MOLECULAR ANALYSIS OF MAMMALIAN ADENYLYL CYCLASES AND EDEMA FACTOR, A BACTERIAL ADENYLYL CYCLASE TOXIN

BY

Srividya Suryanarayana
M.Sc, Osmania University, India, 2002

Submitted to the Graduate Degree program in Biochemistry and Biophysics
and the Graduate Faculty of the University of Kansas
in partial fulfillment of the requirements for the degree of
Doctorate of Philosophy

Dissertation Committee:

_____
Mark Richter, PhD (Chairperson)

_____
Roland Seifert, M.D., PhD

_____
William Picking, PhD

_____
Krzysztof Kuczera, PhD

_____
Jackob Moskovitz, PhD

Date Defended: 15th December 2008

The Dissertation Committee for Srividya Suryanarayana certifies
that this is the approved version of the following dissertation:

MOLECULAR ANALYSIS OF MAMMALIAN ADENYLYL CYCLASES AND EDEMA FACTOR, A BACTERIAL ADENYLYL CYCLASE TOXIN

Dissertation Committee:

_____
Mark Richter, PhD (Chairperson)

_____
Roland Seifert, M.D., PhD

_____
William Picking, PhD

_____
Krzysztof Kuczera, PhD

_____
Jackob Moskovitz, PhD

Date Approved: 15th December 2008

Abstract

Adenylyl cyclases (ACs) catalyze the conversion of ATP to cAMP, an important second messenger central to many signaling pathways. Nine different isoforms of mammalian ACs (mACs) are present, each with distinct localization, physiological function and regulatory mechanisms by activators and inhibitors. In addition to mACs, bacterial AC toxins such as edema factor (EF) from Bacillus anthracis and CyaA from Bordetella pertussis have also been identified. Following infection, the AC toxins cause a dramatic increase in cAMP levels, thereby disrupting several intracellular signaling pathways.

This thesis is broadly divided into two parts and is aimed at validating the active-site nucleotide analogs of mACs and EF. The first part of the thesis focuses on understanding mAC regulation and the mechanism of interaction of mACs with fluorescent 2', 3'-O-(2, 4, 6-Trinitrophenyl) (TNP)- nucleotides. Using purified catalytic subunits of mAC (C1/C2) as model for mACs, we have observed the binding of TNP-nucleotides to C1/C2 and the resulting conformational changes monitored by fluorescence spectroscopy. The enzymatic assays have shown that TNP-nucleotides potently inhibit C1/C2 as well as holo-AC isoforms. An isoform-selective inhibition of AC1, AC2 and AC5 by TNP-nucleotides has been reported for the first time indicating that TNP-nucleotides can serve as models for rational design of potent isoform-specific AC inhibitors. Furthermore, biophysical and biochemical analysis of

the effects of TNP- and 2’ (3’)-O-(N-methylanthraniloyl) (MANT) -nucleotides on the individual subunits C1 and C2 show that C1 and C2 can exist as homodimers. This homodimerization may play an important physiological role in cAMP signaling.

The second part of the thesis addresses the structure-activity relationship in regulating the catalytic activity of EF and its interaction with calmodulin (CaM) using MANT derivatives of ATP and GTP as probes. Our enzymatic assays have shown that MANT-nucleotides are highly potent at inhibiting EF. MANT-nucleotides are also favorable for FRET studies indicating that our robust fluorescence assays can be used for High-Throughput Screening (HTS) of EF inhibitors. Additionally, EF-CaM interaction was probed by MANT-nucleotides. We have observed that binding and activation of EF by CaM are two independent processes in the presence and absence of calcium. Furthermore, our fluorescence assays to monitor binding of oxidized CaM to EF also indicate that methionine residues in CaM play an important role in binding to EF.

Acknowledgements

First and foremost, I would like to thank God for blessing me with this opportunity to pursue my Ph.D in the United States of America. I thank Him for supporting me through the best and toughest years of my life.

Next, I am extremely thankful to my advisors Dr. Roland Seifert and Dr.Mark Richter for their invaluable guidance, support and for sharing their expertise and research insight. Thanks for helping me make a smooth transition in the U.S and giving me a sense of direction during my doctoral studies. Thanks for believing in me during the toughest times and boosting my morale to do better every day. Thanks for helping me develop my presentation, writing and research skills and providing me with financial support to complete my PhD studies. I am deeply grateful to both of them and I wouldn't have been able to fulfill this dream without their constant encouragement and support. I would also like to acknowledge Dr.William Picking, Dr. Krzysztof Kuczera and Dr. Jackob Moskovitz for serving on my defense committee and providing helpful suggestions.

I am greatly indebted to Dr.Jackob Moskovitz for allowing me to continue my PhD research in his lab. I am also grateful to my dear lab mate Dr.Cibele Pinto (University of Kansas Medical Center) for the enthusiasm, inspiration help and a wonderful friendship, which was always there when I needed it and to Dr.Andreas Gille for initiating the projects I worked on and for all the

support provided. I also wish to thank Derek Oien (graduate student) for all his help in the lab.

Many thanks are also due for all the collaborators at various stages of my PhD studies. I wish to thank Dr.Stephen Sprang and Dr.T.C.Mou (University of Texas Southwestern Medical Center) for providing us generously with C1/C2 and Gsa proteins. I also wish to acknowledge Dr.Wei-Jen Tang (Ben-May institute of Cancer Research, University of Chicago) for kindly providing us with EF and EF3 proteins. I would also like to thank Dr. Gerald Lushington for providing me with all the help on molecular modeling. Grant support for my research projects were provided by the American Heart Association.

I don’t have enough words to describe how grateful I am to my sister Usha. Without her, my dream to become a researcher would always be unfulfilled. She has been the guiding angel in my life, helped me realize what I was capable of, encouraged me, helped me achieve my goals and to stay focused, in short, I owe her all my success.

I did specially like to thank my parents (Mr. Suryanarayanan and Mrs. Janaki Suryanarayanan) for their tremendous sacrifices so that I could achieve my dream. I thank them for teaching me values to be a good person, for always being supportive of my decisions, for letting me come to the United States, thousands of miles away from them, to pursue my goal.

I thank all my family, my sisters (Uma, Bhagyam), my brothers-in-law (Natarajan, Ravi, Kushal and Kaushik), my nieces (Priya and Hemshikha), my in-laws (Mr.Viswanathan and Mrs. Shobha Viswanathan)for being very supportive and proud of my achievements. In particular, I would specially like to acknowledge my father-in-law Mr.Viswanathan for his constant encouragement that will always help me remain grounded and work even harder to achieve my goals.

Lastly, and most importantly, I thank Karthik, my husband for being my pillar of strength without whom this journey would have been incomplete. I am extremely grateful to him for always being there for me, for believing in me and my capabilities, for all his unconditional support, inspiration, love and for his loads of patience in handling difficult situations.

Many thanks are due to Ms. Geetha Vani Chittoor, Dr.Vamsee Mohan Yaganti and many others for providing emotional support and for making my stay in Kansas a very memorable one.

Table of Contents

Chapter 3: Biochemical and biophysical analysis of the C1 and C2 catalytic subunits of mammalian adenylyl cyclase

Chapter 5: Future directions

List of Tables

List of Figures

Chapter 1: Introduction

Adenylyl cyclases (AC) catalyze the conversion of adenosine 5'-triphosphate (ATP) to 3', 5'-cyclic adenosine monophosphate (cAMP), an important second messenger that mediates several intracellular signaling pathways (Sutherland and Rall, 1958; Hurley, 1998; Hanoune and Defer, 2001). cAMP is central to various functions ranging from activation of protein kinase A to cell growth, differentiation and regulation of transcription (Robison et al., 1968; Rodbell, 1980).

Mammalians ACs are typically transmembrane proteins with the exception of one soluble form of AC (sAC) identified in testes (Buck et al., 1999). Nine different AC isoforms have been identified in mammals that differ in tissue distribution, activation and inhibition by different mediators (Tang and Hurley, 1998; Hanoune and Defer, 2001; Sunahara and Taussig, 2002).

In addition to mACs, several microorganisms such as *Bacillus anthracis, Bordetella pertussis and Pseudomonas aeroginosa*, release AC toxins that play an important role in disrupting several host intracellular signaling pathways (Seigel et al., 1977; Wolff et al., 1980; Leppla, 1982). These exotoxins enter the host cells via different mechanisms and bring about a dramatic increase in cAMP levels (Seigel et al., 1977; Wolff et al., 1980; Leppla, 1982). One such toxin is Edema Factor, released by *Bacillus*

anthracis that alters water homeostasis and causes edema by increasing cAMP levels (O' Brien et al., 1985; Drum et al., 2002)

Though mACs and EF are structurally distinct, both these enzymes are important cAMP modulators and they both constitute potential drug targets. By regulating cAMP levels, mACs play an important role in several diseases such as congestive heart failure, asthma etc (Hanoune and Defer, 2001; Sunahara and Taussig, 2002). By increasing cAMP levels, EF contributes significantly to cutaneous and systemic forms of anthrax (Sirisanthana et al., 1988; Bhatnagar and Batra, 2001).

1.1 Mammalian membranous adenylyl cyclases (mACs)

Mammalian adenylyl cyclases play an important role in the G-protein signaling cascade (Robison et al., 1968; Sunahara et al., 1996). Following activation of G-protein-coupled receptors (GPCRs) by extracellular signals such as hormones and neurotransmitters, GPCRs in turn activate the heterotrimeric G-proteins. G-proteins then bind to AC mediating activation of AC and subsequent conversion of ATP to cAMP (Smigel et al., 1985; Gilman, 1987).

After AC1 gene was first cloned by Krupinski et al (1989), nine different isoforms of mAC were cloned and characterized. Each AC isoform is

differentially regulated and has unique functional attributes (Taussig and Gilman, 1995; Sunahara et al., 1996; Smit and Iyengar, 1998). All nine AC isoforms are stimulated by the $G_s\alpha$ subunit of G-proteins and metal ions (Taussig and Zimmerman, 1998; Sunahara and Taussig, 2002). With the exception of AC9, AC1-AC8 are also stimulated by the diterpene activator, forskolin (FS), isolated from the root of the Indian herb *Coleus forskolhii* (Seamon and Daly, 1981; Premont et al., 1996; Yan et al., 1998). In addition to the nine membranous AC isoforms, a tenth distinct soluble AC isoform (sAC) has been identified in the testes (Neer, 1978; Buck et al., 1999). cAMP production by sAC is bicarbonate dependent and sAC is not activated by any of the mAC effectors (Braun, 1991; Buck et al., 1999).

All nine AC isoforms share a common structural topology featuring a short variable cytoplasmic N-terminus followed by two transmembrane domains (M1 and M2). M1 and M2 have 6 transmembrane spans that alternate with two cytoplasmic domains C1 and C2 (Sunahara et al., 1996; Sunahara and Taussig, 2002) as indicated in Figure 1. Though initially transmembrane domains M1 and M2 were thought to play a role in anchoring and coordinating C1/C2 interaction, there is growing evidence of an important role for M1 and M2 in AC dimerization and regulation. ACs are now known to dimerize *via* their transmembrane domains (Gu et al., 2002; Cooper and Crossthwaite, 2006). M1 and M2 also serve as isoform-specific sites for glycosylation (Wu et al., 2001). C1 and C2 domains are further divided into

C1a, C1b and C2a, C2b respectively. C1a and C2a share ~50% sequence similarity and are highly conserved in all AC isoforms (Sunahara et al., 1997). C1a and C2a form the catalytic core of the enzyme and constitute the binding sites for ATP, $G_s\alpha$, divalent metal ions and forskolin (Tang and Gilman, 1995; Dessauer and Gilman, 1996; Whisnant et al., 1996; Yan et al., 1996). The C1b and C2b regions are poorly conserved in all AC isoforms. The C1b domain serves as an important regulatory subunit and an isoform-specific binding site for $\beta\gamma$ subunits of G-proteins (Yan et al., 2001; Beeler et al., 2004). Recent evidence suggests that C1 and C2 domains, in association with other proteins, can target specific AC isoforms to lipid raft regions of the plasma membrane (Fagan et al., 2000; Ostrom et al., 2000; Smith et al, 2002).

Figure 1-1 Structure of mammalian membranous adenylyl cyclases

Schematic representation of the structure of mammalian adenylyl cyclases. Shown are transmembrane domains M1 and M2 (tan color), a short variable N-terminus and cytoplasmic domains C1 and C2. C1 and C2 domains are divided into C1a, C1b (light grey) and C2a, C2b regions (dark grey). C1a and C2a together constitute the catalytic core of the enzyme and possess binding site for ATP, $G_s\alpha$ subunit of G-protein, FS and divalent metal ions.

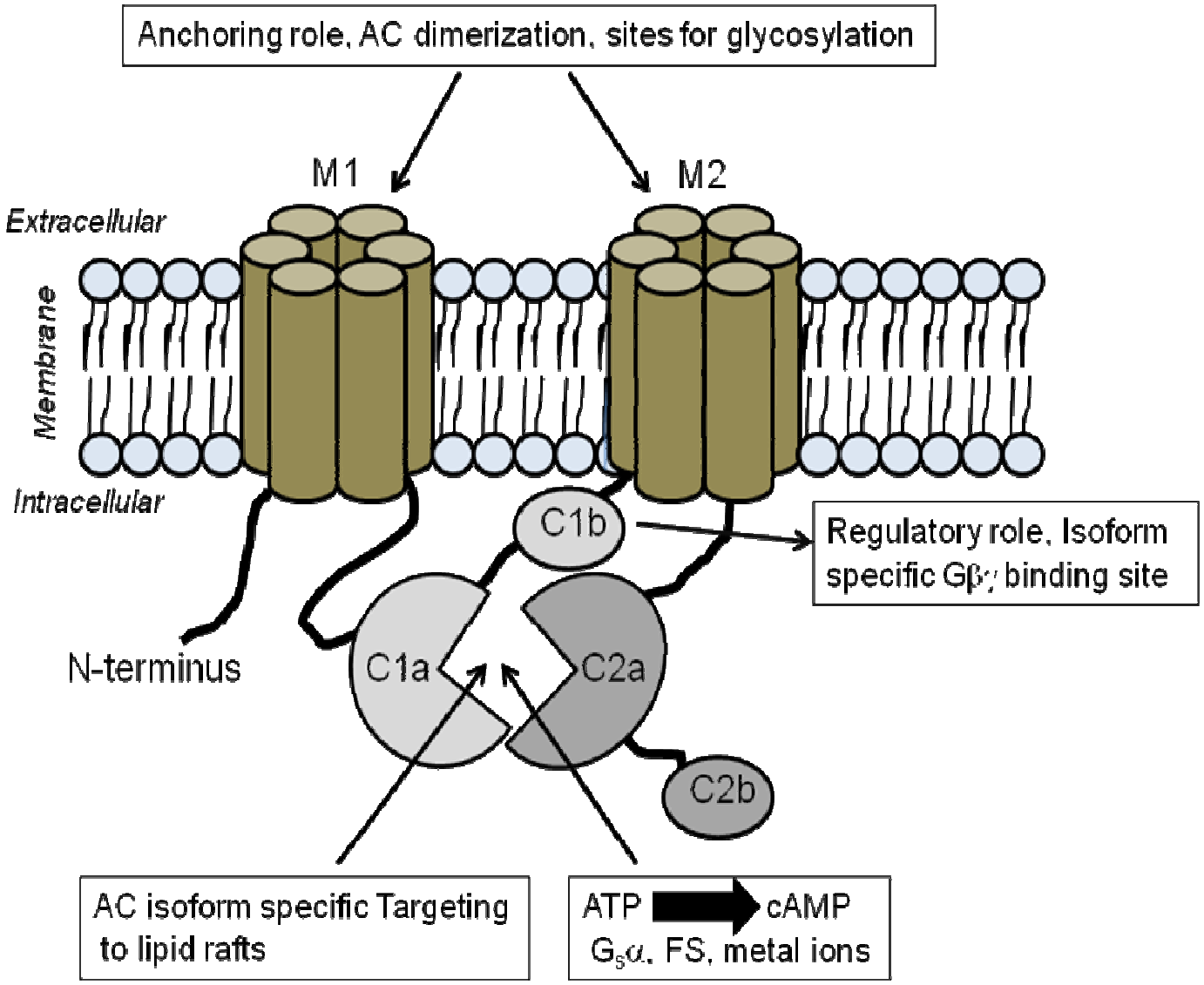
Anchoring role, AC dimerization, sites for glycosylation
M1
M2
Extracellular
Membrane
Intracellular
C1b
Regulatory role, Isoform specific Gβγ binding site
N-terminus
C1a
C2a
C2b
AC isoform specific Targeting to lipid rafts
ATP
cAMP
$G_s\alpha$, FS, metal ions

1.1.1 AC isoforms - tissue distribution, physiological role and potential therapeutic targets

To gain a better understanding of the expression patterns of AC isoforms in different tissues and their role in signaling, a variety of approaches such as RT-PCR, confocal immunofluorescence studies, knock out and transgenic animal models for ACs have been used. Growing evidence suggests that, depending on the localization of AC isoforms, ACs play an important functional role in regulating cAMP levels in these tissues.

Overlapping expression patterns of AC isoforms have been observed in different tissues, nonetheless some isoforms are more predominant compared to other isoforms in different tissues. For example all AC isoforms are expressed in the brain; however AC1, AC2 and AC8 are the predominant ones in the brain and are the major contributors to long term potentiation (LTP), learning and memory. AC1 is expressed in the brain, retina and adrenal medulla (Xia et al., 1993). AC1 is neurospecific and plays an important role in cAMP dependent synaptic plasticity (Wu et al., 1995; Abdel-Majid et al., 1998, Lev-Ram et al., 2002). AC1 is also known to regulate circadian expression of melatonin biosynthesis (Borjigin et al., 1995; Tzavara et al., 1996; Chan et al., 2001). AC1 being neurospecific, may play a role in neurodegenerative diseases, stroke and Huntington's disease (Wang et al., 2007; Fan and Raymond, 2006). AC8 is not neurospecific and is expressed in

lung, heart, pancreas and parotid glands (Muglia et al., 1999; Watson et al., 2000, Guenifi et al., 2000). Transgenic animal studies have shown that AC8 in the heart may play a role in myocardial contractility and AC8 expression in parotid glands may be important for regulation of parotid function (Esposito et al., 2008; Watson et al., 2000). Studies with double AC1 and AC8 knockout mice have shown defects in learning and memory (Wong et al., 1999). The AC2 isoform is expressed in the brain and lung (Furuyama et al, 1993; Jourdan et al, 2001). AC2 and AC8 in the lung contribute to cAMP regulation and cAMP mediated pathways in pulmonary artery myocytes (Jourdan et al, 2001).

AC3 was first identified in the olfactory epithelium and later in other tissues such as heart, pancreas and lung (Bakalyar and Reed, 1990; Xia et al., 1992; Ishikawa et al., 2000). Gene disruption studies in mice have demonstrated that the AC3 isoform is important for olfaction and implicated in cAMP mediated detection of odorants in the olfactory epithelium (Wong et al., 2000). Immunofluorescence studies have shown that AC3 and AC8 are expressed in pancreas and may play a role in glucose mediated insulin secretion (Guenifi et al., 2000) and in type 2 diabetes (Ishikawa et al., 2000). Expression of AC4 is widespread and along with other AC isoforms, AC4 is expressed in rodent outer retina and may play a role in photoreception (Abdel-Majid et al, 2002).

AC5 and AC6 are the predominant isoforms expressed in heart (Ostrom et al, 2002). AC6 is widely expressed in many other tissues (Roth et al., 1999). Several knockout studies have indicated that AC5 and AC6 are particularly important isoforms in the cardiovascular system (D' Angelo et al., 1997; Gao et al., 2002; Okumura et al., 2003). AC5 and AC6 knockouts serve as suitable models to study congestive heart failure. Recent studies have suggested that AC5 knockout mice are resistant to cardiac stress (Yan et al, 2007). Selective AC5 antagonists may have a therapeutic value against depression and anxiety (Krishnan et al., 2008). AC5 gene disruption also played a role in longevity and stress and AC5 knockouts have been useful models for studying pain mechanisms (Yan et al., 2007; Kim et al., 2007). In sharp contrast, AC6 knockout can cause abnormal left ventricular function (Tang et al, 2008). AC6 plays a cardioprotective role and may be very important for congestive heart failure therapy (Phan et al., 2007).

The AC7 isoform is expressed in the brain and in several other tissues. Using a combination of approaches, Hines et al (2006) have shown that AC7 may play a sex-specific role in depression. Recent studies also reveal that alcohol interacts directly with AC molecules and AC7 has been identified as the most ethanol sensitive AC isoform (Yoshimura et al., 2006). This suggests a possible role for AC7 in the development and predisposition to alcoholism. AC9 is the least characterized and FS- insensitive AC isoform (Premont et al, 1996). AC9 is expressed in the brain as well as in many other major tissues

(Hacker et al., 1998; Paterson et al., 2000). In the brain, AC9 is expressed in regions important for learning and memory (Antoni et al., 1998). sAC, the soluble isoform found in testes, is important for sperm maturation and sAC inhibitors can act as potential male contraceptives (Marquez and Suarez, 2008).

AC isoforms are important potential therapeutic targets because cAMP is directly or indirectly implicated to play a major role in several diseases ranging from depression, heart failure to diabetes. However, there are very few known activators and inhibitors of specific AC isoforms. P-site inhibitors and several other small molecule inhibitors such as calmidazolium and tyrphostin A25 have been identified that are isoform-selective to a certain extent (Ahlijanian and Cooper, 1987; Jaleel et al., 2004). FS and FS analogs activate and inhibit various AC isoforms with some specificity (Pinto et al., 2008). Keeping in view the different roles of different AC isoforms, there is a good possibility that isoform-specific and therefore tissue-specific AC inhibitors can be developed.

Table 1-1 A summary of tissue distribution and putative function of mammalian membranous adenylyl cyclase

AC isoforms	Tissue distribution	Putative function	References
AC1	Brain, heart, adrenal medulla, retina	Neuroplasticity, Long term memory (LTM), long term potentiation (LTP)	Xia et al., 1993; Wu et al., 1995; Lev-Ram et al., 2002; Wong et al., 1999
AC2	Brain, lung, smooth muscle	Cell differentiation, learning, memory	Furuyama et al, 1993; Jourdan et al, 2001
AC3	Brain, olfactory epithelium, pancreas	Olfaction, glucose mediated insulin release	Bakalyar and Reed, 1990; Xia et al.,1992; Ishikawa et al., 2000; Wong et al., 2000;
AC4	Widespread	Photoreception	Abdel-Majid et al., 2002
AC5	Brain, heart, kidney	Heart rate regulation, longevity, stress	Yan et al, 2007; Kim et al., 2007
AC6	Heart, kidney, widely expressed	Heart function	Tang et al, 2008; Roth et al., 1999; Gao et al, 2002
AC7	Brain, ubiquitous expression	Alcohol sensitivity	Hines et al., 2006; Yoshimura et al., 2006
AC8	Brain, lung, heart, pancreas, parotid gland	LTM, LTP, synaptic plasticity, glucose mediated insulin release	Muglia et al., 1999; Watson et al., 2000, Wong et al., 1999, Jourdan et al, 2001
AC9	Brain, skeletal muscle, heart	Learning and memory	Hacker et al., 1998; Antoni et al., 1998

1.1.2 AC isoforms - regulation

Adenylyl cyclases can be broadly divided into five groups based on regulation by G-proteins and ions. The first group consists of Ca^{2+}-Calmodulin (CaM) sensitive AC1, AC3 and AC8. This group is stimulated by Ca^{2+}-CaM and AC1 and AC8 are inhibited by $G\beta\gamma$ subunits of G-proteins (Krupinski et al., 1989; Cali et al., 1994; Choi et al., 1992; Tang and Gilman, 1991; Taussig et al., 1993). In addition to regulation by G-proteins and ions, post-translational modifications such as phosphorylation, glycosylation and nitrosylation of ACs are commonly observed. AC1 and AC3 are stimulated by protein kinase C (PKC) and inhibited by CaM kinase IV and CaM kinase II, respectively, in a feedback regulation (Yoshimura and Cooper, 1993; Zimmermann and Taussig, 1996; Wayman et al., 1996; Wei et al., 1996). PAM (protein associated with myc) is known to interact with AC1, thereby inhibiting cAMP production (Scholich et al., 2001). AC3 is also known to interact with RGS2 (Regulators of G-protein signaling) (Sinnarajah et al., 2001).

The second group of ACs, namely AC2, AC4, and AC7, is directly stimulated by $G\beta\gamma$ subunits of G-proteins and are insensitive to calcium (Gao and Gilman, 1991; Lustig et al., 1993; Yoshimura et al., 1996; Cooper et al., 1998). AC2 is activated by PKC, and AC4 is inhibited by PKC (Ebina et al.,

1997; Zimmermann and Taussig, 1996). However, modulation of AC activity by PKC is not clearly known.

The third group of ACs, namely AC5 and AC6, are the best studied isoforms and are inhibited by micromolar concentrations of calcium and $G_i\alpha$ proteins ($G_o\alpha$, $G_i\alpha1$, $G_i\alpha2$, $G_i\alpha3$, $G_z\alpha$) (Guillou et al., 1999; Cooper et al., 1995; Taussig et al., 1993; Kozasa et al., 1995). PKC activates and inhibits AC5 and AC6 respectively (Lai et al., 1997). AC5 and AC6 are also directly phosphorylated and inhibited by PKA (Iwami et al., 1995). AC5 and AC6 are glycosylated at the extracellular loops of their transmembrane domains. However, the physiological role of these glycosylation events is not clearly understood. Blocking AC6 glycosylation decreases inhibition by PKC (Wu et al., 2001). AC5 and AC6 are also nitrosylated and can be inhibited by nitric oxide (NO) (McVey et al., 1999; Ostrom et al., 2004). RGS2 is known to bind to the C1a regions of AC5 and AC6 causing inhibition of cAMP production (Salim et al., 2003; Roy et al., 2003). PAM is also known to physically interact with the C2 region of AC5 and AC6 (Gao and Patel, 2005; Scholich et al., 2001). Patel's group has shown that specific hormones such as EGF (Epidermal growth factor) can indirectly activate AC5 by phosphorylating specific residues on $G_s\alpha$. This increase in cAMP levels has a positive inotropic effect (increase in strength of muscular contractions) on the heart (Nair et al., 1989; Nair and Patel, 1993). AC6 also specifically interact with Raf1, a protein in the MAPK/ERK signaling pathway (Mitrogen activated

protein kinase/extracellular signal regulated kinase) and Snapin, a component of the SNAP-25/SNARE complex of proteins. Raf1 binds to C1b region and the intracellular loop of M2 and is predicted to play a role in heterologous sensitization of AC6 (Ueda et al., 1996). Snapin interacts with the N-terminus of AC6 and, therefore, AC6 is speculated to play a role in synaptic signaling and vesicle fusion (Chou et al., 2004).

AC9, the FS-insensitive AC isoform, is poorly characterized and the only member of the fourth group of ACs. AC9 is activated by $G_s\alpha$ and inhibited by $G_i\alpha$, PKC and Ca^{+2}/Calcineurin (Hacker et al., 1998). AC9 also undergoes glycosylation which is known to determine AC9's relative sensitivity to $G_s\alpha$ (Cumbay and Watts., 2004).

The fifth group of ACs is comprised of sAC, a soluble isoform found in testes and other bicarbonate sensitive tissues. sAC is distinct from other mammalian AC isoforms and is regulated by Ca^{2+} and bicarbonate. sAC is closely related to cyanobacterial ACs and may provide a link between bacterial and mammalian signaling pathways (Buck et al., 1999). sAC plays a role in cAMP mediated sperm maturation and motility in the testes and is implicated to play a very important role in male fertility (Marquez and Suarez, 2008).

Figure 1-2. Regulation of Mammalian membranous AC isoforms and soluble AC

Figure A – Schematic representation of the regulation of nine AC isoforms. Stimulating effectors are represented in red, inhibitors are shown in blue. PKA, Protein Kinase A; PKC, protein kinase C; CaM, Calmodulin; EGF, epidermal growth factor; RTK, receptor tyrosine kinase. All the AC isoforms are stimulated by $G_s\alpha$. All isoforms except for AC9 are also stimulated by forskolin.

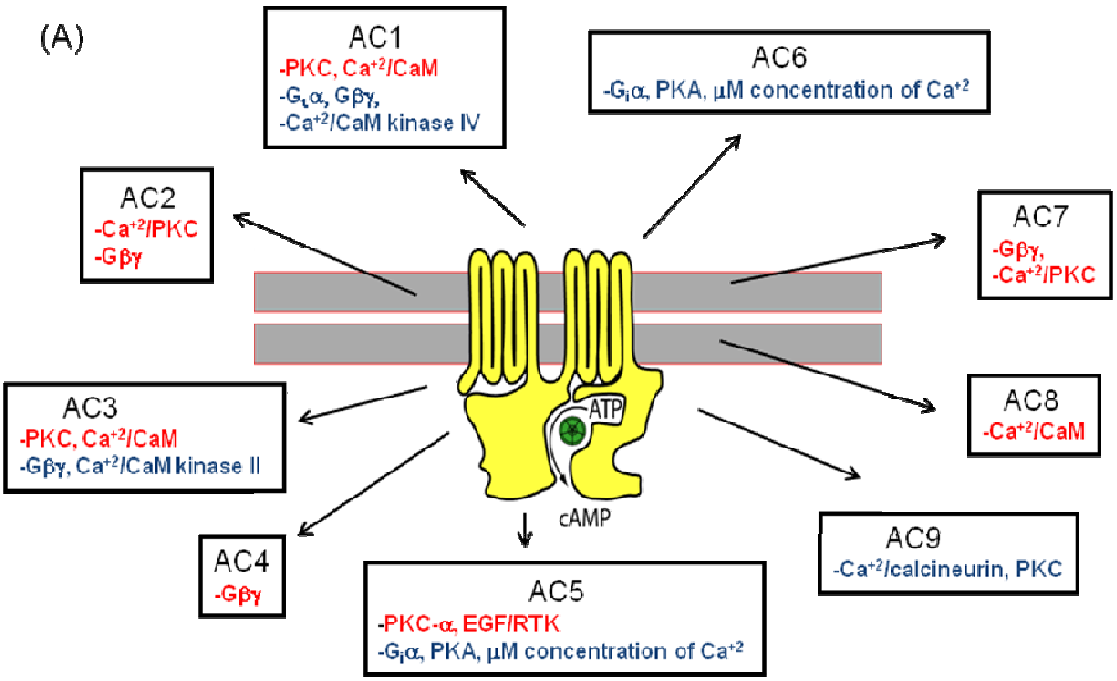

Figure B – Crystal structure of CyaC, a sAC homolog from Cyanobacterium *Spirulina platensis* in complex with an ATP analog and calcium (Steegborn et al., 2005). sACs are stimulated by bicarbonate and calcium. Two sAC homodimers (one in red and one in blue) form the catalytic site for ATP conversion to cAMP.

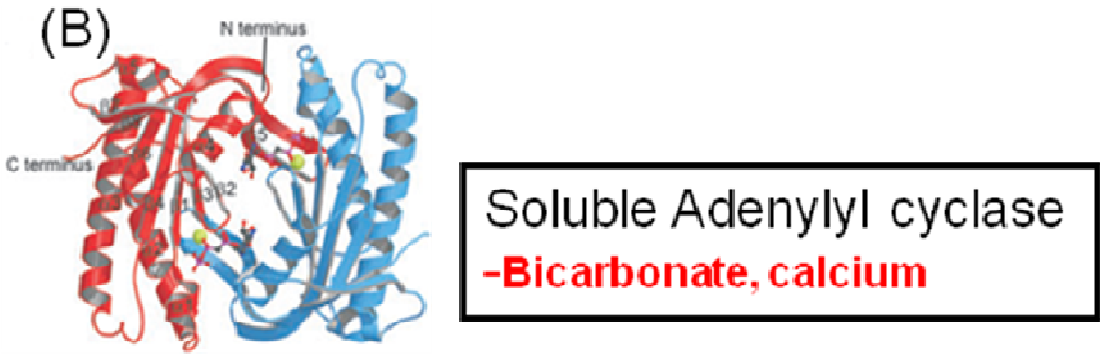

1.1.3 Catalytic mechanism of AC

Several crystallographic, kinetic, mutational and modeling studies have been carried out to gain insight into the catalytic mechanism of AC. First the crystal structure of C1 and C2 in complex with FS and $G_s\alpha$.GTPγS was solved by Tesmer's group (Figure 1-3). They showed that the interfacial surface of C1 and C2 buried approx. 3300 Å of solvent – accessible surface area and two pseudosymmetric regions were observed at the interface. ATP binds to one region, and $G_s\alpha$ and FS bind to the other. Modeling studies have demonstrated that ATP binding changes the conformation of AC from an inactive and open to an active and closed state (Tesmer et al., 1997).

A detailed study of the $G_s\alpha$ and FS binding sites has shown that seventy five percent of $G_s\alpha$ is accommodated by C2 and the remainder by C1. F379 of C1 has been identified as an important residue for interaction with $G_s\alpha$. Binding of $G_s\alpha$ changes the relative orientation of C1/C2 and prepares the active site for catalysis.

The crystal structure of the C2 homodimer possesses two binding sites for FS (Zhang et al., 1997). Since C1 and C2 share at least 30% sequence homology, it was predicted that C1/C2 would also have two FS binding sites similar to C2 homodimers. However, the consensus is that C1/C2 possesses only one FS binding site. FS and $G_s\alpha$, both together and separately, increase

the affinity of C1 for C2, promoting their dimerization, and also increase the V_{max} of the enzyme (Sunahara et al., 1997).

Several critical amino acid residues have been identified that are important for ATP binding and catalysis. For example, R1029 is a very important amino acid residue in C2 that helps to stabilize the α-phosphate intermediate in ATP conversion. N1025 on C2 coordinates a water molecule that forms a hydrogen bond with ATP. Mutational studies have shown that E518 is important for ATP binding because the E518A mutation reduces the affinity for an ATP analog (Dessauer et al., 1997). ACs catalyze the conversion of ATP to cAMP using a two metal ion mechanism. The two - metal ions catalyze the phosphoryl transfer and are coordinated by D396 and D440 residues on C1 (Tesmer et al., 1999).

P-site inhibitors have been extensively used as probes to understand the catalytic mechanism of AC. These inhibitors possess an intact ring and are dead end inhibitors of product (PP_i) release. They bind to the active site and stabilize the enzyme-PP_i complex. P-site inhibitors are non-competitive/uncompetitive depending on metal-ATP and regulators and are known to inhibit only the stimulated forms of AC (Johnson et al., 1989; Tesmer et al., 2000).

Fluorescent nucleotides have also been used as probes to study the conformational changes in C1/C2 upon binding of activators such as $G_s\alpha$ and

FS. Gille et al., (2004) showed that the fluorescent 2' (3')-O-(N-methylanthraniloyl) MANT derivatives of ATP and GTP are highly potent inhibitors of C1/C2 as well as AC isoforms with K_i values in the 10 to 100 nM range. The crystal structure of C1/C2 with MANT-GTP and MANT-ATP, solved by Mou et al., (2005) showed that the MANT substituent of MANT-ATP and MANT-GTP make van der Waals contacts with C1 and C2 (Figure 1-4a). The MANT group prevents movement of the β1-α1-α2 loop of C1 and the α4'-β5' and β7'-β8' loops of C2, thus preventing the change from the inactive (open) to the active (closed) conformation (Gille et al., 2003; Mou et al., 2005).

2', 3'-O-(2, 4, 6-Trinitrophenyl) (TNP) nucleotides were also studied in our laboratory to monitor conformational changes in ACs (the results will be described in some detail in later chapters). TNP nucleotides have been widely used to study conformational changes in proteins. In collaboration with Mou and group, the crystal structure of C1/C2 was solved in complex with TNP-ATP (Figure 1-4b). We observed that the TNP group acts as a wedge preventing the change from the inactive (open) to active (closed) conformation, very similar to MANT-ATP and MANT-GTP. The relative orientations of MANT-ATP, MANT-GTP and TNP-ATP are slightly different in the catalytic pocket of C1/ C2. Nonetheless, all three nucleotides reside in the same pocket formed by C1/C2. This indicates that mAC has a broad nucleotide binding specificity because the catalytic pocket is flexible enough

to accommodate different bases and fluorophore. Therefore, a general tripartite mAC pharmacophore model was generated where the inhibitor binding site overlaps the substrate binding site and contains a spacious base-binding pocket, a hydrophobic pocket for the fluorophore (ribose substituent) and a polar phosphate binding region (Figure 1-5) (Mou et al., 2006).

Figure 1-3. Crystal structure of C1/C2 in complex with $G_s\alpha$, FS and ATP as shown in Tesmer et al., 1999.

C1a and C2a are shown in tan and mauve colors respectively. $G_s\alpha$ is shown in red, ATP and FS in stick models bind at the interface between C1 and C2. C1/C2 is shown to interact with the switch II region of $G_s\alpha$.

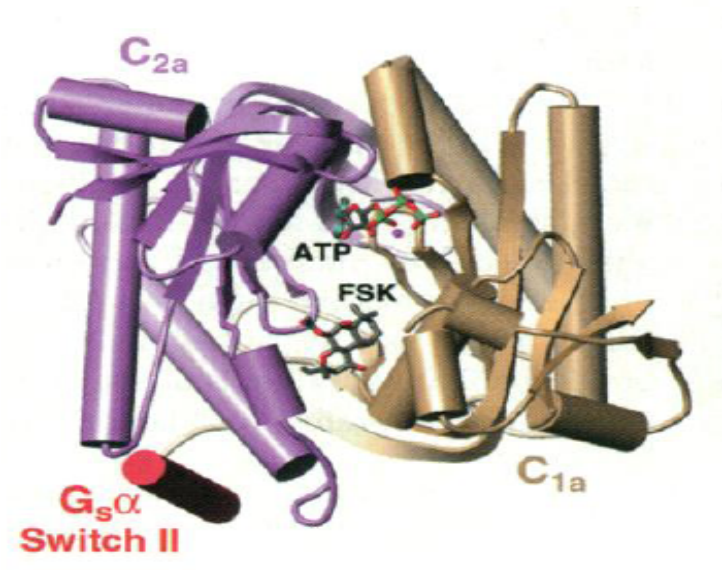

Figure 1-4. (a)Crystal structure of C1/C2, $G_s\alpha$ and FS in complex with MANT-GTP

C1 in mauve, C2 in tan and $G_s\alpha$ is shown gray. Switch II of $G_s\alpha$ is shown in red. FS, MANT-GTP and metal ions occupy the cleft formed by C1 and C2.

(b) Crystal structure of C1/C2, $G_s\alpha$ and FS in complex with TNP-ATP (Mou et al., 2006)

C1 in tan, C2 in mauve and $G_s\alpha$ is shown grey. Switch II of $G_s\alpha$ is shown in red. FS, TNP-ATP and metal ions occupy the cleft formed by C1 and C2. α helices and β-loops in respective C1 and C2 domains involved in change from inactive open to active closed conformation are also highlighted.

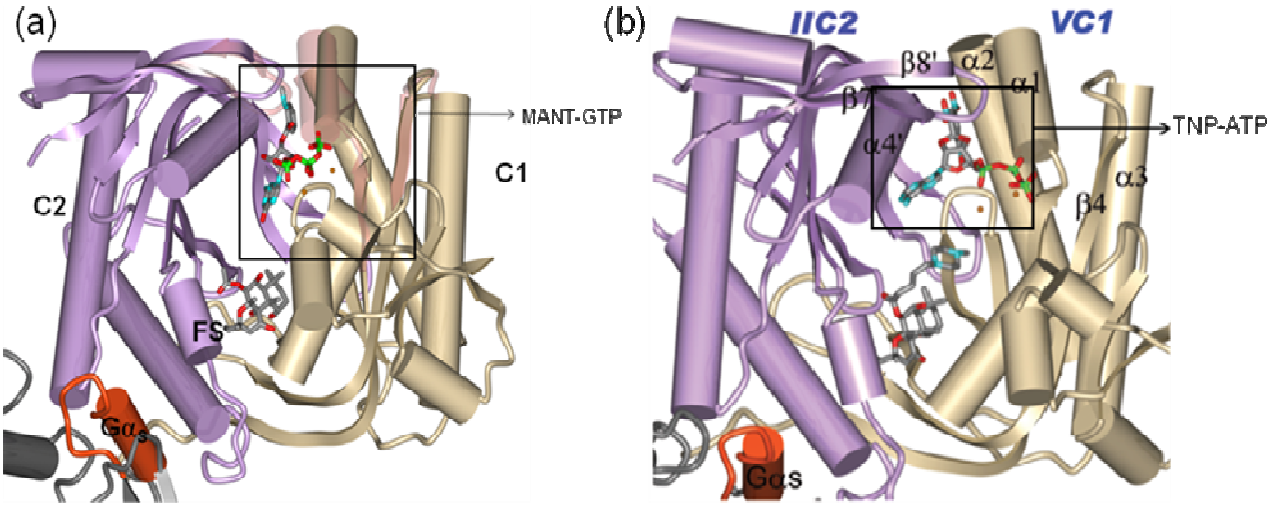

Figure 1-5. (a) Superimposition of MANT-ATP, MANT-GTP and TNP-ATP bound to the C1/C2/ $G_s\alpha$ /FS complex. (Mou et al., 2006)

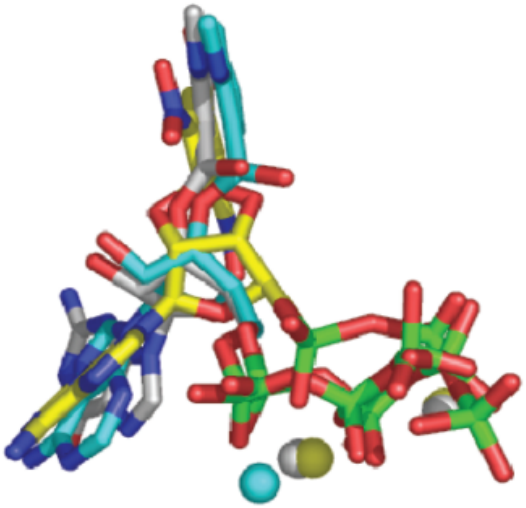

(b) General tripartite AC pharmacophore model for AC inhibitors based on (a). (Mou et al., 2006)

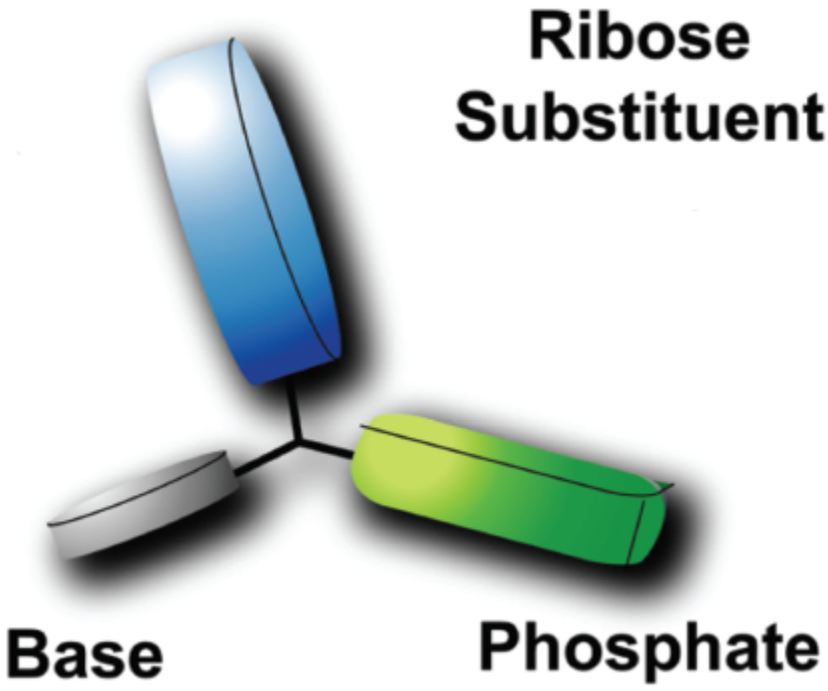

1.1.4 Challenges, limitations and future directions of AC research

Purifying AC protein in its intact membrane bound form has been one of the most difficult challenges faced by AC researchers to date. Fortunately, C1 and C2 have been expressed as separate polypeptides and, when mixed together, they retain many properties of the intact enzyme. Using C1/C2 as a model for ACs, the first crystal structure was solved by Tesmer et al in 1997 and the structure provided considerable information about the catalytic mechanism of ACs and the conformational changes that occur when $G_s\alpha$ and FS bind. In the last 20 years, several biochemical, kinetic and structural studies using C1/C2 have been carried out that have also provided insight into the catalytic mechanism, its regulation and inhibition.

Gene knockout studies and studies using transgenic animal models have helped to understand the physiological roles of some AC isoforms. However, the roles of other specific AC isoforms are not clearly evident due to overlapping expression patterns of AC isoforms in tissues which is due in part to the lack of isoform- specific antibodies (Sunahara et al., 1996). It has also been difficult to identify AC isoform-specific activators and inhibitors.

A major and as yet untapped approach to identification of isoform-selective inhibitors is through the application of high throughput screening experiments. This will require development of suitable assays that can be miniaturized for automated screening formats. Once identified, it will be important to study the

effects of AC isoform-specific inhibitors and activators in intact cells or in animal models. Future biochemical studies will also be required to gain a better understanding of the roles of the different AC isoforms and their regulation in different tissues.

Since the cytoplasmic units of C1 and C2 form the catalytic core of the enzyme, a fundamental question is what is the importance of the transmembrane domains when all that are needed for AC catalysis are the cytoplasmic domains? Emerging evidence suggests that the transmembrane domains play an important role in AC regulation by helping to localize AC, by anchoring the cytoplasmic domains, and by interacting with other regulatory proteins (Wu et al., 2001). Additional information is also needed to describe the exact roles of the C1b and C2b regions in catalysis and regulation. The C1b region is thought to interact with other proteins in some isoforms (Yan et al., 2001; Beeler et al., 2004). Therefore, potential interactions between the C1b and C2b regions with other proteins during the signaling process must also be explored.

G-protein coupled receptors (GPCRs), membrane proteins that are upstream to ACs are known to dimerize as part of their normal function (Prinster et al., 2005). A combination of approaches including co-immunoprecipitation and FRET (fluorescence resonance energy transfer) has suggested that ACs may also dimerize via their transmembrane domains (Gu

et al., 2002). It is speculated that a dimer between two similar or different AC isoforms may constitute a basic functional unit of AC. In addition to interaction with other proteins, transmembrane domains may also participate in AC dimerization.

Recent advancement in AC research has also highlighted the importance of localization of AC isoforms. Some AC isoforms are thought to be localized on lipid rafts and caveolae, a sub set of lipid rafts formed by polymerization of caveolin. Due to localization of ACs, changes in cAMP levels may also be localized in defined cell compartments rather than being distributed throughout the cytoplasm (Gorodinsky et al., 1995; Huang et al., 1997). The possibility of localization of ACs leading to compartmentalization of cAMP production adds a new dimension to the complexity of AC-regulation pathways.

1.2 Bacterial adenylyl cyclase toxin Edema factor (EF) from Bacillus anthracis.

Anthrax, caused by *Bacillus anthracis*, is a deadly epizootic disease primarily affecting cattle and occasionally humans that come in contact with infected animals or animal products (Mock and Fouet, 2001; Mourez et al, 2002). Human anthrax is more common in developing countries of Asia and Africa compared to the developed countries. Anthrax cases have been described as early as 16th century BC in Egypt and several publications describing anthrax were produced in the 1800s (Scorpio et al, 2006; Oncu et al., 2003). More recently, anthrax spores were used during the terrorist attacks in the US in 2001 giving a new meaning to the word bioterrorism.

Bacillus anthracis is a large gram-positive bacterium that forms spores when in contact with oxygen (Figure 1-6). The spores which carry the virulent factors are highly resistant to a wide range of climatic conditions such as high temperature, UV light and high pH (Watson and Keir, 1994). The spores carry three exotoxins namely Edema Factor (EF), Lethal Factor (LF) and Protective Antigen (PA) and a poly-γ-D glutamyl capsule, all of which are released when the spores come in contact with host cells. Crystallographic, biochemical, kinetic and structural studies have greatly improved our understanding of the mode of action of these toxins.

Figure 1-6. (a) Original photomicrograph of Bacillus anthracis by Robert Koch (www.bact.wisc.edu/themicrobialworld/anthrax.html)

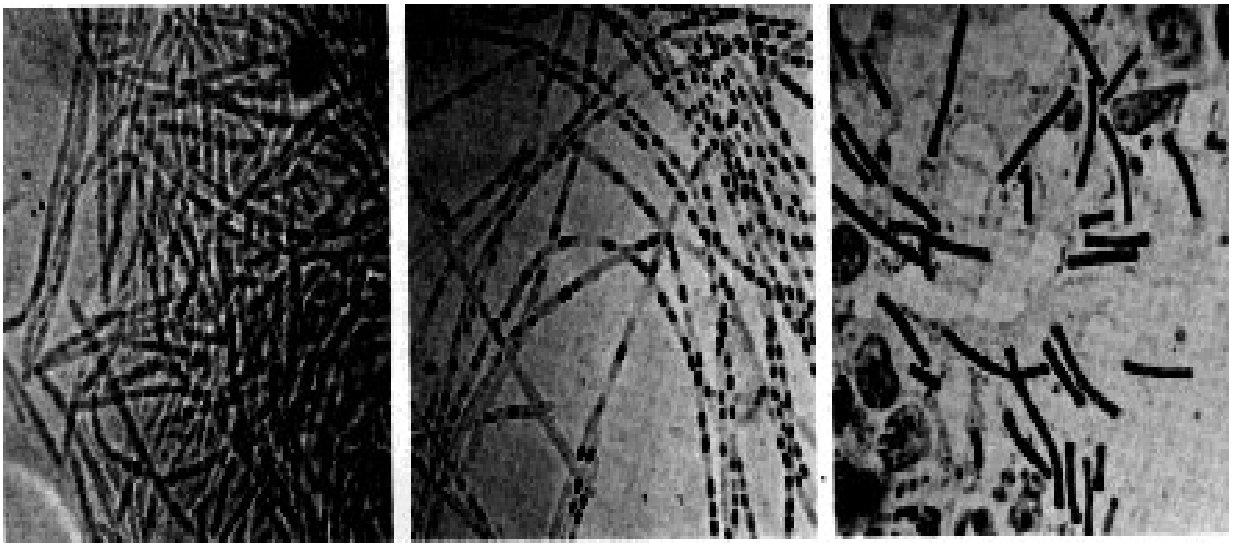

(b) Gram stain photograph of Bacillus anthracis

(www.bact.wisc.edu/themicrobialworld/anthrax.html)

1.2.1 Anthrax – infection, diagnosis, treatment and prevention

Anthrax is primarily divided into three types depending on the mode of entry of the spores into the host. They are (a) cutaneous anthrax (b) inhalational anthrax and (c) gastrointestinal anthrax. There are also some minor and rare forms of anthrax such as anthrax sepsis and renal and ophthalmic forms of anthrax (Oncu et al., 2003).

Cutaneous anthrax

Cutaneous anthrax occurs due to entry of spores through a cut, break or abrasion on the skin. In most cases, cutaneous anthrax in humans is due to handling of infected animals or their products. There have also been reports of some rare cases of cutaneous anthrax due to biting of flies that have fed on anthrax infected animals. The incubation period of spores is typically between 1-12 days. The symptoms start with development of papule on the skin which slowly turns into a vesicle showing necrosis, edema and a characteristic black eschar (lesion) (Figure 1-7). The cutaneous form of anthrax can be effectively treated with antibiotics and can be fatal if left untreated (Oncu et al, 2003; Brey, 2005).

Inhalational anthrax

Inhalational anthrax, also called pulmonary anthrax, is the most lethal form of anthrax. Initial symptoms start with fever and cough. Within a few hours,

more serious symptoms such as dyspnea (shortness of breath), cyanosis (blue coloration of the skin) and respiratory failure develop leading to septicemia, shock and death. Current models for inhalational anthrax assume that spores enter the macrophages in the lungs, multiply and lyse cells, then spread through lymph nodes causing extensive septicemia (Figure 1-8). Inhalational anthrax cases have a high mortality rate and broad-spectrum antibiotic therapies have not been very helpful (Brey, 2005; Ascenzi et al., 2002; http://www.cdc.gov/mmwr/preview/mmwrhtml/mm5510a4.htm) .

Gastrointestinal anthrax (GI anthrax)

The gastrointestinal form of anthrax accounts for less than 5% of anthrax infections. Gastrointestinal anthrax occurs due to ingestion of spores through contaminated food or water. This form of anthrax has a high mortality rate and two subforms i.e. the oropharygeal form where spores get deposited in the upper GI tract and the intestinal or abdominal form with deposition of spores in the lower GI tract have been reported. Extensive edema and necrosis occurs in both forms of GI anthrax. If detected early, GI anthrax can be treated with antibiotics. Once spores invade the bloodstream, they cause toxemia, septicemia and death (http://www.bchealthguide.org/kbase/topic/special/ty6357/sec1.htm).

Figure 1-7 Cutaneous anthrax

(a) Characteristic central eschar with plaque and erythema (b) Necrotic ulcer, black eschar and edema. (www.nlm.nih.gov/medlineplus/anthrax.html)

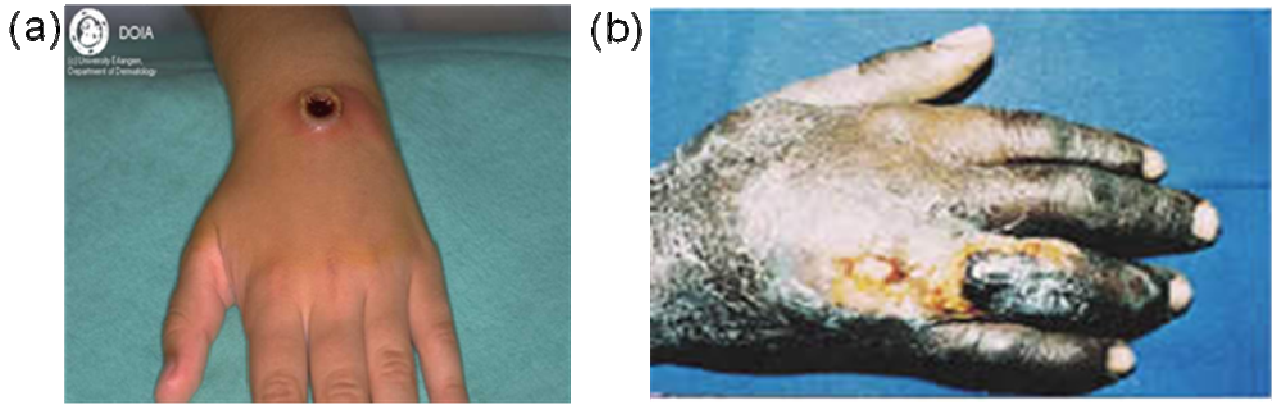

Figure 1-8 Inhalational anthrax

A chest X-ray of an inhalational anthrax infected patient. Clear lungs and mediastinal widening are observed. (http://www.acponline.org/clinical_information/resources/bioterrorism/chest_xray.htm)

Diagnosis, treatment and prevention

Laboratory diagnosis of anthrax includes Gram and polychrome methylene blue staining the specimen from potentially infected patients to identify the polypeptide capsules of *B.anthracis. B.anthracis* from body fluids can also be cultured in blood agar and identified as large colonies, white or grey in color. The anthrax skin test is performed by injecting an attenuated strain and is positive in 85% of cases immediately after infection (Oncu et al., 2003; Shlyakov et al., 1996).

The first vaccine for anthrax was developed by Louis Pasteur by injection of an attenuated *B.anthracis* strain. Protective antigen (PA) was discovered as one of the toxins responsible for virulence by Gladstone (Gladstone, 1946). By the 1950s, the AVA vaccine was developed with PA and small amounts of Edema factor (EF) and lethal factor (LF) from an attenuated strain adsorbed to aluminum hydroxide. AVA, the only vaccine for anthrax approved for use by humans, was licensed by the FDA in the 1970s. AVA with trade name BioThrax® is manufactured by Bioport Corp (Lansing, Michigan), parent company of Emergent Biosolutions (Rockville, MD). Due to problems related to purity, differences in reactivity and manufacturing, a next generation vaccine called rPA is being clinically tested to determine its safety and reactivity. rPA is a recombinant protective antigen purified from an asporogenic *B.anthracis* strain. rPA was clinically tested by VaxGen Inc

(Brisbane, CA) and later acquired by Emergent Biosolutions (Rockville, MD) in 2006 (www.google.com/anthrax news). In addition to vaccines, post exposure treatment for anthrax is aggressive and comprises timely antibiotic therapy with penicillin, doxicyclin and other broad spectrum antibiotics such as fluoroquinolone compounds.

Approaches to development of next generation drugs and vaccines for anthrax are exploring new avenues such as inhibitor design for receptor binding, toxin assembly, endocytosis, enzymatic activity of toxins and targeting virulence of the poly-γ-D glutamyl acid capsule.

Prevention is effective by surveillance and regular check-up of humans working closely associated with animals and military personnel working in higher-risk areas where anthrax spores may be used for potential biological warfare. Timely immunization of animals and humans is also a key to preventing anthrax infections in case of a suspicious exposure to anthrax spores.

1.2.2 Anthrax – Biological warfare and incidence in developing countries

B.anthracis spores have been used as bioweapons and several significant incidents occurred during the last few centuries. Anthrax spores were purportedly used to kill millions of people and cattle during the movement of Huns across Eurasia in 80 AD (http://www.defencejournal.com/dec98/anthrax.htm). In 1941, the British

Government tested the effect of anthrax spores as a bioweapon in Gruinard Island near Scotland. The island was uninhabited until 1986 after several attempts were made to sterilize the soil (Manchee et al., 1981). In 1979, 96 cases of anthrax including 68 deaths resulted due to accidental release of anthrax spores from a military facility in Russia (Meselson et al., 1994). In 1993, an attenuated strain of anthrax was sprayed from the top of a building by the Aum Shinrikyo, a doomsday cult in Tokyo (Keim et al., 2001). In 2001, anthrax spore-laced letters caused widespread panic among people in the United States and worldwide. Due to its high potency, hardiness and resistance to a wide range of conditions, anthrax is classified as Category A bioterrorism agent by the US Centers for Disease Control and Prevention (CDC). It is estimated that a 50 kg of anthrax aerosol spray would result in millions of deaths and, therefore, the potential devastating effects of anthrax cannot be underestimated (Trull et al., 2007).

Naturally occurring anthrax is still a major problem in several developing countries such as India, Turkey, Greece and countries in the African continent. Until 2006, at least 205 cases of anthrax have been reported in parts of Southern India especially in the under-developed regions (Rao et al., 2007; Vijaikumar et al., 2001). Poverty, lack of awareness and lack of vaccinations for both humans and livestock are the primary reasons for high incidence of anthrax infection.

In view of the potential use of anthrax as a bioweapon and the high incidence of naturally occurring infections, there is an urgent need for the development of efficient, accessible and cost-effective drugs, vaccines and other therapeutics to prevent and cure anthrax.

1.2.3 Anthrax tripartite toxin and mechanism of toxin translocation into host cells

Virulence factors of *B.anthracis* are encoded on two plasmids: - pXO1 which contains genes responsible for synthesizing the exotoxins EF, LF and PA, and pXO2 which carries genes that synthesize the poly-γ-D glutamyl capsule. *B.anthracis* toxin is a member of the bacterial binary A-B toxin family where the B moiety acts as a transporter helping the A moiety to translocate into the cytosol. The A moiety exerts its deleterious effects after it enters the cytosol. In the case of *B.anthracis*, PA acts as a transporter protein and translocates EF and LF into the host cell (Mock and Fouet, 2001; Mourez et al., 2002).

Protective antigen (PA) is an 83 kDa protein that binds to specific receptors referred to as ANTXR1 (tumor endothelial marker 8) and ANTXR2 (Capillary morphogenesis protein 2), on host cells. Both ANTXR1 and ANTXR2 are widely expressed in cells and consist of regions similar to the von Willebrand factor type A domain and the Integrin I domain, thus binding to collagen and

collagen/laminin respectively. LRP6, a cell surface protein, can also act as a coreceptor. By interacting directly or indirectly with ANTXR1 and ANTXR2, LRP6 can stimulate PA binding to ANTXR1 and ANTXR2 (Bradley et al., 2001; Scobie et al., 2003; Liu and Leppla, 2003; Nanda et al., 2004; Wei et al., 2006).

After PA_{83} is bound to ANTXR1 or ANTXR2, it is cleaved by a member of the furin family of proteases. The N terminal region of PA_{83} is cleaved, releasing PA_{20} extracellularly, and PA_{63} is bound to the receptors (Klimpel et al., 1992). PA_{63} then self oligomerizes to form a ring-shaped heptamer referred to as prepore conformation. EF and LF bind competitively with high affinity to the PA_{63} heptameric prepore conformation. Several studies have shown that a maximum of three molecules of EF and/or LF can be accommodated by the PA_{63} heptamer. The recognition sites of the interaction of EF and LF with PA_{63} heptamer have been mapped and both EF and LF are positioned with their N termini at the entrance of the PA_{63} prepore and therefore can translocate in the N- to C terminal direction. The PA_{63} heptamer with bound LF and or EF then undergoes receptor-mediated endocytosis and is transferred into an intracellular acidic compartment. The low pH in the endosomal compartment results in structural rearrangements, giving rise to the PA_{63} pore conformation that can now insert itself in the endosomal membrane. The PA_{63} pore is typically a 14-strand transmembrane β barrel with a water-filled central cavity of about 15 Å in diameter (Gao-Sheridan et

al., 2003; Abrami et al., 2003; Lacy et al., 2002 and 2005). EPR (Electron Paramagnetic Resonance) studies have shown that seven F427 residues from the PA_{63} heptamer form a "Φ" (phi) clamp exposing their aromatic rings in the lumen. The Φ clamp causes partial unfolding and translocation of EF and LF through the pore coupled to a positive membrane potential across the membrane (Krantz et al., 2005).

Figure 1-9 Schematic representation of PA binding, assembly, endocytosis and translocation of EF and LF inside the cytosol.

PA_{83} binds to specific receptors on the membrane. Furin endoproteases present on the cell membrane cleave PA_{83}, releasing PA_{20} extracellularly, and PA_{63} bound to the receptor. PA_{63} self-oligomerizes to form a ring-shaped heptamer termed the prepore complex that can bind to EF and or LF. Prepore complex with bound EF and or LF is then endocytosed to an intracellular acidic compartment. The lower pH in the endosome triggers structural rearrangements causing a change in conformation from prepore to pore causing partial unfolding and translocation of EF and LF into the cytosol.

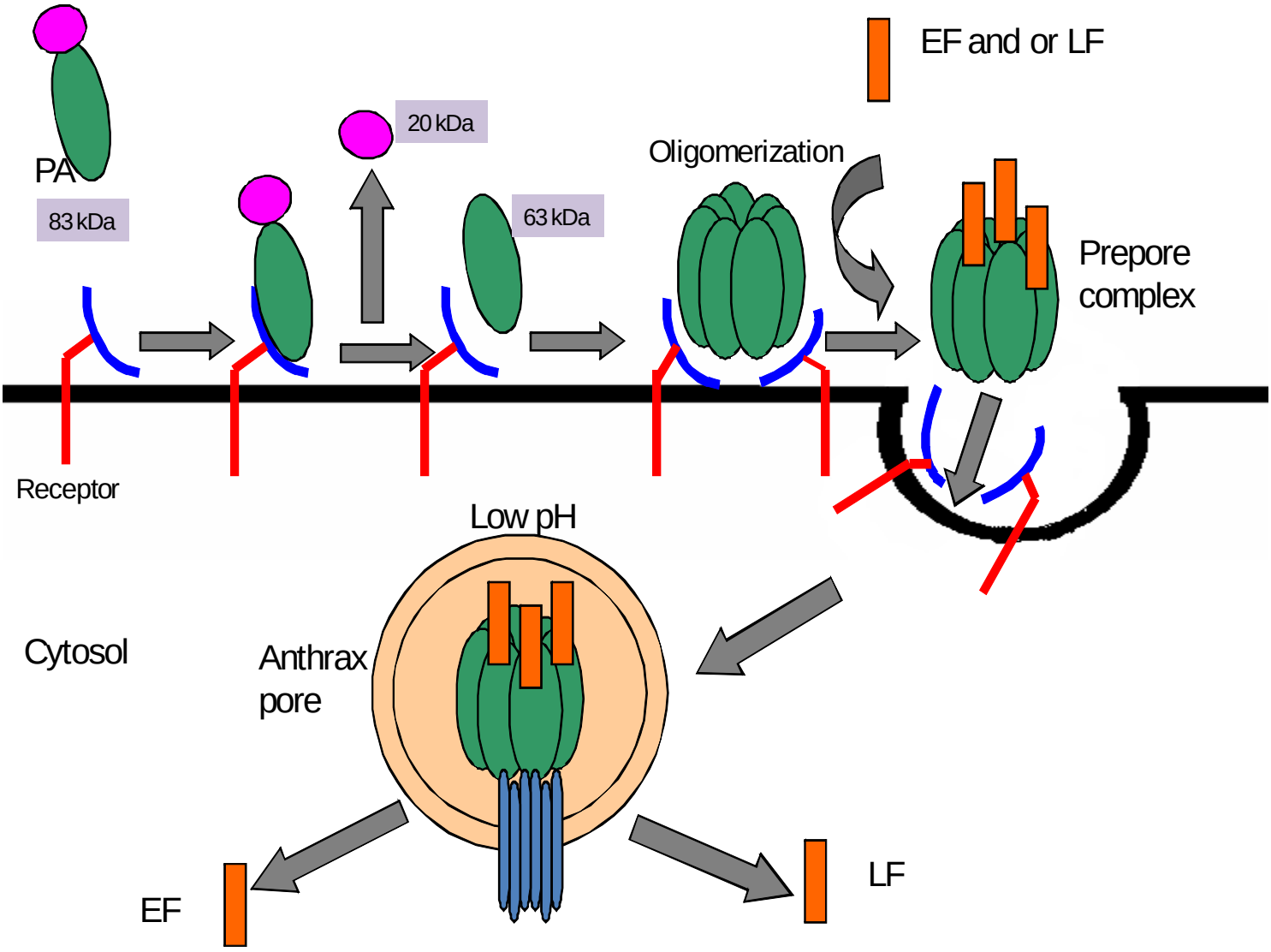
EF and or LF
PA
83 kDa
20 kDa
63 kDa
Oligomerization
Prepore
complex
Receptor
Low pH
Cytosol
Anthrax
pore
EF
LF

1.2.4 Anthrax toxin components and their function

Protective antigen (PA), an 83 kDa protein, is divided into four domains. Domain 1 has a recognition site for Furin-like family endoproteases and part of domain 1 is cleaved giving rise to PA_{20} that is released extracellularly and PA63 which can self oligomerize. Domain 2 undergoes pH-dependent conformational changes and helps in oligomerization, conversion from prepore to pore forms and translocation of EF and LF into the cytosol. Domain 2 from seven PA_{63} monomers forms the transmembrane β barrel and consists of the Φ clamp for unfolding and translocation of EF and LF. Furthermore, it has been shown that K397 from one PA domain 2 can form a salt bridge with D426 of the neighboring PA domain 2 thus giving rise to a loop bringing the F427 residues closer to form the Φ clamp. Mutational studies have shown that Domain 3 is also important for oligomerization of PA_{63}. Domain 4 consists of the receptor-binding domain and is important for the interaction of PA with its cellular receptors ANTXR1 and ANTXR2 (Petosa et al., 1997; Santelli et al., 2004; Mogridge et al., 2001; Young and Collier, 2007).

Lethal factor (LF) is a 90 kDa zinc-dependent metalloprotease that can cleave the proline rich N-terminal of mitogen–activated protein kinase (MAPK) kinases (Meks). LF can cleave and inactivate all Meks except Mek 2. Since Meks serve as important substrates for downstream signaling, proteolytic

inactivation of Meks by LF inhibits the MAP kinase signal transduction pathways that include p38, JNK and ERK. The crystal structure of LF with bound substrate and inhibitor has shown the presence of four domains. The N-terminal domain 1, or LF-N, is the protective antigen binding domain and has residues similar to EF-N. Domain 2 and Domain 3 serve as sites for substrate recognition. The C terminal domain 4 consists of the zinc metalloprotease site (Pannifer et al., 2001; Lacy et al., 2002; Tonello et al., 2003). Though several studies have shown that EF and LF can bind only to PA_{63} heptamers, recent evidence suggests that LF and LF-N (N-terminal region of LF) can bind to PA_{63} monomer, albeit with lower affinity. It has also been shown that PA_{20} interacts with LF-N, though a functional role for this interaction has not been determined (Lacy et al., 2005; Chvyrkova et al., 2007). It has also been demonstrated that low concentrations of LF bind to PA_{63} and higher concentrations inhibit PA_{63} assembly (Christiansen et al., 2006).

Edema Factor (EF) is a 93 kDa calmodulin (CaM) activated adenylyl cyclase that can convert ATP to cAMP (Leppla, 1982). Increased cAMP levels can cause several changes by activating downstream targets such as PKA, in turn disrupting intracellular signaling pathways. EF is thought to be primarily responsible for the cutaneous form of anthrax (Leppla, 1982; Dixon et al., 1999). A detailed analysis of the structure and intracellular activation of EF is dicussed in the following sections.

ET (EF with PA) and LT (LF with PA) can together or separately impair host defenses by promoting bacterial invasion (Firoved et al., 2007). Both ET and LT suppress innate immune responses and impair human neutrophil activity (Kammer et al., 1988; Kyriakis et al., 2001). ET and LT inhibit the generation of superoxides and reactive oxygen species (ROS) by NADPH oxidase activity of human neutrophils needed to cause bacterial killing (Crawford et al., 2006). ET increased cAMP levels of lymphocytes can cause changes in important gene expression resulting in suppression of the immune response. ET can also inhibit chemotaxis in endothelial cells by activating downstream effectors such as Epac and RAP1 (Hong et al., 2007). Also, the PA binding domain of EF is not essential for potency of ET (Hong et al., 2005). Furthermore, ET can inhibit platelet aggregation and cause hemorrhage, an important symptom of anthrax (Alam et al., 2006). It has also been demonstrated that EF and LF are capable of inducing hemolysis (lysis of blood cells) in the presence of neutrophils (Wu et al., 2003).

1.2.5 Edema Factor – structure and intracellular activation

Edema factor can be considered to have two domains, a 30 kDa N-terminal protective antigen binding domain and a 63 kDa CaM sensitive adenylyl cyclase domain or EF3 (Drum et al., 2000; Bhatnagar et al, 2001). The protective antigen binding domain is homologous to the N terminal region of

LF (Collier and Young, 2003). EF3 can be further divided into N terminal EF3 (EF3-N) and a C terminal EF3 (EF3-C). EF3-N is homologous to AC exotoxins from *Bordetella pertussis* and *Pseudomonas aeuroginosa.* It is resistant to protease digestion. EF3-C is sensitive to protease digestion in the absence of CaM (Drum et al., 2000).

After PA-mediated entry of EF into the cells, EF binds to calmodulin (CaM). CaM is a 16.5 kDa protein, ubiquitously expressed in cells. CaM binds and modulates activities in a large number of targets that include enzymes, pumps and ion channels in a calcium-dependent manner, thus playing an important role in several intracellular processes such as signal transduction and gene transcription (Deisseroth et al., 1998; Demaria et al., 2001).

X-ray and NMR studies have shown that CaM exists as a flexible dumbbell-shaped structure with two globular end domains each consisting of two calcium binding motifs. CaM adopts a closed conformation in the absence of calcium and changes to an open conformation exposing a large hydrophobic binding site in the presence of calcium (Babu et al., 1985; Zhang et al., 1995).

The crystal structure of EF with and without CaM and inhibitor, solved by Drum et al (2001), showed that the C terminus of EF consists of three domains, C_A, C_B and a helical domain. A linker region connects C_A to the helical domain and C_A and C_B together form the catalytic core of the enzyme. CaM binding causes large conformational changes in the structure of EF.

CaM is almost completely wrapped by a clamp formed by C_A, linker and the helical domain in such a manner that it causes a 30˚ rotation and a 15Å movement of the helical domain. In addition, three regions, switch A, B and C in EF also undergo large conformational changes due to CaM binding. Switch A (residues 502-551) consists of amino acid residues important for CaM- and nucleotide binding. Switch B (residues 578-591) contains residues important for ATP binding and catalysis. Switch C (residues 630-659) consists of residues from the linker region and swings almost 33Å when CaM binds to EF. The EF-CaM interaction is stabilized and strengthened by a large number of both hydrophobic and hydrophilic contacts. FRET (Fluorescence resonance energy transfer) experiments have also shown that CaM binds to EF in an extended conformation unlike its binding to a number of other proteins (Drum et al., 2000; Ulmer et al., 2003).

Figure 1-10 Schematic illustration of primary structure of EF

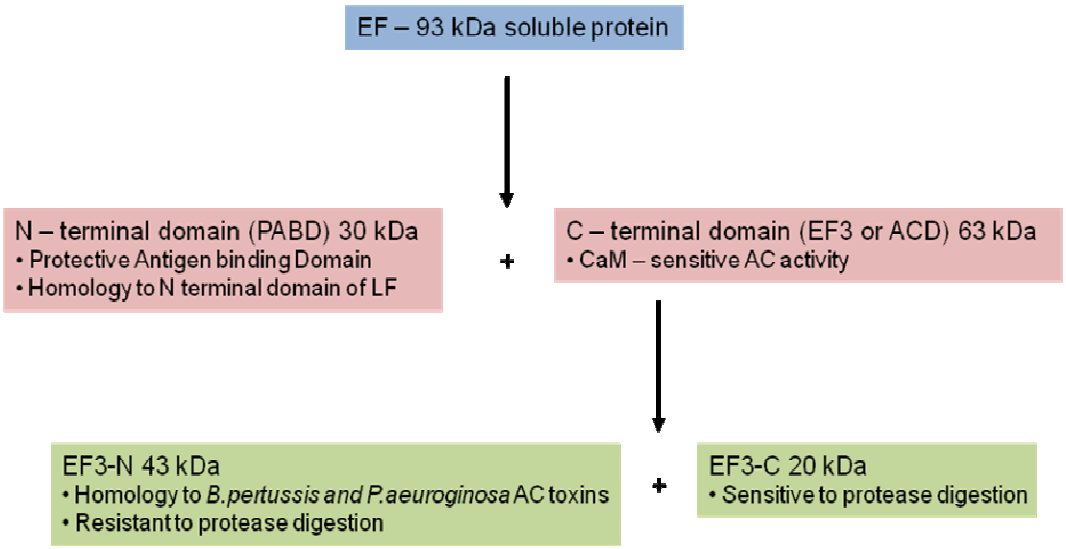

Figure 1-11 Crystal structure of EF (a) EF alone (b) EF with bound CaM and 3'dATP (Drum et al 2002)

C_A and C_B domains of EF are shown in green and the helical domain is shown in yellow. Switch A, B and C regions are shown in blue, orange and magenta respectively. CaM is shown in red and metal ions and 3'dATP are shown in purple. CaM is wrapped by the helical domain and the switch A, C and C_A regions. The C_A and C_B domains form the catalytic core of EF (Drum et al., 2002).

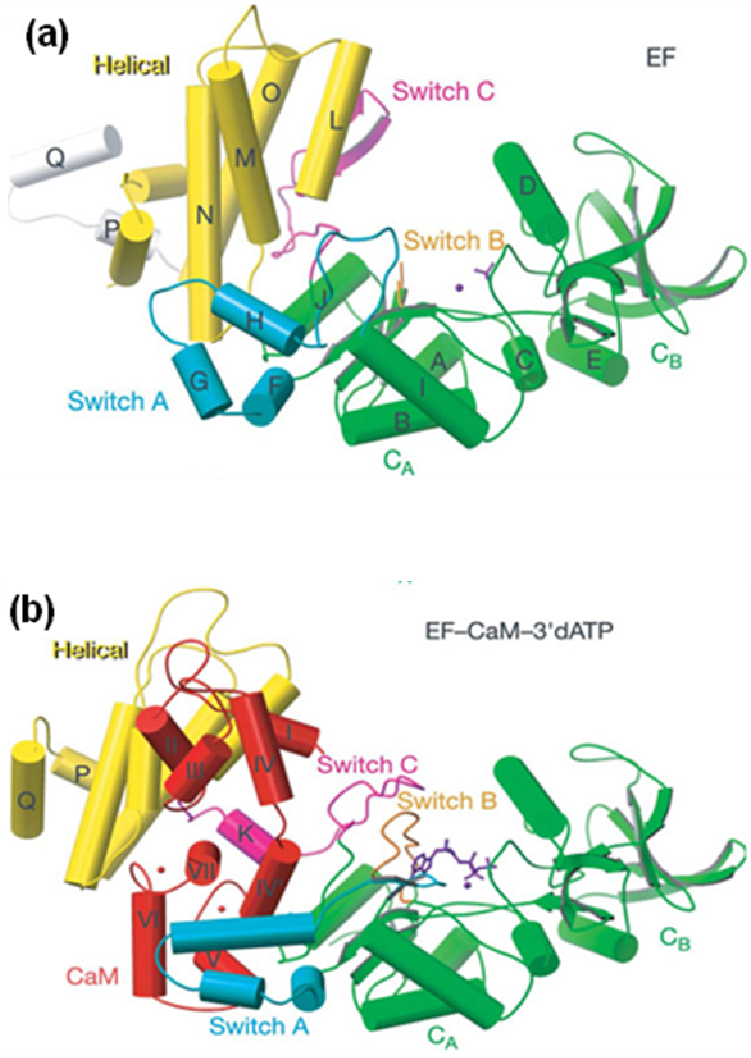

1.2.6 Catalytic mechanism of EF

Following activation of EF by CaM, EF catalyzes conversion of ATP to cAMP. Several crystal structures of EF with bound CaM and nucleotide/inhibitor have been solved that greatly helped to improve our understanding of the ATP binding and catalysis processes. The first crystal structure of EF with bound CaM and 3' d ATP published by Drum et al (2002) indicates a single metal ion-mediated catalytic mechanism unlike the mammalian ACs where two-metal-ion-catalysis is observed. Drum et al (2002) observed that the single metal ion is coordinated by a pair of aspartate residues (D491 and D493) and interacts with the oxygens of the α and β phosphates of the substrate analog 3'dATP. Furthermore, H351 serves as a catalytic base and is thought to interact with the 3'-OH of the substrate to promote nucleophilic attack (Drum et al., 2002). In support of this hypothesis, Gupta et al (2005) have shown in their kinetic studies that when H351 was mutated to alanine, aspargine or phenyl alanine, AC activity was reduced several fold, indicating the importance of H351 in catalysis by EF (Gupta et al., 2005).

Shen et al (2005) refined the first model and found that EF contains two metal ions similar to mammalian ACs and DNA polymerases. Metal ion A is coordinated by the conserved aspartate residues and H577. Metal ion B is coordinated by D493 and the non-bridging oxygens of all three phosphates of

ATP. Furthermore, it was shown that H351 may not act as a catalytic base because it was at least 6Å away from the 3'-OH of the substrate making it unlikely to be able to accept a proton from the 3'-OH during the cyclization reaction. Site directed mutagenesis studies have shown that when H351 was mutated to lysine, there was no change in AC activity or the pH optimum, further confirming that H351 is not the catalytic base but may act to stabilize the 3'-OH group. Nonetheless, both crystal structures have indicated several amino acid residues that are important for interaction of EF with substrate ATP. R329, K346, S354 and K372 interact with the phosphates of 3'dATP and are important for stabilization of the reaction intermediate and the release of the PP_i. The side chain of N583 hydrogen bonds with the ribose ring and holds the 3'-OH group in place for nucleophilic attack.

Shen et al (2004) have also demonstrated an alternate binding mode of ATP to the catalytic core of EF. They showed that AMPCPP (adenosine 5'-(α, β-methylene)-triphosphate) binds to EF differently compared to 3'dATP and 2'd3' ANT-ATP. The ribose ring of AMPCPP is rotated 105° and the adenine ring is rotated by 180° in the catalytic site of EF.

Figure 1-12 Catalytic mechanism of EF

(a) A ball and stick model of the EF active site. EF shown in green, side chains of important residues in blue and ligand in black (Drum et al., 2002);

(b) Proposed catalytic mechanism of EF. Single metal ion-mediated catalysis is shown. H351 is indicated as the catalytic base (Drum et al 2002); (c) Simulated model based on the EF-CaM-3'dATP catalytic site. EF is in green, ligand in black and Mg ions are shown in orange (Shen et al., 2005); (d) Proposed two metal ion catalytic mechanism of EF (Shen et al., 2005).

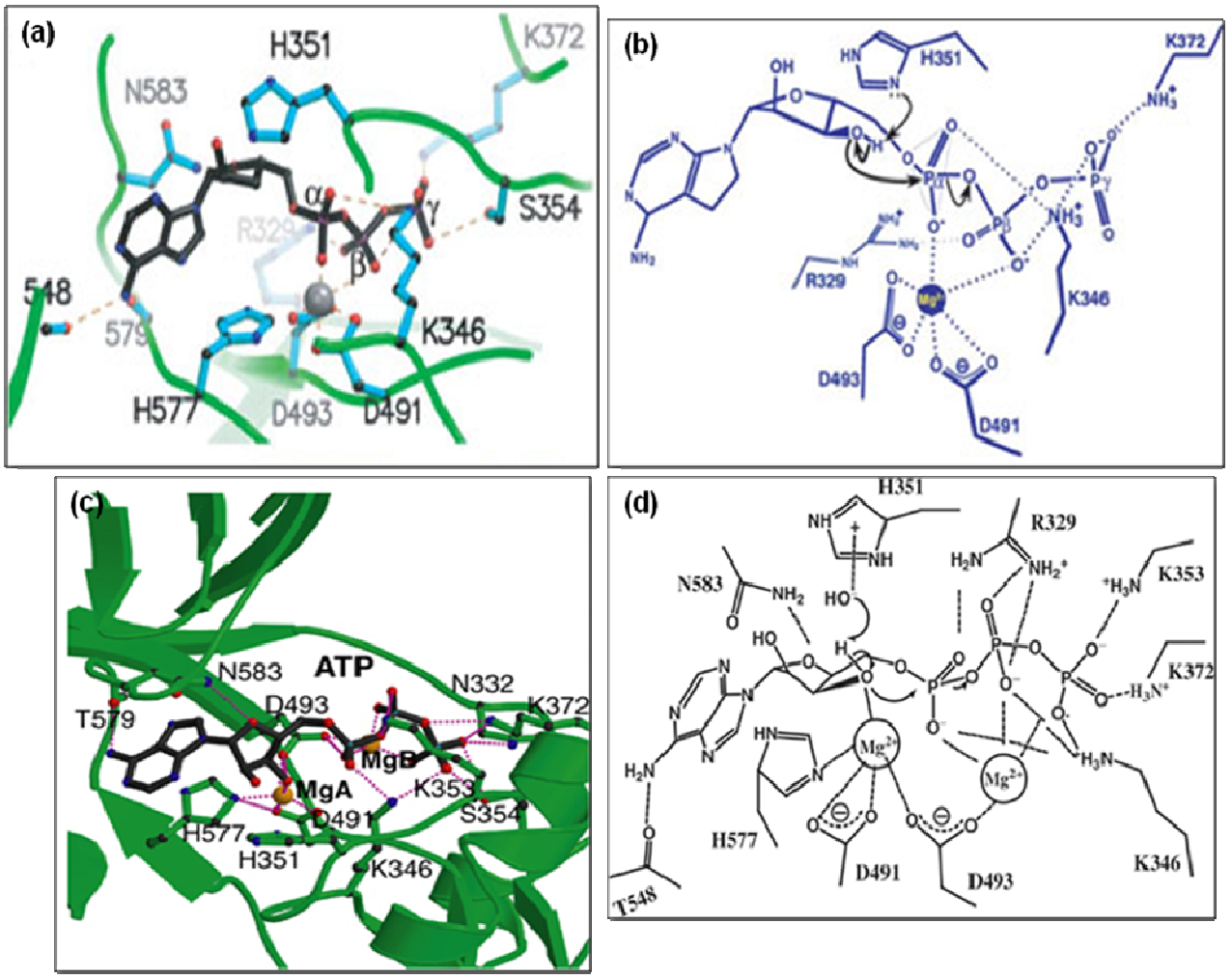
(a)
H351
K372
N583
S354
R329
α
γ
β
548
579
K346
H577
D493
D491
(b)
OH
HN
H351
K372
R329
K346
D493
D491
(c)
N583
ATP
N332
T579
D493
K372
MgB
MgA
K353
D491
S354
H577
H351
K346
(d)
H351
R329
N583
K353
K372
HO
H
HN
H577
D491
D493
K346
T548

1.2.7 Challenges, limitations and future directions of anthrax research with special focus on EF

With a better understanding of the detrimental effects of anthrax, it will become possible to develop highly specific control measures to prevent and treat anthrax infections. The efficacy of the AVA vaccine currently used is a cause for major concern since adverse side effects have been reported in some cases. Another disadvantage of AVA vaccine is that it is available only for military personnel. Antibiotic treatment is effective only against the cutaneous forms of anthrax. Therefore, there is a need for better vaccinations, drugs and other therapeutics to prevent anthrax infection not only in military personnel but also in humans and animals that are at a higher risk of contracting the infection.

With recent evidence that LF binds to monomeric PA, the question arises as to whether monomeric PA could translocate LF and EF into the cytosol? To this end, it has been shown that LF binds to monomeric PA with low affinity and would probably require PA oligomer/heptmer for its translocation. Another important challenge faced by researchers is the lack of crystal structure of PA heptamer since it is a transmembrane protein. Solving the crystal structure of the PA heptamer would substantially improve our understanding of the PA prepore formation, binding of LF and EF, and help develop PA-based inhibitors. With the current model of the PA heptamer, it is

known that the Φ clamp formed by the PA heptamer facilitates the translocation of EF and LF, however, it is not clear how these proteins unfold and refold in the cytosol.

With the solution of crystal structures of both LF and EF we have gained considerable insight into the catalytic mechanisms of these toxins. What remains to be determined is how EF and LF carry out a synergistic action to impair the immune system and whether or not they must interact with other proteins as part of this process.

Using various approaches to study the anthrax toxins, several steps in the intoxication mechanism can be blocked and studied for future rational drug design. For example, the binding sites of EF on PA have been mapped, so it would be interesting to study inhibitors that would block EF-PA interaction, thus preventing entry of EF into the cytosol. Once inside the cell, inhibitors can be developed to block two important processes of EF. One is CaM-dependent activation of EF, the second is the catalytic activity of EF. The crystal structure of EF-CaM shows that EF makes extensive contacts with CaM and CaM changes the conformation of EF from a closed to an open conformation, thus exposing the substrate binding site. An important challenge here is to understand the specificity of this interaction, since CaM is a ubiquitously expressed protein that binds to several other protein targets. Although several small molecules have been designed to block the catalytic

activity of EF both *in vitro* and *in vivo*, there is a critical need for more potent and cell-permeable inhibitors (Chen et al., 2008; Pini et al., 2006).

In summary, early detection, appropriate timely treatment and improved vaccines combined with a better understanding of the molecular basis of the biological action of anthrax toxins are critical for control and prevention of anthrax.

1.3 Research presented in this thesis

This thesis is comprised of two independent yet interconnected projects aimed at improving our overall understanding of the regulation of mammalian adenylyl cyclases and bacterial adenylyl cyclase toxins. The specific aims are:

- Monitor binding and conformational changes in mACs and EF using fluorescent nucleotides as probes;
- Characterize different AC isoforms using fluorescent nucleotides and identify potent isoform-specific mAC inhibitors;
- Characterize individual catalytic subunits, C1 and C2, of mACs using biochemical and biophysical approaches;

- Studying EF-Calmodulin interaction and identify potent EF inhibitors for rational drug design.

Chapter 2 describes the interaction of fluorescent nucleotides with purified C1/C2 subunits as well as with the holo AC isoforms. Earlier studies in our lab have shown that MANT and TNP-nucleotides are potent inhibitors of C1/C2 and bind in a similar but non-identical way to the catalytic site formed by C1 and C2. A detailed analysis of MANT nucleotide binding to C1/C2 has been carried out. However it is not known if TNP nucleotides inhibit holo AC isoforms, and if so, are they isoform specific? The studies focus on interaction of TNP purine and pyrimidine nucleotides with both C1/C2 and holo AC isoforms and on the specificity of TNP nucleotides for ACs and G-proteins.

Recent evidence suggests that AC dimerization occurs via transmembrane domains and that the cytoplasmic domains are essential for catalytic activity. The cytoplasmic domains C1 and C2 can heterodimerize to form the catalytic core of the enzyme. However it is not clear if C1 and C2 can homodimerize and if they did then how does this dimerization affect the catalytic activity and regulation of mACs? The studies described in Chapter 3 are aimed at studying the individual catalytic subunits C1 and C2 of mACs using a variety of techniques and addresses the possibility of homodimerization of the C1 and C2 subunits and a potential role of this dimerization in regulation of mACs.

The primary goal of studies described in Chapter 4 is to study, in detail, the inhibitory effects of several MANT nucleotide analogs on EF/CaM. These studies also focus on understanding the mechanism of interaction between EF and CaM using MANT nucleotides and the effects of modulating this interaction. The importance of calcium binding to CaM and the effect of partial oxidation of CaM on EF function has been examined.

Future perspectives of Chapters 2-4 are discussed in Chapter 5. Preparation of manuscripts for the research presented in Chapters 2-4 are in progress.

References

Abdel-Majid RM, Leong WL, Schalkwyk LC, Smallman DS, Wong ST, Storm DR, Fine A, Dobson MJ, Guernsey DL and Neumann PE (1998) Loss of adenylyl cyclase I activity disrupts patterning of mouse somatosensory cortex. *Nat Genet* **19**(3):289-291.

Abdel-Majid RM, Tremblay F and Baldridge WH (2002) Localization of adenylyl cyclase proteins in the rodent retina. *Brain Res* **101**(1-2):62-70.

Abrami L, Liu S, Cosson P, Leppla SH and van der Goot FG (2003) Anthrax toxin triggers endocytosis of its receptor via a lipid raft-mediated clathrin-dependent process. *J Cell Biol* **160**(3):321-328.

Ahlijanian MK and Cooper DM (1987) Antagonism of calmodulin-stimulated adenylate cyclase by trifluoperazine, calmidazolium and W-7 in rat cerebellar membranes. *J Pharmacol Exp Ther* **241**(2):407-414.

Alam S, Gupta M and Bhatnagar R (2006) Inhibition of platelet aggregation by anthrax edema toxin. *Biochem Biophys Res Commun* **339**(1):107-114.

Antoni FA, Palkovits M, Simpson J, Smith SM, Leitch AL, Rosie R, Fink G and Paterson JM (1998) Ca^{2+}/calcineurin-inhibited adenylyl cyclase, highly

abundant in forebrain regions, is important for learning and memory. *J Neurosci* **18**(23):9650-9661.

Ascenzi P, Visca P, Ippolito G, Spallarossa A, Bolognesi M and Montecucco C (2002) Anthrax toxin: a tripartite lethal combination. *FEBS Lett* **531**(3):384-388.

Babu YS, Sack JS, Greenhough TJ, Bugg CE, Means AR and Cook WJ (1985) Three-dimensional structure of calmodulin. *Nature* **315**(6014):37-40.

Bakalyar HA and Reed RR (1990) Identification of a specialized adenylyl cyclase that may mediate odorant detection. *Science (New York, NY* **250**(4986):1403-1406.

Beeler JA, Yan SZ, Bykov S, Murza A, Asher S and Tang WJ (2004) A soluble C1b protein and its regulation of soluble type 7 adenylyl cyclase. *Biochemistry* **43**(49):15463-15471.

Bhatnagar R and Batra S (2001) Anthrax toxin. *Crit Rev Microbiol* **27**(3):167-200.

Borjigin J, Wang MM and Snyder SH (1995) Diurnal variation in mRNA encoding serotonin N-acetyltransferase in pineal gland. *Nature* **378**(6559):783-785.

Bradley KA, Mogridge J, Mourez M, Collier RJ and Young JA (2001) Identification of the cellular receptor for anthrax toxin. *Nature* **414**(6860):225-229.

Braun T (1991) Purification of soluble form of adenylyl cyclase from testes. *Methods Enzymol* **195**:130-136.

Brey RN (2005) Molecular basis for improved anthrax vaccines. *Adv Drug Deliv Rev* **57**(9):1266-1292.

Buck J, Sinclair ML, Schapal L, Cann MJ and Levin LR (1999) Cytosolic adenylyl cyclase defines a unique signaling molecule in mammals. *Proc Natl Acad Sci U S A* **96**(1):79-84.

Cali JJ, Zwaagstra JC, Mons N, Cooper DM and Krupinski J (1994) Type VIII adenylyl cyclase. A Ca^{2+}/calmodulin-stimulated enzyme expressed in discrete regions of rat brain. *J Biol Chem* **269**(16):12190-12195.

Chan GC, Lernmark U, Xia Z and Storm DR (2001) DNA elements of the type 1 adenylyl cyclase gene locus enhance reporter gene expression in neurons and pinealocytes. *Eur J Neurosci* **13**(11):2054-2066.

Chen D, Misra M, Sower L, Peterson JW, Kellogg GE and Schein CH (2008) Novel inhibitors of anthrax edema factor. *Bioorg Med Chem* **16**(15):7225-7233.

Choi EJ, Xia Z and Storm DR (1992) Stimulation of the type III olfactory adenylyl cyclase by calcium and calmodulin. *Biochemistry* **31**(28):6492-6498.

Chou JL, Huang CL, Lai HL, Hung AC, Chien CL, Kao YY and Chern Y (2004) Regulation of type VI adenylyl cyclase by Snapin, a SNAP25-binding protein. *J Biol Chem* **279**(44):46271-46279.

Christensen KA, Krantz BA and Collier RJ (2006) Assembly and disassembly kinetics of anthrax toxin complexes. *Biochemistry* **45**(7):2380-2386.

Chvyrkova I, Zhang XC and Terzyan S (2007) Lethal factor of anthrax toxin binds monomeric form of protective antigen. *Biochem Biophys Res Commun* **360**(3):690-695.

Collier RJ and Young JA (2003) Anthrax toxin. *Annu Rev Cell Dev Biol* **19**:45-70.

Cooper DM and Crossthwaite AJ (2006) Higher-order organization and regulation of adenylyl cyclases. *Trends Pharmacol Sci* **27**(8):426-431.

Cooper DM, Karpen JW, Fagan KA and Mons NE (1998) Ca^{2+}-sensitive adenylyl cyclases. *Adv Second Messenger Phosphoprotein Res* **32**:23-51.

Cooper DM, Mons N and Karpen JW (1995) Adenylyl cyclases and the interaction between calcium and cAMP signalling. *Nature* **374**(6521):421-424.

Crawford MA, Aylott CV, Bourdeau RW and Bokoch GM (2006) *Bacillus anthracis* toxins inhibit human neutrophil NADPH oxidase activity. *J Immunol* **176**(12):7557-7565.

Cumbay MG and Watts VJ (2004) Novel regulatory properties of human type 9 adenylate cyclase. *J Pharmacol Exp Ther* **310**(1):108-115.

D'Angelo DD, Sakata Y, Lorenz JN, Boivin GP, Walsh RA, Liggett SB and Dorn GW, 2nd (1997) Transgenic $G\alpha_q$ overexpression induces cardiac contractile failure in mice. *Proc Natl Acad Sci U S A* **94**(15):8121-8126.

Defer N, Best-Belpomme M and Hanoune J (2000) Tissue specificity and physiological relevance of various isoforms of adenylyl cyclase. *Am J Physiol Renal Physiol* **279**(3):F400-416.

Deisseroth K, Heist EK and Tsien RW (1998) Translocation of calmodulin to the nucleus supports CREB phosphorylation in hippocampal neurons. *Nature* **392**(6672):198-202.

Dessauer CW and Gilman AG (1996) Purification and characterization of a soluble form of mammalian adenylyl cyclase. *J Biol Chem* **271**(28):16967-16974.

Dixon TC, Meselson M, Guillemin J and Hanna PC (1999) Anthrax. *N Engl J Med* **341**(11):815-826.

Drum CL, Yan SZ, Bard J, Shen YQ, Lu D, Soelaiman S, Grabarek Z, Bohm A and Tang WJ (2002) Structural basis for the activation of anthrax adenylyl cyclase exotoxin by calmodulin. *Nature* **415**(6870):396-402.

Drum CL, Yan SZ, Sarac R, Mabuchi Y, Beckingham K, Bohm A, Grabarek Z and Tang WJ (2000) An extended conformation of calmodulin induces interactions between the structural domains of adenylyl cyclase from *Bacillus anthracis* to promote catalysis. *J Biol Chem* **275**(46):36334-36340.

Ebina T, Kawabe J, Katada T, Ohno S, Homcy CJ and Ishikawa Y (1997) Conformation-dependent activation of type II adenylyl cyclase by protein kinase C. *J Cell Biochem* **64**(3):492-498.

Esposito G, Perrino C, Ozaki T, Takaoka H, Defer N, Petretta MP, De Angelis MC, Mao L, Hanoune J, Rockman HA and Chiariello M (2008) Increased myocardial contractility and enhanced exercise function in transgenic mice overexpressing either adenylyl cyclase 5 or 8. *Basic Res Cardiol* **103**(1):22-30.

Fagan KA, Graf RA, Tolman S, Schaack J and Cooper DM (2000) Regulation of a Ca^{2+}-sensitive adenylyl cyclase in an excitable cell. Role of voltage-gated versus capacitative Ca^{2+}entry. *J Biol Chem* **275**(51):40187-40194.

Firoved AM, Moayeri M, Wiggins JF, Shen Y, Tang WJ and Leppla SH (2007) Anthrax edema toxin sensitizes DBA/2J mice to lethal toxin. *Infect Immun* **75**(5):2120-2125.

Furuyama T, Inagaki S and Takagi H (1993) Distribution of type II adenylyl cyclase mRNA in the rat brain. *Brain Res* **19**(1-2):165-170.

Gao BN and Gilman AG (1991) Cloning and expression of a widely distributed (type IV) adenylyl cyclase. *Proc Natl Acad Sci U S A* **88**(22):10178-10182.

Gao MH, Bayat H, Roth DM, Yao Zhou J, Drumm J, Burhan J and Hammond HK (2002) Controlled expression of cardiac-directed adenylyl cyclase type VI provides increased contractile function. *Cardiovasc Res* **56**(2):197-204.

Gao X and Patel TB (2005) Histidine residues 912 and 913 in protein associated with Myc are necessary for the inhibition of adenylyl cyclase activity. *Mol Pharmacol* **67**(1):42-49.

Gao-Sheridan S, Zhang S and Collier RJ (2003) Exchange characteristics of calcium ions bound to anthrax protective antigen. *Biochem Biophys Res Commun* **300**(1):61-64.

Gille A and Seifert R (2003) 2'(3')-*O*-(*N*-methylanthraniloyl)-substituted GTP analogs: a novel class of potent competitive adenylyl cyclase inhibitors. *J Biol Chem* **278**(15):12672-12679.

Gilman AG (1987) G proteins: transducers of receptor-generated signals. *Annu Rev Biochem***56**:615-649.

Gorodinsky A and Harris DA (1995) Glycolipid-anchored proteins in neuroblastoma cells form detergent-resistant complexes without caveolin. *J Cell Biol* **129**(3):619-627.

Gu C, Cali JJ and Cooper DM (2002) Dimerization of mammalian adenylate cyclases. *Eur J Biochem / FEBS* **269**(2):413-421.

Guenifi A, Portela-Gomes GM, Grimelius L, Efendic S and Abdel-Halim SM (2000) Adenylyl cyclase isoform expression in non-diabetic and diabetic Goto-Kakizaki (GK) rat pancreas. Evidence for distinct overexpression of type-8 adenylyl cyclase in diabetic GK rat islets. *Histochem Cell Biol* **113**(2):81-89.

Guillou JL, Nakata H and Cooper DM (1999) Inhibition by calcium of mammalian adenylyl cyclases. *J Biol Chem* **274**(50):35539-35545.

Gupta M, Alam S and Bhatnagar R (2006) Kinetic characterization and ligand binding studies of His351 mutants of *Bacillus anthracis* adenylate cyclase. *Arch Biochem Biophys* **446**(1):28-34.

Hacker BM, Tomlinson JE, Wayman GA, Sultana R, Chan G, Villacres E, Disteche C and Storm DR (1998) Cloning, chromosomal mapping, and regulatory properties of the human type 9 adenylyl cyclase (ADCY9).

Genomics **50**(1):97-104.

Hanoune J and Defer N (2001) Regulation and role of adenylyl cyclase isoforms. *Annu Rev Pharmacol Toxicol* **41**:145-174.

Hines LM, Hoffman PL, Bhave S, Saba L, Kaiser A, Snell L, Goncharov I, LeGault L, Dongier M, Grant B, Pronko S, Martinez L, Yoshimura M and Tabakoff B (2006) A sex-specific role of type VII adenylyl cyclase in depression. *J Neurosci* **26**(48):12609-12619.

Hong J, Beeler J, Zhukovskaya NL, He W, Tang WJ and Rosner MR (2005) Anthrax edema factor potency depends on mode of cell entry. *Biochem Biophys Res Commun* **335**(3):850-857.

Hong J, Doebele RC, Lingen MW, Quilliam LA, Tang WJ and Rosner MR (2007) Anthrax edema toxin inhibits endothelial cell chemotaxis via Epac and Rap1. *J Biol Chem* **282**(27):19781-19787.

Huang C, Hepler JR, Chen LT, Gilman AG, Anderson RG and Mumby SM (1997) Organization of G proteins and adenylyl cyclase at the plasma membrane. *Mol Biol Cell* **8**(12):2365-2378.

Hurley JH (1998) The adenylyl and guanylyl cyclase superfamily. *Curr Opin Struct Biol* **8**(6):770-777.

Ishikawa Y, Grant BS, Okumura S, Schwencke C and Yamamoto M (2000) Immunodetection of adenylyl cyclase protein in tissues. *Mol Cell Endocrinol* **162**(1-2):107-112.

Iwami G, Kawabe J, Ebina T, Cannon PJ, Homcy CJ and Ishikawa Y (1995) Regulation of adenylyl cyclase by protein kinase A. *J Biol Chem* **270**(21):12481-12484.

Jaleel M, Shenoy AR and Visweswariah SS (2004) Tyrphostins are inhibitors of guanylyl and adenylyl cyclases. *Biochemistry* **43**(25):8247-8255.

Johnson RA, Yeung SM, Stubner D, Bushfield M and Shoshani I (1989) Cation and structural requirements for P site-mediated inhibition of adenylate cyclase. *Mol Pharmacol* **35**(5):681-688.

Jourdan KB, Mason NA, Long L, Philips PG, Wilkins MR and Morrell NW (2001) Characterization of adenylyl cyclase isoforms in rat peripheral pulmonary arteries. *Am J Physiol Lung Cell Mol Physiol* **280**(6):L1359-1369.

Kammer GM (1988) The adenylate cyclase-cAMP-protein kinase A pathway and regulation of the immune response. *Immunol Today* **9**(7-8):222-229.

Keim P, Smith KL, Keys C, Takahashi H, Kurata T and Kaufmann A (2001) Molecular investigation of the Aum Shinrikyo anthrax release in Kameido, Japan. *J Clin Microbiol* **39**(12):4566-4567.

Kim KS, Kim J, Back SK, Im JY, Na HS and Han PL (2007) Markedly attenuated acute and chronic pain responses in mice lacking adenylyl cyclase-5. *Genes Brain Behav* **6**(2):120-127.

Klimpel KR, Molloy SS, Thomas G and Leppla SH (1992) Anthrax toxin protective antigen is activated by a cell surface protease with the sequence specificity and catalytic properties of furin. *Proc Natl Acad Sci U S A* **89**(21):10277-10281.

Kozasa T and Gilman AG (1995) Purification of recombinant G proteins from Sf9 cells by hexahistidine tagging of associated subunits. Characterization of α12 and inhibition of adenylyl cyclase by α z. *J Biol Chem* **270**(4):1734-1741.

Krantz BA, Melnyk RA, Zhang S, Juris SJ, Lacy DB, Wu Z, Finkelstein A and Collier RJ (2005) A phenylalanine clamp catalyzes protein translocation through the anthrax toxin pore. *Science* **309**(5735):777-781.

Krishnan V, Graham A, Mazei-Robison MS, Lagace DC, Kim KS, Birnbaum S, Eisch AJ, Han PL, Storm DR, Zachariou V and Nestler EJ (2008) Calcium-sensitive adenylyl cyclases in depression and anxiety: behavioral and biochemical consequences of isoform targeting. *Biol Psychiatry* **64**(4):336-343.

Krupinski J, Coussen F, Bakalyar HA, Tang WJ, Feinstein PG, Orth K, Slaughter C, Reed RR and Gilman AG (1989) Adenylyl cyclase amino acid sequence: possible channel- or transporter-like structure. *Science* **244**(4912):1558-1564.

Kyriakis JM and Avruch J (2001) Mammalian mitogen-activated protein kinase signal transduction pathways activated by stress and inflammation. *Physiol Rev* **81**(2):807-869.

Lacy DB, Lin HC, Melnyk RA, Schueler-Furman O, Reither L, Cunningham K, Baker D and Collier RJ (2005) A model of anthrax toxin lethal factor bound to protective antigen. *Proc Natl Acad Sci U S A* **102**(45):16409-16414.

Lacy DB, Mourez M, Fouassier A and Collier RJ (2002) Mapping the anthrax

protective antigen binding site on the lethal and edema factors. *J Biol Chem* **277**(4):3006-3010.

Lai HL, Yang TH, Messing RO, Ching YH, Lin SC and Chern Y (1997) Protein kinase C inhibits adenylyl cyclase type VI activity during desensitization of the A2α-adenosine receptor-mediated cAMP response. *J Biol Chem* **272**(8):4970-4977.

Leppla SH (1982) Anthrax toxin edema factor: a bacterial adenylate cyclase that increases cyclic AMP concentrations of eukaryotic cells. *Proc Natl Acad Sci USA* **79**(10):3162-3166.

Lev-Ram V, Wong ST, Storm DR and Tsien RY (2002) A new form of cerebellar long-term potentiation is postsynaptic and depends on nitric oxide but not cAMP. *Proc Natl Acad Sci U S A* **99**(12):8389-8393.

Liu S and Leppla SH (2003) Cell surface tumor endothelium marker 8 cytoplasmic tail-independent anthrax toxin binding, proteolytic processing, oligomer formation, and internalization. *J Biol Chem* **278**(7):5227-5234.

Lustig KD, Conklin BR, Herzmark P, Taussig R and Bourne HR (1993) Type II adenylylcyclase integrates coincident signals from G_s, G_i, and G_q. *J Biol Chem* **268**(19):13900-13905.

Manchee RJ, Broster MG, Henstridge RM, Stagg AJ and Melling J (1982) Anthrax island. *Nature* **296**(5858):598.

Marquez B and Suarez SS (2008) Soluble adenylyl cyclase is required for activation of sperm but does not have a direct effect on hyperactivation. *Reprod Fertil Dev* **20**(2):247-252.

McVey M, Hill J, Howlett A and Klein C (1999) Adenylyl cyclase, a coincidence detector for nitric oxide. *J Biol Chem* **274**(27):18887-18892.

Meselson M, Guillemin J, Hugh-Jones M, Langmuir A, Popova I, Shelokov A and Yampolskaya O (1994) The Sverdlovsk anthrax outbreak of 1979. *Science* **266**(5188):1202-1208.

Mock M and Fouet A (2001) Anthrax. *Annu Rev Microbiol* **55**:647-671.

Mogridge J, Mourez M and Collier RJ (2001) Involvement of domain 3 in oligomerization by the protective antigen moiety of anthrax toxin. *J Bacteriol* **183**(6):2111-2116.

Mou TC, Gille A, Fancy DA, Seifert R and Sprang SR (2005) Structural basis for the inhibition of mammalian membrane adenylyl cyclase by 2 '(3')-*O*-(*N*-Methylanthraniloyl)-guanosine 5 '-triphosphate. *J Biol Chem* **280**(8):7253-7261.

Mou TC, Gille A, Suryanarayana S, Richter M, Seifert R and Sprang SR (2006) Broad specificity of mammalian adenylyl cyclase for interaction with 2',3'-substituted purine- and pyrimidine nucleotide inhibitors. *Mol Pharmacol* **70**(3):878-886.

Mourez M, Lacy DB, Cunningham K, Legmann R, Sellman BR, Mogridge J and Collier RJ (2002) 2001: a year of major advances in anthrax toxin research. *Trends Microbiol* **10**(6):287-293.

Muglia LM, Schaefer ML, Vogt SK, Gurtner G, Imamura A and Muglia LJ (1999) The 5'-flanking region of the mouse adenylyl cyclase type VIII gene imparts tissue-specific expression in transgenic mice. *J Neurosci* **19**(6):2051-2058.

Nair BG and Patel TB (1993) Regulation of cardiac adenylyl cyclase by epidermal growth factor (EGF). Role of EGF receptor protein tyrosine kinase activity. *Biochem Pharmacol* **46**(7):1239-1245.

Nair BG, Rashed HM and Patel TB (1989) Epidermal growth factor stimulates rat cardiac adenylate cyclase through a GTP-binding regulatory protein. *Biochem J* **264**(2):563-571.

Nanda A, Carson-Walter EB, Seaman S, Barber TD, Stampfl J, Singh S, Vogelstein B, Kinzler KW and St Croix B (2004) TEM8 interacts with the cleaved C5 domain of collagen α 3(VI). *Cancer Res* **64**(3):817-820.

Neer EJ (1978) Physical and functional properties of adenylate cyclase from mature rat testis. *J Biol Chem* **253**(16):5808-5812.

O'Brien J, Friedlander A, Dreier T, Ezzell J and Leppla S (1985) Effects of anthrax toxin components on human neutrophils. *Infect Immun* **47**(1):306-310.

Okumura S, Takagi G, Kawabe J, Yang G, Lee MC, Hong C, Liu J, Vatner DE, Sadoshima J, Vatner SF and Ishikawa Y (2003) Disruption of type 5 adenylyl cyclase gene preserves cardiac function against pressure overload. *Proc Natl Acad Sci U S A* **100**(17):9986-9990.

Oncu S, Oncu S and Sakarya S (2003) Anthrax--an overview. *Med Sci Monit*

9(11):RA276-283.

Ostrom RS, Bundey RA and Insel PA (2004) Nitric oxide inhibition of adenylyl cyclase type 6 activity is dependent upon lipid rafts and caveolin signaling complexes. *J Biol Chem* **279**(19):19846-19853.

Ostrom RS, Liu X, Head BP, Gregorian C, Seasholtz TM and Insel PA (2002) Localization of adenylyl cyclase isoforms and G protein-coupled receptors in vascular smooth muscle cells: expression in caveolin-rich and noncaveolin domains. *Mol Pharmacol* **62**(5):983-992.

Ostrom RS, Violin JD, Coleman S and Insel PA (2000) Selective enhancement of β-adrenergic receptor signaling by overexpression of adenylyl cyclase type 6: colocalization of receptor and adenylyl cyclase in caveolae of cardiac myocytes. *Mol Pharmacol* **57**(5):1075-1079.

Pannifer AD, Wong TY, Schwarzenbacher R, Renatus M, Petosa C, Bienkowska J, Lacy DB, Collier RJ, Park S, Leppla SH, Hanna P and Liddington RC (2001) Crystal structure of the anthrax lethal factor. *Nature* **414**(6860):229-233.

Paterson JM, Smith SM, Simpson J, Grace OC, Sosunov AA, Bell JE and Antoni FA (2000) Characterisation of human adenylyl cyclase IX reveals inhibition by $Ca(^{2+})$/Calcineurin and differential mRNA plyadenylation. *J Neurochem* **75**(4):1358-1367.

Petosa C, Collier RJ, Klimpel KR, Leppla SH and Liddington RC (1997) Crystal structure of the anthrax toxin protective antigen. *Nature* **385**(6619):833-838.

Phan HM, Gao MH, Lai NC, Tang T and Hammond HK (2007) New signaling pathways associated with increased cardiac adenylyl cyclase 6 expression: implications for possible congestive heart failure therapy. *Trends Cardiovasc Med* **17**(7):215-221.

Pini A, Runci Y, Falciani C, Lelli B, Brunetti J, Pileri S, Fabbrini M, Lozzi L, Ricci C, Bernini A, Tonello F, Dal Molin F, Neri P, Niccolai N and Bracci L (2006) Stable peptide inhibitors prevent binding of lethal and oedema factors to protective antigen and neutralize anthrax toxin in vivo. *Biochem J* **395**(1):157-163.

Pinto C, Papa D, Hubner M, Mou TC, Lushington GH and Seifert R (2008) Activation and inhibition of adenylyl cyclase isoforms by forskolin analogs. *J Pharmacol Exp Ther* **325**(1):27-36.

Premont RT, Matsuoka I, Mattei MG, Pouille Y, Defer N and Hanoune J (1996) Identification and characterization of a widely expressed form of adenylyl cyclase. *J Biol Chem* **271**(23):13900-13907.

Prinster SC, Hague C and Hall RA (2005) Heterodimerization of G protein-coupled receptors: specificity and functional significance. *Pharmacol Rev* **57**(3):289-298.

Rao GR, Padmaja J, Lalitha MK, Rao PV, Kumar HK, Gopal KV, Jaideep M and Mohanraj P (2007) Cutaneous anthrax in a remote tribal area--Araku Valley, Visakhapatnam district, Andhra Pradesh, southern India. *Int J Dermatol* **46**(1):55-58.

Robison GA, Butcher RW and Sutherland EW (1968) Cyclic AMP. *Annu Rev Biochem* **37**:149-174.

Rodbell M (1980) The role of hormone receptors and GTP-regulatory proteins in membrane transduction. *Nature* **284**(5751):17-22.

Roth DM, Gao MH, Lai NC, Drumm J, Dalton N, Zhou JY, Zhu J, Entrikin D and Hammond HK (1999) Cardiac-directed adenylyl cyclase expression improves heart function in murine cardiomyopathy. *Circulation* **99**(24):3099-3102.

Roy AA, Lemberg KE and Chidiac P (2003) Recruitment of RGS2 and RGS4 to the plasma membrane by G proteins and receptors reflects functional interactions. *Mol Pharmacol* **64**(3):587-593.

Salim S, Sinnarajah S, Kehrl JH and Dessauer CW (2003) Identification of RGS2 and type V adenylyl cyclase interaction sites. *J Biol Chem* **278**(18):15842-15849.

Santelli E, Bankston LA, Leppla SH and Liddington RC (2004) Crystal structure of a complex between anthrax toxin and its host cell receptor. *Nature* **430**(7002):905-908.

Scholich K, Pierre S and Patel TB (2001) Protein associated with Myc (PAM) is a potent inhibitor of adenylyl cyclases. *J Biol Chem* **276**(50):47583-47589.

Scobie HM, Rainey GJ, Bradley KA and Young JA (2003) Human capillary morphogenesis protein 2 functions as an anthrax toxin receptor. *Proc Natl Acad Sci U S A* **100**(9):5170-5174.

Scorpio A, Blank TE, Day WA and Chabot DJ (2006) Anthrax vaccines:

Pasteur to the present. *Cell Mol Life Sci* **63**(19-20):2237-2248.

Seamon KB and Daly JW (1981) Forskolin: a unique diterpene activator of cyclic AMP-generating systems. *J Cyclic Nucleotide Res* **7**(4):201-224.

Shen Y, Guo Q, Zhukovskaya NL, Drum CL, Bohm A and Tang WJ (2004) Structure of anthrax edema factor-calmodulin-adenosine 5'-(α,β-methylene)-triphosphate complex reveals an alternative mode of ATP binding to the catalytic site. *Biochem Biophys Res Commun* **317**(2):309-314.

Shen Y, Zhukovskaya NL, Guo Q, Florian J and Tang WJ (2005) Calcium-independent calmodulin binding and two-metal-ion catalytic mechanism of anthrax edema factor. *Embo J* **24**(5):929-941.

Shlyakhov E and Rubinstein E (1996) Anthraxin skin testing: an alternative method for anthrax vaccine and post-vaccinal immunity assessment. *Zentralbl Veterinarmed B J Vet Med* **43**(8):483-488.

Siegel LS, Hylemon PB and Phibbs PV, Jr. (1977) Cyclic adenosine 3',5'-monophosphate levels and activities of adenylate cyclase and cyclic adenosine 3',5'-monophosphate phosphodiesterase in *Pseudomonas* and Bacteroides. *J Bacteriol* **129**(1):87-96.

Sinnarajah S, Dessauer CW, Srikumar D, Chen J, Yuen J, Yilma S, Dennis JC, Morrison EE, Vodyanoy V and Kehrl JH (2001) RGS2 regulates signal transduction in olfactory neurons by attenuating activation of adenylyl cyclase III. *Nature* **409**(6823):1051-1055.

Sirisanthana T, Nelson KE, Ezzell JW and Abshire TG (1988) Serological studies of patients with cutaneous and oral-oropharyngeal anthrax from northern Thailand. *Am J Trop Med Hyg* **39**(6):575-581.

Smigel MD, Ferguson KM and Gilman AG (1985) Control of adenylate cyclase activity by G proteins. *Adv Cyclic Nucleotide Protein Phosphorylation Res* **19**:103-111.

Smit MJ and Iyengar R (1998) Mammalian adenylyl cyclases. *Adv Second Messenger Phosphoprotein Res* **32**:1-21.

Smith KE, Gu C, Fagan KA, Hu B and Cooper DM (2002) Residence of adenylyl cyclase type 8 in caveolae is necessary but not sufficient for regulation by capacitative $Ca(^{2+})$ entry. *J Biol Chem* **277**(8):6025-6031.

Sunahara RK, Dessauer CW and Gilman AG (1996) Complexity and diversity

of mammalian adenylyl cyclases. *Annu Rev Pharmacol Toxicol* **36**:461-480.

Sunahara RK, Dessauer CW, Whisnant RE, Kleuss C and Gilman AG (1997) Interaction of $G_s\alpha$ with the cytosolic domains of mammalian adenylyl cyclase. *J Biol Chem* **272**(35):22265-22271.

Sunahara RK and Taussig R (2002) Isoforms of mammalian adenylyl cyclase: multiplicities of signaling. *Mol Interv* **2**(3):168-184.

Sutherland EW and Rall TW (1958) Fractionation and characterization of a cyclic adenine ribonucleotide formed by tissue particles. *J Biol Chem* **232**(2):1077-1091.

Tang T, Gao MH, Lai NC, Firth AL, Takahashi T, Guo T, Yuan JX, Roth DM and Hammond HK (2008) Adenylyl cyclase type 6 deletion decreases left ventricular function via impaired calcium handling. *Circulation* **117**(1):61-69.

Tang WJ and Gilman AG (1991) Type-specific regulation of adenylyl cyclase by G protein $\beta\gamma$ subunits. *Science* **254**(5037):1500-1503.

Tang WJ and Gilman AG (1995) Construction of a soluble adenylyl cyclase activated by $G_s\alpha$ and forskolin. *Science* **268**(5218):1769-1772.

Tang WJ and Hurley JH (1998) Catalytic mechanism and regulation of mammalian adenylyl cyclases. *Mol Pharmacol* **54**(2):231-240.

Taussig R and Gilman AG (1995) Mammalian membrane-bound adenylyl cyclases. *J Biol Chem* **270**(1):1-4.

Taussig R, Iniguez-Lluhi JA and Gilman AG (1993) Inhibition of adenylyl cyclase by $G_i\alpha$. *Science* **261**(5118):218-221.

Taussig R and Zimmermann G (1998) Type-specific regulation of mammalian adenylyl cyclases by G protein pathways. *Adv Second Messenger Phosphoprotein Res* **32**:81-98.

Tesmer JJ, Dessauer CW, Sunahara RK, Murray LD, Johnson RA, Gilman AG and Sprang SR (2000) Molecular basis for P-site inhibition of adenylyl cyclase. *Biochemistry* **39**(47):14464-14471.

Tesmer JJ, Sunahara RK, Gilman AG and Sprang SR (1997) Crystal structure of the catalytic domains of adenylyl cyclase in a complex with $G_s\alpha$.GTPγS. *Science* **278**(5345):1907-1916.

Tesmer JJ, Sunahara RK, Johnson RA, Gosselin G, Gilman AG and Sprang SR (1999) Two-metal-Ion catalysis in adenylyl cyclase. *Science* **285**(5428):756-760.

Tonello F, Ascenzi P and Montecucco C (2003) The metalloproteolytic activity of the anthrax lethal factor is substrate-inhibited. *J Biol Chem* **278**(41):40075-40078.

Trull MC, du Laney TV and Dibner MD (2007) Turning biodefense dollars into products. *Nat Biotechnol* **25**(2):179-184.

Tzavara ET, Pouille Y, Defer N and Hanoune J (1996) Diurnal variation of the adenylyl cyclase type 1 in the rat pineal gland. *Proc Natl Acad Sci U S A* **93**(20):11208-11212.

Ueda Y, Hirai S, Osada S, Suzuki A, Mizuno K and Ohno S (1996) Protein kinase C activates the MEK-ERK pathway in a manner independent of Ras and dependent on Raf. *J Biol Chem* **271**(38):23512-23519.

Ulmer TS, Soelaiman S, Li S, Klee CB, Tang WJ and Bax A (2003) Calcium dependence of the interaction between calmodulin and anthrax edema factor. *J Biol Chem* **278**(31):29261-29266.

Vijaikumar M, Thappa DM and Jeevankumar B (2001) Cutaneous anthrax: still a reality in India. *Pediatr Dermatol* **18**(5):456-457.

Watson EL, Jacobson KL, Singh JC, Idzerda R, Ott SM, DiJulio DH, Wong ST and Storm DR (2000) The type 8 adenylyl cyclase is critical for Ca^{2+} stimulation of cAMP accumulation in mouse parotid acini. *J Biol Chem* **275**(19):14691-14699.

Wayman GA, Wei J, Wong S and Storm DR (1996) Regulation of type I adenylyl cyclase by calmodulin kinase IV in vivo. *Mol Cell Biol* **16**(11):6075-6082.

Wei J, Wayman G and Storm DR (1996) Phosphorylation and inhibition of type III adenylyl cyclase by calmodulin-dependent protein kinase II in vivo. *J Biol Chem* **271**(39):24231-24235.

Wei W, Lu Q, Chaudry GJ, Leppla SH and Cohen SN (2006) The LDL receptor-related protein LRP6 mediates internalization and lethality of anthrax toxin. *Cell* **124**(6):1141-1154.

Whisnant RE, Gilman AG and Dessauer CW (1996) Interaction of the two

cytosolic domains of mammalian adenylyl cyclase. *Proc Natl Acad Sci U S A* **93**(13):6621-6625.

Wolff J, Cook GH, Goldhammer AR and Berkowitz SA (1980) Calmodulin activates prokaryotic adenylate cyclase. *Proc Natl Acad Sci U S A* **77**(7):3841-3844.

Wong ST, Athos J, Figueroa XA, Pineda VV, Schaefer ML, Chavkin CC, Muglia LJ and Storm DR (1999) Calcium-stimulated adenylyl cyclase activity is critical for hippocampus-dependent long-term memory and late phase LTP. *Neuron* **23**(4):787-798.

Wong ST, Trinh K, Hacker B, Chan GC, Lowe G, Gaggar A, Xia Z, Gold GH and Storm DR (2000) Disruption of the type III adenylyl cyclase gene leads to peripheral and behavioral anosmia in transgenic mice. *Neuron* **27**(3):487-497.

Wu AG, Alibek D, Li YL, Bradburne C, Bailey CL and Alibek K (2003) Anthrax toxin induces hemolysis: an indirect effect through polymorphonuclear cells. *J Infect Dis* **188**(8):1138-1141.
Wu GC, Lai HL, Lin YW, Chu YT and Chern Y (2001) N-glycosylation and residues Asn805 and Asn890 are involved in the functional properties of type VI adenylyl cyclase. *J Biol Chem* **276**(38):35450-35457.

Wu ZL, Thomas SA, Villacres EC, Xia Z, Simmons ML, Chavkin C, Palmiter RD and Storm DR (1995) Altered behavior and long-term potentiation in type I adenylyl cyclase mutant mice. *Proc Natl Acad Sci U S A* **92**(1):220-224.

Xia Z, Choi EJ, Wang F, Blazynski C and Storm DR (1993) Type I calmodulin-sensitive adenylyl cyclase is neural specific. *J Neurochem* **60**(1):305-311.

Xia Z, Choi EJ, Wang F and Storm DR (1992) The type III calcium/calmodulin-sensitive adenylyl cyclase is not specific to olfactory sensory neurons. *Neurosci Lett* **144**(1-2):169-173.

Yan L, Vatner DE, O'Connor JP, Ivessa A, Ge H, Chen W, Hirotani S, Ishikawa Y, Sadoshima J and Vatner SF (2007) Type 5 adenylyl cyclase disruption increases longevity and protects against stress. *Cell* **130**(2):247-258.

Yan SZ, Beeler JA, Chen Y, Shelton RK and Tang WJ (2001) The regulation of type 7 adenylyl cyclase by its C1b region and Escherichia coli peptidylprolyl isomerase, SlyD. *J Biol Chem* **276**(11):8500-8506.

Yan SZ, Hahn D, Huang ZH and Tang WJ (1996) Two cytoplasmic domains

of mammalian adenylyl cyclase form a $G_s\alpha$ - and forskolin-activated enzyme in vitro. *J Biol Chem* **271**(18):10941-10945.

Yan SZ, Huang ZH, Andrews RK and Tang WJ (1998) Conversion of forskolin-insensitive to forskolin-sensitive (mouse-type IX) adenylyl cyclase. *Mol Pharmacol* **53**(2):182-187.

Yoshimura M and Cooper DM (1993) Type-specific stimulation of adenylylcyclase by protein kinase C. *J Biol Chem* **268**(7):4604-4607.

Yoshimura M, Ikeda H and Tabakoff B (1996) μ-Opioid receptors inhibit dopamine-stimulated activity of type V adenylyl cyclase but enhance dopamine-stimulated activity of type VII adenylyl cyclase. *Mol Pharmacol* **50**(1):43-51.

Yoshimura M, Pearson S, Kadota Y and Gonzalez CE (2006) Identification of ethanol responsive domains of adenylyl cyclase. *Alcohol Clin Exp Res* **30**(11):1824-1832.

Young JA and Collier RJ (2007) Anthrax toxin: receptor binding, internalization, pore formation, and translocation. *Annu Rev Biochem***76**:243-265.

Zhang G, Liu Y, Ruoho AE and Hurley JH (1997) Structure of the adenylyl cyclase catalytic core. *Nature* **386**(6622):247-253.

Zhang M, Tanaka T and Ikura M (1995) Calcium-induced conformational transition revealed by the solution structure of apo calmodulin. *Nat Struct Biol* **2**(9):758-767.

Zimmermann G and Taussig R (1996) Protein kinase C alters the responsiveness of adenylyl cyclases to G protein α and $\beta\gamma$ subunits. *J Biol Chem* **271**(43):27161-27166.

Chapter 2: Molecular Analysis of the Interaction of 2', 3'-O-(2, 4, 6-trinitrophenyl) (TNP) nucleotides with Purified Catalytic C1/C2 subunits of mammalian Adenylyl cyclase and holo Adenylyl cyclase isoforms

2.1 Introduction

Fluorescent nucleotides are excellent probes for investigating receptor-mediated processes and enzymatic reactions (Jameson and Eccleston, 1997). The 2', 3'-O-(2, 4, 6-trinitrophenyl) (TNP) nucleotides are environmentally sensitive fluorescent probes that have been extensively used to study conformational changes in proteins especially in nucleotide binding proteins such as P-glycoprotein multidrug transporters and histidine protein kinases (Liu and Sharom, 1997; Stewart et al., 1998).

Our earlier studies have shown that MANT-substituted nucleotides are potent inhibitors of the soluble C1/C2 as well as several mAC isoforms (Gille and Seifert, 2003; Gille et al., 2004). Crystallographic studies also showed that TNP-substituted nucleotides can bind to C1/C2 with high affinity (Mou et al., 2006). Both TNP and MANT-nucleotides bind to the same catalytic site of mAC but in different conformations. Both TNP and MANT-nucleotides are environmentally sensitive fluorescent probes, however MANT-nucleotides have a high basal fluorescence and the MANT-group isomerizes between the

2’ and the 3’ position of the ribosyl moiety of the nucleotide (Gille et al., 2004; Mou et al., 2005). In contrast, TNP-nucleotides are more rigid molecules attached to both the 2’ and the 3’ position of the ribose moiety and their basal fluorescence is almost negligible (Hiratsuka, 2003).

A detailed analysis of the substrate binding site in the crystal structure of C1/C2 with TNP-ATP suggests that TNP-ATP may hamper important movement of protein loops, preventing a conformational change from the inactive and open state to the active and closed state (Mou et al., 2006) (Figure 2-1). TNP-ATP makes several contacts with residues on both C1 and C2. The two amino groups of TNP-ATP form hydrogen bonds with the amino groups of N1022 and N1025 of C2 and the backbone oxygen of A409 of C1. K1029 of C2 interacts with phosphates of the substrate ATP to promote formation of the active, closed conformation and catalysis. TNP-nucleotide-binding prevents this interaction. N6 and N7 of the adenine ring of TNP-ATP hydrogen bonds with S1028 of C2. Metal ion A is coordinated by D396 and D440 of C1. Metal ion B is coordinated by the β and γ phosphates of TNP-ATP and three residues on C1, D396, I397 and D440 (Mou et al., 2006).

An inhibitory effect of TNP-nucleotides on purified C1/C2 has been observed in the Seifert laboratory (Gille et al., 2004). Since, UTPγS and CTPγS inhibited ACs (Gille et al., 2004), we examined the effect of TNP pyrimidine nucleotides on C1/C2. TNP purine and pyrimidine nucleotides are

moderately potent inhibitors of C1/C2 (K_i in the nanomolar range) (Table 2-1). TNP-nucleotide triphosphates (TNP-ATP, TNP-GTP, TNP-UTP and TNP-CTP) are more potent compared to TNP-ADP, TNP-GDP and TNP-AMP. TNP-nucleotides were more potent when C1/C2 was maximally activated, i, e in the presence of both $G\alpha_s$ and FS when compared to submaximal activation (only FS, no $G\alpha_s$). This effect was more pronounced with some TNP-nucleotides compared to others. The phosphate chain of TNP-nucleotides played an important role in inhibition. We observed that removal of the γ-phosphate of TNP-ATP caused a six fold decrease in affinity for C1/C2. Removal of both the β and γ phosphates caused an additional thirteen fold decrease in affinity for C1/C2. From the crystal structure of C1/C2 with bound TNP-ATP, it is clear that metal ion B interacts with the β and γ phosphates of TNP-ATP. Since metal ions are critical for catalysis (Tesmer et al., 1997 and 1999), removal of these phosphates explains the decrease in affinity of TNP-ADP and TNP-AMP for C1/C2. Compared with K_i values for other proteins inhibited by TNP-ATP, TNP-ATP has the lowest K_i (81 nM) for AC and thus a higher affinity than previously observed (Hiratsuka, 1982; Broglie and Takahashi, 1983; Thomas et al., 1991).

Differential regulation, localization and function of AC isoforms suggest a possible way for development of potent AC isoform specific inhibitors (Sunahara et al., 1996; Hanoune and Defer, 2001). We have observed that

MANT-nucleotides are potent inhibitors of C1/C2. However isoform-specific inhibition of MANT-nucleotides was not clearly observed (Gille et al., 2004). This chapter primarily focuses on the inhibitory effects of TNP-nucleotides on holo-AC isoforms and identification of potent AC isoform-specific inhibitors for rational drug design.

Figure 2-1 Crystal structure of C1/C2-FS- $G\alpha_s$-TNP-ATP (Mou et al., 2006)

A detailed analysis of the substrate binding site of C1/C2 is shown here. C1 in tan, C2 in mauve and $G_s\alpha$ is shown grey. FS, TNP-ATP and metal ions occupy the cleft formed by C1 and C2. TNP-ATP making contacts with important amino acid residues in C1 and C2 are also highlighted. FS and TNP-ATP are shown as stick models. Colors of atoms are depicted as C = gray, N = blue, O = red and P = green. The two Mn^{2+} ions are depicted as orange metallic spheres.

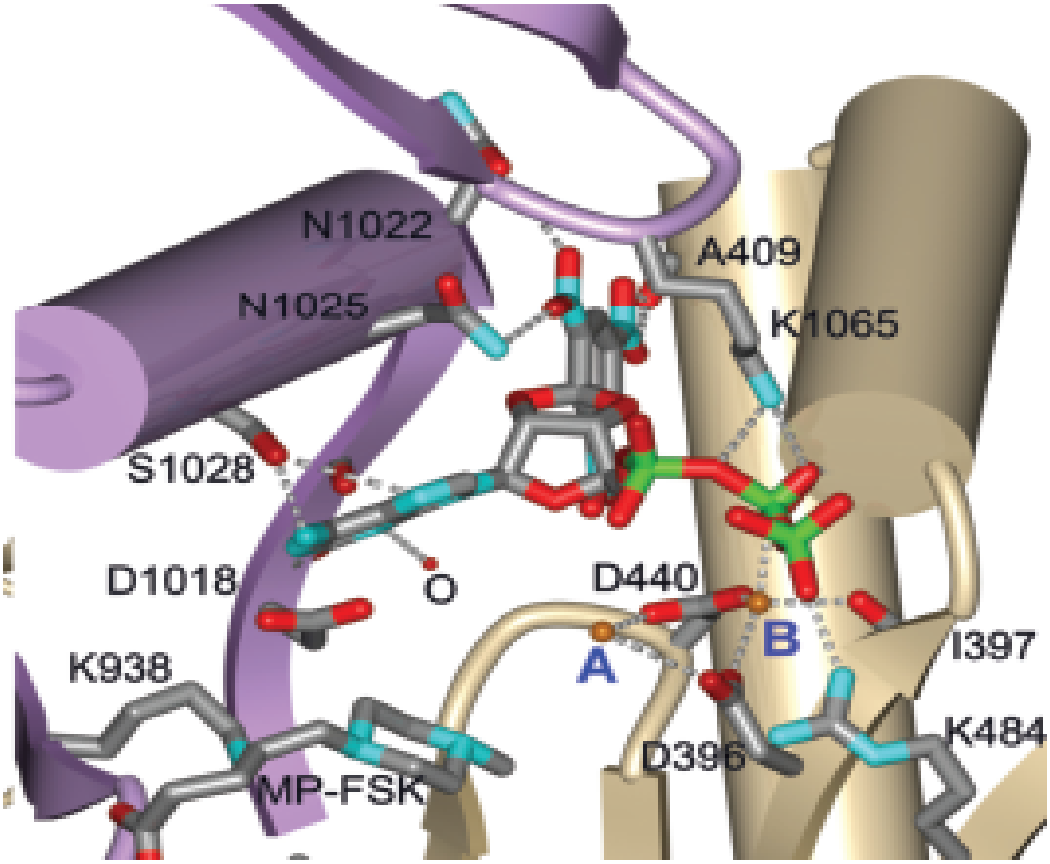

Table 2-1 Inhibition of the Catalytic activity of C1/C2 by TNP-nucleotides (Mou et al., 2006)

Nucleotide	VC1:IIC2 + FSK K_i (nM)	VC1:IIC2 + FSK + $G\alpha_s$ K_i (nM)
TNP-nucleotides		
TNP-ATP	100 ± 30	81 ± 27
TNP-ADP	2,000 ± 660	1,300 ± 280
TNP-AMP	21,000 ± 7,200	17,000 ± 6,000
TNP-GTP	430 ± 130	83 ± 22
TNP-GDP	8,100 ± 2,900	9,400 ± 1,800
TNP-UTP	92 ± 9	92 ± 36
TNP-CTP	110 ± 16	310 ± 76

2.2 Specific Aims and hypothesis

Although from earlier studies, it is clear that TNP-nucleotides inhibit C1/C2 with great affinity (Ki in the nanomolar range) (Mou et al., 2006), the inhibitory properties of TNP-nucleotides for understanding AC isoform-specific inhibition has not yet been studied. In the present study, we examine: 1) How TNP-purine and pyrimidine nucleotides effect the catalytic activity of C1/C2 in its native form i.e., in the absence of the activators $G\alpha_s$ and or Forskolin (FS); 2) The inhibitory effect of TNP-nucleotides on holo-AC isoforms, mainly focusing on AC1, AC2 and AC5; 3) The conformational changes in C1/C2 due to binding of TNP-nucleotides observed by fluorescence spectroscopy; 4) DMB-FS-induced conformational changes in C1/C2 probed by TNP-nucleotides; 5) The specificity of TNP substituted adenine and guanine nucleotides, TNP-ATP and TNP-GTP for G-proteins in view of the fact that guanine nucleotides and adenine nucleotides bind to $G\alpha_s$- and $G\alpha_i$- with high affinity and low affinity respectively (Gilman, 1987; Birnbaumer et al., 1990). 6) How the TNP-nucleotide interacts with C1/C2 compared to those of the MANT-nucleotides as indicated by fluorescence spectroscopy and enzymatic analysis.

Based on previous studies using purified C1/C2 and studies carried out in our laboratory, we hypothesize that TNP-nucleotides bind with low affinity to C1/C2 alone in the absence of its activators, $G\alpha_s$ and or FS, and that both

purine and pyrimidine TNP-nucleotides bind to and bring about a major conformational change in the C1/C2 catalytic core.

In earlier studies of the interaction of MANT-nucleotides with C1/C2, we observed that there are subtle differences in binding of MANT-ATP to C1/C2 compared to MANT-GTP (Mou et al., 2005; Mou et al., 2006). Therefore, we predict that there might be similar differences in binding of TNP-ATP to C1/C2 compared to TNP-GTP and that such differences might be exploited for the rational design of AC isoforms-selective inhibitors.

2.3 Materials and methods

2.3.1 Materials

VC1, IIC2 and $G\alpha_s$-GTPγS proteins kindly provided by Drs. S.Sprang and T.C.Mou (University of Texas Southwestern Medical Center, Dallas, TX), were expressed, purified and stored as described previously (Taussig et al., 1994; Sunahara et al., 1997; Tesmer et al., 2002). Baculoviruses encoding ACs 1, 2 and 5 were generously donated by Drs. A.G. Gilman and R.K.Sunahara (University of Texas Southwestern Medical Center, Dallas, TX). Sf9 cells were obtained from the American Type Cell Culture Collection (Rockville, MD). TNP-ATP, TNP-ADP and TNP-AMP were purchased from Invitrogen. TNP-GTP, TNP-GDP, TNP-UTP, TNP-CTP, MANT-ADP and MANT-GDP were obtained from Jena Bioscience (Jena, Germany). An overview of the structure of all the TNP-nucleotides (except TNP-AMP) is shown in Figure 2-2. FS and DMB-FS (water-soluble analog of FS) were obtained from Calbiochem (La Jolla, CA) or Sigma-Aldrich (St.Louis, MO). 2'5' dd 3'ATP, myokinase, creatine phosphate (CP), creatine kinase (CK) and nucleoside diphosphokinase (NDPK) were obtained from Sigma. [α-^{32}P] ATP (6000 Ci/mmol) and [γ-^{32}P]GTP were purchased from PerkinElmer Life sciences. Sources of cell culture reagents and other materials have been described elsewhere (Gille and Seifert, 2003; Pinto et al., 2008). Construction of cDNA, cell culture and membrane preparation of formyl peptide receptor

(FPR) coupled to $G\alpha_i$ proteins and the β_2-adrenoreceptor coupled to $G\alpha_s$ splice variants are as described previously (Wenzel-Seifert et al., 1999; Seifert et al., 1998).

Figure 2-2 Structure of TNP-nucleotides

Chemical structure of TNP-nucleotides utilized in this chapter and chapter 3.

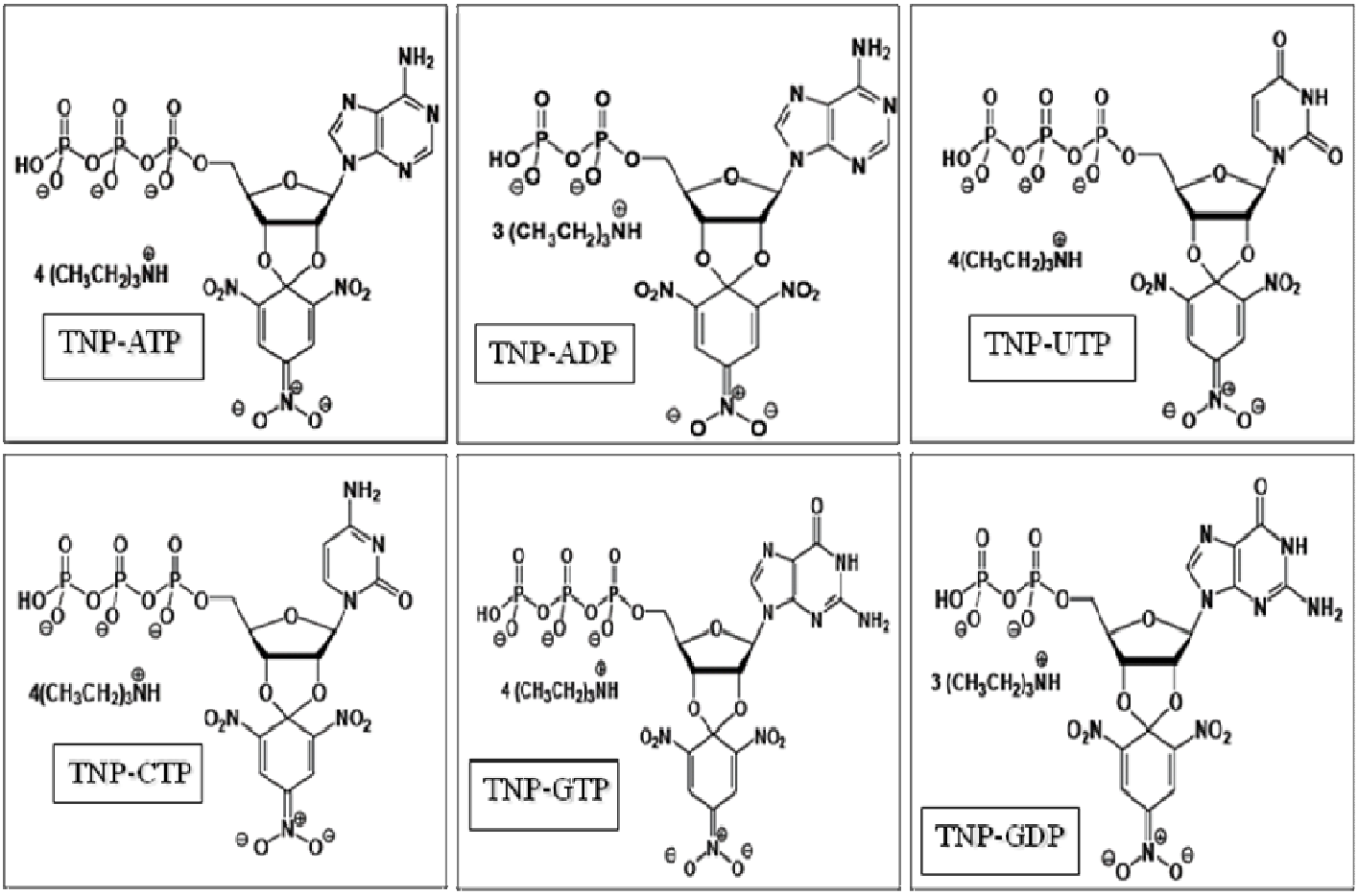

2.3.2 Experimental methods

- Cell culture, expression and membrane preparation of recombinant holo-AC isoforms

Cell culture, expression and membrane preparation were carried out as described previously (Seifert et al., 1998; Gille et al., 2002; Houston et al., 2002). Briefly, Sf9 cells were cultured in SF 900 II medium with 5% (vol/vol) FBS and 0.1 mg/ml gentamycin. High-titer baculoviruses were produced in two amplification steps as described elsewhere (Houston et al., 2002) and the supernatant fluid from each step was harvested and stored at 4˚C. Sf9 cells were then infected with the corresponding baculovirus encoding different ACs and cultured for 48 hours (1:10 – 1:10,000 dilutions incase of high titer virus stocks). Membranes from uninfected Sf9 cells and each AC construct were prepared as described previously (Seifert et al., 1998). Briefly, cells were harvested and suspensions centrifuged for 10 mins (1,000 x g at 4˚C). Pellets were resuspended in lysis buffer following lysis using a Dounce homogenizer. Lysis buffer contained 1 mM EDTA, 0.2 mM phenylmethyl-sulfonyl fluoride, 10 μg/ml each of leupeptine and benzamide with a pH of 7.4. The resultant suspension was centrifuged for 5 mins (500 x g at 4˚C) for nuclei sedimentation. The supernatant fluid containing the cell membranes was transferred to 30 ml tubes and centrifuged for 20 mins (30,000 x g at 4˚C). The resultant pellet was then collected and resuspended in buffer containing

75 mM Tris/HCl, 12.5 mM $MgCl_2$ and 1mM EDTA, pH 7.4. Protein concentration for each membrane was measured using Bio-Rad DC protein assay kit (Bio-Rad, Hercules, CA). 0.5 to 1 ml of membrane aliquots were prepared and stored at -80C.

- ***AC activity assay***

AC activity assays using C1/C2 was determined as described previously (Mou et al., 2005 and 2006). To carry out AC activity assays with C1/C2, assay tubes contained 7 nM VCI and 35 nM IIC2 respectively. For inhibition experiments with TNP and MANT-nucleotides, concentrations of the nucleotides ranging from 1 nM to 100 μM were added to the assay tubes before addition of the protein. Reactions were conducted in the presence and absence of 45 nM $G\alpha_s$-GTPγS and 100 μM FS. After an initial preincubation for 2 min at 30˚C, 20 μl of reaction mixture containing 100 μM cAMP, 40 μM ATP, 10 mM $MnCl_2$, 100 μM KCl, 25 mM Na+ HEPES pH 7.4 and 1 – 1.5 μCi/tube [α-^{32}P]ATP were added to the assay tubes. After incubation for 20 min at 30˚C, reactions were terminated by adding 20 μl of 2.2 N HCl. Denatured protein was sedimented by a 1-min centrifugation at 25˚C and 15,000 x g followed by application of 65 μl of the supernatant onto disposable alumina columns (1.3 g neutral alumina, Sigma A-1522, super I, WN-6). To separate [^{32}P]cAMP from [^{32}P]ATP, 4 ml of 0.1 M ammonium acetate was added for elution of [^{32}P] cAMP. Recovery of [^{32}P]cAMP was approx. 80% as

assessed with [^{3}H]cAMP set as standard. [^{32}P]cAMP was determined by liquid scintillation counting using Ecolume scintillation cocktail or Cerenkov radiation. AC assays in the absence of FS and Gα_s were carried out using 6 – 6.5 μCi/tube [α-^{32}P] ATP and incubated for 1 hour at 30˚C before stopping the reaction.

AC assays using membranes from Sf9 cells expressing AC1, 2 and 5 were conducted as described previously (Gille 2004). Membranes were first centrifuged for 15 min (15,000 x g at 4˚C) and the pellets were resuspended in binding buffer. Each assay tube contained membrane expressing AC (15 – 20 μg of protein/tube), 10 μM GTPγS, 40 μM ATP, 100 μM FS, 1 mM $MnCl_2$ and 100 μM cAMP and increasing concentrations of TNP-nucleotides ranging from 1 nM to 100 μM. Reactions were carried out as described above for C1/C2.

In AC experiments shown in Table 2.8, the AC5 isoform was used and additionally reaction mix contained NTP-regenerating system consisting of 2.7 mM mono(cyclohexyl)ammonium phosphoenol pyruvate, 0.125 IU pyruvate kinase and 1 IU myokinase was used as described previously (Gille 2004) to study the effect of phosphorylation of TNP-NDPs. In AC experiments with nucleoside-diphosphate kinase (NDPK), 1 IU NDPK was added either to the protein mix (C1/C2/ Gα_s) or to the reaction tubes with nucleotides and preincubated for 15 minutes before addition of C1/C2. No major differences

were observed between the two conditions. AC experiments with 1 IU CP/CK (creatine phosphate/creatine kinase) were carried out in the same manner.

- ***Fluorescence spectroscopy***

All experiments were carried out using a Cary eclipse fluorescence spectrophotometer at 25C (Varian, Walnut Creek, CA). Measurements were performed using a quartz fluorescence microcuvette (Hellma, Plainview, NY) and the final assay volume was 150 μl. For TNP-nucleotides, steady-state emission spectra were recorded at low speed with λ_{ex} = 405 nm (λ_{em} = 500 – 600 nm). Reaction mixture containing 100 mM KCl, 10 mM $MnCl_2$ in 25 mM HEPES/NaOH pH 7.4 was added followed by sequential addition of TNP-nucleotide, VCI/IIC2 and DMB-FS (water soluble analog of FS) to final concentrations of 5 μM, 4 μM/25 μM and 100 μM respectively. All the experiments were also carried out in the presence of 10 mM $MgCl_2$. For the TNP-nucleotides, measurements were also carried out in the kinetic mode with the range 405-550 nm to measure the rate of binding of TNP-nucleotides to C1/C2. For competition experiments with 2'5' dd 3' ATP, experiments were carried out similarly except that 2'5' dd 3' ATP was added in place of DMB-FS. Reactions were also carried out in the kinetic mode to observe the displacement of TNP-nucleotides by 2'5' dd 3'ATP.

- ***Steady-state GTPase assay***

GTPase assays were carried out as described previously (Gille et al., 2004). Membranes with β_2AR- Gα_s and FPR- Gα_i fusion proteins were thawed and centrifuged for 15 min (15,000 x g at 4˚C) to eliminate any endogenous nucleotides. Pellets were resuspended in Tris-HCl, pH 7.4. Assay tubes contained, in a final volume of 80 μl, 10 μg of protein/tube, 1 mM AppNHp, 100 nM unlabeled GTP, 100 μM unlabeled ATP, 1 mM $MgCl_2$, 100 μM EDTA, 0.2% (mass/vol) bovine serum albumin, 5 mM creatine phosphate, 40 μg creatine kinase in 50 mM Tris-HCl, pH 7.4, TNP-ATP or TNP-GTP at varying concentrations and 10 μM isoproterenol and *N*-formyl-L-methionyl-L-leucyl-L-phenylalanine (FMLP) to fully activate β_2AR- Gα_s and FPR- Gα_i fusion proteins respectively. Assay tubes were incubated for 3 min at 25˚C following addition of 20 μl of [γ-^{32}P]GTP (0.2 μCi/tube). Reactions were carried out for 20 min at 25˚C and terminated by adding 900 μl of slurry (5% mass/vol) activated charcoal and 50 mM NaH_2PO_4, pH 2.0). Charcoal terminated reaction mixtures were centrifuged for 15 min (15,000 x g at room temperature). 700 μl of supernatant liquid were removed from each assay tube and $^{32}P_i$ was determined by liquid scintillation counting. In the presence of 1 mM unlabelled GTP, non-enzymatic degradation of [γ-^{32}P]GTP was determined and was < 1% of the total amount of radioactivity added.

- ***Molecular Docking and scoring method***

Docking studies were carried out in collaboration with Mou's group. The X-ray crystal structure of VC1:IIC2:FSK:Gαs-GTPγS in complex with TNP-ATP and two Mn^{2+} ions (PDB ID:1GVD) was used as a model for docking other TNP-nucleotides. TNP-ATP and all the other atoms and associated residues within 5 Å of the ligand were used to define the active site of the mAC catalytic core complex. In the first step, modeled TNP-ATP was aligned to the one in the crystal structure. Using the rigid docking method, several conformations were generated and the most aligned TNP-ATP model was used since it closely mimics the actual TNP-ATP in the crystal structure. Similar conformations were generated for all the other TNP-nucleotides using the rigid docking procedure.

- ***Data Generation and Statistics***

All the enzymatic assays with saturation curves for inhibitors, were analyzed by nonlinear regression using Prism 4.0 software (Graphpad, San Deigo, CA). K_i values expressed in nM were calculated using non-linear regression. Data shown are the mean values ± standard deviations of 3-4 experiments performed in duplicate. In GTP hydrolysis assays, K_i values expressed as μM or μmol/L (???) and 95% confidence intervals were also calculated using nonlinear regression.

Fluorescence recordings were analyzed using the spectrum package of the Cary Eclipse software and final graphs were prepared using Graphpad prism 4.0 software. Similar results were obtained from 3 – 4 independent experiments using three different batches of VCI and two different batches of IIC2.

Docking calculations were carried out using the GOLD 3.0.1 docking software. The Goldscore and Chemscore scoring functions were used to rank different binding poses. GOLD 3.0.1 GA parameter was used to encode the ligand hydrogen-binding interactions.

2.4 Results and discussion

2.4.1 Enzymatic analysis of the interaction of TNP-nucleotides with C1/C2

As was reported previously (Mou et al., 2006) the purine-substituted nucleotides TNP-ATP, TNP-GTP and the pyrimidine-substituted nucleotides TNP-UTP, TNP-CTP potently inhibited C1/C2 when maximally stimulated by FS, $G\alpha_s$ and Mn^{2+} (K_i values in the 100 nM range) (Table 2-1). It is also very clear that with the elimination of γ phosphate in TNP-ATP and TNP-GTP, the Ki values increased several fold. With the elimination of both the β and γ phosphates in TNP-ATP, the Ki value was further increased.

In order to fully understand the structure-activity relationship for the inhibition of C1/C2 by different TNP-nucleotides, the potencies of TNP-nucleotides in inhibiting C1/C2 in the absence of both the activators, $G\alpha_s$ and FS, was determined (Table 2-2). By omission of the activators the Ki increased several-fold. This is in accordance with earlier findings that FS and $G\alpha_s$ together and separately change the relative conformation of C1/C2 and promote catalysis (Sunahara et al., 1997). This indicates that FS, a non physiological activator, and $G\alpha_s$, a physiological activator, are important for mAC catalysis. Furthermore, in the absence of $G\alpha_s$ and FS, the reduced apparent affinity for C1/C2 was different for different TNP-nucleotides. Even in the absence of $G\alpha_s$ and FS, TNP-ATP was the most potent inhibitor (Ki =

3.3 μM) of C1/C2 compared to other TNP-nucleotides. This reduced affinity of TNP-nucleotides for C1/C2 can also be explained by the fact that FS and $G\alpha_s$ binding to C1/C2 gives rise to a tighter binding and change in conformation. Therefore, in the absence of these activators, C1/C2 is in its native state with a completely different conformation prior to $G\alpha_s$ and FS binding.

It must be noted that in our AC experiments Mn^{2+} was used because Mn^{2+} is a more effective activator than Mg^{2+} (Dessauer and Gilman, 1997; Johnson et al., 1989). We have also observed that the inhibitor affinity is greatly reduced when Mn^{2+} is replaced by Mg^{2+}(data not shown).

Though TNP-ATP and TNP-GTP have very similar potencies for C1/C2 in the presence of FS and $G\alpha_s$, we shall explore the differences in their binding to C1/C2 in the later sections of this chapter.

Table 2-2 Inhibitory potencies of TNP-nucleotides under different experimental conditions

Catalytic activity assays of C1/C2 were performed as described in section 2.3.2. Assay tubes contained 7 nM VCI and 35 nM IIC2. Concentrations of TNP-nucleotides ranging from 1 nM to 100 μM were added to the assay tubes before addition of the protein. Reactions were conducted in the presence and absence of 45 nM $G\alpha_s$-GTPγS and 100 μM FS. Reaction mixture (20 μl) containing 100 μM cAMP, 40 μM ATP, 10 mM $MnCl_2$, 100 μM KCl, 25 mM HEPES/NaOH pH 7.4 and 1 – 1.5 μCi/tube [α-^{32}P]ATP were added to the assay tubes. AC assays in the absence of FS and $G\alpha_s$ were carried out using 6-6.5 μCi/tube [α-^{32}P] ATP (25 μl) and incubated for 1 h at 30˚C before stopping the reaction. All enzymatic assays with saturated inhibition curves were analyzed by nonlinear regression using Prism 4.0 software (Graphpad, San Deigo, CA). K_i values are expressed in nM and data shown are the mean values ± SD of 3-4 experiments performed in duplicates.

TNP-nucleotides	C1/C2+ Mn^{2+}+FS	C1/C2+ Mn^{2+}+FS+ $G\alpha_s$	C1/C2+ Mn^{2+}
TNP-ATP	100 ± 30	81 ± 27	3,300 ± 1400
TNP-ADP	2,000 ± 660	1,300 ± 280	11,400 ± 5900
TNP-AMP	21,000 ± 7,200	17,000 ± 6,000	-
TNP-GTP	430 ± 130	83 ± 22	6,420 ± 2000
TNP-GDP	8,100 ± 2,900	9,400 ± 1,800	15,200 ± 400
TNP-UTP	92 ± 9	92 ± 36	14,300 ± 0
TNP-CTP	110 ± 16	310 ± 76	8,570 ± 0

Figure 2-3 Inhibition of catalytic activity of C1/C2 by TNP-nucleotides under different experimental conditions

Saturation curves for different TNP-nucleotides under three different experimental conditions are shown. A, in the presence of FS (sub maximal activation of C1/C2. B, in the presence of $G\alpha_s$ and FS (maximal activation of C1/C2). C, in the absence of both $G\alpha_s$ and FS (C1/C2 in native state). Catalytic activity assays of C1/C2 inhibited by TNP-nucleotides were carried out as described in section 2.3.2. Saturated curves shown are representative of 3-4 independent experiments performed in duplicates.

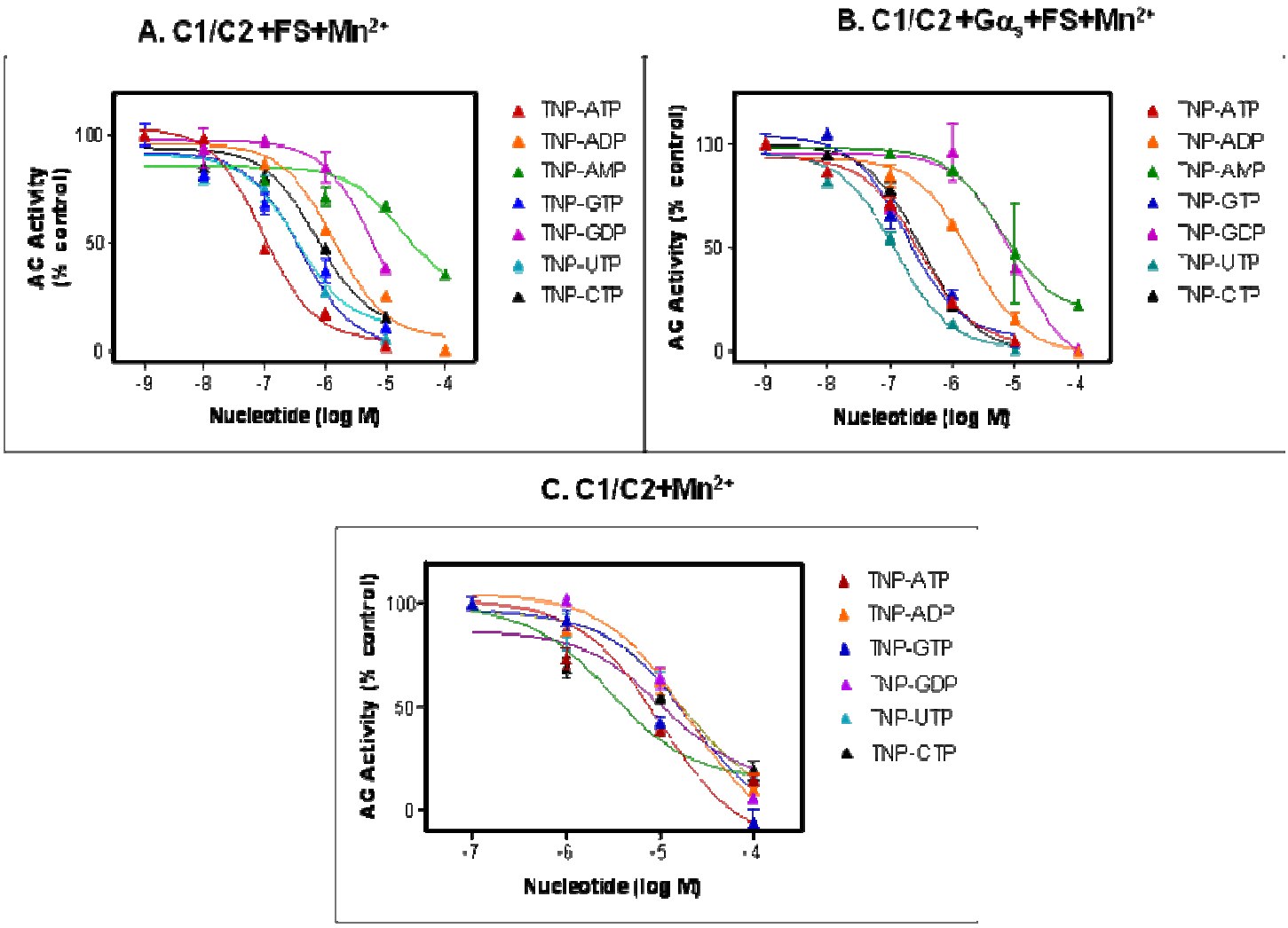
A. C1/C2+FS+Mn2+
B. C1/C2+Gαs+FS+Mn2+
AC Activity (% control)
100
50
0
-9
-8
-7
-6
-5
-4
Nucleotide (log M)
TNP-ATP
TNP-ADP
TNP-AMP
TNP-GTP
TNP-GDP
TNP-UTP
TNP-CTP

C. C1/C2+Mn2+
AC Activity (% control)
100
50
0
-7
-6
-5
-4
Nucleotide (log M)
TNP-ATP
TNP-ADP
TNP-GTP
TNP-GDP
TNP-UTP
TNP-CTP

2.4.2 Enzymatic analysis of the interaction of TNP-nucleotides with holo-AC isoforms

Crystallographic studies have provided us with insight into TNP-ATP binding and interaction with important amino acid residues in the catalytic pocket formed by C1 and C2 (Mou et al., 2006). Enzymatic studies have helped to show that TNP-nucleotides are potent inhibitors of C1/C2. However it is important to examine the effects of TNP-nucleotides on holo enzymes in membrane preparations to identify isoform-specific inhibitors.

Baculovirus encoded AC1, 2 and 5 isoforms were expressed in Sf9 cells. Sf9 cells have been widely used to express recombinant proteins and are excellent expression systems for mACs (Feinstein et al., 1991; Tang et al., 1991; Taussig et al., 1993). Since Sf9 cells express an unidentified endogenous membrane AC, it is also important to measure basal AC activity in uninfected Sf9 AC membranes to make sure that cAMP signaling is partly (??) due to endogenous ACs in Sf9 and not due to over-expression of mammalian ACs (Tang et al., 1991; Mouillac et al., 1992; Houston et al., 2002). Furthermore, in order to ensure a smaller background activity, Sf9 cells with virus encoded GAIP protein was used to study AC activity. GAIP protein is a GTPase-activating protein that interacts with $G\alpha_i$ and is irrelevant with respect to AC regulation (De Vries et al., 1995). Moreover, Sf9 cells do

not express Gi, GAIP proteins act as controls when measuring AC activity in Sf9 membranes, both infected and uninfected.

Before examining the effects of TNP-nucleotides on recombinant AC isoforms, it was important to confirm that the AC isoform retained its natural properties, i,e, if it is activated by mediators such as FS and $G\alpha_s$. Experiments were carried out under four different conditions: 1, Basal AC activity; 2, AC activity with FS as activator; 3, AC activity with GTPγS; 4, AC activity with both FS and GTPγS. ACs 1, 2 and 5 were compared in parallel with uninfected Sf9 membranes and GAIP membranes. Membranes were analyzed in duplicate and three different batches of membranes were used. Membranes expressing AC1, 2 and 5 when activated by both FS and GTPγS showed maximal AC activity. In addition, as expected, AC activity was several fold higher in membranes with AC1, 2 and 5 isoforms (266 ± 12, 120 ± 8, 108 ± 7 pmol/mg/min respectively) when compared to uninfected Sf9 membrane and in membranes with GAIP.

Figure 2-4 AC activity in membranes from uninfected Sf9 cells and membranes from Sf9 cells expressing GAIP, AC1, AC2 and AC5 under different experimental conditions

AC activity was measured in membranes from uninfected Sf9 cells, GAIP and holo-AC isoforms under four different experimental conditions: 1, Basal condition with no activation; 2, 100 μM FS; 3, 10 μM GTPγS; 4, 100 μM FS/10 μM GTPγS. Each assay tube contained ~20 μg membrane/tube, 40 μM unlabelled ATP, 5 mM $MnCl_2$, 100 μM cAMP and 1 – 1.5 μCi/tube [α-32P]ATP. AC activity assay was carried out as described in section 2.3.2. AC activity measured in pmol/mg/min was calculated by non-linear regression. Data were obtained from 2-3 independent experiments from different membrane batches and experiments were performed in duplicate.

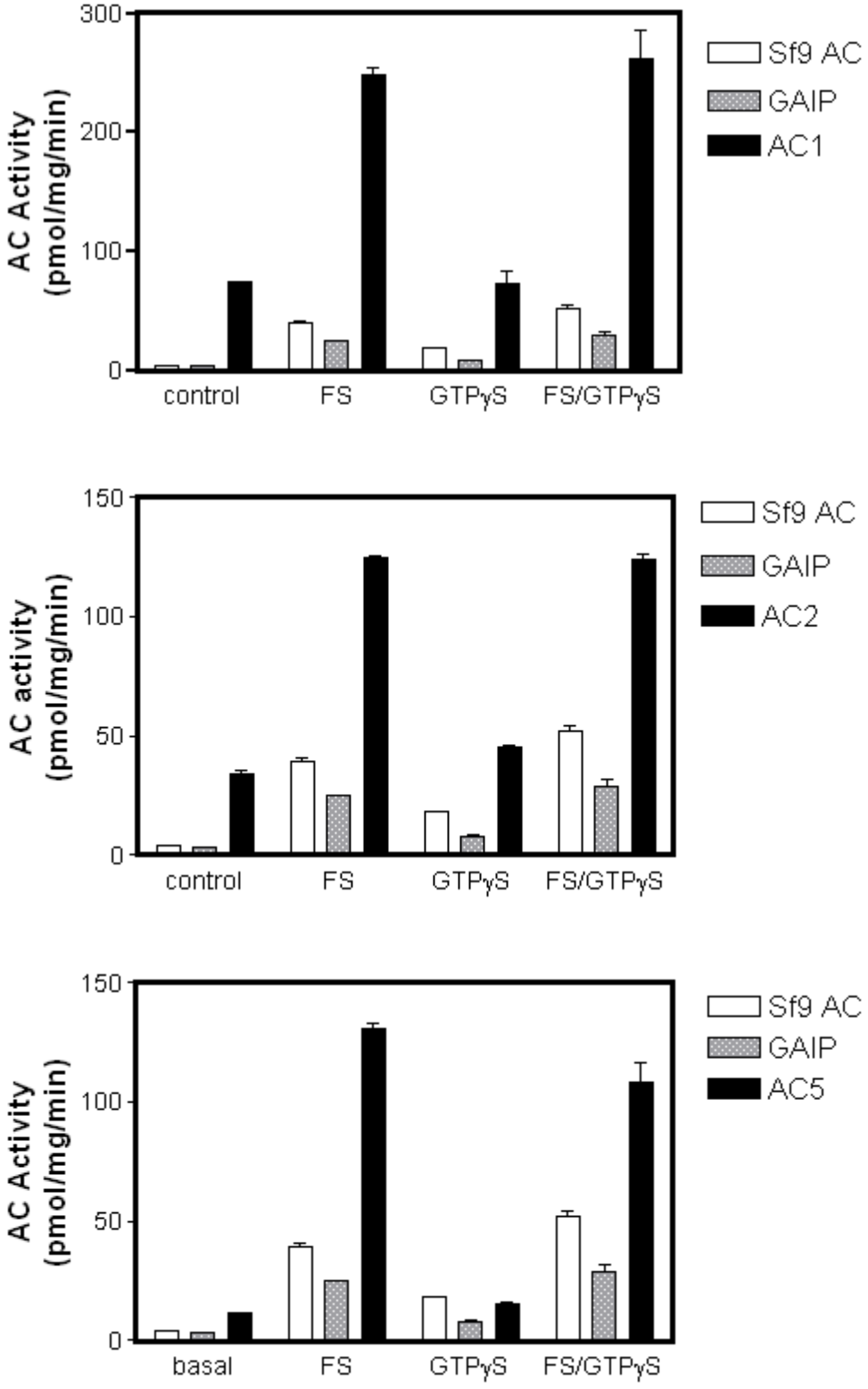
AC Activity (pmol/mg/min)
300
200
100
0
control
FS
GTPγS
FS/GTPγS
Sf9 AC
GAIP
AC1
AC activity (pmol/mg/min)
150
100
50
0
control
FS
GTPγS
FS/GTPγS
Sf9 AC
GAIP
AC2
AC Activity (pmol/mg/min)
150
100
50
0
basal
FS
GTPγS
FS/GTPγS
Sf9 AC
GAIP
AC5

A systematic analysis of the structure-activity relationship of TNP-nucleotides with holo-AC1, AC2 and AC5 isoforms was carried out to identify possible isoform-specific inhibitors and for a detailed comparison with results from C1/C2 inhibition described in section 2.4.1

In general, all four TNP-NTPs, i,e, TNP-ATP, TNP-GTP, TNP-UTP and TNP-CTP are potent inhibitors of AC1, 2 and 5 isoforms (K_i values in the nanomolar range). Among all AC isoforms studied, AC1 exhibited the highest sensitivity to inhibition by TNP-nucleotides and AC2 showed lower inhibitor sensitivity when compared AC1 and AC5. TNP-ATP and TNP-UTP were the most potent inhibitors of AC1 isoform (K_i = 9 and 7 nM respectively). TNP-ATP was the most potent inhibitor for AC5 and was at least 25-fold more potent at inhibiting AC5 than AC2. TNP-UTP was the most potent inhibitor for AC2. Although most TNP-nucleotides showed a higher selectivity for AC5 compared to AC2, the differences between specificities of TNP-UTP for AC1, AC2 and AC5 were negligible. TNP-CTP also showed very small differences in selectivity between AC1, AC2 and AC5 indicating that TNP-pyrimidine nucleotides probably bind to AC isoforms in a different manner compared the TNP-purine nucleotides. Also, since pyrimidine nucleotides are smaller in size, it is possible that they could fit into smaller catalytic pockets in AC isoforms when compared to purine nucleotides.

Upon comparing soluble C1/C2 and holo-AC isoforms, a common similarity between the two is that holo-AC isoforms are also highly sensitive to inhibition by TNP-NTPs than TNP-NDPs. For example, in the case of AC1, removal of the γ-phosphate in TNP-ATP reduces the inhibitor affinity by 15-fold. Removal of both the β- and γ– phosphates of TNP-ATP reduces the affinity by an additional 33-fold. We have observed a similar pattern in Table 2-2 in the case of C1/C2. A major difference between C1/C2, and holo-AC isoforms in general, is that C1/C2 is several-fold less sensitive to inhibition by TNP-nucleotides. This difference in sensitivity could be attributed to the fact that holo-AC isoforms have transmembrane domains that probably orient the catalytic domains in a position favorable for tighter binding and better inhibition by TNP-nucleotides. Since C1/C2 are soluble catalytic subunits without the transmembrane domains, the positioning of the hydrophobic pocket may be relatively different than in the holo-AC isoforms. It must also be noted that C1 and C2 subunits are from AC5 and AC2 respectively. Therefore, it is also possible that C2(AC2) dominates C1(AC5) and confers low inhibitor affinity to the cyclase since TNP-nucleotides have a lower affinity for AC2.

TNP-nucleotides also differ in their AC-inhibition pattern compared to MANT-nucleotides. C1/C2 are more sensitive to inhibition by MANT-nucleotides compared to holo-AC isoforms whereas the reverse is true for TNP-nucleotides. TNP-nucleotides are also more isoform-selective in their

inhibition compared to MANT-nucleotides. Earlier, crystallographic studies have shown differences in MANT-ATP, MANT-GTP and TNP-ATP binding to the catalytic site of C1/C2 (Mou et al., 2006). Although all three nucleotides bind to a common site in C1/C2, there are slight differences in their orientations. It is not clear if these differences in orientation may also exist in holo-AC isoforms. It is, however, possible that MANT and TNP-nucleotides have different binding modes to AC isoforms thus giving rise to properties important for rational design of novel, isoform-specific cyclase inhibitors.

Table 2-3 Inhibition of catalytic activity of AC1, AC2 and AC5 isoforms by TNP-nucleotides

AC assays using membranes from Sf9 cells expressing AC1, 2 and 5 were conducted as described previously (Gille et al., 2004) and in section 2.3.2. Each assay tube contained membrane expressing AC (15 – 20 μg of protein/tube), 10 μM GTPγS, 40 μM ATP, 100 μM FS, 1 mM $MnCl_2$, 100 μM cAMP, 1 – 1.5 μCi/tube [α-^{32}P] ATP and increasing concentrations of TNP-nucleotides ranging from 1 nM to 100 μM in a final volume of 50 μl. K_i values are expressed in nM and were calculated by non-linear regression. Data shown are mean values ± S.D. of 3-5 experiments performed in duplicate with atleast 3 different batches of AC membranes.

TNP-nucleotides	*AC1*	*AC2*	*AC5*
TNP-ATP	9 ± 4	99 ± 2	3.7 ± 2
TNP-ADP	143 ± 17	1105 ± 176	367 ± 45
TNP-AMP	4801 ± 1000	7383 ± 518	4784 ± 1191
TNP-GTP	23 ± 2	216 ± 30	27 ± 4
TNP-GDP	410 ± 76	3355 ± 1262	1179 ± 277
TNP-UTP	7 ± 3	24 ± 12	15 ± 2
TNP-CTP	24 ± 12	112 ± 35	31 ± 3

Figure 2-5 AC activity inhibition in AC1, AC2 and AC5 isoforms by TNP-nucleotides

Shown are saturation curves of the relative inhibitory activities of TNP-nucleotides on the catalytic activity of AC1, AC2 and AC5. AC assays using membranes from Sf9 cells expressing AC1, 2 and 5 were conducted as described previously (Gille et al., 2004) and in section 2.3.2. Each assay tube contained membrane expressing AC (15 – 20 μg of protein/tube), 10 μM GTPγS, 40 μM ATP, 100 μM FS, 1 mM $MnCl_2$, 100 μM cAMP, 1 – 1.5 μCi/tube [α-^{32}P] ATP and increasing concentrations of TNP-nucleotides ranging from 1 nM to 100 μM in a final volume of 50 μl. AC activity was calculated by non-linear regression and is expressed in pmol/mg/min. Data shown are representative of 3-5 experiments performed in duplicate with at least three different batches of AC membranes.

A

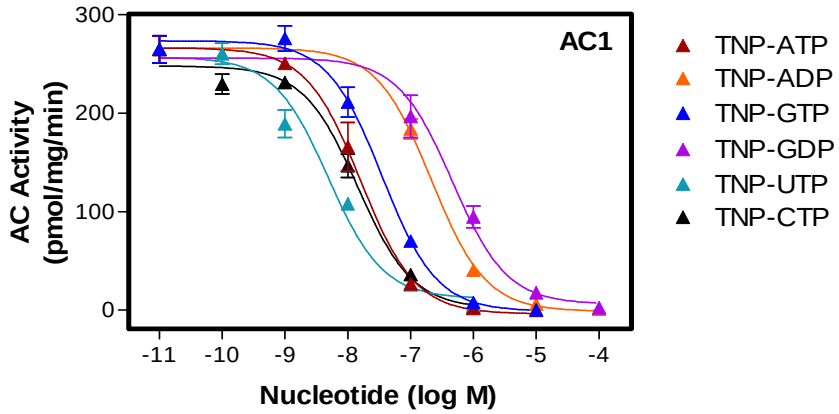
AC1
AC Activity (pmol/mg/min)
300
200
100
0
-11
-10
-9
-8
-7
-6
-5
-4
Nucleotide (log M)
TNP-ATP
TNP-ADP
TNP-GTP
TNP-GDP
TNP-UTP
TNP-CTP

B

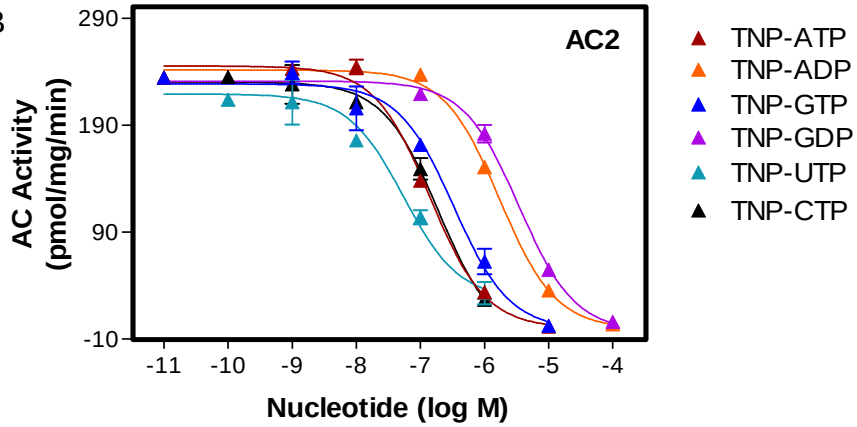
AC2
AC Activity (pmol/mg/min)
290
190
90
-10
-11
-10
-9
-8
-7
-6
-5
-4
Nucleotide (log M)
TNP-ATP
TNP-ADP
TNP-GTP
TNP-GDP
TNP-UTP
TNP-CTP

C

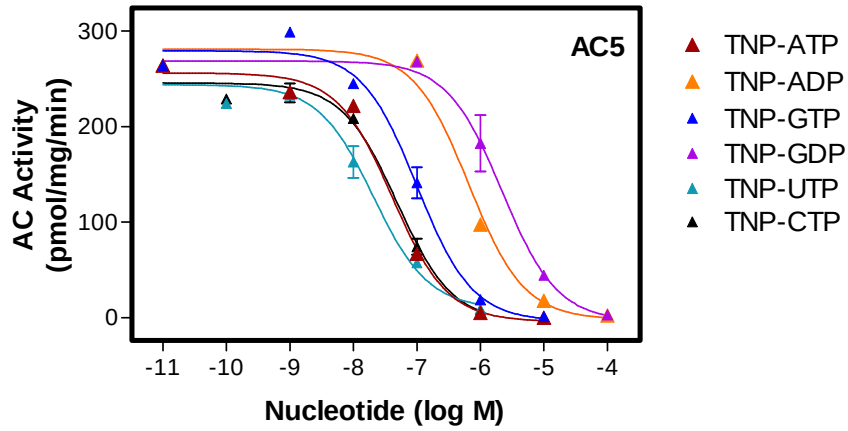
AC5
AC Activity (pmol/mg/min)
300
200
100
0
-11
-10
-9
-8
-7
-6
-5
-4
Nucleotide (log M)
TNP-ATP
TNP-ADP
TNP-GTP
TNP-GDP
TNP-UTP
TNP-CTP

2.4.3 Characterization of C1/C2 interaction with TNP-nucleotides by fluorescence spectroscopy.

TNP-nucleotides are environmentally sensitive probes with a λ_{max} emission at 550 nm and are weakly fluorescent in aqueous solutions (Hiratsuka 1982 and 2003). However, when placed in a hydrophobic environment, the quantum yield of TNP-nucleotides greatly increases making them suitable for studying the active site or nucleotide binding sites of proteins. TNP-nucleotide binding, particularly TNP-ATP, has been studied in relation to myosin, protein kinases, ATPases, enzymes and nucleotide binding proteins to monitor conformational changes in these systems (Grubmeyer and Penefsky, 1981; Cheng and Koland, 1996; Weber and Senior, 1996). In this study, we monitor the binding of TNP-nucleotides to C1/C2 catalytic subunits of mAC.

Fluorescence emission spectra from TNP-nucleotides were measured in the presence and absence of C1/C2 and DMB-FS. TNP-nucleotides show a fluorescence peak at 550 nm when excited at 405 nm. The experiments were conducted in the presence of either Mn^{2+} or Mg^{2+}. With the addition of C1/C2, the fluorescence increases 3-5 fold with TNP-ATP, TNP-GTP, TNP-CTP and TNP-UTP and 50-100-fold in the case of TNP-ADP and TNP-GDP indicating a strong interaction between the nucleotide and C1/C2 (Figure 2-6). Crystallographic studies of C1/C2 in complex with TNP-ATP (Mou et al.,

2006) have shown that the amino groups of TNP-ATP form hydrogen bonds with A409 on C1 and N1022 and M1025 on C2. It is possible that this interaction is responsible for the increase in fluorescence and stabilization of TNP-ATP in the hydrophobic pocket of C1/C2. In addition to a several-fold increase in fluorescence, we observed that the emission peak shifted to a shorter wavelength. The blue shift is due to the binding of the nucleotide in a strongly hydrophobic pocket formed by the C1/C2. The magnitude of the blue shift was different for different TNP-nucleotides. The adenine nucleotides (TNP-ATP and TNP-ADP) and the pyrimidine nucleotides (TNP-UTP and TNP-CTP) showed a larger blue shift when compared to the guanine nucleotides (TNP-GTP and TNP-GDP) (Table 2-4). Furthermore, there was a decrease in fluorescence observed when DMB-FS was added. This reduction in fluorescence was most apparent for the adenine and the pyrimidine nucleotides and least apparent with the guanine nucleotides (Figure 2-6).

All of the nucleotide binding experiments were carried out in the presence of Mn^{2+}. When $Mg^{2+}$was used in place of Mn^{2+}, only a small increase in TNP fluorescence was observed when C1/C2 was added (Figure 2-7) and the blue shift and decrease in TNP fluorescence upon addition of DMB-FS was less pronounced. Collectively, enzymatic, crystallographic and fluorescence data indicate that TNP-nucleotides bind to C1/C2 with higher affinity in the presence of Mn^{2+} than in the presence of Mg^{2+}.

In comparison with MANT-nucleotides, several similarities and differences in TNP binding to C1/C2 were observed. Differences in the magnitude of the blue shift and in fluorescence amplitude due to FS binding indicate that TNP-adenine nucleotides interact differently with C1/C2 compared to TNP-guanine nucleotides. These results are similar to those obtained for MANT-nucleotides where it has been observed that there are slight differences in the interaction of MANT-ATP and MANT-GTP with C1/C2 (Mou et al., 2006). Also, the apparent affinity of MANT and TNP-nucleotides for C1/C2 is higher in the presence of Mn^{2+} than Mg^{2+}. However, a reduction in TNP-nucleotide fluorescence due to FS binding is in striking contrast to MANT-nucleotides where an increase in fluorescence was observed with addition of DMB-FS. This difference is likely due to the fact that, although MANT-nucleotides and TNP-nucleotides bind to a common site in C1/C2, slight differences in their orientations may cause a change in the relative conformation of C1/C2 which in turn can influence the positioning of DMB-FS.

In order to measure the displacement of bound TNP-nucleotides from C1C2, a competitive P-site inhibitor of C1/C2, 2’ 5’ dd 3’ ATP, was added (Desaubry et al., 1996). 2’ 5’ dd 3’ ATP almost completely displaced TNP-ATP from the catalytic site of C1/C2 in a concentration dependent manner. However not all TNP-ATP was displaced indicating that some of the TNP-ATP interaction with C1/C2 is may be non-specific. It is also possible that the inhibited conformation of C1/C2 by TNP-ATP is somewhat different from the

conformation of C1/C2 in the presence of 2’5’ dd 3’ ATP. This incomplete displacement of bound TNP-ATP has also been observed in other nucleotide binding proteins (karkaria and Rosen, 1991; Liu and Sharom, 1997) and though it has been difficult to explain why this happens, it is still clear that TNP-ATP binding is largely reversible and competes with ATP or ATP analogs for binding to catalytic site of C1/C2.

Figure 2-6 Fluorescence emission spectra of TNP-nucleotides in the absence and presence of C1/C2 and DMB-FS

Fluorescence experiments were conducted as described in section 2.3.2. Steady state emission spectra of TNP-nucleotides were recorded at λ_{ex} = 405 nm (λ_{em} = 500 – 600 nm). Cuvettes containing 4 μM/25 μM of VCI/IIC2, 100 μM DMB-FS, and10 mM $MnCl_2$ were equilibrated for 10 min at 25˚C with 5 μM TNP-nucleotide in a final volume of 150 μl. Representative fluorescence emission spectra are shown for TNP-nucleotide alone (dashed line), TNP-nucleotide in the presence of C1/C2 (bold line), TNP-nucleotide in the presence of C1/C2 and DMB-FS (dotted line). Fluorescence intensities are measured as percentage of the maximum emission. Fluorescence recordings were analyzed using the spectrum package of the Cary Eclipse software. Similar results were obtained from 3 – 4 independent experiments.

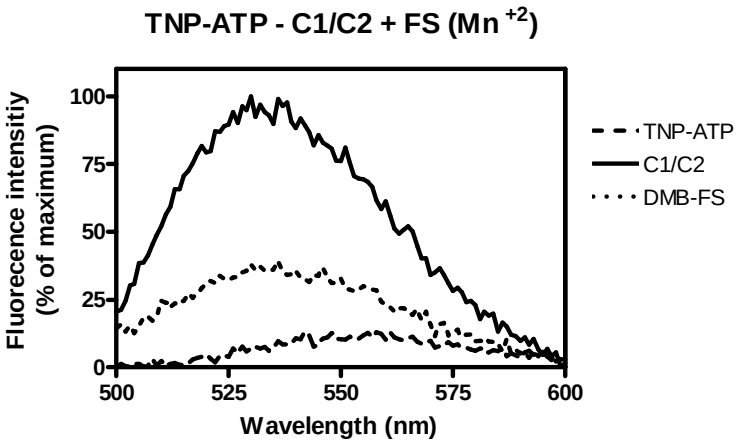
TNP-ATP - C1/C2 + FS (Mn +2)
Fluorecence intensitiy (% of maximum)
Wavelength (nm)
TNP-ATP
C1/C2
DMB-FS

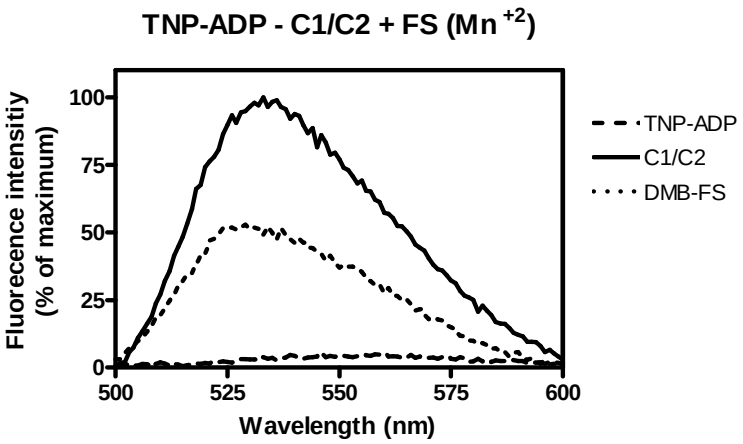
TNP-ADP - C1/C2 + FS (Mn +2)
Fluorecence intensitiy (% of maximum)
Wavelength (nm)
TNP-ADP
C1/C2
DMB-FS

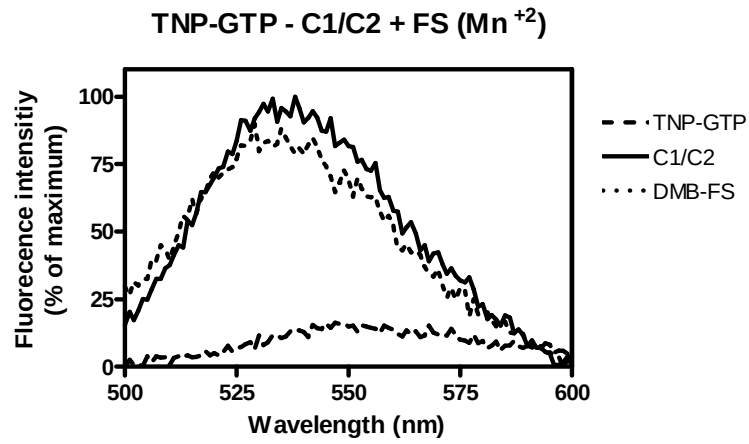
TNP-GTP - C1/C2 + FS (Mn +2)
Fluorecence intensitiy (% of maximum)
Wavelength (nm)
TNP-GTP
C1/C2
DMB-FS

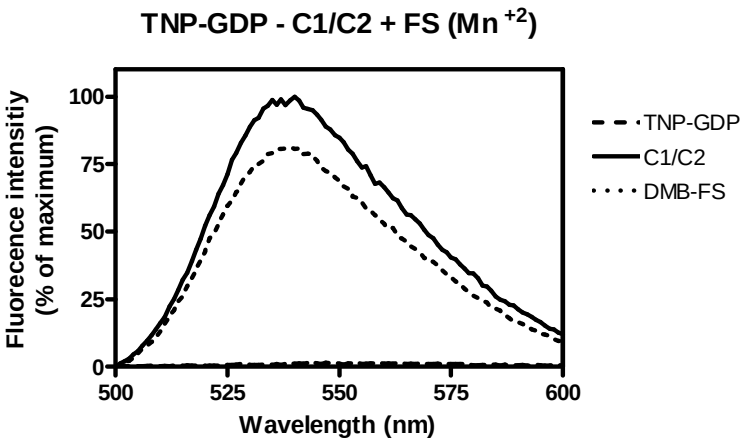
TNP-GDP - C1/C2 + FS (Mn +2)
Fluorecence intensitiy (% of maximum)
Wavelength (nm)
TNP-GDP
C1/C2
DMB-FS

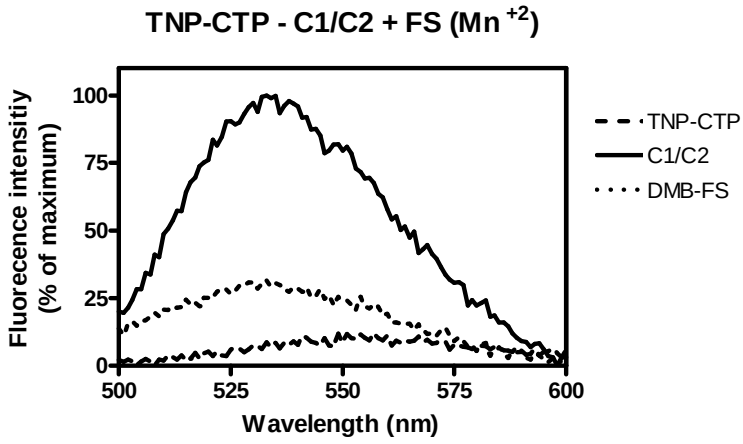
TNP-CTP - C1/C2 + FS (Mn +2)
Fluorecence intensitiy (% of maximum)
Wavelength (nm)
TNP-CTP
C1/C2
DMB-FS

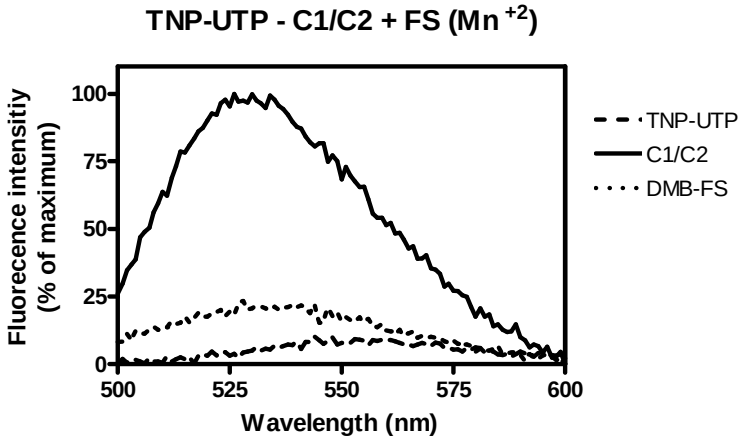
TNP-UTP - C1/C2 + FS (Mn +2)
Fluorecence intensitiy (% of maximum)
Wavelength (nm)
TNP-UTP
C1/C2
DMB-FS

Table 2-4 Blue shift of TNP-nucleotides in the presence of C1/C2

Fluorescence experiments were conducted as described in section 2.3.2. Steady state emission spectra of TNP-nucleotides were recorded at λ_{ex} = 405 nm (λ_{em} = 500 – 600 nm) in the presence of 4 μM/25 μM of VCI/IIC2, 5 μM TNP-nucleotide and 10 mM $MnCl_2$ in a final volume of 150 μl. The magnitude of the blue shift was calculated by the difference between the normal emission maxima (550 nm) and the emission maxima of TNP-nucleotides in the presence of C1/C2. Fluorescence recordings were analyzed using the spectrum package of the Cary Eclipse software. Similar results were obtained from 3 – 4 independent experiments.

Nucleotides	**Emission peak (nm)**	**Blue shift by (nm)**
TNP-ATP	531.5 ± 2	13.5 ± 2
TNP-ADP	532 ± 1	13 ± 1
TNP-GTP	537 ± 1	8 ± 1
TNP- GDP	540 ± 0	5 ± 0
TNP-CTP	532.5 ± 0.7	12.5 ± 0.7
TNP-UTP	528 ± 2.8	17 ± 2.8

Figure 2-7 A comparison of emission spectra of TNP-ATP and TNP-GTP in the absence and presence of C1/C2 and DMB-FS and with Mn^{2+} or Mg^{2+}

Fluorescence experiments were conducted as described in section 2.3.2. Steady state emission spectra of TNP-nucleotides were recorded at λ_{ex} = 405 nm (λ_{em} = 500 – 600 nm). Cuvettes containing 4 μM/25 μM of VCI/IIC2 and 100 μM DMB-FS in the presence of 10 mM $MnCl_2$ or 10 mM $MgCl_2$ were equilibrated for 10 min at 25˚C with 5 μM of TNP-nucleotide in a final volume of 150 μl. Representative fluorescence emission spectra are shown for TNP-nucleotide alone (dotted line), TNP-nucleotide in the presence of C1/C2 (bold line), TNP-nucleotide in the presence of C1/C2 and DMB-FS (dashed line). A and C are emission spectra of TNP-ATP and TNP-GTP respectively in the presence of Mn^{2+}. B and D are emission spectra of TNP-ATP and TNP-GTP in the presence of Mg^{2+}. Fluorescence intensities are shown in arbitrary units. Fluorescence recordings were analyzed using the spectrum package of the Cary Eclipse software. Similar results were obtained from 3 – 4 independent experiments.

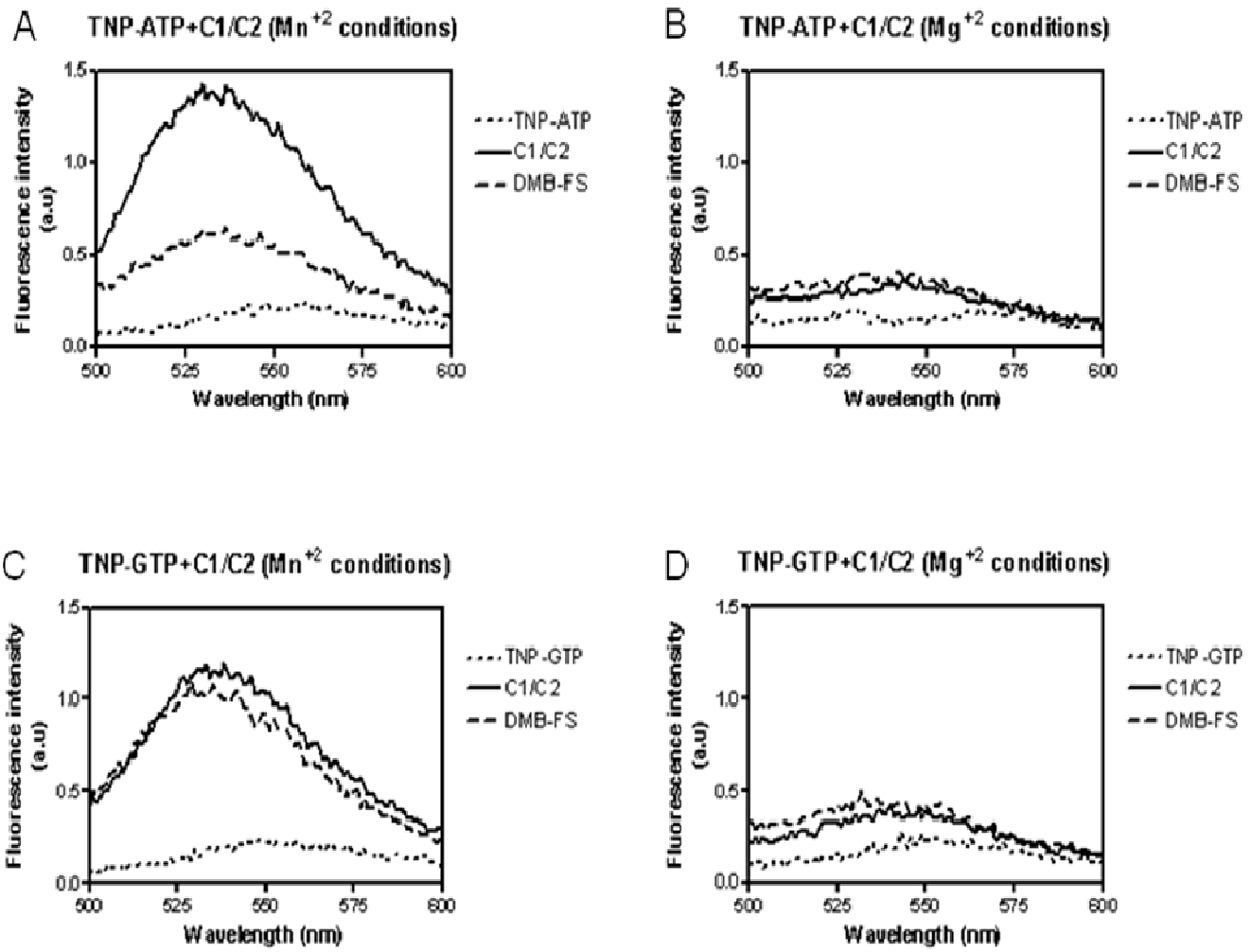
A
TNP-ATP+C1/C2 (Mn+2 conditions)
Fluorescence intensity (a.u)
Wavelength (nm)
TNP-ATP
C1/C2
DMB-FS
B
TNP-ATP+C1/C2 (Mg+2 conditions)
C
TNP-GTP+C1/C2 (Mn+2 conditions)
TNP-GTP
D
TNP-GTP+C1/C2 (Mg+2 conditions)

Figure 2-8 Displacement of bound TNP-ATP from C1/C2 by 2'5' dd 3' ATP

Fluorescence experiments were conducted as described in section 2.3.2. Steady state emission spectra of TNP-nucleotides were recorded at λ_{ex} = 405 nm (λ_{em} = 500 – 600 nm). Cuvettes containing 4 μM/25 μM of VCI/IIC2 in the presence of 10 mM $MnCl_2$ were equilibrated for 10 min at 25˚C with 5 μM TNP-ATP and concentrations of 2'5' dd 3' ATP varying from 10 mM to 200 mM. Panel A shows the kinetics of TNP-ATP displacement by 2'5' dd 3' ATP from C1/C2 in a concentration dependent manner. Fluorescence intensity in arbitrary units is measured as a function of time in min. Panel B shows the fluorescence emission spectra of TNP-ATP alone (dotted line), TNP-ATP in the presence of C1/C2 (bold line), TNP-ATP in the presence of C1/C2 and 2'5' dd 3' ATP (dashed line). Fluorescence intensities are shown as percentage of the emission maxima in the respective experiment. Fluorescence recordings were analyzed using the spectrum package of the Cary Eclipse software. Similar results were obtained from 3 – 4 independent experiments.

A 2' 5' dd 3' ATP : 10 – 200 mM

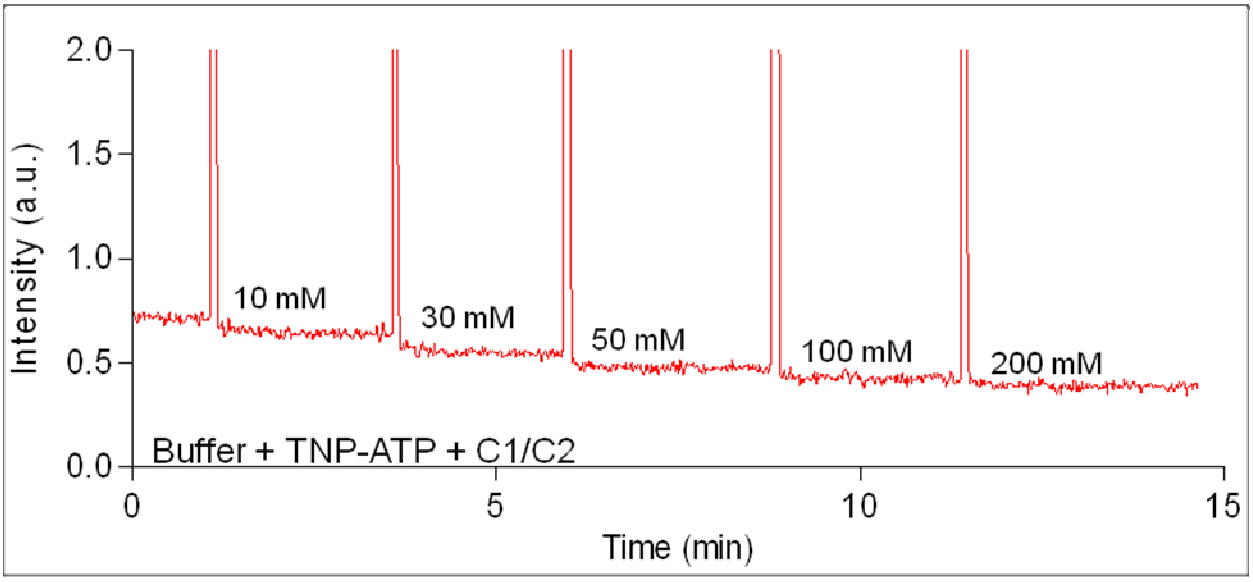

B

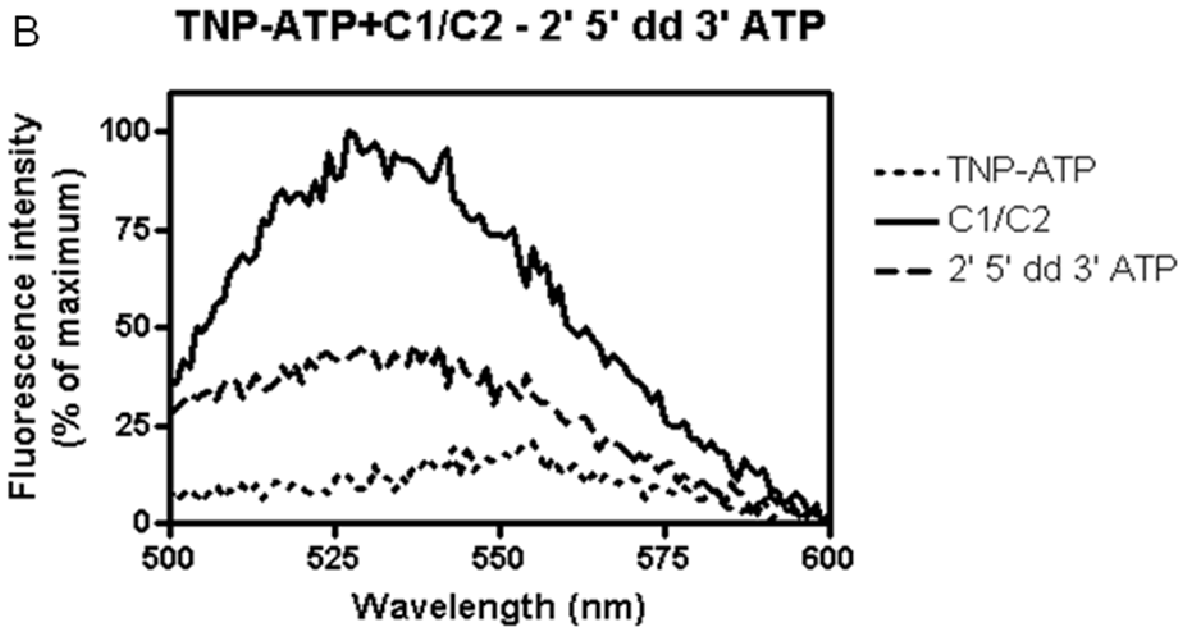

2.4.4. Molecular modeling of C1/C2 with bound TNP-ATP and TNP-GTP

To explore differences in the interaction of TNP-ATP and TNP-GTP with C1/C2, molecular docking experiments were carried out in collaboration with Dr. Mou (University of Texas Southwestern Medical Center). TNP-nucleotides were rigidly docked into the AC receptor derived from the crystal structure of C1/C2 in complex with TNP-ATP in the presence of $G\alpha_s$, FS and Mn^{2+}. Docking calculations were performed using GOLD 3.0.1 docking software (Table 2-5). TNP-GTP was the top-scoring structure (indicating the best-aligned TNP-nucleotide model) for docking into the catalytic site of C1/C2. This is surprising in view of the fact that TNP-ATP is the most potent inhibitor of C1/C2 as well as for holo-AC isoforms compared to TNP-GTP. However, it should be stressed that docking calculations were made using the C1/C2 structure in the presence of $G\alpha_s$ and FS. Therefore it must be noted that in the presence of $G\alpha_s$ and FS, there is no difference in the Ki values of TNP-ATP and TNP-GTP at inhibiting C1/C2 (Mou et al., 2006). Furthermore, though all four TNP-NTPs have relatively small differences in their docking scores, their scores are higher than their corresponding TNP-NDPs. This observation also corroborates with our data that TNP-NTPs are more potent compared to their respective TNP-NDPs. Also, TNP-UTP and TNP-CTP were docked with high scores indicating a strong interaction of these pyrimidine nucleotides with the catalytic site of C1/C2.

Using the rigid docking procedure, models of TNP-ATP and TNP-GTP docked into C1/C2 were generated. A superimposition of the TNP-ATP conformer with the TNP-GTP conformer indicates that though both these nucleotides occupy a common site in the catalytic pocket of C1/C2, small but significant differences in their interaction can be observed (Figure 2-9). It is observed that TNP-ATP and TNP-GTP interact with several amino acid residues on C1 and C2, i.e. N1025, K1065 and D1018. These results are similar to our crystallography data indicating that these amino acid residues are important for binding, stabilization and fluorescence of TNP-nucleotides (Mou et al., 2006). Though the TNP-groups and the phosphate chains of TNP-ATP and TNP-GTP are aligned along the same sub-sites in C1/C2, there is a small difference in the orientation of the purine moiety of TNP-ATP and TNP-GTP in the purine binding subsite. A closer look at the purine binding site of TNP-GTP docked in the C1/C2 catalytic core indicates that the N-2 atom of the guanine ring of TNP-GTP could hydrogen bond with D1018 (Figure 2-10). It is possible that these differences in TNP-ATP and TNP-GTP binding are responsible for the differences observed in fluorescence emission, interaction with FS and the blue shift. Collectively, our enzymatic, fluorescence and modeling data suggests that TNP-ATP and TNP-GTP interact differently at the catalytic site of C1/C2, nonetheless all TNP-NTPs are potent inhibitors of C1/C2 because C1/C2 has a spacious base binding pocket that can accommodate different purine and pyrimidine nucleotides.

Table 2-5 Docking scores of TNP-nucleotides with C1/C2. Comparison with K_i values obtained from AC inhibition assays under three different conditions

Docking studies were carried out in collaboration with Mou's group. The X-ray crystal structure of VC1:IIC2:FSK:Gα_s-GTPγS in complex with TNP-ATP and two Mn^{2+} ions (PDB ID:1GVD) was used as a model for docking other TNP-nucleotides. TNP-ATP and all the other atoms and associated residues within 5 Å of the ligand were used to define the active site of the mAC catalytic core complex. In the first step, modeled TNP-ATP was aligned to the one in the crystal structure. Using the rigid docking method, several conformations were generated and the most aligned TNP-ATP model was used since it closely mimicked the actual TNP-ATP in the crystal structure. Docking calculations were carried out using the GOLD 3.0.1 docking software. The Goldscore and Chemscore scoring functions were used to rank different binding poses. GOLD 3.0.1 GA parameter was used to encode the ligand hydrogen-bonding interactions. Docking scores are compared side-by-side with K_i values of TNP-nucleotides obtained from AC inhibition assays carried out under three different conditions.

Dock Ranking (Arbitrary score)	TNP-nucleotides	C1/C2 + Mn^{2+}+FS	C1/C2 + Mn^{2+}+FS+ $G\alpha_s$	C1/C2 + Mn^{2+}
1 (122.94)	TNP-GTP	430 ± 130	83 ± 22	6,420 ± 2000
2 (122.78)	TNP-CTP	110 ± 16	310 ± 76	8,570 ± 0
3 (111.05)	TNP-UTP	92 ± 9	92 ± 36	14,300 ± 0
4 (105.61)	TNP-ATP	100 ± 30	81 ± 27	3,300 ± 1400
5 (105.10)	TNP-GDP	8,100 ± 2,900	9,400 ± 1,800	15,200 ± 400
6 (95.43)	TNP-ADP	2,000 ± 660	1,300 ± 280	11,400 ± 5900
7 (78.47)	TNP-AMP	21,000 ± 7,200	17,000 ± 6,000	-

Figure 2-9 Models of superimposed TNP-ATP and TNP-GTP docked into the active site of C1/C2

Docking studies were carried out in collaboration with Mou's group. The X-ray crystal structure of VC1:IIC2:FSK:Gαs-GTPγS in complex with TNP-ATP and two Mn^{2+} ions (PDB ID:1GVD) was used as a model for docking other TNP-nucleotides. TNP-ATP and all the other atoms and associated residues within 5 Å of the ligand were used to define the active site of the mAC catalytic core complex. In the first step, modeled TNP-ATP was aligned to the one in the crystal structure. Using the rigid docking method, several conformations were generated and the most aligned TNP-ATP model was used since it closely mimicked the actual TNP-ATP in the crystal structure. Docking calculations were carried out using the GOLD 3.0.1 docking software.

A. Models of the superimposed inhibitor TNP-ATP and TNP-GTP docked to the active site of mAC catalytic core. Ligands are shown as stick models; carbon atoms are *gray* for TNP-ATP and *cyan* for TNP-GTP. Nitrogen, oxygen and phosphorus are shown in *blue*, *red*, and *green respectively*. Mn^{2+} ions are shown in *orange*. (The same coloring scheme is shown in B and in Figure 2-10). Important amino acid residues on C1/C2 are also indicated.

A

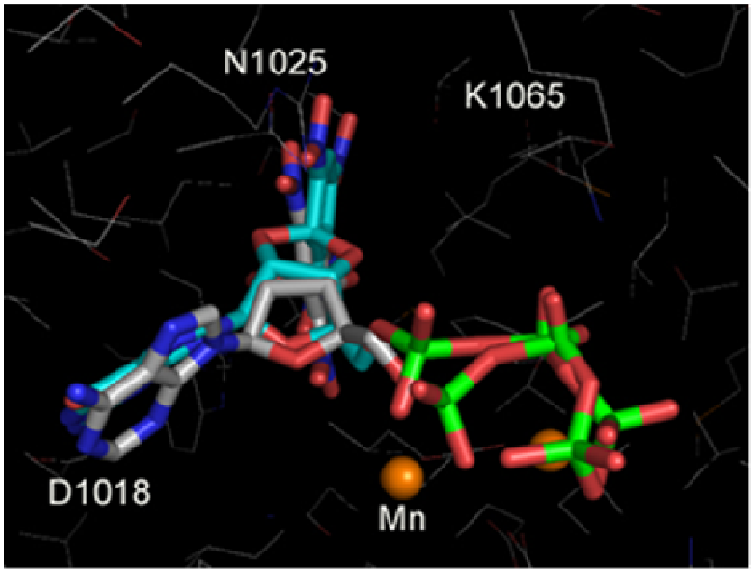

B. TNP-ATP and TNP-GTP docked to the active site of mAC catalytic core. The molecular surface was calculated using the program PYMOL (DeLano Scientific, San Carlos, CA).

B

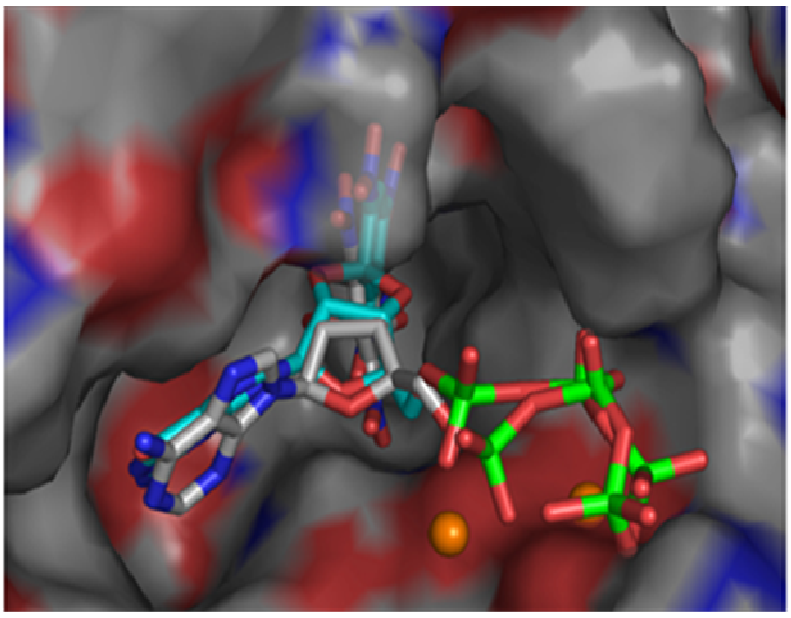

Figure 2-10 Model of the purine binding site of TNP-GTP docked into the C1/C2 catalytic core

Models of the purine binding sites of the superimposed inhibitor TNP-ATP and TNP-GTP docked to the active site of mAC catalytic core. Ligands are shown as stick models; carbon atoms are *gray* for TNP-ATP and *cyan* for TNP-GTP. Nitrogen, oxygen and phosphorus are shown in *blue*, *red*, and *green* respectively. Mn^{2+} ions are shown in *orange*. The N-2 of the guanine ring of TNP-GTP could form hydrogen bonds with D1018 of C2.

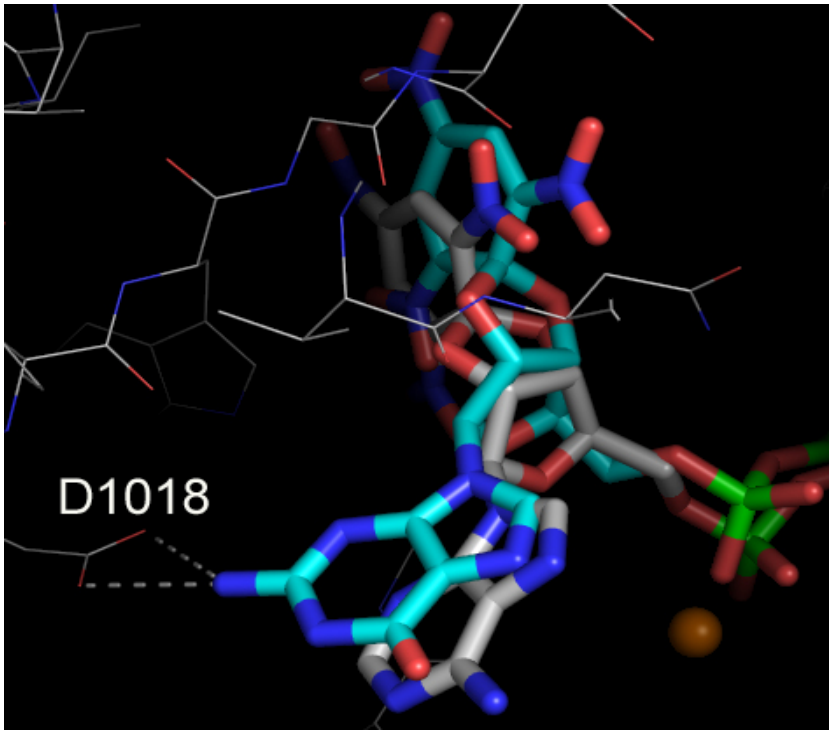

2.4.5 Effects of TNP-ATP and TNP-GTP on $G\alpha_s$ - and $G\alpha_i$ -protein mediated signaling

Heterotrimeric G-proteins ($\alpha\beta\gamma$) mediate signaling from GPCRs to effector systems such as ACs (Gilman, 1987; Birnbaumer et al., 1990). Ligand-bound GPCRs activate $G\alpha$ by catalyzing GTP binding to $G\alpha$. $G\alpha$–GTP then dissociates itself from GPCRs as well as from the $\beta\gamma$ subunits. After activation of ACs, $G\alpha$ returns to its ground state when its GTPase activity causes hydrolysis of GTP to release GDP and P_i. GTP and ATP bind to G-proteins with high and low affinity respectively (Gilman, 1987; Birnbaumer et al., 1990). To answer the question whether TNP-nucleotides bind to ACs with high specificity, we examined the functional effects of TNP-ATP and TNP-GTP on $G\alpha_s$ - and $G\alpha_i$ -protein mediated signaling.

Fusion proteins of β_2AR with $G\alpha_s$s, $G\alpha_s$L and $G\alpha_s$olf respectively and fusion proteins of FPR with $G\alpha_i$1, $G\alpha_i$2 and $G\alpha_i$3 respectively expressed in Sf9 cells, were studied as models to examine the effects of TNP-ATP and TNP-GTP. Steady-state GTPase activity was carried out and we found that TNP-ATP and TNP-GTP bind to $G\alpha_s$ - and $G\alpha_i$ -proteins with low affinities (Table 2-6). $G\alpha_s$ - and $G\alpha_i$ -proteins bound to TNP-ATP with several-fold lower affinity than TNP-GTP. Our results are not surprising in view of the fact that although G-proteins can bind ATP and GTP, the nucleotide binding pocket of $G\alpha$ is tight (Rens-Domiano and Hamm, 1995; Sprang, 1997; Zera et

al., 1996). Therefore, substitution of the TNP-group at the ribose moiety yielding TNP-ATP and TNP-GTP hinders proper binding of these nucleotides to the binding pocket of G-proteins and reduces the affinities of ATP and GTP for G proteins. Our results are very similar to those obtained for MANT-nucleotides. MANT-nucleotides are also highly specific for ACs and MANT-GTPγS and MANT-GppNHp bind to Gα_s - and Gα_i- with low affinities (Gille and Seifert, 2003). Collectively, it is clear that TNP-ATP and TNP-GTP are highly specific for ACs and bind to G-proteins with low affinity and therefore are almost ineffective at activating Gα.

Table 2-6 Affinities of TNP-ATP and TNP-GTP for $G\alpha_s$ - and $G\alpha_i$- proteins

GTPase assays were carried out as described previously (Gille et al., 2004) and in section 2.3.2. Briefly, assay tubes contained 10 μg of protein/tube (fusion proteins), increasing concentrations of TNP-ATP or TNP-GTP ranging from 1 μM to 1 mM, unlabelled ATP and GTP. Additionally assay tubes contained 10 μM isoproterenol and *N*-formyl-L-methionyl-L-leucyl-L-phenylalanine (FMLP) to fully activate β_2AR- $G\alpha_s$ and FPR- $G\alpha_i$ fusion proteins respectively. Data was analyzed by non-linear regression and 95% confidence intervals have been reported. K_i values are reported in μM unless otherwise noted.

	TNP-ATP	TNP-GTP
β_2AR- Gα_{sS}	53	12
95% confidence interval	27 to 104.8 mmol/l	7.9 -19
β_2AR- Gα_{sL}	164.1 mmol/l	17.4
95% confidence interval	90 to 296.2 mmol/l	8.8 - 34
β_2AR-Gα_{olf}	50	26
95% confidence interval	34 to 74	19 - 35
FPR- Gα_{i1}	332 mmol/l	12
95% confidence interval	244.5 mmol/l to 451 mmol/l	9.6 - 15
FPR- Gα_{i2}	263 mmol/l	6.9
95% confidence interval	112 mmol/l to 616.3 mmol/l	5.2 - 9.3
FPR- Gα_{i3}	329 mmol/l	10
95% confidence interval	174 mmol/l to 621 mmol/l	7.6 - 13

2.4.6 Effect of kinases on the potency of MANT and TNP-NDPs at inhibiting ACs

A nucleoside triphosphate (NTP) regenerating system was used previously in AC assays routinely conducted in our laboratory, primarily to help reduce the degradation of NTPs by phosphatases especially in membrane preparations thereby keeping the NTP concentrations constant (Johnson, 1980). It is possible that, in the presence of an NTP-regenerating system, MANT-NDPs and TNP-NDPs get phosphorylated to MANT-NTPs and TNP-NTPs in AC assays, therefore rendering both NDPs and NTPs equally potent.

To examine the effect of the NTP regenerating system on the potency of MANT and TNP-NDPs at inhibiting ACs, three different systems were used. Experiments were carried out with MANT-ADP, MANT-GDP, TNP-ADP and TNP-GDP using C1/C2 in the presence and absence of creatine kinase (CK) and nucleoside-diphosphate kinase (NDPK) respectively. CK catalyzes the phosphorylation of ADP to ATP in the presence of creatine phosphate (Tanzer and Gilwarg, 1959). With C1/C2, in the presence of CK, MANT-ADP and TNP-ADP are at least 19-fold and 2-fold respectively more potent than in the absence of CK indicating that MANT-ADP and TNP-ADP serve as good substrates for CK. However, no change was observed in the affinities of MANT-GDP and TNP-GDP for CK in the presence of C1/C2. This demonstrates that CK is highly selective towards adenine nucleotides and

can phosphorylate MANT-ADP and TNP-ADP to MANT-ATP and TNP-ATP respectively.

Sf9 cell membranes possess NDPK that catalyzes the conversion of NDP to NTP (Gille et al., 2002; Otero, 1990). With C1/C2, using NDPK, there was no change in the potencies of MANT- and TNP-NDPs indicating that these nucleotides do not serve as substrates for NDPK (Table 2-7).

Experiments were carried out with TNP-AMP, TNP-ADP and TNP-ATP using AC5 isoform in the presence and absence of a regenerating system consisting of pyruvate kinase and myokinase. Pyruvate kinase catalyzes the following reaction (Johnson, 1980):

phosphoenol pyruvate + ADP $\longrightarrow$ pyruvate + ATP

It was observed that TNP-AMP was at least 500-fold more potent in the presence of the regenerating system than in its absence (Table 2-8). TNP-ADP was found to be 50-fold more potent in the presence of the regenerating system. As expected, there was no change in the affinity of TNP-ATP in the presence and absence of the regenerating system. These data indicate that with AC5, pyruvate kinase catalyzes phosphorylation of both TNP-AMP and TNP-ADP to TNP-ATP, thus accounting for high potencies of TNP-AMP and TNP-ADP at inhibiting AC5. TNP-nucleotide analysis with AC5 was conducted in the absence of external NDPK-regenerating system. It must however be noted that though AC5 membrane preparations may contain

NDPK, the phosphorylation of TNP-AMP and TNP-ADP in this case is solely due to pyruvate kinase because we earlier observed that TNP- and MANT-nucleotides do not serve as substrates for NDPK.

Collectively, these studies indicate that in the presence of a regenerating system, the potencies of TNP and MANT-NDPs must be more carefully analyzed. Also, this furthers shows that both β and γ phosphates of TNP and MANT-nucleotides are important for inhibiting C1/C2 as well as holo-AC isoforms, reconfirming the importance of the phosphate groups in AC inhibition.

Table 2-7 Inhibitory effects of MANT-ADP, MANT-GDP, TNP-ADP and TNP-GDP on C1/C2 in the presence of a NTP-regenerating system

AC assays using C1/C2 with CPK and NDPK were conducted as described previously (Gille 2004) and in section 2.3.2. Assay tubes contained 7 nM VCI and 35 nM IIC2. For experiments with NDPK, concentrations of TNP and MANT-nucleotides ranging from 1 μM to 100 μM were added to the assay tubes before addition of the protein. For experiments with CPK, 1 nM to 100 μM concentrations of TNP and MANT-nucleotides were added in the assay tubes. One IU NDPK or CPK was added to half the reaction tubes and preincubated for 15 minutes before addition of C1/C2. Reactions were conducted in the presence of 45 nM $G\alpha_s$-GTPγS and 100 μM FS. Saturated curvesd for Inhibition and 95% confidence intervals were analyzed by nonlinear regression using Prism 4.0 software (Graphpad, San Deigo, CA). K_i values are expressed in μM and numbers with +++ sign indicate more potency.

	Control	CPK	Control	NDPK
MANT-ADP	3.4 (+)	0.18 (+++)	3.8 (+)	4.3 (+)
95% confidence interval	1.6 – 6.8	0.93 – 0.36	1.5 – 9.2	2.7 – 6.9
MANT-GDP	1.27 (+)	2.6 (+)	1.02 (+)	1.67 (+)
95% confidence interval	0.3 – 4.05	1.8 – 3.6	0.4 – 2.5	0.85 – 3.3
TNP-ADP	1.09 (+)	0.516 (+++)	0.51 (+)	1.9 (+)
95% confidence interval	0.5 – 2.09	0.29 – 0.92	0.2 – 1.2	1.5 – 2.4
TNP-GDP	2.7 (+)	2.6 (+)	3.3 (+)	5.6 (+)
95% confidence interval	1.4 – 5.1	1.1 – 5.8	2.5 – 4.2	2.7 – 12

Table 2-8 Inhibitory effects of TNP-AMP, TNP-ADP and TNP-ATP on AC5 in the presence of an NTP-regenerating system

AC assay was carried out as described previously (Gille et al., 2004) and in section 2.3.2. Each assay tube contained 32 μg of AC5 protein, 10 μM GTPγS, 40 μM ATP, 100 μM FS, 5 mM $MnCl_2$ and 100 μM cAMP. TNP-nucleotides at final concentrations varying from 0.1 nM to 1 μM were added to the assay tubes. Additionally, the reaction mix contained an NTP-regenerating system consisting of 2.7 mM mono(cyclohexyl)ammonium phosphoenol pyruvate, 0.125 IU pyruvate kinase and 1 IU myokinase. Experiments were performed in duplicate and data were analyzed by non-linear regression. K_i values are expressed in nM and numbers with +++ sign indicate more potency.

	Control	**Pyruvate kinase**
TNP-AMP	4784 (+)	9.7 (+++)
TNP-ADP	367 (++)	4.4 (+++)
TNP-ATP	3.7 (+++)	11 (+++)

2.5 Conclusions

Enzymatic, fluorescence and molecular modeling studies of ACs with TNP-nucleotides as probes reveal that TNP-nucleotides are a novel class of potent AC isoform-selective inhibitors. A systematic inhibitor analysis of purified C1/C2 with TNP-nucleotides under various conditions confirm that ACs have a broad base specificity and can accommodate different purine and pyrimidine nucleotides. Our studies also show that TNP-NTPs are more potent compared to their respective NDPs and NMPs, highlighting the role of the $\beta-$ and the γ-phosphate in AC inhibition. Furthermore, we observed that FS and $G\alpha_s$ bring about a dramatic change in the conformation of C1/C2 thus allowing TNP-nucleotides to bind and inhibit AC activity much more potently than in the absence of the activators. In the absence of FS and $G\alpha_s$, it was observed that TNP-nucleotides weakly bind to C1/C2 bringing us back to the question: what the native conformation of C1/C2 is? Since the crystal structure of C1/C2 in the absence of FS and $G\alpha_s$ is not yet available, future biochemical and crystallographic studies in this area of AC research must be carried out to understand the exact conformational change in C1/C2 that occurs upon FS and $G\alpha_s$ binding.

Enzymatic studies also highlight an important role of TNP-nucleotides in isoform-selective inhibition. TNP-ATP and TNP-UTP are the most potent inhibitors of the AC1 isoform. For the AC2 isoform, we have observed that the

pyrimidine nucleotides TNP-UTP and TNP-CTP are more potent compared to purine nucleotides. As indicated earlier that AC2 may have a smaller catalytic pocket compared to AC5, we predict that pyrimidine TNP-nucleotides are better at inhibiting AC2 due to their smaller size compared to purine TNP-nucleotides. AC1 and AC2 play an important role in learning, memory and synaptic plasticity (Wu et al., 1995; Jourdan et al., 2001). Therefore, the inhibitory properties of TNP-nucleotides can be very important for isoform-specific inhibition of AC1 and AC2.

TNP-ATP is the most potent inhibitor of AC5 known so far. Intriguingly, the AC5 KO in mouse reduces development of cardiac failure and enhances longevity (Okumura et al., 2003; Yan et al., 2007). Thus, AC5 inhibitors may become of therapeutic relevance in the future. We have also observed that TNP-nucleotides have a higher specificity for holo-AC isoforms compared to purified C1/C2 indicating an important role for transmembrane domains in AC catalysis. Collectively, since both purine and pyrimidine TNP-nucleotides display isoform-selective inhibition, they serve as excellent starting points for development of potent isoform-specific AC inhibitors.

We have also observed that TNP-nucleotides are highly specific to some kinases. Our data clearly show that TNP-nucleotides serve as substrates for creatine kinase and pyruvate kinase. Since these enzymes are expressed in

several tissues, TNP-nucleotides can be used as prodrugs of AC inhibitors and can be valuable in studying AC isoform-selective inhibition in intact cells.

Fluorescence spectroscopic studies showed an enhancement in TNP-nucleotide fluorescence when bound to C1/C2 confirming that TNP-nucleotides bind to a hydrophobic/non-polar site in the C1/C2 catalytic core. Our fluorometric data fit with our crystallographic studies carried out earlier showing that TNP-nucleotides interact and form hydrogen bonds with important amino acid residues on C1 and C2. This interaction of TNP-nucleotides with C1 and C2 is responsible for stabilization and fluorescence of TNP-nucleotides in the C1/C2 catalytic core. Furthermore, fluorescence studies also revealed differences between the interactions of TNP and MANT-nucleotides with C1/C2. Our data clearly show that FS binding to C1/C2 causes a decrease in TNP fluorescence and an increase in MANT fluorescence indicating their differential interaction with C1/C2. This observation is also supported by our crystallographic studies showing that MANT-nucleotides are stabilized by interacting with a completely different set of amino acid residues on C1 and C2 compared to TNP-nucleotides. Additionally, our fluorescence studies have highlighted differences between TNP-ATP and TNP-GTP, especially differences in their binding to C1/C2 and in the blue shift in fluorescence. This further allowed us to explore their differences through molecular modeling. The modeling data revealed that

there is a small difference in the orientation of TNP-ATP and TNP-GTP and we predict that TNP-GTP but not TNP-ATP may hydrogen bond with D1018.

Finally, these studies identified TNP-nucleotides as potent isoform-selective inhibitors similar yet different from MANT-nucleotides and as important probes to study conformational changes in ACs. It is anticipated that TNP-nucleotides will be used as valuable tools in understanding regulation of ACs and will aid in identification and development of cell permeable isoform-selective inhibitors.

References

Birnbaumer L, Abramowitz J and Brown AM (1990) Receptor-effector coupling by G proteins. *Biochim Biophys Acta* **1031**(2):163-224.

Broglie KE and Takahashi M (1983) Fluorescence studies of threonine-promoted conformational transitions in aspartokinase I using the substrate analogue 2'(3')-*O*-(2,4,6-trinitrophenyl)adenosine 5'-triphosphate. *J Biol Chem* **258**(21):12940-12946.

Cheng K and Koland JG (1996) Nucleotide binding by the epidermal growth factor receptor protein-tyrosine kinase. Trinitrophenyl-ATP as a spectroscopic probe. *J Biol Chem* **271**(1):311-318.

De Vries L, Mousli M, Wurmser A and Farquhar MG (1995) GAIP, a protein that specifically interacts with the trimeric G protein $G\alpha_{i3}$, is a member of a protein family with a highly conserved core domain. *Proc Natl Acad Sci U S A* **92**(25):11916-11920.

Desaubry L, Shoshani I and Johnson RA (1996) 2',5'-Dideoxyadenosine 3'-polyphosphates are potent inhibitors of adenylyl cyclases. *J Biol Chem* **271**(5):2380-2382.

Dessauer CW and Gilman AG (1997) The catalytic mechanism of mammalian adenylyl cyclase. Equilibrium binding and kinetic analysis of P-site inhibition. *J Biol Chem* **272**(44):27787-27795.

Feinstein PG, Schrader KA, Bakalyar HA, Tang WJ, Krupinski J, Gilman AG and Reed RR (1991) Molecular cloning and characterization of a Ca^{2+}/calmodulin-insensitive adenylyl cyclase from rat brain. *Proc Natl Acad Sci U S A* **88**(22):10173-10177.

Gille A, Liu HY, Sprang SR and Seifert R (2002) Distinct interactions of GTP, UTP, and CTP with G_s proteins. *J Biol Chem* **277**(37):34434-34442.

Gille A, Lushington GH, Mou TC, Doughty MB, Johnson RA and Seifert R (2004) Differential inhibition of adenylyl cyclase isoforms and soluble guanylyl cyclase by purine and pyrimidine nucleotides. *J Biol Chem* **279**(19):19955-19969.

Gille A and Seifert R (2003) 2'(3')-*O*-(N-methylanthraniloyl)-substituted GTP analogs: a novel class of potent competitive adenylyl cyclase inhibitors. *J Biol Chem* **278**(15):12672-12679.

Gilman AG (1987) G proteins: transducers of receptor-generated signals. *Annu Rev Biochem* **56**:615-649.

Grubmeyer C and Penefsky HS (1981) The presence of two hydrolytic sites on beef heart mitochondrial adenosine triphosphatase. *J Biol Chem* **256**(8):3718-3727.

Hanoune J and Defer N (2001) Regulation and role of adenylyl cyclase isoforms. *Annu Rev Pharmacol Toxicol* **41**:145-174.

Hiratsuka T (1982) Biological activities and spectroscopic properties of chromophoric and fluorescent analogs of adenine nucleoside and nucleotides, 2',3'-*O*-(2,4,6-trinitrocyclohexadienylidene) adenosine derivatives. *Biochim Biophys Acta* **719**(3):509-517.

Hiratsuka T (2003) Fluorescent and colored trinitrophenylated analogs of ATP and GTP. *Eur J Biochem / FEBS* **270**(17):3479-3485.

Houston C, Wenzel-Seifert K, Burckstummer T and Seifert R (2002) The human histamine H2-receptor couples more efficiently to Sf9 insect cell Gs-proteins than to insect cell G_q-proteins: limitations of Sf9 cells for the analysis of receptor/G_q-protein coupling. *J Neurochem* **80**(4):678-696.

Jameson DM and Eccleston JF (1997) Fluorescent nucleotide analogs: synthesis and applications. *Methods Enzymol* **278**:363-390.

Johnson RA (1980) Stimulatory and inhibitory effects of ATP-regenerating systems on liver adenylate cyclase. *J Biol Chem* **255**(17):8252-8258.

Johnson RA, Yeung SM, Stubner D, Bushfield M and Shoshani I (1989) Cation and structural requirements for P site-mediated inhibition of adenylate cyclase. *Mol Pharmacol* **35**(5):681-688.

Jourdan KB, Mason NA, Long L, Philips PG, Wilkins MR and Morrell NW (2001) Characterization of adenylyl cyclase isoforms in rat peripheral pulmonary arteries. *Am J Physiol Lung Cell Mol Physiol* **280**(6):L1359-1369.

Karkaria CE and Rosen BP (1991) Trinitrophenyl-ATP binding to the ArsA protein: the catalytic subunit of an anion pump. *Arch Biochem Biophys* **288**(1):107-111.

Liu R and Sharom FJ (1997) Fluorescence studies on the nucleotide binding domains of the P-glycoprotein multidrug transporter. *Biochemistry* **36**(10):2836-2843.

Mou TC, Gille A, Fancy DA, Seifert R and Sprang SR (2005) Structural basis for the inhibition of mammalian membrane adenylyl cyclase by 2 '(3')-*O*-(N-Methylanthraniloyl)-guanosine 5 '-triphosphate. *J Biol Chem* **280**(8):7253-7261.

Mou TC, Gille A, Suryanarayana S, Richter M, Seifert R and Sprang SR (2006) Broad specificity of mammalian adenylyl cyclase for interaction with 2',3'-substituted purine- and pyrimidine nucleotide inhibitors. *Mol Pharmacol* **70**(3):878-886.

Mouillac B, Caron M, Bonin H, Dennis M and Bouvier M (1992) Agonist-modulated palmitoylation of β2-adrenergic receptor in Sf9 cells. *J Biol Chem* **267**(30):21733-21737.

Okumura S, Takagi G, Kawabe J, Yang G, Lee MC, Hong C, Liu J, Vatner DE, Sadoshima J, Vatner SF and Ishikawa Y (2003) Disruption of type 5 adenylyl cyclase gene preserves cardiac function against pressure overload. *Proc Natl Acad Sci U S A* **100**(17):9986-9990.

Otero AD (1990) Transphosphorylation and G protein activation. *Biochem Pharmacol* **39**(9):1399-1404.

Pinto C, Papa D, Hubner M, Mou TC, Lushington GH and Seifert R (2008) Activation and inhibition of adenylyl cyclase isoforms by forskolin analogs. *J Pharmacol Exp Ther* **325**(1):27-36.

Rens-Domiano S and Hamm HE (1995) Structural and functional relationships of heterotrimeric G-proteins. *Faseb J* **9**(11):1059-1066.

Seifert R, Wenzel-Seifert K, Lee TW, Gether U, Sanders-Bush E and Kobilka BK (1998) Different effects of $G_s\alpha$ splice variants on β2-adrenoreceptor-mediated signaling. The β2-adrenoreceptor coupled to the long splice variant of $G_s\alpha$ has properties of a constitutively active receptor. *J Biol Chem* **273**(18):5109-5116.

Sprang SR (1997) G protein mechanisms: insights from structural analysis. *Annu Rev Biochem* **66**:639-678.

Stewart RC, VanBruggen R, Ellefson DD and Wolfe AJ (1998) TNP-ATP and TNP-ADP as probes of the nucleotide binding site of CheA, the histidine protein kinase in the chemotaxis signal transduction pathway of Escherichia coli. *Biochemistry* **37**(35):12269-12279.

Sunahara RK, Dessauer CW and Gilman AG (1996) Complexity and diversity of mammalian adenylyl cyclases. *Annu Rev Pharmacol Toxicol* **36**:461-480.

Sunahara RK, Dessauer CW, Whisnant RE, Kleuss C and Gilman AG (1997) Interaction of $G_s\alpha$ with the cytosolic domains of mammalian adenylyl cyclase. *J Biol Chem* **272**(35):22265-22271.

Tang WJ, Krupinski J and Gilman AG (1991) Expression and characterization of calmodulin-activated (type I) adenylylcyclase. *J Biol Chem* **266**(13):8595-8603.

Tanzer ML and Gilvarg C (1959) Creatine and creatine kinase measurement. *J Biol Chem* **234**:3201-3204.

Taussig R, Quarmby LM and Gilman AG (1993) Regulation of purified type I and type II adenylylcyclases by G protein beta gamma subunits. *J Biol Chem* **268**(1):9-12.

Taussig R, Tang WJ and Gilman AG (1994) Expression and purification of recombinant adenylyl cyclases in Sf9 cells. *Methods Enzymol* **238**:95-108.

Tesmer JJ, Sunahara RK, Fancy DA, Gilman AG and Sprang SR (2002) Crystallization of complex between soluble domains of adenylyl cyclase and

activated $G_s\alpha$. *Methods Enzymol* **345**:198-206.

Tesmer JJ, Sunahara RK, Gilman AG and Sprang SR (1997) Crystal structure of the catalytic domains of adenylyl cyclase in a complex with $G_s\alpha$.GTPγS. *Science,NY* **278**(5345):1907-1916.

Tesmer JJ, Sunahara RK, Johnson RA, Gosselin G, Gilman AG and Sprang SR (1999) Two-metal-Ion catalysis in adenylyl cyclase. *Science, NY* **285**(5428):756-760.

Thomas PJ, Shenbagamurthi P, Ysern X and Pedersen PL (1991) Cystic fibrosis transmembrane conductance regulator: nucleotide binding to a synthetic peptide. *Science, NY* **251**(4993):555-557.

Weber J and Senior AE (1996) Binding and hydrolysis of TNP-ATP by Escherichia coli F1-ATPase. *J Biol Chem* **271**(7):3474-3477.

Wenzel-Seifert K, Arthur JM, Liu HY and Seifert R (1999) Quantitative analysis of formyl peptide receptor coupling to $g_i\alpha_1$, $g_i\alpha_2$, and $g_i\alpha_3$. *J Biol Chem* **274**(47):33259-33266.

Wu ZL, Thomas SA, Villacres EC, Xia Z, Simmons ML, Chavkin C, Palmiter RD and Storm DR (1995) Altered behavior and long-term potentiation in type I adenylyl cyclase mutant mice. *Proc Natl Acad Sci U S A* **92**(1):220-224.

Yan L, Vatner DE, O'Connor JP, Ivessa A, Ge H, Chen W, Hirotani S, Ishikawa Y, Sadoshima J and Vatner SF (2007) Type 5 adenylyl cyclase disruption increases longevity and protects against stress. *Cell* **130**(2):247-258.

Zera EM, Molloy DP, Angleson JK, Lamture JB, Wensel TG and Malinski JA (1996) Low affinity interactions of GDPβS and ribose- or phosphoryl-substituted GTP analogues with the heterotrimeric G protein, transducin. *J Biol Chem* **71**(22):12925-12931.

Chapter 3: Biochemical and Biophysical analysis of the C1 and C2 catalytic subunits of Mammalian Adenylyl Cyclase

3.1 INTRODUCTION

Mammalian adenylyl cyclases (mACs) that catalyze the conversion of ATP to cAMP play an important role in the G-protein signaling cascade (Tang and Hurley, 1998; Ishikawa and Homcy, 1997; Hanoune and Defer, 2001). Upon activation of G-protein coupled receptors (GPCRs) by extracellular signals such as hormones or neurotransmitters, GPCRs transmit signals to G-proteins which in turn activate ACs thus producing cAMP (Cooper et al., 1995; Defer et al., 2000). Though originally known to act as monomers, it is now well accepted that GPCRs can form dimers or oligomers as part of their normal function (Jordan and Devi, 1999; Marshall, 2001; George et al., 2002). However it is not clearly known if ACs can dimerize or oligomerize and if this dimerization of ACs could play an important role in the complex cAMP signaling system.

Nine different isoforms of mAC have been characterized (AC1-9) and all the isoforms share a common topology (Sunahara et al., 1996; Sunahara and Taussig, 2002). The AC molecule typically possesses two transmembrane domains, TM1 and TM2, and two associated cytoplasmic

domains, C1 and C2 respectively (Zhang et al., 1997; Tesmer et al., 1997). The C1 and C2 domains share a high degree of sequence homology and are further divided into C1a and C1b, C2a and C2b regions respectively. C1a and C2a together form the catalytic core of the enzyme as well as sites for activation by $G\alpha_s$ and FS. Previous studies have shown that C1a or C2a are catalytically inactive but when expressed separately and then mixed together, they retain the properties of the original enzyme such as conversion of ATP to cAMP and activation by $G\alpha_s$ and FS (Tang and Gilman, 1995; Whisnant et al., 1996; Dessauer et al., 1998).

Hydrodynamic properties of holo-ACs studied using gel filtration and density-gradient ultracentrifugation showed that ACs have a molecular weight of ~220 kDa, though the normal molecular weight is ~120 kDa (Haga et al.,1977). This indicated that ACs may form dimeric complexes or higher order assemblies with other signaling proteins. Target-size analysis of ACs in hepatic membranes demonstrated that ACs in both the ground (no activators bound) and active state can form multimeric complexes with regulatory proteins such as $G\alpha_s$ as well as receptor proteins (Schlegel et al.,1979). Several independent studies using a variety of techniques have demonstrated that ACs may exist in dimeric or oligomeric forms interacting with G-proteins and GPCRs (Neer et al., 1984; Yeager et al., 1985; Smigel, 1986). In addition, ACs belong to the ABC (ATP-binding cassette) transporter protein family. Several members of this family such as glutamate transporter and

cystic fibrosis transmembrane conductance regulator (CFTR), are multimeric in their active forms (Krupinski et al., 1989; Haugeto et al., 1996; Wang et al., 2000). Coimmunoprecipitation and fluorescence resonance energy transfer (FRET) evidence suggests that ACs may undergo dimerization via their transmembrane domains, TM1 and TM2 (Gu et al., 2001 and 2002; Cooper and Crossthwaithe, 2006). The transmembrane domains are thought to function as sites for regulation and oligomerization and the catalytic domains constitute the site for AC enzyme activity (Figure 3-1). Baragli et al., (2008) have shown that AC2 and AC5 can form heterodimers and this AC2/5 complex retains all the properties of the original enzyme including activation by $G\alpha_s$ and forskolin. In addition, there is also growing evidence that ACs in other organisms dimerize *via* their catalytic domains. FRET measurements of *Bordetella pertussis* AC toxin have revealed their oligomeric behavior in solution (Lee et al., 2005). In *Mycobacterium tuberculosis*, Rv1625c is an AC enzyme that shows a high degree of sequence similarity to mammalian ACs (Shenoy et al., 2003). The Rv1625c AC is a transmembrane protein with a single cytosolic catalytic domain and is known to homodimerize to give rise to the functionally active form of the enzyme with two catalytic centers. In simpler organisms such as *Trypanosoma brucei*, AC dimerization occurs through their catalytic domains (Beiger and Essen, 2001). Therefore, it cannot be ruled out that catalytic domains in mACs also play an important role in dimerization.

Based on sequence similarity between the C1 and C2 catalytic subunits of mAC, a crystal structure of C2 homodimer was determined and used as a model for the AC catalytic core (Zhang et al., 1997). These studies suggest that dimerization of monomers must occur for catalysis, a process further promoted by FS. FS is thought to play a key role in bringing the two monomers together as well as in interacting with the active site of the enzyme. Using gel filtration and sedimentation equilibrium centrifugation approaches, Sunahara and group (1997) have shown that C1 and C2 subunits of mammalian AC may individually exist as homodimers in solution. However, when mixed together they found that C1 and C2 subunits have a higher propensity to form heterodimers in a manner that is dependent on the presence of FS and $G\alpha_s$ (Sunahara et al., 1997). Earlier studies have also shown that C1 homodimers may exist but they are catalytically inactive. In contrast, a C2 homodimer was shown to have very low catalytic activity and could bind ATP analogues (Mitterauer et al., 1998).

This chapter primarily focuses on analyzing the nucleotide binding and catalytic properties of C1 (AC5, C1a region) and C2 (AC2, C2a region) domains of mammalian AC using a variety of approaches such as fluorescence studies, enzymatic assays, native gel electrophoresis and molecular modeling to understand the dimerizing/oligomerizing properties of C1 and C2.

Figure 3-1 A schematic representation of intra and inter-molecular heterodimerization between two AC8 isoforms.

Shown here are two AC8 isoforms with transmembrane domains as TM1 and TM2 and cytosolic domains as C1a, C1b, C2a and C2b. C1a and C2a form the catalytic core of the enzyme (from Cooper and Crossthwaithe, 2006). FRET analysis also showed that AC8 is capable of intra (between TM1 and TM2 of the same molecule) and inter-molecular heterodimerization (between TM2 and TM2 of two AC8 isoforms).

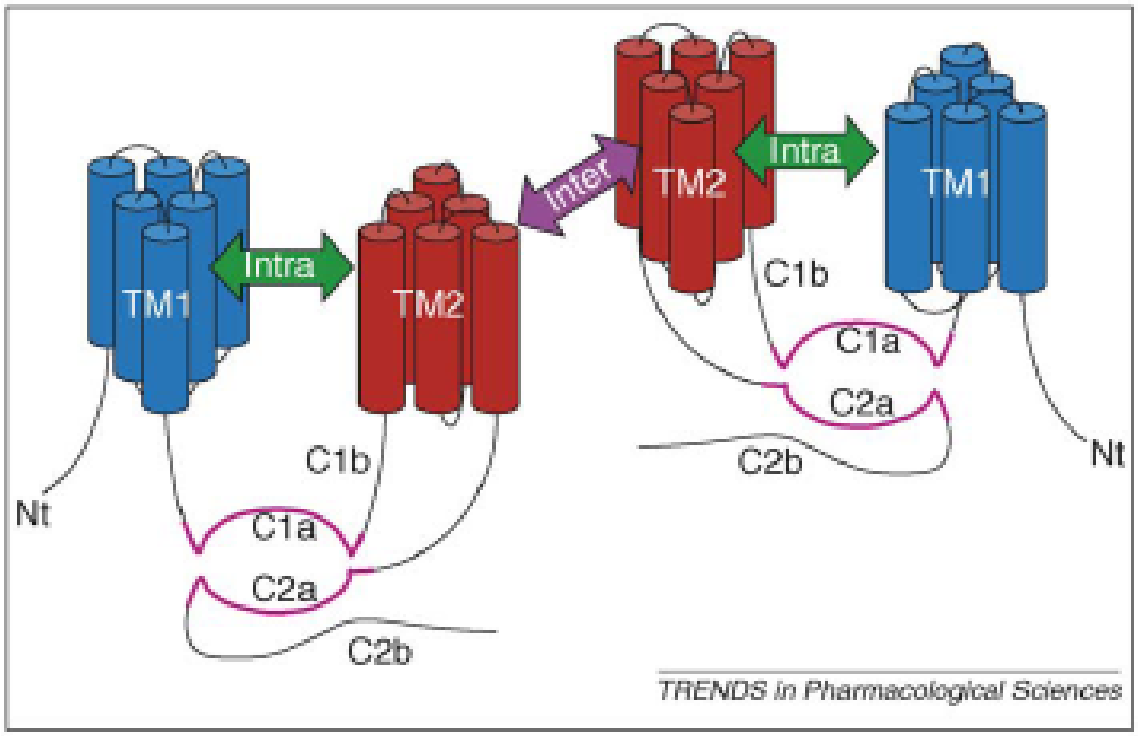

3.2 Specific aims and hypothesis

ACs dimerize *via* their transmembrane domains, however, we still do not know if the catalytic subunits C1 and C2 play an important role in this dimerization. The research described in this chapter aims at answering the following questions.

1. Do C1 and C2 subunits homodimerize in solution?

2. If C1 and C2 homodimerize, are they catalytically active?

3. If C1 and C2 homodimerize, do they have a functional nucleotide binding site?

4. If C1 and C2 homodimerize, what is the possible physiological role of this dimerization event *in vivo*?

Using MANT and TNP-nucleotides as probes, we have studied the binding, conformational changes and catalytic activities of C1 and C2. Based on the available evidence, we hypothesize that C1 and C2 homodimerize and that the homodimerization may have an important functional significance in AC regulation since production and regulation of cAMP is central to several important signaling pathways.

3.3 Materials and Methods

3.3.1 Materials

C1, C2 and $G\alpha_s$-GTPγS were kindly donated by TC.Mou and S.Sprang (University of Texas Southwestern Medical Center, Dallas, TX). FS and DMB-FS were obtained from Sigma and Calbiochem respectively. TNP-nucleotides and MANT-nucleotides were obtained from Jena Bioscience (Jena, Germany) (Figure 2-2 and 3-2). [α-^{32}P]ATP (3000 Ci/mmol) was obtained from Perkin Elmer Life Sciences. Novex® Tris-Glycine native gels (4-12%) and SDS-PAGE gels were obtained from Invitrogen. Sources of all other materials have been indicated in chapter 2.

Figure 3-2 Structure of MANT-nucleotides

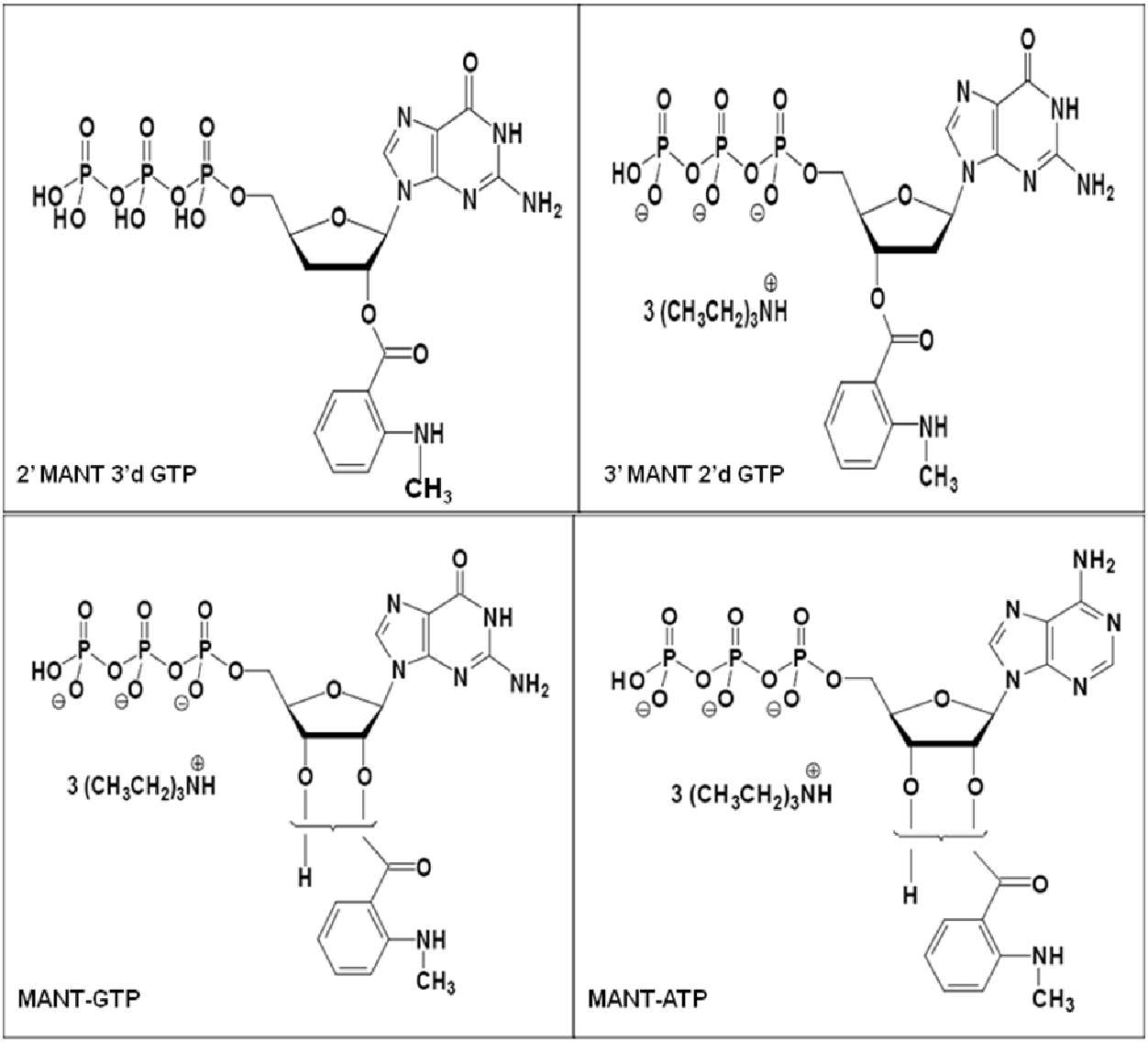

3.3.2 Experimental methods

- ***AC activity assay***

AC activity assays were performed as described in chapter 2. To carry out assays with C1 alone and C2 alone, assay tubes contained 1 μM CI and/or 5 μM C2. Reactions were conducted in the presence and absence of 5 μM $G\alpha_s$-GTPγS and 100 μM FS. Twenty μl of reaction mixture containing 100 μM cAMP, 40 μM ATP, 10 mM $MnCl_2$, 100 μM KCl, 25 mM HEPES/NaOH pH 7.4 and 6 – 6.5 μCi/tube [α-^{32}P]ATP were added to each assay tube. For inhibition experiments with TNP and MANT-nucleotides, nucleotides at final concentrations ranging from 1 nM to 100 μM were added to the assay tubes before addition of the protein.

- ***Fluorescence spectroscopy***

All experiments were carried out at 25°C using a Cary Eclipse fluorescence spectrophotometer (Varian, Walnut Creek, CA). Measurements were performed using a quartz fluorescence microcuvette (Hellma, Plainview, NY). Reaction mixture containing 100 mM KCl, 10 mM $MnCl_2$ in 25 mM HEPES/NaOH, pH 7.4 was added to the cuvette and the final assay volume was 150 μl. For TNP-nucleotides, measurements were carried out as described in chapter 2 with 4 μM CI or 25 μM C2 and 100 μM DMB-FS.

For experiments with MANT-nucleotides, steady-state emission spectra were recorded with λ_{ex} = 280 nm (λ_{em} = 300 – 500 nm) and λ_{ex} = 350 nm (λ_{em} = 370 – 500 nm). Assays were performed as described above except that final concentration of 1 μM of MANT-nucleotide, 5 μM C1 and 35 μM C2 were used. In order to measure the binding stoichiometry between C1 and TNP-ATP/GDP, experiments were carried out in the kinetic mode with 4 μM C1 and increasing concentrations of TNP-ATP and TNP-GDP. K_d values were calculated after correction for the inner filter effect based on absorbance of the TNP-nucleotides (Lakowicz, 1999).

- ***Native and SDS gel electrophoresis***

C1 and C2 were electrophoresed on 4-12% Novex ® Tris-Gylcine gels under native conditions and 10% Bis-Tris gels under denaturing conditions. Proteins were visualized using coomassie blue staining.

- ***Molecular modeling studies***

Molecular models of the C1 homodimer and C1/C2 heterodimer were generated in collaboration with Dr. G. Lushington (University of Kansas, Lawrence). To generate the C1+C1 homodimer, the first C1 unit was obtained from the crystal structure solved by Tesmer et al. (1997), and the second C1

unit was obtained via homology modeling. Sequence alignment between the C1 target and the C2 template was performed via the Clustal-W program (Thompson et al., 1994), using the BLOSUM-30 substitution matrix (Henikoff and Henikoff, 1993), and standard gap penalties of 10 for opening and 0.1 for extension.

- ***Data Generation and statistics***

For AC activity assays and inhibition experiments, V_{max}, K_m, turn over number, K_i values and saturation curves for inhibitors were analyzed by nonlinear regression using Prism 4.0 software (Graphpad, San Diego, CA). The K_i values calculated are apparent K_i values since the protein concentration is higher than the ligand concentrations in the experiments performed.

Fluorescence recordings were analyzed using the spectrum package of the Cary Eclipse software and final graphs were prepared using Graphpad prism 4.0 software. Similar results were obtained from 3 – 4 independent experiments using three different batches of C1 and two different batches of C2.

3.4 Results and Discussion

3.4.1 Kinetic studies of C1 and C2 subunits of mAC

Previous biochemical studies have shown that C1 is catalytically inactive and C2 possesses low catalytic activity (Zhang et al., 1997; Mitterauer et al., 1998). Since C1 and C2 domains were highly homologous, the C2 homodimer crystal structure solved by Zhang et al (1997) was used as the preliminary model for C1/C2 interaction. However, the structure of C1 has not been solved and studies of C1 have been limited to biochemical and biophysical approaches.

To study the properties of the individual subunits C1 and C2, AC activity expressed as turnover numbers for C1 and C2 was first determined. The catalytic properties of C1 and C2 were examined under four different conditions as indicated in Table 3-1. AC activity was observed only in the presence of both the activators, $G\alpha_s$ and FS. Catalytic rates for both C1 and C2 were very low although significant. Interestingly, the activity of C1 was more than 20-fold higher than that of C2. This is surprising in view of the fact that C2 was shown previously to display exceedingly low catalytic activity whereas C1 was essentially inactive (Mitterauer et al., 1998). The same group further showed that C2 alone could bind ATP analogs and this binding was further enhanced by Mn^{2+}.

The V_{max} and K_m values for C1 were calculated in the presence of the activators, $G\alpha_s$, FS and Mn^{2+} (Figure 3-2). The K_m values for C1 ranged between 32 and 70 μM and the V_{max} value was 110 pmol/mg/min. The V_{max} value for C1 was much lower than that of the C1/C2 heterodimer (Gille et al., 2004). Compared to the C1/C2 heterodimer (Gille et al., 2004), the K_m value of C1 for ATP was several-fold lower, indicating that, although C1 has a very low catalytic activity, it has a high affinity for substrate ATP.

Table 3-1 AC activity of C1 and C2 in the presence and absence of FS and $G\alpha_s$

AC assays were carried out under four different conditions: 1) Basal; 2) In the presence of FS; 3) In the presence of $G\alpha_s$; and 4) in the presence of both FS and $G\alpha_s$. Assay tubes contained 1 μM C1 or 5 μM C2. Reactions were carried out in the presence or absence of 5 μM $G\alpha_s$-GTPγS and 100 μM FS. 20 μl of reaction mixture containing 100 μM cAMP, 40 μM ATP, 10 mM $MnCl_2$, 100 μM KCl, 25 mM HEPES/NaOH pH 7.4 and 6 – 6.5 μCi/tube [α-^{32}P]ATP was added to each assay tube. AC activity was calculated as turnover numbers and analyzed by non-linear regression using the Prism 4.0 software (Graphpad, San Diego, CA). Data shown are the mean values ± SD of 2-3 experiments performed in duplicate.

Additions	**C1 (AC activity/min)**	**C2 (AC activity/min)**
Basal	ND	ND
FS	ND	ND
$G\alpha_s$	ND	ND
FS+$G\alpha_s$	0.0026 ± 0.0001	0.000132 ± 0.0

Figure 3-2 C1 AC activity – K_m and V_{max} determination

C1 AC activity assays were performed as described in section 3.3.2. Assay tubes contained 1 μM C1, 5 μM $G\alpha_sGTP\gamma S$, 100 μM FS and 10 mM $MnCl_2$. Vmax is expressed in pmol/mg/min, K_m is expressed in μM and 95% confidence intervals were analyzed by non-linear regression using Prism 4.0 software (Graphpad, San Deigo, CA).

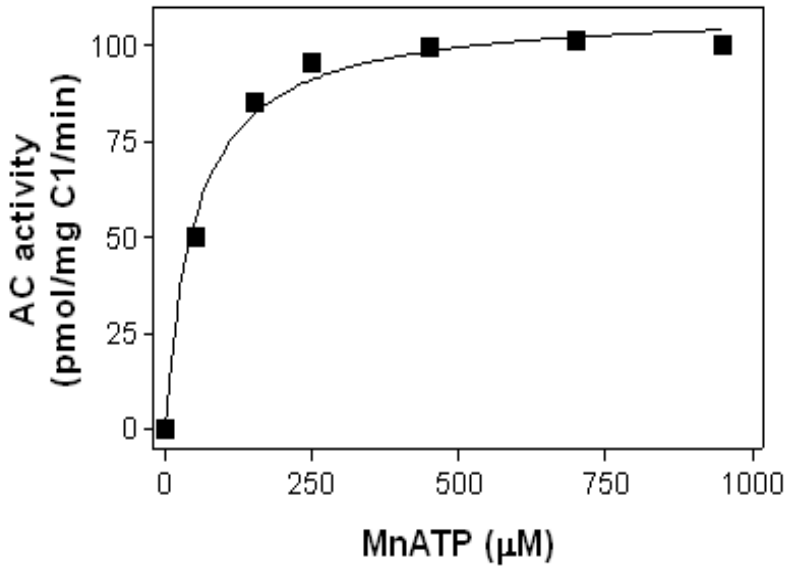

V_{max} 95% confidence interval	110 pmol/mg/min 102-117
K_m 95% confidence interval	51 μM 32- 70

3.4.2 Inhibition of C1 AC activity by MANT and TNP-nucleotides

Since C2 AC activity was too small to measure reliably, we examined the inhibitory properties of MANT-GTP, TNP-ATP and TNP-GDP on C1 AC activity (Figure 3-3). The reason for selection of MANT-GTP and TNP-ATP was due to the fact that earlier studies had shown MANT-GTP is the most potent inhibitor (K_i = 11 nM) of C1/C2 among the MANT substituted nucleotides (Gille et al., 2004; Gille and Seifert, 2003; Mou et al., 2005) and TNP-ATP was reported as the most potent (K_i = 81 nM) when compared to other TNP-nucleotides (Mou et al., 2006). TNP-GDP was selected because, though TNP-GDP poorly inhibited C1/C2 (K_i = 9.4 μM), it showed the largest fluorescence change (Figure 3-5) upon binding to C1 alone compared to other TNP-nucleotides.

MANT-GTP was the most potent inhibitor of C1 activity with a K_i value of 4.6 nM following maximal activation by $G\alpha_s$, FS and Mn^{2+} (Figure 3-3). TNP-ATP also potently inhibited C1 with a K_i value of 8.9 nM. TNP-GDP inhibited C1 activity with a K_i value of 645 nM. We observed that all three nucleotides show higher affinity for C1 when compared to C1/C2. This again points to our earlier observation that though C1 has low catalytic activity, it has a high affinity for substrate ATP and ATP analogues modified at the ribosyl moiety. It must be noted that all the K_i values reported in these experiments are

apparent K_i values due to the fact that the concentrations of C1 and C2 were higher than those of the nucleotides used in these experiments.

Figure 3-3 Inhibition of C1 AC catalytic activity by TNP and MANT-nucleotides

Experiments aimed at measuring C1 AC activity inhibition by TNP-ATP, TNP-GDP and MANT-GTP were performed as described in section 3.3.2. Assay tubes contained 1 μM C1, 5 μM $G\alpha_s$-GTPγS and 100 μM FS. Concentrations of the TNP and MANT-nucleotides ranging from 1 nM to 100 μM were added to the assay tubes before addition of the protein. K_i values (nM) and 95% confidence intervals were analyzed by non-linear regression using Prism 4.0 software (Graphpad, San Deigo, CA).

Nucleotides	K_i values
MANT-GTP	4.6
95% confidence intervals	3.7 – 5.6
TNP-ATP	8.9
95% confidence intervals	6.7 – 11
TNP-GDP	645
95% confidence intervals	381 – 1092

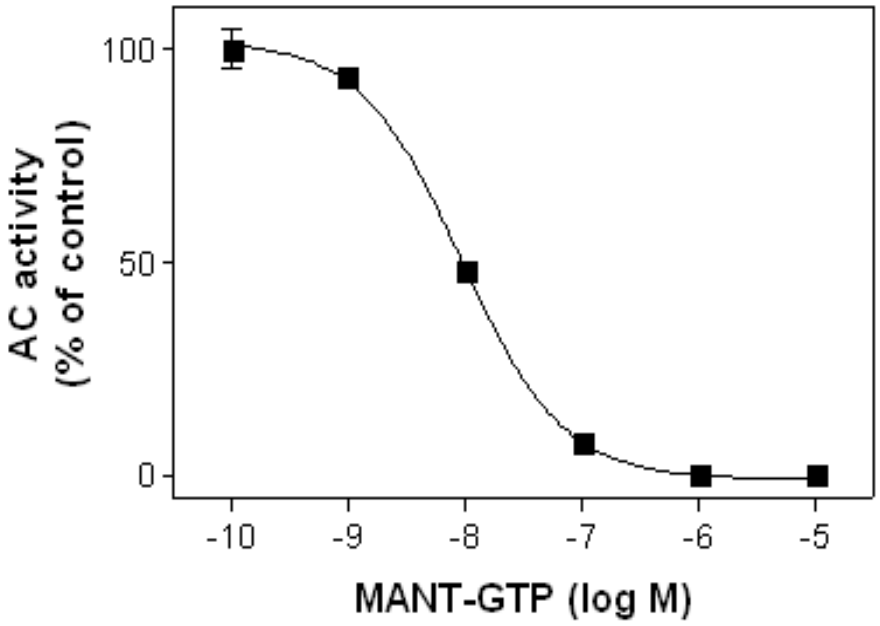
100
50
0
AC activity
(% of control)
-10
-9
-8
-7
-6
-5
MANT-GTP (log M)

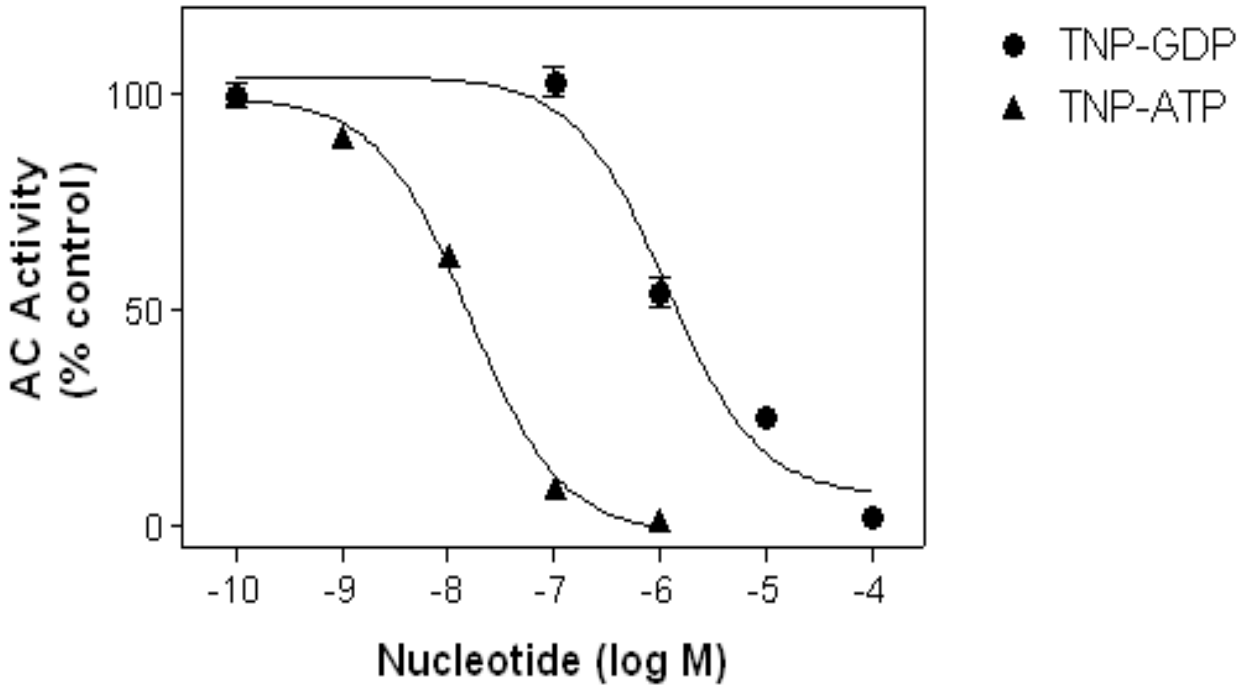
100
50
0
AC Activity
(% control)
-10
-9
-8
-7
-6
-5
-4
Nucleotide (log M)
TNP-GDP
TNP-ATP

3.4.3 Fluorescence analysis of the interaction of TNP-nucleotides with C1 and C2

TNP and MANT-nucleotides bind to a hydrophobic site formed by C1/C2 as monitored by fluorescence spectroscopy (Mou et al., 2005; Chapter 2). Crystal structures of C1/C2 with bound TNP-ATP or MANT-GTP/ATP have shown that these nucleotides have slightly different orientations but bind to a common site at the C1/C2 interface (Mou et al., 2006). Mitterauer et al., (1998) have observed that TNP-ATP fluorescence increases in the presence of C2 alone and fluorescence is further enhanced by the addition of $MnCl_2$. However, experiments with C1 alone have not been reported so far and it is not known if C1 alone can bind TNP and MANT-nucleotides. If so, then it is important to see if the nucleotides bind to C1 monomer or a dimer.

When TNP-GDP, TNP-ATP and TNP-UTP were excited at 408 nm, they emitted a fluorescence peak at ~550 nm (Figure 3-5). With the addition of C1 to the cuvette containing TNP-nucleotides in the presence of Mn^{2+}, a 3-6-fold increase in fluorescence was observed (Figure 3-5 A, B and C). The fluorescence increase was dependent on the specific nucleotide studied. A 6-fold increase in fluorescence was observed with TNP-GDP when bound to C1 (Figure 3-5A). Additionally, a blue-shift in the emission maximum of TNP-nucleotides was observed indicating that the TNP-group resided in a hydrophobic pocket. The magnitude of the blue-shift was dependent on the

respective nucleotide studied. TNP-GDP fluorescence shifted to ~ 537 nm from 550 nm (Fig. 3-5A). Similarly with TNP-ATP and TNP-UTP in the presence of C1, the emission peak shifted to ~ 533 nm (Figure 3-5B) and ~ 530 nm (Figure 3-5C) respectively. Furthermore, upon addition of DMB-FS, a decrease in fluorescence was observed and was dependent on the specific nucleotide studied. Collectively, the data indicate that all three nucleotides bind to C1 but interact in slightly different ways with residues within the hydrophobic site on C1.

With the addition of C2 to the cuvette containing TNP-nucleotides alone, there was no increase in fluorescence observed irrespective of the specific nucleotide studied (Figure 3-6 A, B and C). Moreover, there was no change in fluorescence observed with the addition of DMB-FS. These results are in striking contrast to earlier studies (Mitterauer et al., 1998) which showed an increase in fluorescence of TNP-ATP with C2. Therefore our data indicate that none of the three TNP-nucleotides studied bind tightly to C2 in the absence of C1.

To estimate the affinity of TNP-nucleotides for C1, fluorescence experiments were carried out with increasing concentrations of TNP-ATP and TNP-GDP in the presence of a constant concentration of C1. K_d values were calculated after correction for the inner filter effect and substraction of baseline TNP-nucleotide-fluorescence in the absence of C1. Apparent K_d

values of 0.51 μM and 0.07 μM were calculated for TNP-ATP and TNP-GDP respectively at 4 μM C1 (Figure 3-7). These values do not match with the K_i values calculate for these nucleotides. It is possible that that this approach underestimates the actual affinity of TNP-nucleotides for C1 because higher concentrations of C1 are required to observe changes in fluorescence. Also, a difference in the binding of TNP-GDP and TNP-ATP to C1 was observed. At a constant concentration of C1 (4 μM), with 2 μM TNP-GDP, an increase in fluorescence was observed. Beyond 2 μM concentration of TNP-GDP, fluorescence intensity constantly decreased. In the case of TNP-ATP, with 2 μM concentration, an increase in fluorescence intensity was observed. Higher concentrations of TNP-ATP did not decrease the fluorescence intensity. Based on our observation in chapter 1 that TNP adenine nucleotides interact differently with C1/C2 compared to TNP guanine nucleotides, it may be possible that TNP-adenine nucleotides interact differently with C1 compared to TNP-guanine nucleotides. Nonetheless, saturation of 4 μM C1 was observed with 2 μM of TNP-ATP or TNP-GDP. The 1:2 binding stoichiometry between nucleotide and C1 strongly indicates that C1 is present as a dimer.

Figure 3-5 Fluorescence analysis of the interaction of TNP-nucleotides with C1

The buffered solution consisted of 100 mM KCl, 10 mM $MnCl_2$ in 25 mM HEPES/NaOH pH 7.4. 5 μM (final concentration) of TNP-GDP, ATP or UTP (A, B and C respectively - green trace) was added followed by addition of 4 μM C1 (red trace). 100 μM DMB-FS was added following C1 addition (blue trace). Emission spectra were recorded in the emission range 500-600 nm with an excitation wavelength of 405 nm. Fluorescence is shown as arbitrary units (a.u.). Baseline fluorescence (buffer alone) was subtracted from each curve. Similar data were obtained from 3-4 independent experiments using three different batches of C1 and two different batches of C2.

A

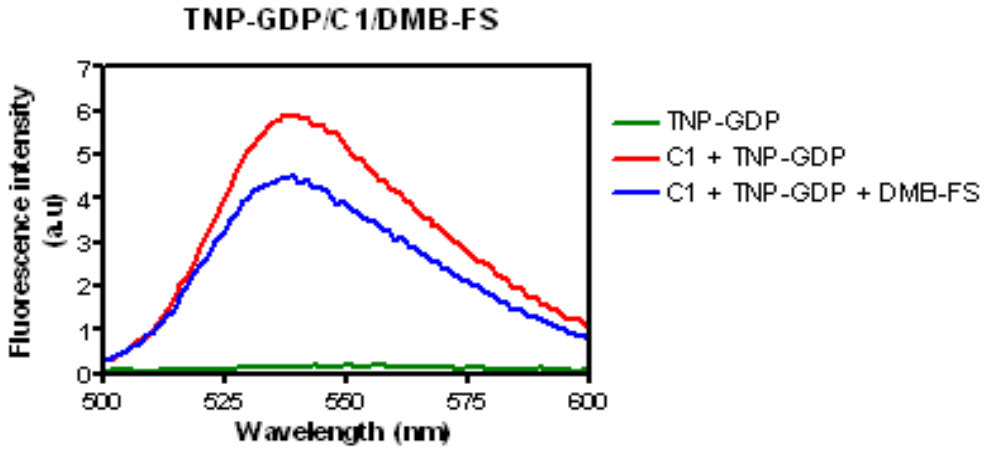
TNP-GDP/C1/DMB-FS
Fluorescence intensity (a.u)
Wavelength (nm)
TNP-GDP
C1 + TNP-GDP
C1 + TNP-GDP + DMB-FS

B

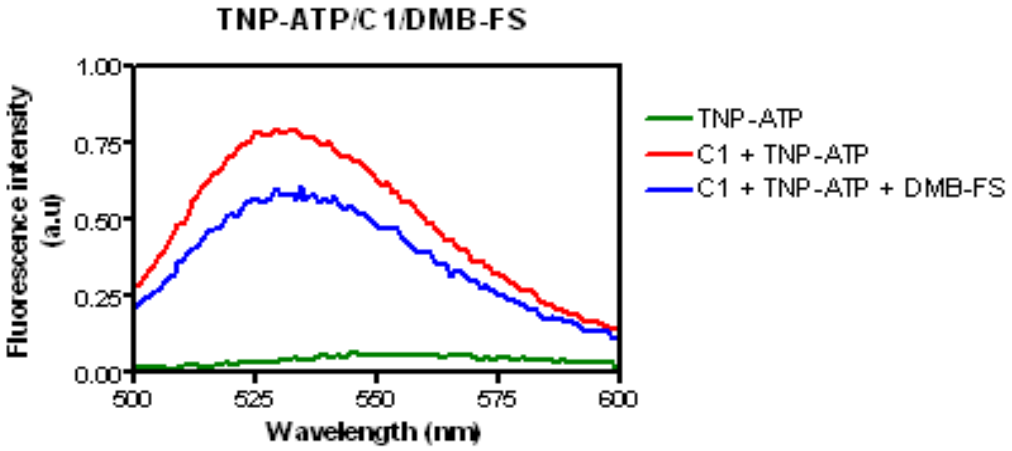
TNP-ATP/C1/DMB-FS
Fluorescence intensity (a.u)
Wavelength (nm)
TNP-ATP
C1 + TNP-ATP
C1 + TNP-ATP + DMB-FS

C

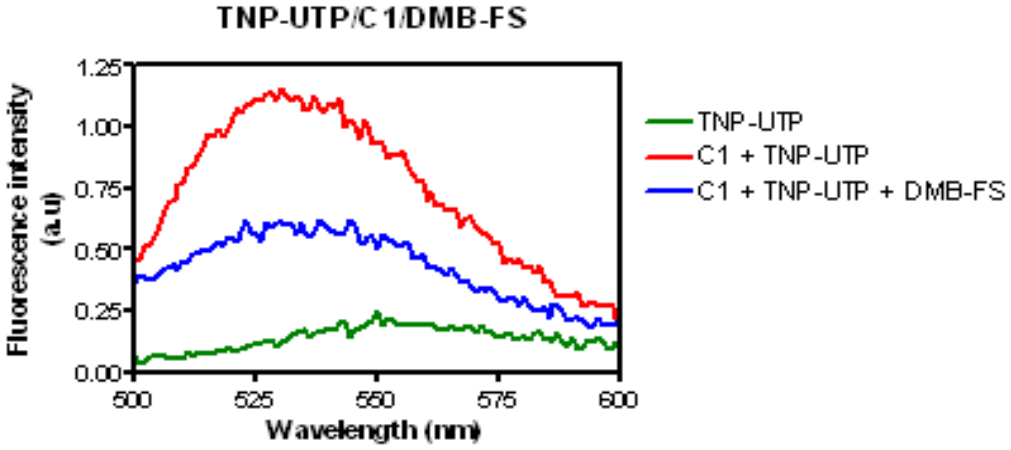
TNP-UTP/C1/DMB-FS
Fluorescence intensity (a.u)
Wavelength (nm)
TNP-UTP
C1 + TNP-UTP
C1 + TNP-UTP + DMB-FS

Figure 3-6 Fluorescence analysis of the interaction of TNP-nucleotides with C2

The buffered solution consisted of 100 mM KCl, 10 mM $MnCl_2$ in 25 mM HEPES/NaOH pH 7.4. 5 μM (final concentration) of TNP-nucleotide (3-6 A, B and C respectively, green trace) was added followed by addition of 25 μM C2 (red trace). 100 μM DMB-FS was added following addition of C2 (blue trace). Emission spectra were recorded in the emission range of 500-600 nm with an excitation wavelength of 405 nm. Fluorescence is shown as arbitrary units (a.u.). Baseline fluorescence (buffer alone) was subtracted from each curve. Similar data were obtained from 3-4 independent experiments using three different batches of C1 and two different batches of C2.

A

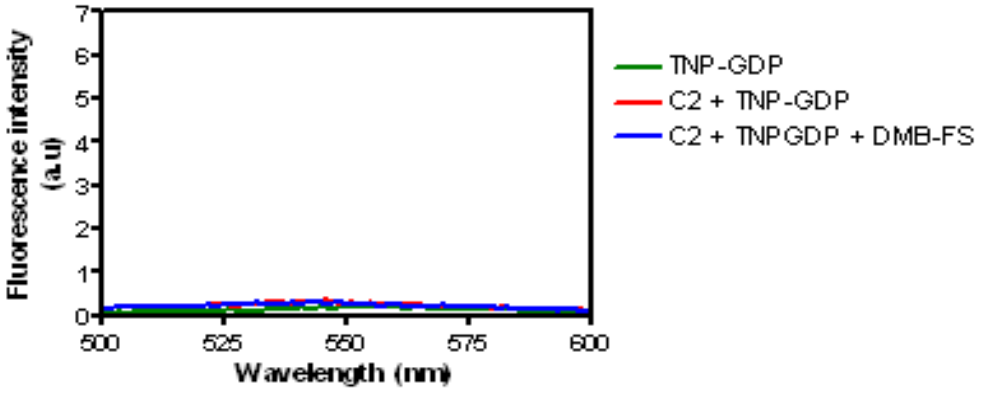
TNP-GDP/C2/DMB-FS
Fluorescence intensity (a.u)
Wavelength (nm)
TNP-GDP
C2 + TNP-GDP
C2 + TNPGDP + DMB-FS

B

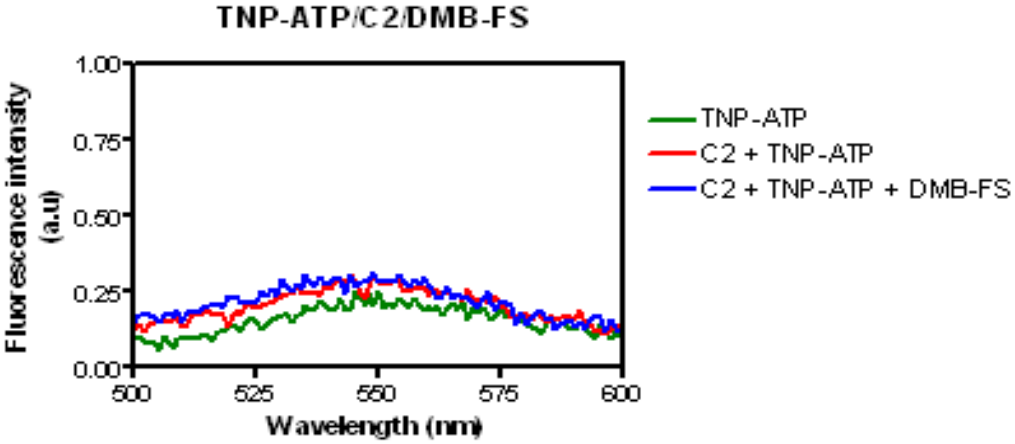
TNP-ATP/C2/DMB-FS
Fluorescence intensity (a.u)
Wavelength (nm)
TNP-ATP
C2 + TNP-ATP
C2 + TNP-ATP + DMB-FS

C

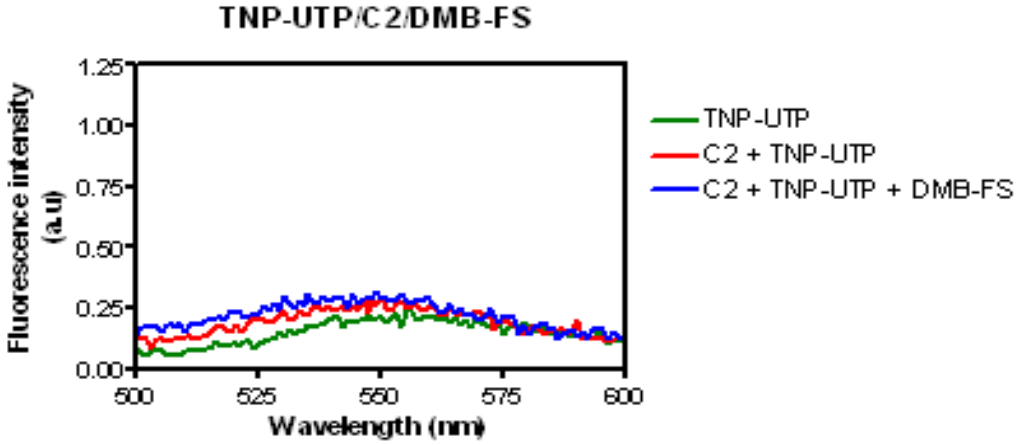
TNP-UTP/C2/DMB-FS
Fluorescence intensity (a.u)
Wavelength (nm)
TNP-UTP
C2 + TNP-UTP
C2 + TNP-UTP + DMB-FS

Figure 3-7 Fluorescence spectra of increasing concentrations of TNP-ATP and TNP-GDP in the presence of C1.

4 μM C1 was incubated in buffer containing 100 mM KCl, 10 mM $MnCl_2$ in 25 mM HEPES/NaOH, pH 7.4 followed by increasing concentrations of TNP-ATP or TNP-GDP as indicated.

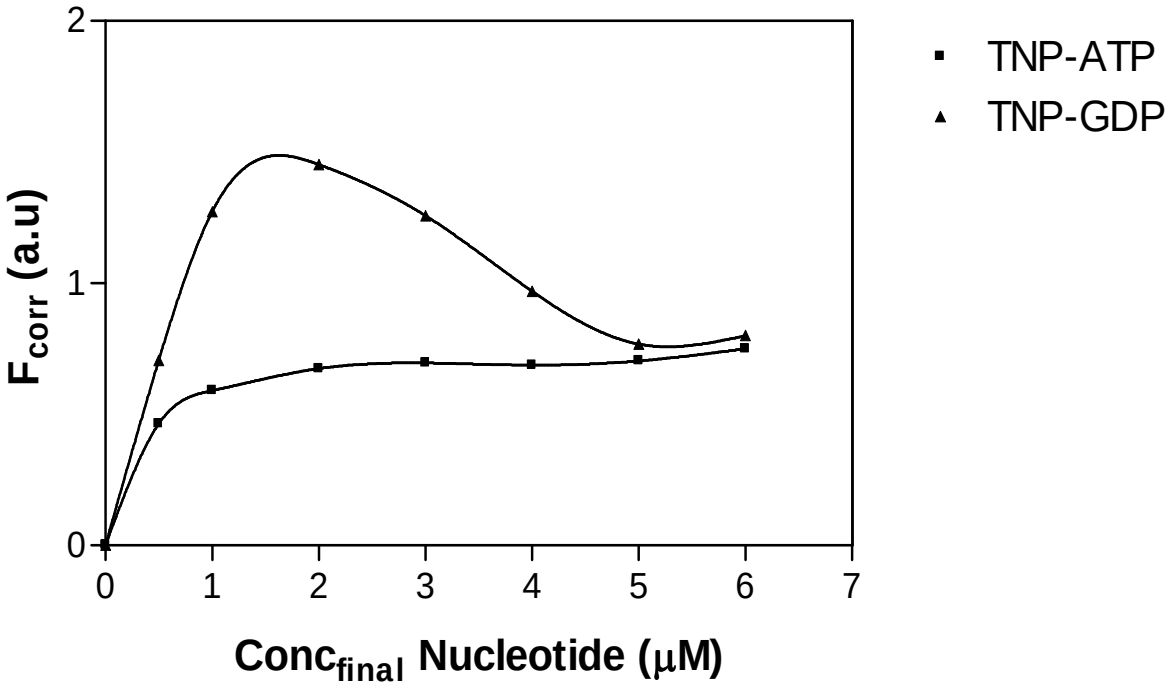

3.4.4 Fluorescence analysis of the interaction of MANT-nucleotides with C1 and C2

In previous studies we have observed that MANT-nucleotides bind to a hydrophobic site on C1/C2 as indicated by an increase in fluorescence at 350 nm (Mou et al., 2005 and 2006). With the addition of DMB-FS, a further increase in fluorescence was observed. In addition, at 280 nm, fluorescence resonance energy transfer (FRET) was observed between the aromatic amino acid residues such as W1020 residue of C2 and the MANT group. FRET is a distance-dependent interaction occurring between a donor and an acceptor. If the donor and acceptor lie between 10 – 100 Å, a transfer of energy occurs from the donor to the acceptor (Lacowicz, 1999). In this case, when the MANT-nucleotide in the presence of C1/C2 is excited at 280 nm, energy from neighboring groups such as W1020 is transferred to the MANT group which in turn gets excited and subsequently emits at ~420 nm (Figure 3-8). However, it is not known if MANT-nucleotides bind to C1 and C2 alone. Therefore, fluorescence experiments were conducted to analyze the changes both in intrinsic protein fluorescence via FRET and changes in MANT-nucleotide fluorescence in the presence of C1 or C2.

- ***Interaction of MANT-nucleotides with C1 – FRET measurements***

For FRET measurements, we used MANT-GTP and its analogs, 2’ MANT 3’d GTP and 3’ MANT 2’d GTP. When excited at 280 nm, a small increase in fluorescence of MANT-nucleotide was observed around 450 nm (Fig 3-9 A, B and C). With the addition of C1, tyrosine and tryptophan fluorescence occurred at 350 nm (red trace). Additionally a smaller peak was observed at around 430 nm due to FRET from C1 to the MANT-nucleotide. A C1 alone trace without bound nucleotide (green trace, Figure 3-9 A, B and C) was superimposed on the graphs to indicate the magnitude of FRET. The magnitude of FRET was dependent on the specific nucleotide studied. MANT-GTP showed the lowest FRET compared to 2’ MANT 3’d GTP and 3’ MANT 2’d GTP.

For FRET to occur, the MANT-nucleotide must lie close between 10-100 Å of tyrosine/tryptophan residue of C1. When FRET measurements were performed using 295 nm as the excitation wavelength (tryptophan specific excitation, Lakowicz, 1999), we observed a 2-fold decrease in fluorescence at 350 nm as well as a decrease in FRET at 430 nm (data not shown). Thus, both tyrosine and tryptophan residues must be excited in order to obtain the maximum FRET. Based on the primary structure of C1, it is clear that the MANT-nucleotide lies in the vicinity of tryptophan residues W502, W507 and

tyrosine residues Y383, Y442, Y443, Y535, Y540 and Y557 and these are the most likely candidate residues contributing to the observed FRET.

We also observed that, in the presence of 2' MANT 3'd GTP, the intrinsic C1 fluorescence decreased at 350 nm with a corresponding increase at 430 nm (FRET) (3-9 B, red trace). However, in the case of MANT-GTP and 3' MANT 2'd GTP, although FRET was observed, there was no decrease in intrinsic C1 fluorescence (Figure 3-9 A and C, red trace). The data indicates that the three MANT-nucleotides studied interact differently with C1.

We also observed that with the addition of DMB-FS (Blue trace, Figure 3-9 A, B and C) there was a slight decrease in intrinsic C1 fluorescence and FRET. These results are in striking contrast to our earlier studies with C1/C2. When DMB-FS was added to C1/C2, a decrease in intrinsic C1/C2 fluorescence with corresponding increase in FRET was observed (Mou et al., 2005 and 2006).

Figure 3-8 Schematic representation of fluorescence resonance energy transfer (FRET)

A schematic representation of FRET between C1/C2 and the MANT group of MANT-ATP is shown. Upon excitation at 280 nm (intrinsic protein fluorescence), tryptophan and tyrosine residues of C1/C2 emit at 350 nm. From the crystal structure of C1/C2 in complex with MANT-ATP, it is clear that the MANT group lies in the vicinity of W1020 of C2. Therefore, an energy transfer from W1020 to the MANT group causes MANT-ATP to emit at 420 nm.

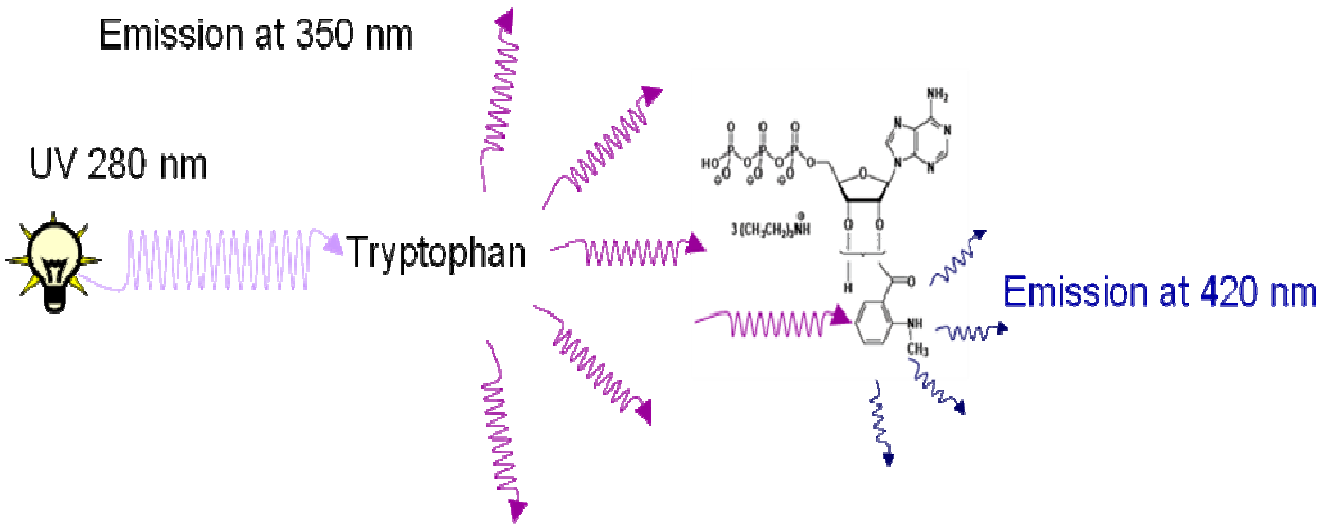

Figure 3-9 FRET analysis of MANT-GTP and its 2' and 3' analogs in the presence of C1 and DMB-FS

Fluorescence measurements were conducted as described in section 3.3.2. A, B and C are FRET measurements with 1 μM MANT-GTP, 2' MANT-3'-d-GTP or 3' MANT-2'-d-GTP respectively. Steady-state emission spectra were recorded at λ_{ex} = 280 nm (λ_{em} = 300 – 500 nm). Five μM C1 and 100 μM DMB-FS were included as indicated. Representative emission spectra of MANT-nucleotide alone (purple trace), C1 alone (green trace), MANT-nucleotide in the presence C1 (red trace) and MANT-nucleotide in the presence of both C1 and DMB-FS (blue trace) are shown. Fluorescence intensity is measured as percentage of the maximal emission spectra recorded in the respective experiments. Fluorescence tracings are representative for three or four independent experiments using different batches of C1.

A

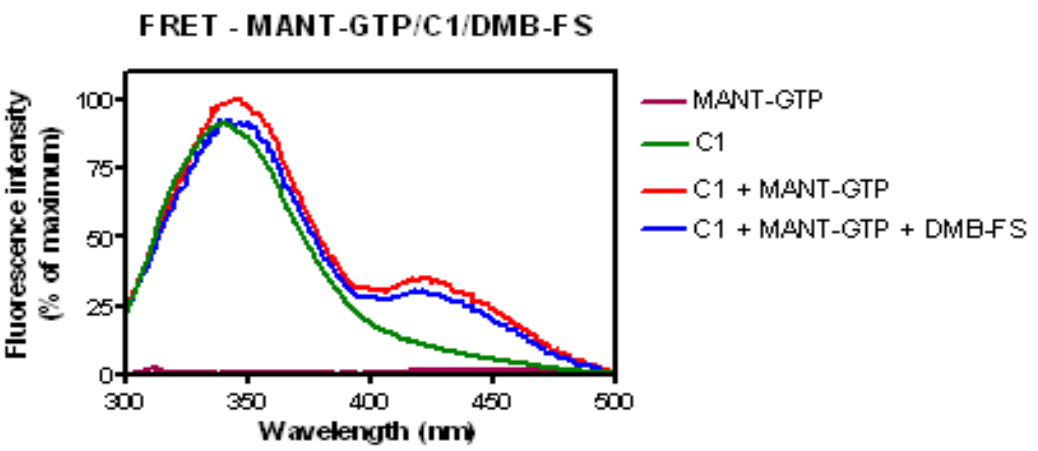
FRET - MANT-GTP/C1/DMB-FS
Fluorescence intensity (% of maximum)
100
75
50
25
0
300
350
400
450
500
Wavelength (nm)
MANT-GTP
C1
C1 + MANT-GTP
C1 + MANT-GTP + DMB-FS

B

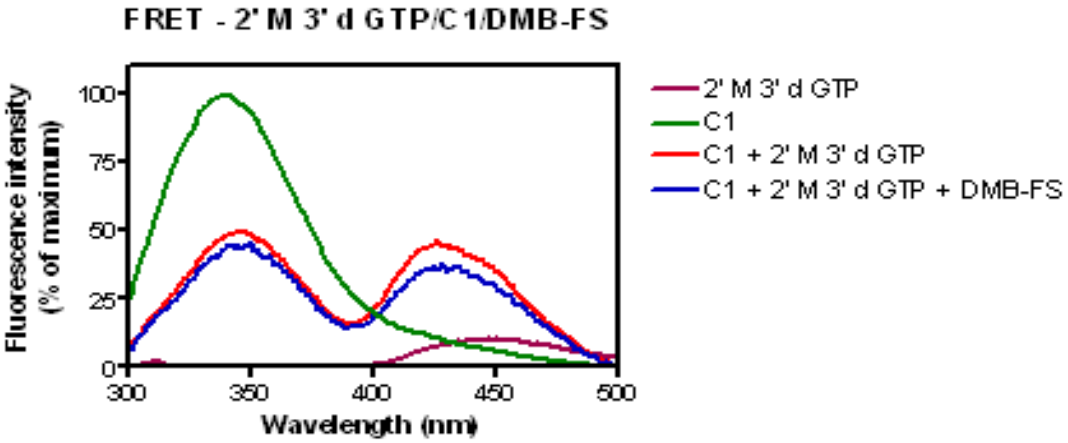
FRET - 2' M 3' d GTP/C1/DMB-FS
Fluorescence intensity (% of maximum)
100
75
50
25
0
300
350
400
450
500
Wavelength (nm)
2' M 3' d GTP
C1
C1 + 2' M 3' d GTP
C1 + 2' M 3' d GTP + DMB-FS

C

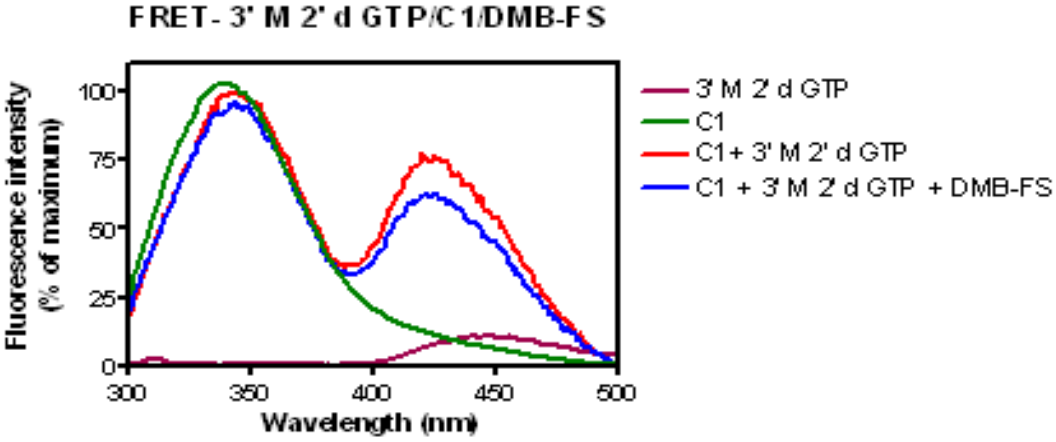
FRET - 3' M 2' d GTP/C1/DMB-FS
Fluorescence intensity (% of maximum)
100
75
50
25
0
300
350
400
450
500
Wavelength (nm)
3' M 2' d GTP
C1
C1 + 3' M 2' d GTP
C1 + 3' M 2' d GTP + DMB-FS

- ***Interaction of MANT-nucleotides with C1 – Direct fluorescence measurements***

When excited at 350 nm, MANT-GTP, 2’ MANT 3’d GTP and 3’ MANT 2’d GTP emit at 450 nm (green trace, Figure 3-10 A, B and C). With the addition of C1 (red trace, Figure 3-10 A, B and C), an increase in fluorescence was observed. Additionally, the emission maxima of the MANT-nucleotides studied showed a shift to shorter wavelengths (Blue shift). The emission maxima for MANT-GTP, 2’ MANT 3’d GTP and 3’ MANT 2’d GTP shifted to 439 nm, 441 nm and 432 nm respectively. An increase in fluorescence is indicative of MANT-nucleotides binding to C1 and the blue shift is indicative of MANT-nucleotide residing in a hydrophobic pocket of C1. With the addition of DMB-FS (blue trace, Figure 3-10 A, B and C), there was no change in fluorescence observed. It was observed previously that addition of DMB-FS to C1/C2 caused an increase in fluorescence (Mou et al., 2005 and 2006). The lack of effect of DMB-FS observed here with C1 indicates that DMB-FS probably induces a conformational change in C1 different from that with C1/C2.

Figure 3-10 Direct fluorescence analysis of MANT-GTP and its 2' and 3' analogs in the presence of C1 and DMB-FS

Fluorescence measurements were conducted as described in section 3.3.2. A, B and C are direct fluorescence measurements with MANT-GTP, 2' MANT-3'-d-GTP and 3' MANT-2'-d-GTP respectively. Steady state emission spectra was recorded at λ_{ex} = 350 nm (λ_{em} = 370 – 500 nm). Final concentrations of 1 μM MANT-nucleotide, 5 μM C1 and 100 μM DMB-FS were used. Representative emission spectra of MANT-nucleotide (green trace), MANT-nucleotide in the presence of C1 (red) and MANT-nucleotide in the presence of C1 and DMB-FS (blue) are shown. Fluorescence intensity is measured as percentage of the maximal emission spectra recorded in the respective experiments. Black arrows indicate the emission maxima of MANT-nucleotides alone and in the presence of C1 and DMB-FS. Fluorescence tracings are representative for three – four independent experiments using different batches of C1.

A

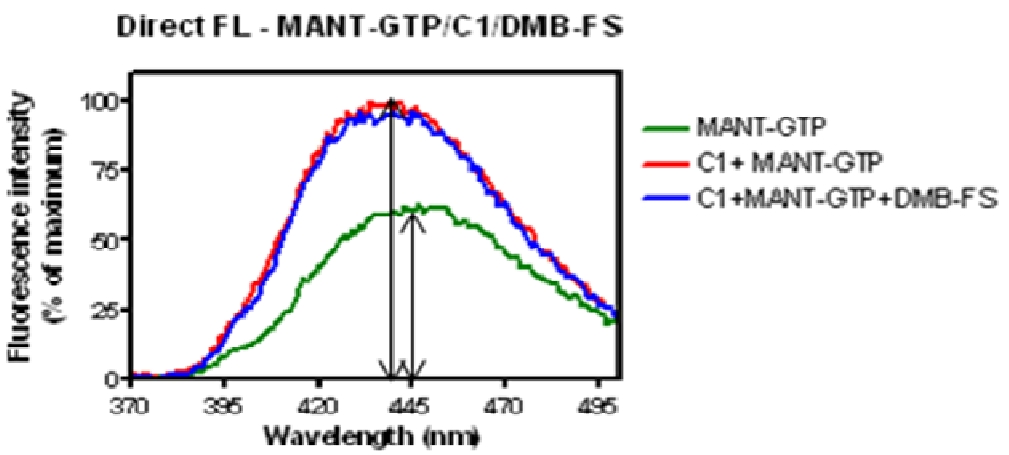
Direct FL - MANT-GTP/C1/DMB-FS
Fluorescence intensity (% of maximum)
100
75
50
25
0
370
395
420
445
470
495
Wavelength (nm)
MANT-GTP
C1+ MANT-GTP
C1+MANT-GTP+DMB-FS

B

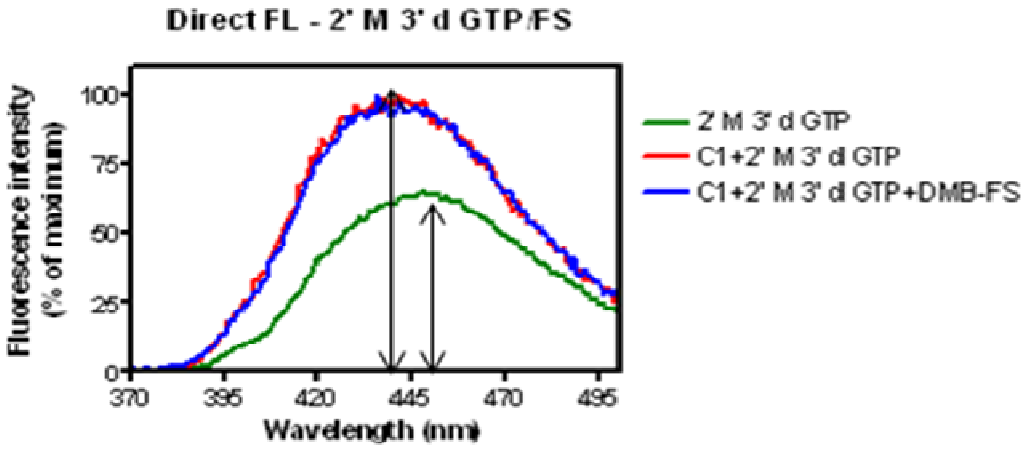
Direct FL - 2' M 3' d GTP/FS
Fluorescence intensity (% of maximum)
100
75
50
25
0
370
395
420
445
470
495
Wavelength (nm)
2' M 3' d GTP
C1+2' M 3' d GTP
C1+2' M 3' d GTP+DMB-FS

C

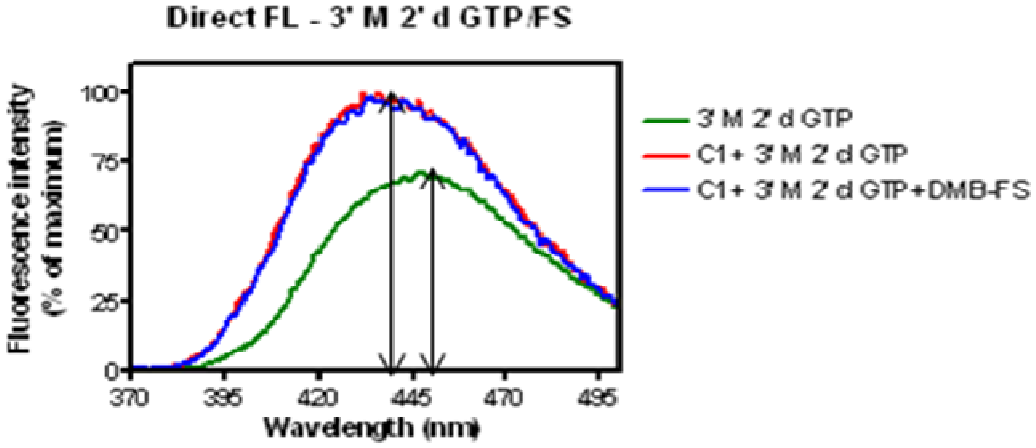
Direct FL - 3' M 2' d GTP/FS
Fluorescence intensity (% of maximum)
100
75
50
25
0
370
395
420
445
470
495
Wavelength (nm)
3' M 2' d GTP
C1+ 3' M 2' d GTP
C1+ 3' M 2' d GTP+DMB-FS

- ***Interaction of MANT-nucleotides with C2 – FRET and direct fluorescence measurements***

MANT-ATP and MANT-GTP were used as probes for FRET measurements of C2. With the addition of C2 to the cuvette containing MANT-ATP or MANT-GTP, an increase in fluorescence was observed at 350 nm when excited at 280 nm (red trace, Figure 3-11 A and B). However, there was no FRET observed from C2 to MANT group as in the case of C1. A C2 alone trace (black trace, Figure 3-11 A and B) was superimposed to observe the magnitude of FRET, if any. There was no change in fluorescence observed with the addition of DMB-FS (blue trace, Figure 3-11 A and B).

In direct fluorescence measurements, when MANT-ATP or MANT-GTP were excited at 350 nm, the emission maximum was observed at 450 nm (green trace, Fig. 4C and D). When C2 was added, there was no change in fluorescence observed for MANT-ATP (red trace, Fig. 4C). A slight decrease in fluorescence was observed for MANT-GTP (red trace, Fig. 4D). This decrease is probably due to the presence of MANT-GTP in a hydrophilic environment. With the addition of DMB-FS (blue trace, Fig. 4C and D), again there was no change in fluorescence observed. Collectively, these studies indicate that MANT-nucleotides do not bind to C2.

Figure 3-11 FRET and direct fluorescence analysis of MANT-ATP and MANT-GTP in the presence of C2 and DMB-FS

Fluorescence measurements were conducted as described in 3.3.2. A and B are FRET measurements; C and D are direct fluorescence measurements. A and C are measurements with MANT-ATP; B and D are measurements with MANT-GTP. Steady state emission spectra was recorded at λ_{ex} = 280 nm (λ_{em} = 300 – 500 nm) in A and B; λ_{ex} = 350 nm (λ_{em} = 370 – 500 nm) in C and D. Final concentrations of 1 μM MANT-nucleotide, 35 μM C2 and 100 μM DMB-FS were used. Representative emission spectra of MANT-ATP/MANT-GTP only (green trace) and C2 only (black trace) in A and B, MANT-nucleotide in the presence C2 (red trace) and MANT-nucleotide in the presence of both C2 and DMB-FS (blue trace) are shown. Fluorescence intensity is measured as arbitrary units (a.u). Fluorescence tracings are representative for three – four independent experiments using different batches of C2

A

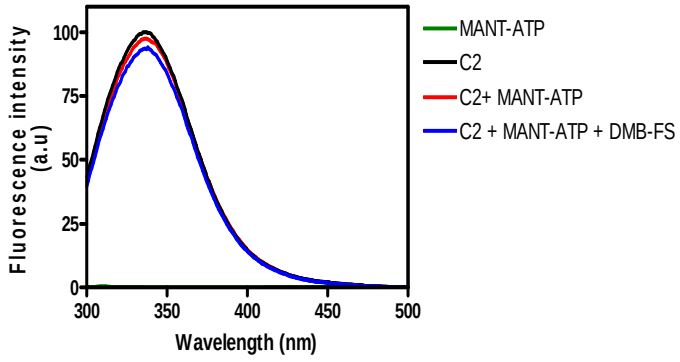
FRET - MANT-ATP/C2/DMB-FS
Fluorescence intensity (a.u)
100
75
50
25
0
300
350
400
450
500
Wavelength (nm)
MANT-ATP
C2
C2+ MANT-ATP
C2 + MANT-ATP + DMB-FS

B

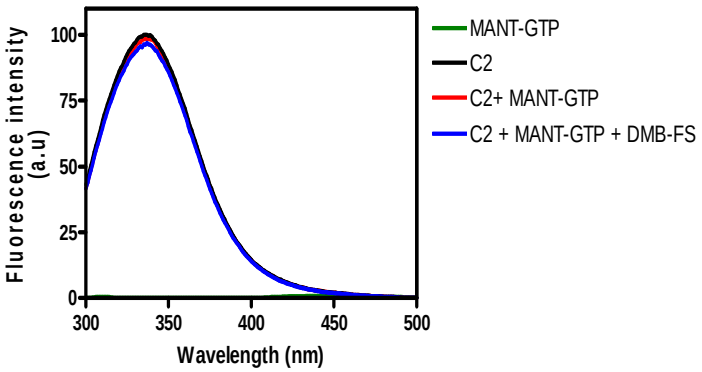
FRET - MANT-GTP/C2/DMB-FS
Fluorescence intensity (a.u)
100
75
50
25
0
300
350
400
450
500
Wavelength (nm)
MANT-GTP
C2
C2+ MANT-GTP
C2 + MANT-GTP + DMB-FS

C

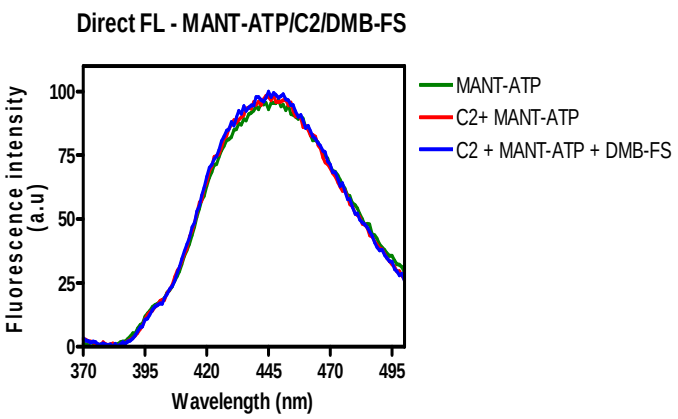
Direct FL - MANT-ATP/C2/DMB-FS
Fluorescence intensity (a.u)
100
75
50
25
0
370
395
420
445
470
495
Wavelength (nm)
MANT-ATP
C2+ MANT-ATP
C2 + MANT-ATP + DMB-FS

D

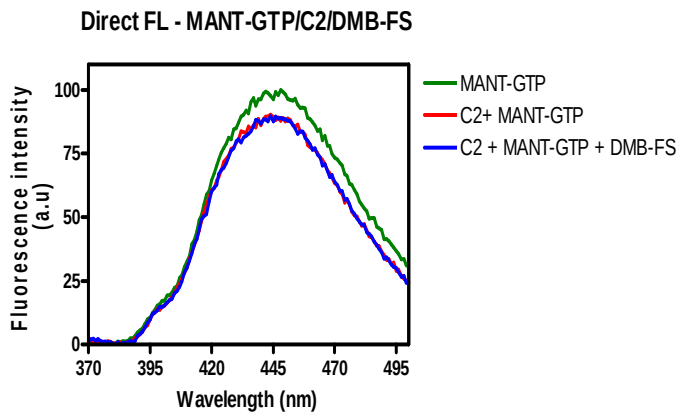
Direct FL - MANT-GTP/C2/DMB-FS
Fluorescence intensity (a.u)
100
75
50
25
0
370
395
420
445
470
495
Wavelength (nm)
MANT-GTP
C2+ MANT-GTP
C2 + MANT-GTP + DMB-FS

3.4.5 Native and SDS gel electrophoresis of C1, C2 and C1/C2

C1 and C2 are each 25 kDa and together form a 50 kDa heterodimer which constitutes the catalytic core of the enzyme (Sunahara et al., 1997). C1, C2 and C1/C2 were resolved on Tris-glycine gels under native conditions (Figure 3-12 A). We observed that C1 alone (lane 2, Figure 3-12 A) and C2 alone (lane 3, Figure 3-12 A) migrated with different electrophoretic mobility. C1/C2 did not migrate together as one band (lane 4, Figure 3-12A). Under native conditions, proteins migrate based on their charge: mass ratio. Therefore it is clear that C1 and C2 have different charge densities causing them to migrate differently. In case of C1/C2 together, it is not surprising that they do not migrate as one band. This is probably due to the fact that they are loosely associated in the absence of activators such as $G\alpha_s$ and FS. Our results indicate that C1 and C2, under native conditions, exist in different forms. As a control, we carried out gel electrophoresis experiments under denaturing conditions, as expected, C1 and C2 each migrated at ~25 kDa (Figure 3-12 B).

Figure 3-12 Native and SDS gel electrophoresis of C1, C2 and C1/C2

A and B are electrophoresis under native and denaturing conditions respectively. Lane 1 is a protein marker, Lane 2 is 4.5 μg C1, lane 3 is 5 μg C2 and lane 4 is 2 μg C1 plus 2 μg C2. Proteins were visualized using coomassie staining. Shown here are representative results from 3-4 independent experiments performed with 3 different batches of C1 and C2.

A. Native PAGE

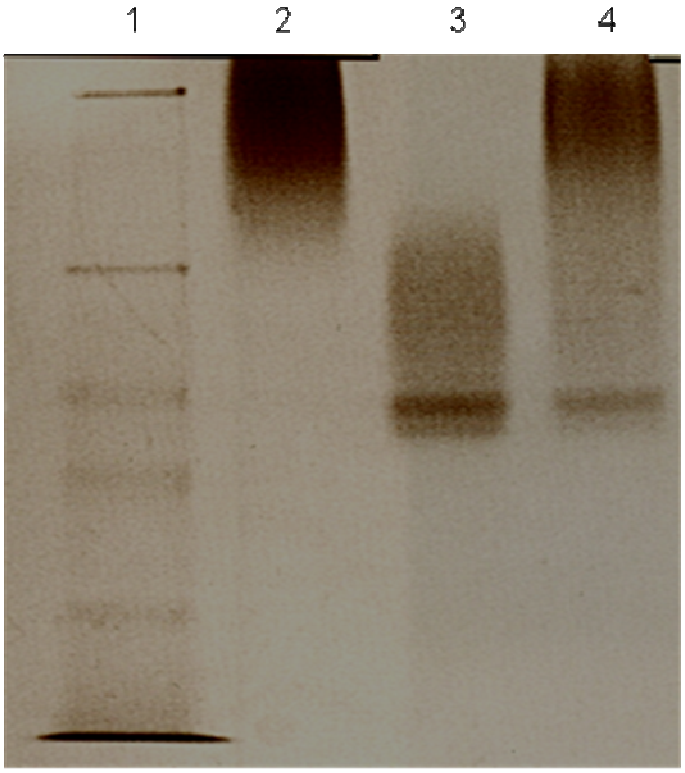

-Lane 1 – Marker (kDa)
-Lane 2 – C1 alone
-Lane 3 – C2 alone
-Lane 4 – C1+ C2

B. SDS-PAGE

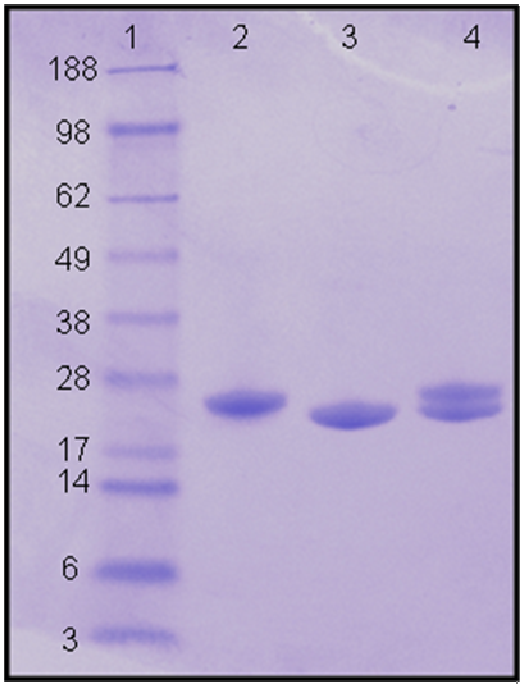

-Lane 1 – Marker (kDa)
-Lane 2 – C1 alone
-Lane 3 – C2 alone
-Lane 4 – C1+ C2

3.4.6 Molecular modeling of C1 homodimer and C1/C2 heterodimer

We have observed that, although C1 exhibits low catalytic activity and C2 possesses almost no measurable catalytic activity, TNP and MANT-nucleotides bind to C1 with high affinity. In fluorescence assays, we have seen that TNP and MANT-nucleotides bind to C1 with an increase in fluorescence and FRET that are indicative of a hydrophobic binding site in C1 formed probably due to dimerization. The crystal structure of C1 has not been solved yet and we know that C2 exist as dimers. Therefore, in collaboration with Dr.G. Lushington (Molecular modeling laboratory, University of Kansas, Lawrence), based on the crystal structure of C1/C2 (Tesmer et al., 1997), a C1 dimer was obtained using homology modeling (Figure 3-13). A straightforward explanation for our observation of strong ligand affinity to C1C1 but a low catalytic activity is that the R1029 residue in C1.C2 is replaced in C1.C1 by a histidine. R1029 is critical for catalysis as it is the immediate destination of the proton stripped from the ribosyl 3-hydroxy that initiates the cyclization reaction (Tesmer et al., 1997). The reason for low catalytic activity in C1/C1 is probably due to histidine because it may be too weak a base to serve this role and, perhaps more importantly, has a shorter side chain that likely doesn't come close enough to the ribose to perform this role effectively.

Interestingly, Tesmer et al (1997), claim that an alanine mutation of R1029 does not diminish the K_m of 2', 3' d-ATP. This indicates that, from the perspective of P-site inhibition, stronger interactions of 2', 3'd-ATP with R1029 (both van der Waals and electrostatic) actually correlate with somewhat weaker observed affinity. Therefore, the presence of a smaller and electrostatically weaker histidine may actually improve non-catalytic binding affinity.

Molecular modeling studies predict that MANT-nucleotides are stabilized by hydrophobic and hydrophilic interactions with C1 homodimer. Based on the hydrophobic pocket formed by C1/C1, within a distance of 3 Å and 20 Å, the MANT-group can be predicted to interact with lipophilic residues A409, L413, W507 and polar residues Q410, S508 and N509. Furthermore, between a distance of 3 Å and 20 Å, MANT-group is predicted to interact with the tryptophan residues W502, W507 and tyrosine residues Y383, Y442, Y443, Y535, Y540 and Y557 of C1. Therefore these are the most likely amino acid residues contributing to the FRET observed on interaction with C1.

Figure 3-13 Computational modeling of C1/C1 homodimer and C1/C2 heterodimer

Molecular modeling of C1 homodimer and C1/C2 heterodimer was undertaken in collaboration with Dr.Gerald Lushington (University of Kansas, Lawrence). To generate the C1+C1 homodimer, based on the crystal structure solved by Tesmer et al (1997), the first C1 unit was retained and the second C1 unit was mapped to the framework via homology modeling. Sequence alignment between the C1 target and the C2 template was effected *via* the Clustal-W program (Thompson et al., 1994), using the BLOSUM-30 substitution matrix (Hanikoff and Hanikoff, 1993), and standard gap penalties of 10 for opening and 0.1 for extension. In the graphic, the ligand shown is 2'3' d-ATP bound to C1/C2 heterodimer alternated by C1/C1 homodimer. Carbon atoms of R1029 in C1/C2 dimer and the corresponding histidine residue in the C1/C1 dimer are shown in green and orange respectively.

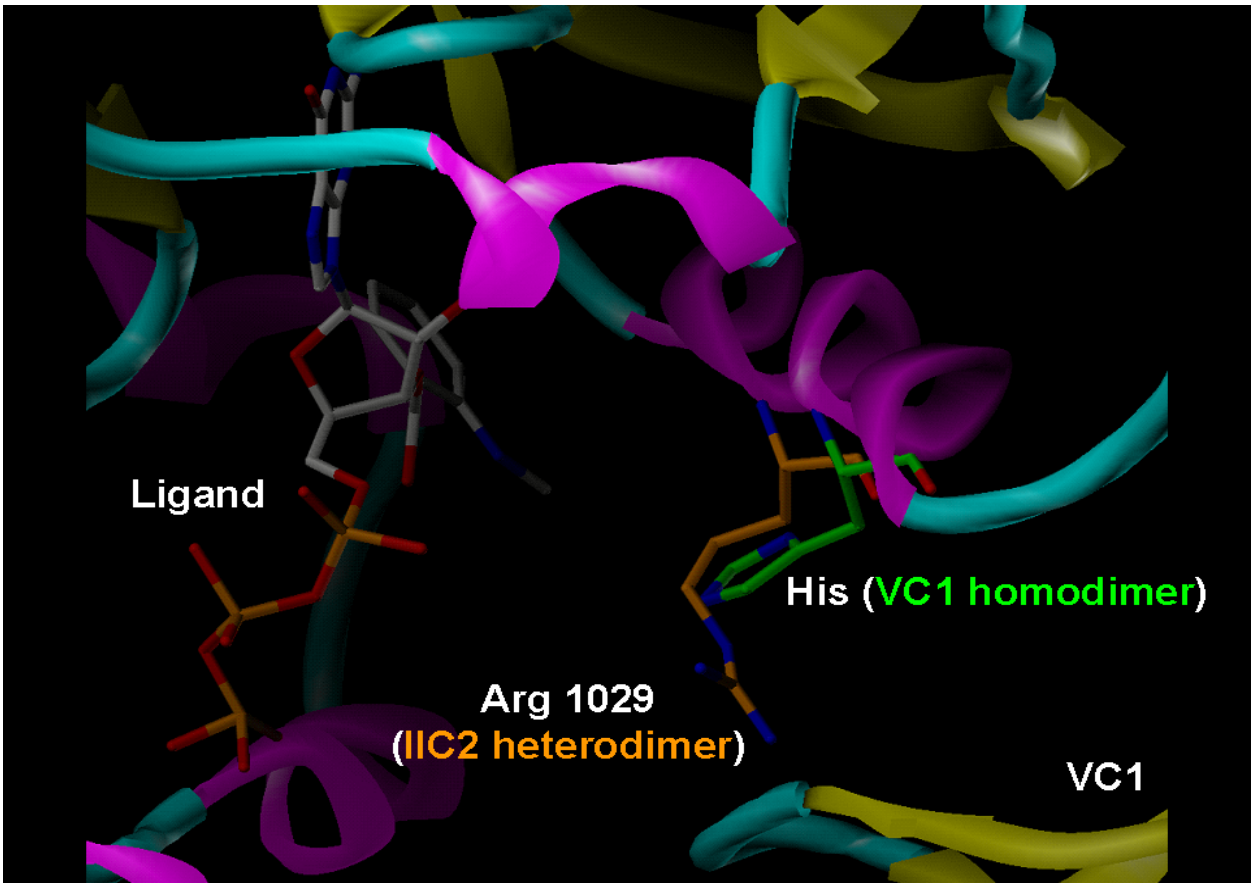
Ligand
His (VC1 homodimer)
Arg 1029
(IIC2 heterodimer)
VC1

3.5 Conclusions

In this chapter, using a variety of approaches, we have provided a demonstration that soluble catalytic subunits of mAC, C1 and C2 can exist as homodimers in solution. This homodimerization of C1 and C2 subunits may play an important physiological role in signaling.

Based on our earlier studies of the C1/C2 heterodimer with bound MANT-ATP, MANT-GTP or TNP-ATP, we have observed that the C2 domain contributes a site for purine binding and the C1 domain accommodates nucleotide phosphates and metal ions. The MANT or the TNP-group binds at the interface between C1 and C2 (Mou et al., 2006). However, we have observed an increase in fluorescence and FRET when TNP or MANT-nucleotide binds to C1. Keeping in mind the fact that C1 accommodates only the nucleotide phosphates, it is almost impossible for TNP or MANT-nucleotide to bind to a monomer of C1. Therefore, we predict that TNP and MANT-nucleotides bind to a hydrophobic site formed by two subunits of C1.

In our fluorescence assays with C1 alone, we found that FRET occurred between C1 and MANT-nucleotide indicating that MANT-nucleotide was in close proximity to tyrosine and tryptophan residues of C1. It is interesting to note that none of the C1 amino acid residues were responsible for FRET to occur between the C1/C2 heterodimer and bound MANT-nucleotide. In fact W1020 of C2 was most likely to be mainly responsible for FRET to the MANT

group (Mou et al., 2005). This indicates that C1 alone is in an altogether different conformation when compared to C1/C2 dimer thus making tyrosine and tryptophan residues more accessible for interaction with MANT-nucleotides. On the contrary, in the case of C2 with MANT-nucleotide, we did not observe any FRET between C2 and the MANT group indicating that W1020 is not accessible for interaction with MANT-nucleotides. This also suggests that the C2/C2 dimer does not have a nucleotide binding site. It would be extremely important to solve the crystal structure of C1 homodimer and carry out site-directed mutagenesis studies to identify the important residues involved in nucleotide binding and the residues responsible for FRET to the MANT group of MANT-nucleotides.

In addition to the above mentioned differences between C1 homodimers and C1/C2 heterodimer, we have also observed that FS interacts differently with the C1 homodimer when compared to the C1/C2 heterodimer. In enzymatic assays, in the case of C1/C2, submaximal activation of catalytic activity was observed in the presence of either $G\alpha_s$ or FS. When both $G\alpha_s$ and FS were present together, maximal activation of catalytic activity was observed. However, in the case of C1 homodimers or C2 homodimers, to observe measurable catalytic activity, both $G\alpha_s$ and FS must be present. In fluorescence experiments, addition of DMB-FS increased fluorescence of MANT-nucleotides when bound to C1/C2 (Mou et al., 2005 and 2006). In striking contrast, we found that when DMB-FS was added, a decrease or no

change in MANT-nucleotide fluorescence was observed when bound to C1 homodimer and C2 homodimer respectively. All these differences point to the fact that FS induces different conformational changes in homodimers vs. the heterodimers.

Based on our enzymatic studies, it is also clear that C1 shows low catalytic activity but a high affinity for substrate ATP, and C2 has extremely low catalytic activity. Our molecular modeling data support the above observation of strong ligand binding affinity to the C1 homodimer but an absence of catalytic activity due to replacement of Arg1029 in C1/C2 with a histidine in C1/C1. In electrophoresis experiments, C1 forms higher order aggregates in native PAGE, probably dimers but the interaction is probably unstable under the electrophoresis conditions. However based on the observed results, we predict that a dimer is a minimum that C1 can form with a low catalytic activity but a functional nucleotide binding site.

Earlier studies by Mitterauer et al. have shown that TNP-ATP can bind to C2 (Mitterauer et al., 1998). These results were surprising because our fluorescence experiments suggest that TNP-nucleotides do not bind to C2. There have been some differences in the experimental protocols, namely, the C2 used by Mitterauer et al, had a hexa-His tag at the N-terminus whereas the C2 used in our experiments was C terminal His-tagged. Also, the concentrations of TNP-nucleotide used were different, since fluorescence

assays are extremely sensitive and concentration dependent, we have used 5 μM TNP-nucleotide final concentration versus 100 μM TNP-ATP used by Mitterauer et al. However, it is not entirely clear if positive results obtained by Mitterauer et al. can be attributed to the above mentioned differences.

In previous studies with AC6 (Ding et al., 2005) and AC8 isoforms (Gu et al., 2001), it was observed that AC6 dimerizes via the TM1 domain and AC8 via the TM2 domain. In both cases, the dimerized forms showed lower plasma membrane expression and AC activity when compared to full length AC6 or AC8. The lower AC activity in AC6 is probably because when the two TM1 domains dimerize, the C1 subunits attached to TM1 domains may also dimerize to form a site with low catalytic activity but high affinity for ATP. Similarly, in the case of AC8, when TM2 regions dimerize, C2 domains may form dimers with low catalytic activity.

- ***Physiological relevance of C1 and C2 homodimers and isoform-specific heterodimers***

Preformed homodimers of C1 and C2 may play several important roles. Since C1 and C2 must dimerize to convert ATP to cAMP, dimerization of individual subunits of C1 and C2 may play an autoinhibitory role to serve as a checkpoint for excessive cAMP production. Since our studies were carried out using only C1a and C2a regions, an important role for C1b regions and the TM regions cannot be ruled out. In an intact molecule, it is well possible that

TM regions may prevent or promote homodimerization of C1 and C2 domains.

So far, we have seen that AC isoforms prefer to dimerize with their own kind instead of different isoforms (Cooper and Crossthwaithe, 2006). However, using a combination of approaches, recent studies have shown that a functional heterodimer of AC2/AC5 was localized on the plasma membrane in live cells (Baragli et al., 2008). AC2 and AC5 alone and together were co-expressed with $G\alpha_s$ in HEK293 cells and treated with FS. It was observed that cAMP accumulation in cells expressing both AC2 and AC5 was 6 times higher when compared to cells expressing either of the two AC isoforms. This production of cAMP was further enhanced by treatment with FS. These properties of the AC2/AC5 heterodimer are very similar to the soluble C1/C2 used as a model for AC catalysis and regulation over the last several years. This indicates the possibility of cross-talk between C1 of AC5 and C1 of AC2 or an interaction between the two C2 subunits in the AC2/AC5 heterodimer.

Furthermore, it has been found that AC2 and AC5 are co-localized in cardiac tissues (Baragli et al., 2008). It has also been demonstrated that AC2 and AC5 in rat ventricular cardiomyocytes are localized in the nuclear membranes (Boivin et al., 2006). This indicates that heterodimers are probably a special and distinct class of ACs with a more complex regulation. Colocalization of two different isoforms such as AC2 and AC5 in cardiac tissues also indicates an intriguing possibility of other tissue-specific

heterodimerization such as AC1 and AC2 in the brain, AC5 and AC6 in the heart and AC3 and AC8 in the pancreas. AC1 and AC2 in the brain are localized in regions important for learning and memory and play an important role in synaptic plasticity (Wu et al., 1995; Abdel-Majid et al., 1998; Furuyama et al, 1993). AC5 and AC6 in the heart play an important role in cardiac stress. AC6 is known to be cardioprotective, whereas AC5 antagonists are important for cardiac stress (Phan et al., 2007; Yan et al, 2007; Krishnan et al., 2008). AC3 and AC8 in the pancreas are implicated in glucose-mediated insulin secretion (Guenifi et al., 2000). Therefore, it would be extremely important to understand if these isoforms in these specific tissues formed heterodimers. It would also be important to study the role of C1 and C2 subunits in the overall regulation of the AC heterodimers.

Future studies in this area of research, using techniques such as FRET and BRET, (bioluminescence resonance energy transfer) will be required to understand the cross-talk between two similar or different AC isoforms. It will also be interesting to study chimeric ACs with TM domains from AC X and catalytic domains from AC Y.

References

Abdel-Majid RM, Leong WL, Schalkwyk LC, Smallman DS, Wong ST, Storm DR, Fine A, Dobson MJ, Guernsey DL and Neumann PE (1998) Loss of adenylyl cyclase I activity disrupts patterning of mouse somatosensory cortex. *Nat Genet* **19**(3):289-291.

Baragli A, Grieco ML, Trieu P, Villeneuve LR and Hebert TE (2008) Heterodimers of adenylyl cyclases 2 and 5 show enhanced functional responses in the presence of $G\alpha_s$. *Cell Signal* **20**(3):480-492.

Bieger B and Essen LO (2001) Structural analysis of adenylate cyclases from Trypanosoma brucei in their monomeric state. *Embo J* **20**(3):433-445.

Boivin B, Lavoie C, Vaniotis G, Baragli A, Villeneuve LR, Ethier N, Trieu P, Allen BG and Hebert TE (2006) Functional β-adrenergic receptor signalling on nuclear membranes in adult rat and mouse ventricular cardiomyocytes. *Cardiovasc Res* **71**(1):69-78.

Cooper DM and Crossthwaite AJ (2006) Higher-order organization and regulation of adenylyl cyclases. *Trends Pharmacol Sci* **27**(8):426-431.

Cooper DM, Mons N and Karpen JW (1995) Adenylyl cyclases and the interaction between calcium and cAMP signalling. *Nature* **374**(6521):421-424.

Defer N, Best-Belpomme M and Hanoune J (2000) Tissue specificity and physiological relevance of various isoforms of adenylyl cyclase. *Am J Physiol Renal Physiol* **279**(3):F400-416.

Dessauer CW, Tesmer JJ, Sprang SR and Gilman AG (1998) Identification of a $G_i\alpha$ binding site on type V adenylyl cyclase. *J Biol Chem* **273**(40):25831-25839.

Ding Q, Gros R, Chorazyczewski J, Ferguson SS and Feldman RD (2005) Isoform-specific regulation of adenylyl cyclase function by disruption of membrane trafficking. *Mol Pharmacol* **67**(2):564-571.

Furuyama T, Inagaki S and Takagi H (1993) Distribution of type II adenylyl cyclase mRNA in the rat brain. *Brain Res* **19**(1-2):165-170.

George SR, O'Dowd BF and Lee SP (2002) G-protein-coupled receptor oligomerization and its potential for drug discovery. *Nat Rev Drug Discov* **1**(10):808-820.

Gille A, Lushington GH, Mou TC, Doughty MB, Johnson RA and Seifert R (2004) Differential inhibition of adenylyl cyclase isoforms and soluble guanylyl cyclase by purine and pyrimidine nucleotides. *J Biol Chem* **279**(19):19955-19969.

Gille A and Seifert R (2003) 2'(3')-*O*-(*N*-methylanthraniloyl)-substituted GTP analogs: a novel class of potent competitive adenylyl cyclase inhibitors. *J Biol Chem* **278**(15):12672-12679.

Gu C, Cali JJ and Cooper DM (2002) Dimerization of mammalian adenylate cyclases. *Eur J Biochem / FEBS* **269**(2):413-421.

Gu C, Sorkin A and Cooper DM (2001) Persistent interactions between the two transmembrane clusters dictate the targeting and functional assembly of adenylyl cyclase. *Curr Biol* **11**(3):185-190.

Guenifi A, Portela-Gomes GM, Grimelius L, Efendic S and Abdel-Halim SM (2000) Adenylyl cyclase isoform expression in non-diabetic and diabetic Goto-Kakizaki (GK) rat pancreas. Evidence for distinct overexpression of type-8 adenylyl cyclase in diabetic GK rat islets. *Histochem Cell Biol* **13**(2):81-89.

Haga T, Haga K and Gilman AG (1977) Hydrodynamic properties of the β-adrenergic receptor and adenylate cyclase from wild type and varient S49 lymphoma cells. *J Biol Chem* **252**(16):5776-5782.

Hanoune J and Defer N (2001) Regulation and role of adenylyl cyclase isoforms. *Annu Rev Pharmacol Toxicol* **41**:145-174.

Haugeto O, Ullensvang K, Levy LM, Chaudhry FA, Honore T, Nielsen M, Lehre KP and Danbolt NC (1996) Brain glutamate transporter proteins form homomultimers. *J Biol Chem* **271**(44):27715-27722.

Henikoff S and Henikoff JG (1993) Performance evaluation of amino acid substitution matrices. *Proteins* **17**(1):49-61.

Ishikawa Y and Homcy CJ (1997) The adenylyl cyclases as integrators of transmembrane signal transduction. *Circ Res* **80**(3):297-304.

Jordan BA and Devi LA (1999) G-protein-coupled receptor heterodimerization modulates receptor function. *Nature* **399**(6737):697-700.

Krishnan V, Graham A, Mazei-Robison MS, Lagace DC, Kim KS, Birnbaum S, Eisch AJ, Han PL, Storm DR, Zachariou V and Nestler EJ (2008) Calcium-

sensitive adenylyl cyclases in depression and anxiety: behavioral and biochemical consequences of isoform targeting. *Biol Psychiatry* **64**(4):336-343.

Krupinski J, Coussen F, Bakalyar HA, Tang WJ, Feinstein PG, Orth K, Slaughter C, Reed RR and Gilman AG (1989) Adenylyl cyclase amino acid sequence: possible channel- or transporter-like structure. *Science, NY* **244**(4912):1558-1564.

Lee SJ, Gray MC, Zu K and Hewlett EL (2005) Oligomeric behavior of *Bordetella pertussis* adenylate cyclase toxin in solution. *Arch Biochem Biophys* **438**(1):80-87.

Marshall FH (2001) Heterodimerization of G-protein-coupled receptors in the CNS. *Curr Opin Pharmacol* **1**(1):40-44.

Mitterauer T, Hohenegger M, Tang WJ, Nanoff C and Freissmuth M (1998) The C2 catalytic domain of adenylyl cyclase contains the second metal ion (Mn^{2+}) binding site. *Biochemistry* **37**(46):16183-16191.

Mou TC, Gille A, Fancy DA, Seifert R and Sprang SR (2005) Structural basis for the inhibition of mammalian membrane adenylyl cyclase by 2 '(3')-*O*-(*N*-Methylanthraniloyl)-guanosine 5 '-triphosphate. *J Biol Chem* **280**(8):7253-7261.

Mou TC, Gille A, Suryanarayana S, Richter M, Seifert R and Sprang SR (2006) Broad specificity of mammalian adenylyl cyclase for interaction with 2',3'-substituted purine- and pyrimidine nucleotide inhibitors. *Mol Pharmacol* **70**(3):878-886.

Neer EJ, Lok JM and Wolf LG (1984) Purification and properties of the inhibitory guanine nucleotide regulatory unit of brain adenylate cyclase. *J Biol Chem* **259**(22):14222-14229.

Phan HM, Gao MH, Lai NC, Tang T and Hammond HK (2007) New signaling pathways associated with increased cardiac adenylyl cyclase 6 expression: implications for possible congestive heart failure therapy. *Trends Cardiovasc Med* **17**(7):215-221.

Schlegel W, Kempner ES and Rodbell M (1979) Activation of adenylate cyclase in hepatic membranes involves interactions of the catalytic unit with multimeric complexes of regulatory proteins. *J Biol Chem* **254**(12):5168-5176.

Shenoy AR, Srinivasan N, Subramaniam M and Visweswariah SS (2003)

Mutational analysis of the Mycobacterium tuberculosis Rv1625c adenylyl cyclase: residues that confer nucleotide specificity contribute to dimerization. *FEBS Lett* **545**(2-3):253-259.

Smigel MD (1986) Purification of the catalyst of adenylate cyclase. *J Biol Chem* **261**(4):1976-1982.

Sunahara RK, Dessauer CW and Gilman AG (1996) Complexity and diversity of mammalian adenylyl cyclases. *Annu Rev Pharmacol Toxicol* **36**:461-480.

Sunahara RK, Dessauer CW, Whisnant RE, Kleuss C and Gilman AG (1997) Interaction of $G_s\alpha$ with the cytosolic domains of mammalian adenylyl cyclase. *J Biol Chem* **272**(35):22265-22271.

Sunahara RK and Taussig R (2002) Isoforms of mammalian adenylyl cyclase: multiplicities of signaling. *Mol Interv* **2**(3):168-184.

Tang WJ and Gilman AG (1995) Construction of a soluble adenylyl cyclase activated by $G_s\alpha$ and forskolin. *Science* **268**(5218):1769-1772.

Tang WJ and Hurley JH (1998) Catalytic mechanism and regulation of mammalian adenylyl cyclases. *Mol Pharmacol* **54**(2):231-240.

Tesmer JJ, Sunahara RK, Gilman AG and Sprang SR (1997) Crystal structure of the catalytic domains of adenylyl cyclase in a complex with $G_s\alpha$ .GTPγS. *Science* **278**(5345):1907-1916.

Thompson JD, Higgins DG and Gibson TJ (1994) CLUSTAL W: improving the sensitivity of progressive multiple sequence alignment through sequence weighting, position-specific gap penalties and weight matrix choice. *Nucleic Acids Res* **22**(22):4673-4680.

Wang S, Yue H, Derin RB, Guggino WB and Li M (2000) Accessory protein facilitated CFTR-CFTR interaction, a molecular mechanism to potentiate the chloride channel activity. *Cell* **103**(1):169-179.

Whisnant RE, Gilman AG and Dessauer CW (1996) Interaction of the two cytosolic domains of mammalian adenylyl cyclase. *Proc Natl Acad Sci U S A* **93**(13):6621-6625.

Wu ZL, Thomas SA, Villacres EC, Xia Z, Simmons ML, Chavkin C, Palmiter RD and Storm DR (1995) Altered behavior and long-term potentiation in type I adenylyl cyclase mutant mice. *Proc Natl Acad Sci U S A* **92**(1):220-224.

Yan L, Vatner DE, O'Connor JP, Ivessa A, Ge H, Chen W, Hirotani S, Ishikawa Y, Sadoshima J and Vatner SF (2007) Type 5 adenylyl cyclase disruption increases longevity and protects against stress. *Cell* **130**(2):247-258.

Yeager RE, Heideman W, Rosenberg GB and Storm DR (1985) Purification of the calmodulin-sensitive adenylate cyclase from bovine cerebral cortex. *Biochemistry* **24**(14):3776-3783.

Zhang G, Liu Y, Ruoho AE and Hurley JH (1997) Structure of the adenylyl cyclase catalytic core. *Nature* **386**(6622):247-253.

Chapter 4: Molecular analysis of edema factor, a Bacillus anthracis adenylyl cyclase toxin and its interaction with calmodulin using MANT-nucleotides as probes.

4.1 Introduction

Edema Factor (EF), one of the exotoxins released by *Bacillus anthracis*, contributes considerably to both cutaneous and systemic forms of anthrax (Leppla, 1982; Dixon et al., 1999). EF, a ~90 kDa protein, consists of a protective antigen binding domain (PABD, ~30 kDa) and an adenylyl cyclase domain (ACD, ~60 kDa) (Drum et al., 2000; Bhatnagar et al, 2001). After protective antigen (PA)- mediated entry into host cells, EF is activated by calmodulin (CaM), a calcium sensor protein and catalyzes the conversion of adenosine 5'-triphosphate (ATP) to adenosine 3':5'-cyclic monophosphate (cAMP) (Drum et al., 2002; Shen et al., 2002). Binding of calmodulin to EF causes a major conformational change in EF giving rise to excessive intracellular levels of cAMP which in turn disrupts several signaling pathways (Shen et al., 2005). EF can severely impair host defenses and suppress innate immune responses (Firoved et al., 2007; Kammer et al., 1988; Kyriakis et al., 2001).

EF plays a crucial role in causing anthrax and therefore, several studies have been carried out to identify potent inhibitors of EF catalytic activity. Using a variety of approaches, several studies have traditionally identified both fluorescent and non-fluorescent analogs of the substrate ATP as potent inhibitors of EF. Johnson et al. (1990) identified polyadenylate (IC_{50} in the mM range) and 2'd 3' AMP (IC_{50} in the μM range) as low - moderate potency inhibitors of EF and *CyaA*, an adenylyl cyclase toxin from *Bordetella pertussis* (Confer and Eaton, 1982; Hewlett et al., 1989; Ladant and Ullmann, 1999). The crystal structure of EF in complex with CaM and 3'd-ATP helped to gain insight into the activation and catalytic mechanism of EF (Drum et al., 2002). Shen et al., (2004a) have observed that adenosine 5'-(α, β-methylene)-triphosphate (AMPCPP) inhibits EF with low potency (K_i = 0.85 mM) and possesses an alternative binding mode in the catalytic pocket of the EF-CaM complex. Shen et al (2004b) also observed that the antiviral drug, adefovir dipivoxil potently inhibits EF AC activity (K_i = 27 nM). Adefovir, approved for treatment of chronic hepatitis B virus infection, is an acyclic nucleotide analog of adefovir monophosphate and is phosphorylated into its active metabolite, adefovir diphosphate (PMEApp). Furthermore, the fluorescent nucleotide 3'-anthraniloyl-2'-deoxy-ATP (3'ANT-2'd-ATP) can bind to both EF and *CyaA* (Sarfati et al., 1990; Gallay et al., 2004). As monitored by fluorescence spectroscopy, the K_d for 3'ANT-2'd-ATP binding to EF-CaM is1 μM. Additionally, the crystal structure of EF-CaM in complex with 3'ANT-2'd-ATP

was comparable to that of EF-CaM-3'd-ATP complex (Drum et al., 2002; Shen et al., 2002). Furthermore, N-methylanthraniloyl (MANT)-substituted nucleotides are potent inhibitors of mammalian ACs and bacterial ACs including EF and *CyaA* (Gille et al., 2004).

Several small molecules structurally dissimilar to ATP analogs and peptide based inhibitors also potently inhibit the catalytic activity of EF. Based on the crystal structure of EF, molecular docking experiments were carried out with ~200,000 commercially available small molecules and identified a specific quinazoline compound that does not affect EF-CaM binding but specifically inhibits EF AC activity (K_i = 20 μM) (Soelaiman et al., 2003). This compound also efficiently inhibited *CyaA* (K_i = 20 μM). A specific anti-protective antigen (anti-PA) branched peptide called MAP3 V/A was also capable of inhibiting EF catalytic activity in several cell lines (Pini et al., 2006). Very recently, 3 out of 19 diverse compounds were identified that are capable of inhibiting EF catalytic activity in cell-based assays (Chen et al., 2008). Based on crystal structures of EF alone and in complex with CaM and several inhibitors, they generated a 3D-pharmacophore model for EF. Using a fragment-based screening approach, at least 10,000 compounds from the ZINC database were virtually docked onto the 3D-pharmacophore model. Out of 19 compounds selected, 3 were chosen for cell based assays depending on various factors such as toxicity, solubility and penetration into the cell.

Although, most of the inhibitor development studies have aimed at blocking EF catalytic activity, it is also important to focus on studying EF-CaM binding. After entry of EF into cells, the EF-CaM interaction is the first step in the intoxication mechanism of EF (Deisseroth et al., 1998; Drum et al., 2000, Leppla, 1982). CaM, composed of 148 residues, possesses N and C terminal globular domains connected by a long α-helix (Babu et al., 1985; Zhang et al., 1995). Each domain consists of two Ca^{2+} binding sites. CaM exists in three different Ca^{2+} loading states namely-a Ca^{2+} free apo-form, a two Ca^{2+}ions-bound C-terminal domain and a four Ca^{2+}-bound form with both N and C-terminal domains being loaded (Ikura, 1996; Nelson et al., 1998). Although lower Ca^{2+} concentrations are required for activation and catalysis of EF, higher Ca^{2+} concentrations inhibit EF catalysis (Shen et al., 2002). EF-CaM binding can alter the Ca^{2+} loading state of CaM. EF interacts with N-CaM in a calcium independent manner but forms a tighter interaction with C-CaM only in the presence of calcium (Ulmer et al., 2003; Shen et al., 2005). Furthermore, FRET experiments with a double-labeled CaM molecule demonstrated that CaM binds to EF in an extended conformation (Drum et al., 2000). A two-cysteine CaM mutant was generated in which T34 and T110 in the N and C-terminal domains of CaM respectively, were replaced with cysteine residues. The distance between the two cysteine residues in the presence of EF was ~49 Å indicating an extended conformation compared to

the compact CaM conformation in complex with several effector proteins (~16 Å).

Though several crystallographic, biochemical and structural studies have helped to understand the EF-CaM interaction, in practice it has been extremely difficult to identify small molecules inhibitors of protein-protein interaction (IPPI) the block EF-CaM binding. Using a combination of spectroscopic and cell-based approaches, a benzene sulfonamide derivative (10506-2A) was identified as an IPPI for the EF-CaM interaction. This compound was capable of binding to EF and preventing activation of EF by CaM thereby blocking EF catalytic activity (Lee et al., 2004).

To promote development of inhibitors for EF catalytic activity and of the EF-CaM interaction, a systemic study of these processes is needed. In this chapter, we study the inhibitory properties of fluorescent nucleotides and examine the EF-CaM interaction using these fluorescent nucleotides as probes.

4.2 Specific aims and hypothesis

This chapter will deal with two different aspects of EF. Firstly, several crystallographic, biochemical, structural and cell-based approaches have revealed the catalytic mechanism of EF and have identified potent inhibitors of EF catalytic activity. Studies conducted in our laboratory have identified MANT-nucleotides as potent inhibitors of mAC and CyaA (Gille and Seifert, 2003; Gille et al., 2004; Gottle et al., 2007). Furthermore, 3' MANT-2'd-ATP was identified as a potent inhibitor of EF. However, in order to fully exploit the properties of MANT-nucleotides as potent EF inhibitors, a systematic analysis of MANT-ATP and MANT-GTP analogs was undertaken. The study is aimed at answering the following questions.

- If MANT-ATP and MANT-GTP analogs inhibit EF in the presence of CaM?
- If MANT-ATP and MANT-GTP analogs bind to EF, as monitored by fluorescence spectroscopy?
- If CaM induced-conformational changes in EF could be probed by MANT-ATP and MANT-GTP analogs?
- If MANT-ATP and MANT-GTP analogs demonstrate a differential binding to EF/CaM?

It is known that EF binds to an extended conformation of CaM (Drum et al., 2000). It has also been observed that the EF-CaM interaction and catalysis are dependent on physiological calcium concentrations and depending on the Ca^{2+} loading state, EF binds differentially to N- and C-CaM (Shen et al., 2002 and 2005). However, molecular analysis of a Ca^{2+} dependent/independent interaction between EF and CaM has not yet been probed by fluorescent nucleotides.

Furthermore, oxidation of CaM can alter its binding to effector proteins (Bartlett et al., 2003; Gao et al., 1998). Paritally oxidized CaM can alter the activation and binding to CaM-dependent kinase II (Robison et al., 2007). In the case of bacterial infections, the primary targets are neutrophils, which when activated, produce reactive oxygen species causing oxidation of both intracellular proteins and foreign proteins. Additionally, CyaA-CaM complex is resistant to oxidation to a certain extent indicating that CyaA can still exert its toxic effect even when CaM is oxidized (Vougier et al., 2004). However, it is not known if oxidized CaM can bind and activate EF. In this chapter, the following questions will be examined in detail.

- Role of calcium in CaM-EF interaction as monitored by fluorescence spectroscopy.
- Effect of CaM oxidation on EF-CaM interaction.

Previous studies have demonstrated that CyaA has a spacious catalytic site that can accommodate 2' (-3')-substituted nucleotides (Gottle et al., 2007). Furthermore, as mentioned in chapters 1 and 2, we have generated a three-site pharmacophore model of the mAC catalytic site with a broad-base specificity, i.e, it can bind to both purine and pyrimidine nucleotides (Mou et al., 2006). Therefore, we predict that

- MANT-nucleotides potently inhibit EF catalytic activity.
- Calcium plays an important role in binding and activation of EF.
- Oxidation of CaM alters its binding to EF.

Based on our studies, we expect to obtain a clear understanding of the properties of the MANT-nucleotide and EF-CaM binding processes which will greatly facilitate the rationale design of potent EF inhibitors.

4.3 Materials and methods

4.3.1 Materials

EF (full length) and EF3 (catalytic domain only) were kindly donated by Dr. W.J.Tang (Ben May Department for Cancer Research, University of Chicago, IL). MANT-nucleotides (MANT-ATP, 2'MANT-3'd-ATP, 3'MANT-2'd-ATP, MANT-GTP, 2'MANT-3'd-GTP, 3'MANT-2'd-GTP) were obtained from Jena Bioscience (Jena, Germany). An overview of the structure of MANT-nucleotides is shown in Figure 4-1. In the case of MANT-ATP and MANT-GTP, the MANT-group isomerizes between the 2' and 3' position of the ribose ring. In other MANT-nucleotides, the MANT-group is fixed either at the 2' or 3' position due to the lack of the neighboring hydroxyl group. Calmodulin purified from bovine brain and calmidazolium chloride were purchased from Calbiochem (La Jolla, CA). 2'5' dd 3'ATP was obtained from Sigma (St. Louis, MO). [α-^{32}P]-ATP (6000 Ci/mmol) was purchased from PerkinElmer Life Sciences. Microcon centrifugal filter devices (YM-30) were obtained from Millipore Corporation. Sources of other materials were described previously (Gille et al., 2004; Mou et al., 2005 and 2006; Gottle et al., 2007) and in chapters 2 and 3 respectively.

Figure 4-1 Structure of MANT-nucleotides

Chemical structures of MANT-ATP, MANT-GTP and its analogs are shown. The MANT-group which spontaneously isomerizes between the 2’ and the 3’ position of the ribose moiety in the case of MANT-ATP and MANT-GTP but not in other MANT-nucleotides shown, confers fluorescent features to the nucleotides.

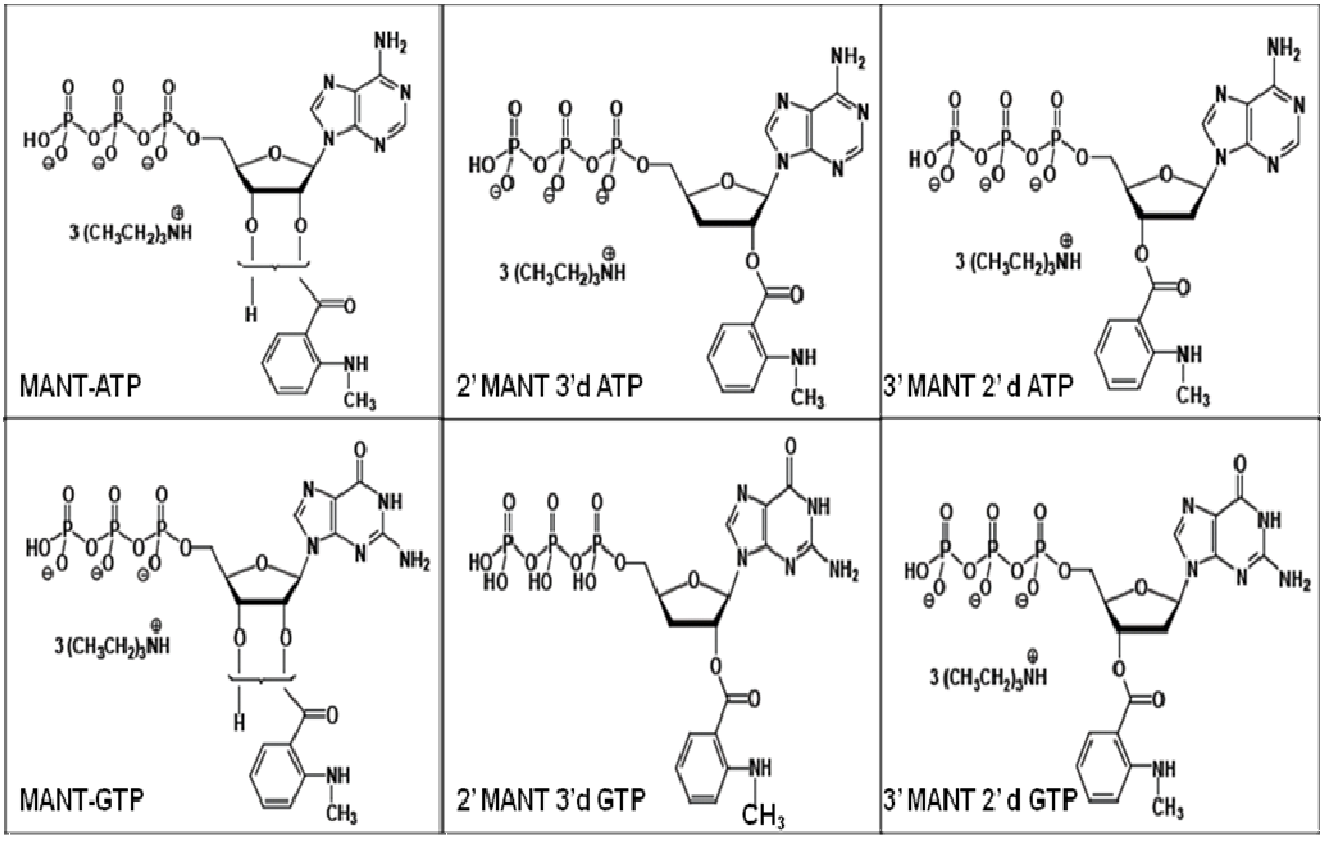

4.3.2 Experimental methods

- ***EF AC activity assay***

EF AC activity assays were conducted as described previously (Gille et al., 2004) and in chapter 2. For determination of potencies of MANT-nucleotides as EF inhibitors, assay tubes contained 10 pM EF/EF3 and 10 μl of MANT-nucleotides with concentrations ranging from 10 nM to 100 μM to obtain inhibition curves. Additionally, reaction mixtures containing 100 μM KCl, 40 μM unlabelled ATP, 5 mM Mn^{2+} or Mg^{2+}, 100 μM EGTA, 100 nM CaM, 100 μM cAMP, 100 μM Ca^{2+} and [α-^{32}P]ATP were added to the assay tubes. AC activity was carried out as described in section 2.3.2 of chapter 2.

- ***Fluorescence spectroscopy***

All experiments were carried out using a Cary Eclipse fluorescence spectrophotometer at 25˚C (Varian, Walnut Creek, CA). Measurements were performed using a quartz fluorescence microcuvette (Hellma, Plainview, NY). Steady-state emission spectra were recorded with λ_{ex} = 280 nm (λ_{em} = 300 – 500 nm) for intrinsic protein fluorescence and λ_{ex} = 350 nm (λ_{em} = 370 – 500 nm) for MANT-nucleotide fluorescence. Reaction mixtures containing 100 mM KCl, 10 mM $MnCl_2$ or $MgCl_2$ and 25 mM HEPES/NaOH, pH 7.4 were added to the cuvette and the final assay volume was 150 μl. Three hundred nM each of MANT-nucleotide, EF/EF3 and CaM were included.

For EF saturation experiments, MANT-nucleotides ranging from 165 nM to 1.3 μM were used to obtain saturation curves. All EF saturation experiments were performed in the presence of 10 mM Mn^{2+} 300 nM each of EF3 and CaM respectively. For determination of K_d values, MANT-nucleotide fluorescence was first corrected for the inner filter effect by recording the absorbance spectra of the respective MANT-nucleotide at the highest concentration in the presence of EF3 and CaM. Since the absorption wavelength depends on the emission properties of the respective nucleotide studied, it varied from nucleotide to nucleotide. The absorption wavelength was then subtracted depending on the concentrations of the MANT-nucleotides used in the saturation experiments.

For competition studies with 2'5' dd 3' ATP and calmidazolium chloride, experiments were carried out similarly except that 2'5' dd 3' ATP or calmidazolium chloride was added in place of CaM. Reactions were first carried out in the kinetic mode to observe the displacement of MANT-nucleotides by increasing concentrations of 2'5' dd 3'ATP. Since calmidazolium chloride inhibits CaM, the rate of change in EF-CaM fluorescence was observed.

To probe Ca^{2+} dependent/independent EF3-CaM interactions using 2' MANT-3'd-ATP, experiments were carried out in the presence and absence of calcium under three different conditions namely (1) in the presence of 100 μM

Ca^{2+} and no EGTA (2) 100 μM EGTA and no Ca^{2+} and (3) no Ca^{2+} and no EGTA. Fluorescence emission spectra were recorded with both λ_{ex} = 280 nm (λ_{em} = 300 – 500 nm) and λ_{ex} = 350 nm (λ_{em} = 370 – 500 nm).

For fluorescence experiments with oxidized calmodulin CaM (O), 10 μM CaM was incubated with 0.06% (vol/vol) of 8.8 M H_2O_2 for 24 h at 37˚C. Ten μM CaM in the absence of H_2O_2 (CaM (N)) was also incubated as control. After incubation, for desalting and efficient concentration of CaM, 25 μl each of normal and oxidized CaM and 175 μl of 25 mM HEPES pH 7.4 were added to microcon centrifugal filter devices (YM-30) and concentrated by centrifugation for 10 min at 11,000 x g. Filter device YM-30 helps desalt and concentrate proteins upto 30 kDa. After repeating the above steps 4-5 times, a Biorad assay was carried out to determine the concentrations of CaM (N) and CaM (O). Fluorescence emission spectra with CaM (O) and CaM (N) were recorded with both λ_{ex} = 280 nm (λ_{em} = 300 – 500 nm) and λ_{ex} = 350 nm (λ_{em} = 370 – 500 nm). Fluorescence experiments were also carried out in the kinetic mode to analyze the rate of binding of CaM (N) and CaM (O) to EF3.

-Molecular modeling studies

Molecular docking studies were carried out in collaboration with Dr. G.H. Lushington (University of Kansas, Lawrence). The six MANT-nucleotides studied in this chapter and 12 MANT-nucleotides studied by Jennifer Schmidt (University of Regensburg, Germany) were used for docking studies. MANT-

nucleotides were docked into the receptor model constructed using the crystal structure of EF3-CaM in complex with 3'-d-ATP as inhibitor (Drum et al., 2002). Amino acid residues with atoms further than 12 Å from the inhibitor 3'-d-ATP were truncated from the model. Except for the *in situ* Mn^{2+}, all of the heteroatoms were omitted. The ligands were docked into the receptor structure and a quantitative structure-activity relationship (QSAR) model was generated. The highest computed binding energy for each ligand was chosen to study the specific interactions between the ligand and the amino acid residues in receptor EF3.

- ***Data generation and statistics***

Saturation inhibition curves for EF AC activity were analyzed by nonlinear regression using Prism 4.0 software (Graphpad, San Diego, CA). Free Ca^{2+} concentrations were calculated using 100 μM EGTA as calcium chelator with WinmaxC 2.05 version (www.stanford.edu/~cpatton/max-c.html). K_i Values were calculated based on K_m values determined previously for EF (Gille et al., 2004). Data shown are the mean values ± SD of 5-6 experiments performed in duplicate.

Fluorescence recordings were analyzed using the spectrum package of the Cary Eclipse software and final graphs were prepared using Graphpad prism 4.0 software. Similar results were obtained from 3 – 4 independent experiments using 3-5 different batches of EF and EF3 respectively. Kinetics

of CaM (N) and CaM (O) binding to EF3 were analyzed by the one-phase exponential association equation in the Graphpad prism 4.0 software.

In Molecular modeling studies, the SYBYL program (SYBYL 7.2, The Tripos Associates, St. Louis, MO) was used to protonate the EF3-CaM receptor model. All the MANT-nucleotides were also sketched and protonated using SYBYL and relaxed via the molecular mechanics optimization settings in SYBYL using the Tripos Force Field (Clark et al., 1989). Ligand-receptor complexes were generated using the FLexX program via flexible docking simulations (Rarey et al., 1996). The QSAR model was generated via the Comparative Binding Energy (COMBINE) method (Ortiz et al., 1995). For each of the 16 ligands, several poses were generated and the pose with the highest computed binding energy was selected to study ligand-receptor interactions.

4.4 Results and Discussion

4.4.1 Inhibition of catalytic activity of EF3 by MANT-nucleotides

In earlier studies carried out in the Seifert laboratory, we have observed that MANT-nucleotides potently inhibit mACs, EF and CyaA (Gille and Seifert, 2003; Gille et al., 2004; Gottle et al., 2007). In mACs, MANT-GTP is more potent than MANT-ATP. Furthermore, crystallographic and molecular modeling studies have demonstrated that the MANT-group at the 2'-*O*-ribosyl position is in a more hydrophobic environment and therefore more favored compared to the MANT-group at the 3'-*O*-ribosyl position (Gille et al., 2004, Mou et al., 2005). In sharp contrast, in the case of both EF and CyaA, the 3' analog of MANT-ATP is the most potent inhibitor reported so far (K_i = 13 nM and 0.2 μM for EF and CyaA respectively) (Gille et al., 2004; Gottle et al., 2007). Additonally, MANT-GTP also moderately inhibits EF (K_i =1.6 μM) (Gille et al., 2004). However, a detailed analysis of the structure-activity relationships with 2' and 3'-MANT-nucleotide isomers and EF has not been studied. Therefore, we examined the properties of 2' and 3'-MANT analogs of ATP and GTP in inhibiting EF and EF3. Since, it is known that there are no major differences between EF and EF3 with respect to inhibition by MANT-nucleotides, the affinities of MANT-nucleotides for EF3 only are reported here.

In the presence of Mn^{2+} and in the presence of Ca^{2+}/CaM, 3' MANT-2'd-ATP is the most potent inhibitor of EF3 (K_i = 11 nM), a result that is similar to results obtained earlier (Gille et al., 2004, K_i = 13 nM) (Table 4-1). The rank order of potency was 3'MANT-2'd-ATP > 2' MANT-3'd-ATP = 2' MANT-3'd-GTP > 3' MANT-2'd-GTP = MANT-ATP > MANT-GTP. Overall MANT-ATP analogs were more potent at inhibiting EF compared to MANT-GTP analogs. MANT-ATP was at least 9-fold and 33 fold less potent than 2' MANT-3'd-ATP and 3' MANT-2'd-ATP respectively. Similarly, MANT-GTP was also at least 2-fold and 3-fold less potent than 2' MANT-3'd-GTP and 3' MANT-2'd-GTP respectively. Most strikingly, 3'MANT-2'd-ATP was 3.6-fold more potent than 2'MANT-3'd-ATP, whereas 2'MANT-3'd-GTP was at least 7-fold more potent than 3'MANT-2'd-GTP. Though the 2' analogs of both MANT-ATP and MANT-GTP showed comparable affinities for EF, a huge difference in the potencies between the 3' analogs of MANT-ATP and MANT-GTP were observed.

Under Mg^{2+} conditions, in the presence of Ca^{2+}/CaM, an overall decrease in the affinity of MANT-nucleotides for EF3 was observed (Table 4-1). The rank order of potency was 3' MANT-2'd-ATP > MANT-ATP > 2' MANT-3'd-ATP = 2' MANT-3'd-GTP > MANT-GTP > 3' MANT-2'd-GTP. Again, 3' MANT-2'd-ATP was the most potent inhibitor of EF in the presence of Mg^{2+}. The affinities of 2' MANT-3'd-ATP and 3' MANT-2'd-ATP for EF3 were at least 115-fold and 68-fold lower in the presence of Mg^{2+} when compared to those obtained in the presence of Mn^{2+} c. Similarly, 2' MANT-3'd-GTP and 3' MANT-

2’d-GTP showed at least 86-fold and 27-fold lower potency in the presence of Mg^{2+}. Surprisingly, it was observed that MANT-ATP and MANT-GTP had comparable affinities to 3’ MANT-2’d-ATP and 3’ MANT-2’d-GTP respectively for EF3 in the presence of Mg^{2+}. This observation possibly indicates that in the presence of the physiological ligand, the 3’-*O*-ribosyl conformer of the MANT-group of both ATP and GTP is preferred over the 2’-*O*-ribosyl conformer.

Based on experiments of MANT-nucleotide affinities for EF3 under Mn^{2+} and Mg^{2+} conditions, it is clear that MANT-nucleotides bind and inhibit EF3 with a higher affinity in the presence of Mn^{2+} than in the presence of Mg^{2+}. This observation also corroborates available literature related to cyclases that indicate a higher sensitivity to inhibition in the presence of Mn^{2+} (Gille and Seifert, 2003; Brandwein et al., 1982; Shoshani et al., 1999; Tesmer et al., 2000). Nonetheless, Mg^{2+} is more relevant under physiological conditions and therefore, it was important to study the inhibitory effects of MANT-nucleotides on EF3 in the presence of Mg^{2+}.

In a detailed comparison of the potencies of MANT-nucleotides for EF3, and mACs, 3’ MANT-2’d-ATP was at least 35-fold more potent at inhibiting EF3 compared to C1/C2. Additionally, though MANT-GTP is the least potent inhibitor of EF3 (K_i = 1.08 μM) and the most potent inhibitor of C1/C2 (K_i = 4.2 nM), 2’ MANT and 3’ MANT analogs of GTP were highly potent at inhibiting

EF3. Furthermore, all the MANT-nucleotides studied were more potent inhibitors of EF3 than CyaA (Gottle et al., 2007).

Overall, the 2’ and 3’ isomers of MANT-ATP and MANT-GTP were more potent at inhibiting EF3 when compared to mACs and CyaA indicating the possibility of structural differences in the catalytic sites of these enzymes. Therefore, the 2’ and 3’ isomers of MANT-ATP and MANT-GTP can be considered for future design of EF3 inhibitors.

Table 4-1 Inhibitory potencies of MANT-nucleotides under Mn^{2+} and Mg^{2+} conditions

EF AC activity assays were conducted as described previously (Gille et al., 2004) and in section 2.3.2 of chapter 2. Assay tubes contained 10 pM EF/EF3 and 10 μl of MANT-nucleotides with concentrations ranging from 10 nM to 100 μM to obtain saturation inhibition curves. Additionally, reaction mixtures containing 100 μM KCl, 40 μM unlabelled ATP, 5 mM Mn^{2+} or Mg^{2+}, 100 μM EGTA, 100 nM CaM, 100 μM cAMP, 100 μM Ca^{2+} and [α-^{32}P]ATP were added to the assay tubes. Data were analyzed by nonlinear regression using the Prism 4.0 software (Graphpad, San Diego, CA) and K_i values, expressed in μM were calculated based on K_m values calculated previously for EF (Gille et al., 2004). Data shown are the mean values ± SD of 5-6 independent experiments performed in duplicate.

Nucleotides	**Mn^{2+}** ***K_i* (μM)**	**Mg^{2+}** ***K_i* (μM)**
MANT-ATP	0.36 ± 0.18	0.9 ± 0.07
2’ MANT-3’d-ATP	0.04 ± 0.002	4.6 ± 0.2
3’ MANT-2’d-ATP	0.011 ± 0.002	0.75 ± 0.04
MANT-GTP	1.08 ± 0.4	8.8 ± 0.3
2’ MANT-3’d-GTP	0.05 ± 0.01	4.3 ± 0.4
3’ MANT-2’d-GTP	0.36 ± 0.1	9.9 ± 1.6

Figure 4-2 Inhibition of the catalytic activity of EF3 by MANT-nucleotides under Mn^{2+} and Mg^{2+} conditions

EF AC activity assay was conducted as described previously (Gille et al., 2004) and in chapter 2. Briefly, assay tubes contained 10 pM EF/EF3 and 10 μl of MANT-nucleotides with concentrations ranging from 10 nM to 100 μM to obtain saturation inhibition curves. Additionally, reaction mixtures containing 100 μM KCl, 40 μM unlabelled ATP, 5 mM Mn^{2+} or Mg^{2+}, 100 μM EGTA, 100 nM CaM, 100 μM cAMP, 100 μM Ca^{2+} and [α-^{32}P]ATP were added to the assay tubes. Saturated inhibition curves were analyzed by nonlinear regression using Prism 4.0 software (Graphpad, San Diego, CA). EF AC activity is expressed in turnover numbers (s^{-1}). Data shown are representative of 5-6 independent experiments performed in duplicate.

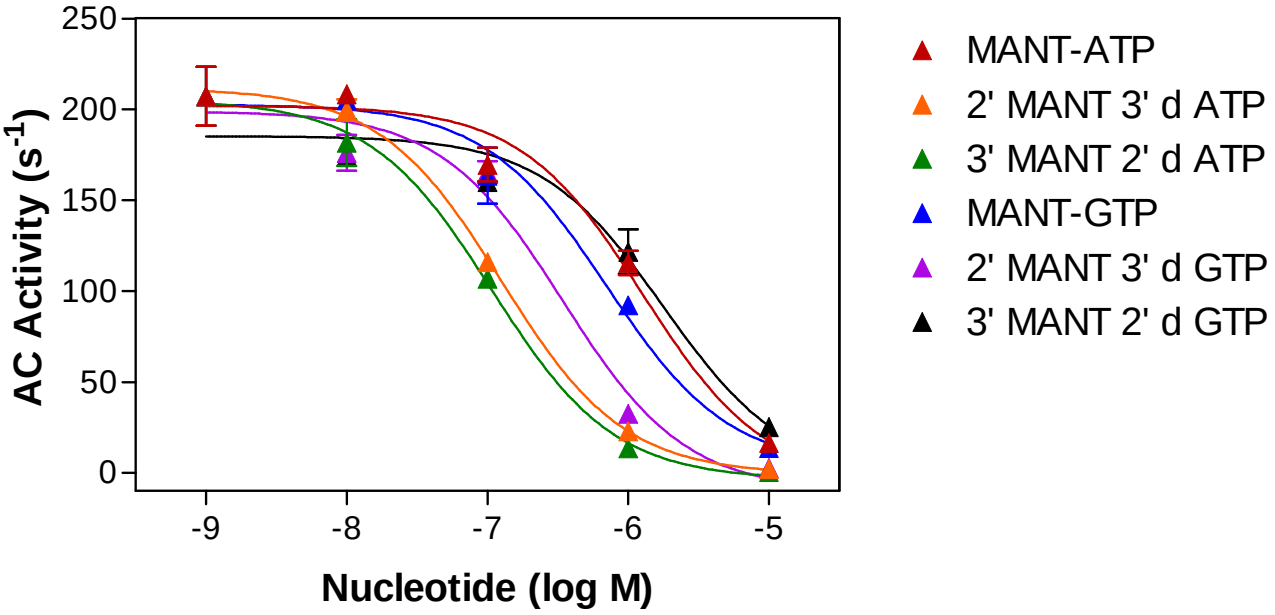
AC Activity (s^{-1})
250
200
150
100
50
0
-9
-8
-7
-6
-5
Nucleotide (log M)
MANT-ATP
2' MANT 3' d ATP
3' MANT 2' d ATP
MANT-GTP
2' MANT 3' d GTP
3' MANT 2' d GTP

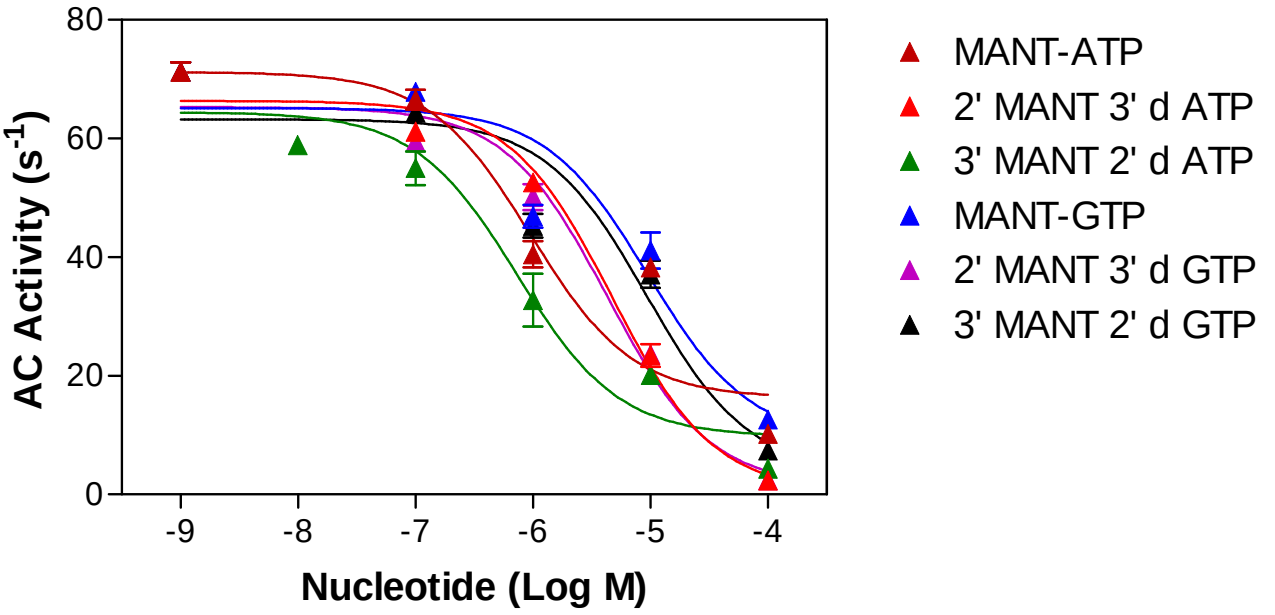
AC Activity (s^{-1})
80
60
40
20
0
-9
-8
-7
-6
-5
-4
Nucleotide (Log M)
MANT-ATP
2' MANT 3' d ATP
3' MANT 2' d ATP
MANT-GTP
2' MANT 3' d GTP
3' MANT 2' d GTP

4.4.2 Characterization of EF interaction with MANT-nucleotides by fluorescence spectroscopy

MANT-nucleotides are environmentally sensitive probes utilized in the study of several nucleotide-binding proteins, structural proteins and enzymes (Hazlett et al., 1993; Bauer et al., 1997; Hiratsuka, 1983; Jameson and Eccleston, 1997). Specifically, MANT-nucleotides have been used to monitor conformational changes in mACs and *CyaA* (Mou et al., 2005 and 2006; Göttle et al., 2007). Crystallographic and fluorimetric data suggest that MANT-nucleotides bind to a hydrophobic pocket formed by C1/C2 resulting in a several-fold increase in fluorescence. MANT-nucleotide interacts with several polar and hydrophobic amino acid residues and thereby is stabilized in the catalytic pocket of C1/C2. This interaction causes an increase in MANT fluorescence indicating the presence of MANT-nucleotide in a hydrophobic environment within C1/C2. Furthermore, the MANT-group lies close to W1020 residue of C2 resulting in energy transfer from W1020 to the MANT-group (Mou et al., 2005 and 2006).

In *CyaA*, MANT-nucleotides interact with the hydrophobic residue F306 in the catalytic site. This interaction is likely to increase fluorescence signals. Additionally, FRET occurs between W69, W242 and multiple tyrosine residues and the MANT-group in *CyaA* (Göttle et al., 2007). Very similar to *CyaA*, crystallographic and fluorescence studies with EF have shown that 2'd-

3’ANT-ATP interacts with F586 of EF, thereby stabilizing the EF-nucleotide interaction in the presence of CaM (Shen et al., 2002).

In contrast to mACs and *CyaA*, a detailed analysis of the conformational changes in EF3 monitored by the binding of the MANT-ATP and MANT-GTP analogs has not yet been presented. Therefore, In order to further investigate the mechanism of conformational changes in EF3 due to MANT-nucleotide binding, a systematic analysis of interaction of the defined 2’ and 3’ isomers of MANT-ATP and MANT-GTP with EF3 was carried out.

Fluorescence experiments were carried out with both EF and EF3. No major differences in the fluorescence properties between EF and EF3 were observed (data not shown). All experiments were carried out under Mn^{2+} and Mg^{2+} conditions. However, EF3 showed a preference for Mn^{2+} compared to Mg^{2+} (data not shown). Similarly, mACs and *CyaA* show a preference for Mn^{2+} in both fluorescence and enzymatic analysis using MANT and TNP-nucleotides (Mou et al., 2005 and 2006; Chapter 2; Göttle et al., 2007). Experiments were carried out at an excitation wavelength of 280 nm to measure the tyrosine and tryptophan fluorescence of EF3 emitted at 350 nm and the possibility of FRET from these residues to the MANT-group, which is excited at 350 nm to emit light at around 420-450 nm. Fluorescence spectra were also recorded at 350 nm to observe possible changes in MANT-nucleotide fluorescence upon binding to EF3.

- ***Interaction of MANT-nucleotides with EF3 – FRET experiments***

When excited at 280 nm under steady-state conditions, EF3 strongly emits at around 339-340 nm in the absence of CaM (Figure 4-3 A, B, C and Figure 4-4 A, B and C – red trace). As mentioned earlier, at 280 nm, though both tryptophan and tyrosine residues are excited, tryptophan residues have higher fluorescence amplitudes compared to tyrosine residues (Lacowicz, 1999). Tryptophan residues alone can be excited at 294 nm. When EF3 was excited at 294 nm, a 50% decrease in fluorescence intensity was observed with the emission maximum at 340 nm (data not shown). Primary structure analysis of EF3 indicates the presence of six tryptophan and twenty-five tyrosine residues, all of which could potentially transfer energy to the nucleotide (www.pdb.org, structure 1k93). The emission maximum for EF3 observed at ~340 nm indicates that the tryptophan residues are buried in the catalytic site.

In the presence of MANT-nucleotide, when CaM was added, a second prominent peak was observed at around 440 nm (Figure 4-3 A, B, C and Figure 4-4 A, B and C – blue trace). This indicated energy transfer (FRET) from the tryptophan and tyrosine residues to the MANT-group of the nucleotide. The magnitude of FRET varied among the nucleotides studied. The 2’ isomer of both MANT-ATP and MANT-GTP showed at least 3-fold larger FRET than their corresponding 3’ isomers. Though 3’MANT-2’d-ATP

was the most potent inhibitor of EF3 reported so far, the 2' isomers of MANT-ATP and MANT-GTP were more favorable for FRET. These findings indicate that the affinity differences do not account for the different fluorescent responses of the nucleotides studied. The fluorescence responses are entirely dependent on the local environment of the specific nucleotide in the catalytic pocket of EF3.

In addition to the emission peak observed at ~440 nm, a very slight shift of the emission maximum from ~340 nm to ~344 nm (± 2 nm) was observed upon the addition of CaM. This shift to longer wavelength reflects a change in the polarity of the tryptophan residues indicating a shift to a more solvent-exposed environment in the presence of CaM.

- Interaction of MANT-nucleotides with EF3 – direct fluorescence experiments

MANT-nucleotides when excited at 350 nm emit at 450 nm (Figure 4-3 D, E, F and Figure 4-4 D, E and F – green trace). Steady-state emission spectra were recorded between 370 nm and 550 nm. No increase in MANT-nucleotide fluorescence was observed with the addition of EF3 (Figure 4-3 D, E, F and Figure 4-4 D, E and F – red trace). Upon addition of CaM, an increase in fluorescence of more than 140% was observed for the 2' isomers of MANT-ATP and MANT-GTP. In the case of MANT-ATP and MANT-GTP, a 40% and a 10% increase in fluorescence was observed respectively. Also, a

70% increase in fluorescence was seen for the 3’ isomer of MANT-ATP and a very slight increase for the 3’ isomer of MANT-GTP (Figure 4-3 D, E, F and Figure 4-4 D, E and F – blue trace). In addition to increases in MANT-nucleotide fluorescence, the emission maxima of MANT-nucleotides shifted to shorter wavelengths (blue shift) in the presence of CaM. This indicates that MANT-nucleotides bind to a hydrophobic pocket in the catalytic site of EF3 in the presence of CaM probably by interacting with the F586 residue in the EF3.

Qualitatively, 2’ MANT-3’d-ATP and 2’ MANT-3’d-GTP behave similarly in direct fluorescence and FRET experiments. The inhibitory properties of these nucleotides in AC assays are also similar. However, the 3’ isomers of MANT-ATP and MANT-GTP do not have the same properties in direct fluorescence, FRET experiments and AC assays. It is possible that, although the 2’ position of the MANT-group is more favorable for FRET, the 3’ position of the MANT-group is more favorable for inhibition of EF3 especially in the case of MANT-adenine nucleotides. It is also clear that the defined 2’ and 3’ isomers of MANT-ATP and MANT-GTP are more favorable for inhibition of EF3 than the MANT-group isomerizing between the 2’ and 3’ position.

In comparison with *CyaA*, an increase of at least a 4-fold in the intrinsic fluorescence of EF3 was observed in the case of EF3 with the same concentration (300 nM). In direct fluorescence experiments, higher

concentrations of *CyaA* and CaM (2.4 μM each) were used in order to observe measurable increase in fluorescence. In sharp contrast, 300 nM EF3 was sufficient to observe changes in MANT- nucleotide fluorescence. Furthermore, there was no difference observed between the defined 2' and 3' isomers of MANT-ATP in their interaction with *CyaA* in both FRET and direct fluorescence experiments (Göttle et al., 2007). However in EF3, higher FRET and fluorescence amplitude changes were observed with the 2' isomer of MANT-ATP. The interaction of 2' and 3' isomers of MANT-GTP with CyaA has not been studied. Collectively, it is clear that MANT-nucleotides interact differently with EF3 and CyaA.

Figure 4-3 Analysis of MANT-ATP and its defined 2' and 3' isomers binding to EF3 using FRET and direct fluorescence measurements

Shown here are FRET measurements (A, B and C) and direct fluorescence measurements (D, E and F) of MANT-ATP and its defined 2' and 3' isomers respectively. Steady-state emission spectra were recorded with λ_{ex} = 280 nm (λ_{em} = 300 – 500 nm) for intrinsic protein fluorescence and λ_{ex} = 350 nm (λ_{em} = 370 – 500 nm) for MANT-nucleotide fluorescence. Experiments were carried out with sequential addition of reaction mixtures containing 100 mM KCl, 10 mM $MnCl_2$ and 25 mM HEPES/NaOH, pH 7.4, 300 nM MANT-nucleotide (green trace), 300 nM EF3 (red trace) and 300 nM CaM (blue trace). The final assay volume was 150 μl. Arrows in D, E and F indicate a blue shift in the emission spectra due to addition of CaM to EF3/MANT-nucleotide. Graphs were generated using Prism 4.0 software. Baseline fluorescence (buffer alone) was subtracted from the spectra. Fluorescence intensities in A, B and C are shown as percentage of the maximal emission data obtained for the respective experiment. Fluorescence intensity in D, E and F are shown as arbitrary units (a.u) to observe differences between the three nucleotides studied. Data shown are representative of 5-6 experiments using 3 different batches of EF3.

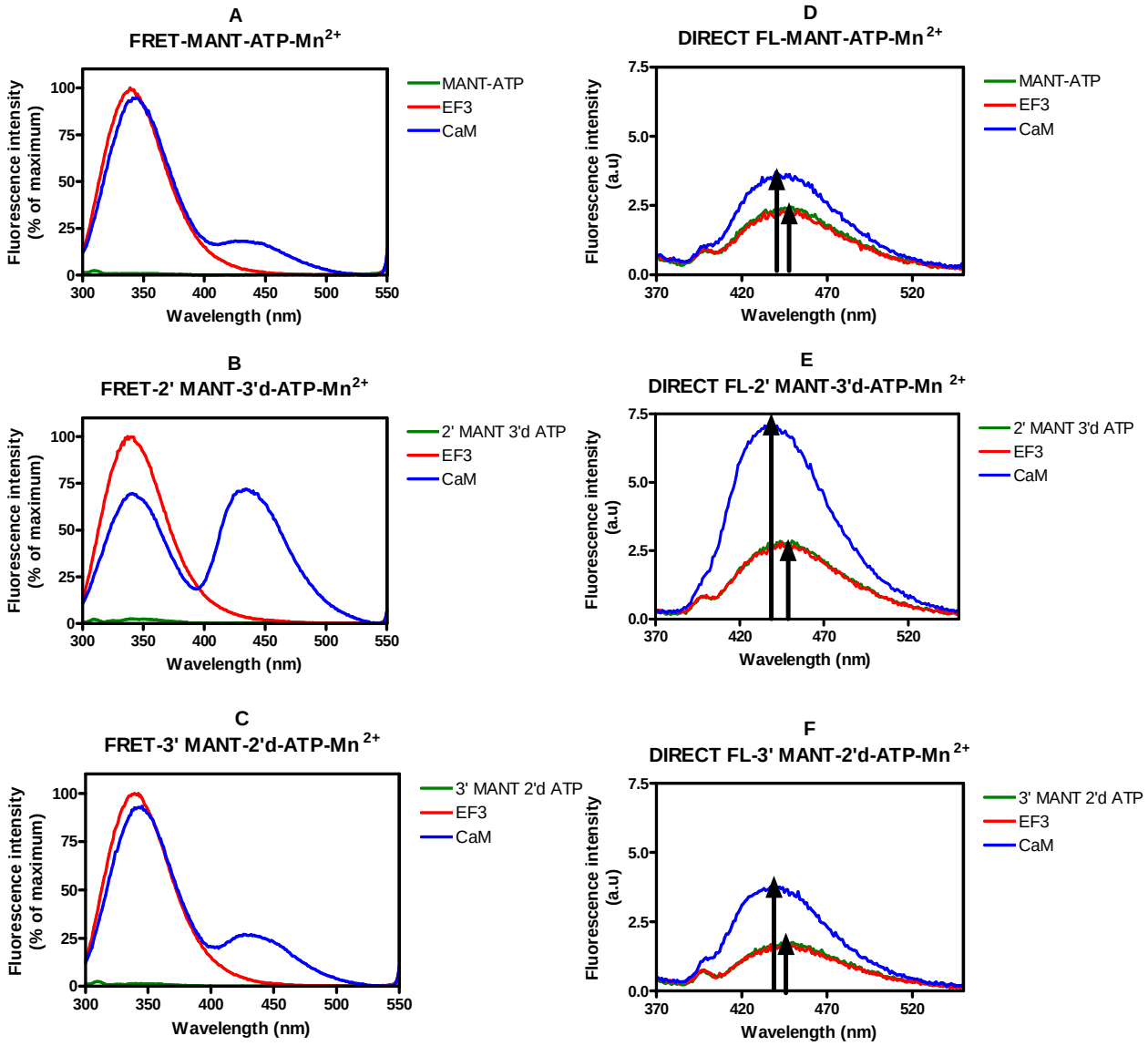
A
FRET-MANT-ATP-Mn2+
Fluorescence intensity (% of maximum)
Wavelength (nm)
MANT-ATP
EF3
CaM
B
FRET-2' MANT-3'd-ATP-Mn2+
2' MANT 3'd ATP
EF3
CaM
C
FRET-3' MANT-2'd-ATP-Mn 2+
3' MANT 2'd ATP
EF3
CaM
D
DIRECT FL-MANT-ATP-Mn 2+
Fluorescence intensity (a.u)
E
DIRECT FL-2' MANT-3'd-ATP-Mn 2+
F
DIRECT FL-3' MANT-2'd-ATP-Mn 2+

Figure 4-4 Analysis of MANT-GTP and its defined 2' and 3' isomers binding to EF3 using FRET and direct fluorescence measurements

Shown here are FRET measurements (A, B and C) and direct fluorescence measurements (D, E and F) of MANT-GTP and its defined 2' and 3' isomers respectively. Steady-state emission spectra were recorded with λ_{ex} = 280 nm (λ_{em} = 300 – 500 nm) for intrinsic protein fluorescence and λ_{ex} = 350 nm (λ_{em} = 370 – 500 nm) for MANT-nucleotide fluorescence. Experiments were carried out with sequential addition of reaction mixtures containing 100 mM KCl, 10 mM $MnCl_2$ and 25 mM HEPES/NaOH, pH 7.4, 300 nM MANT-nucleotide (green trace), 300 nM EF3 (red trace) and 300 nM CaM (blue trace). The final assay volume was 150 μl. Arrows in D, E and F indicate a blue shift in the emission spectra due to addition of CaM to EF3/MANT-nucleotide. Graphs were generated using Prism 4.0 software. Baseline fluorescence was subtracted from the spectra. Fluorescence intensities in A, B and C are shown as percentage of the maximal emission spectra obtained for the respective experiment. Fluorescence intensities in D, E and F are shown as arbitrary units (a.u) to observe differences between the three nucleotides studies. Data shown are representative of 5-6 experiments using 3 different batches of EF3.

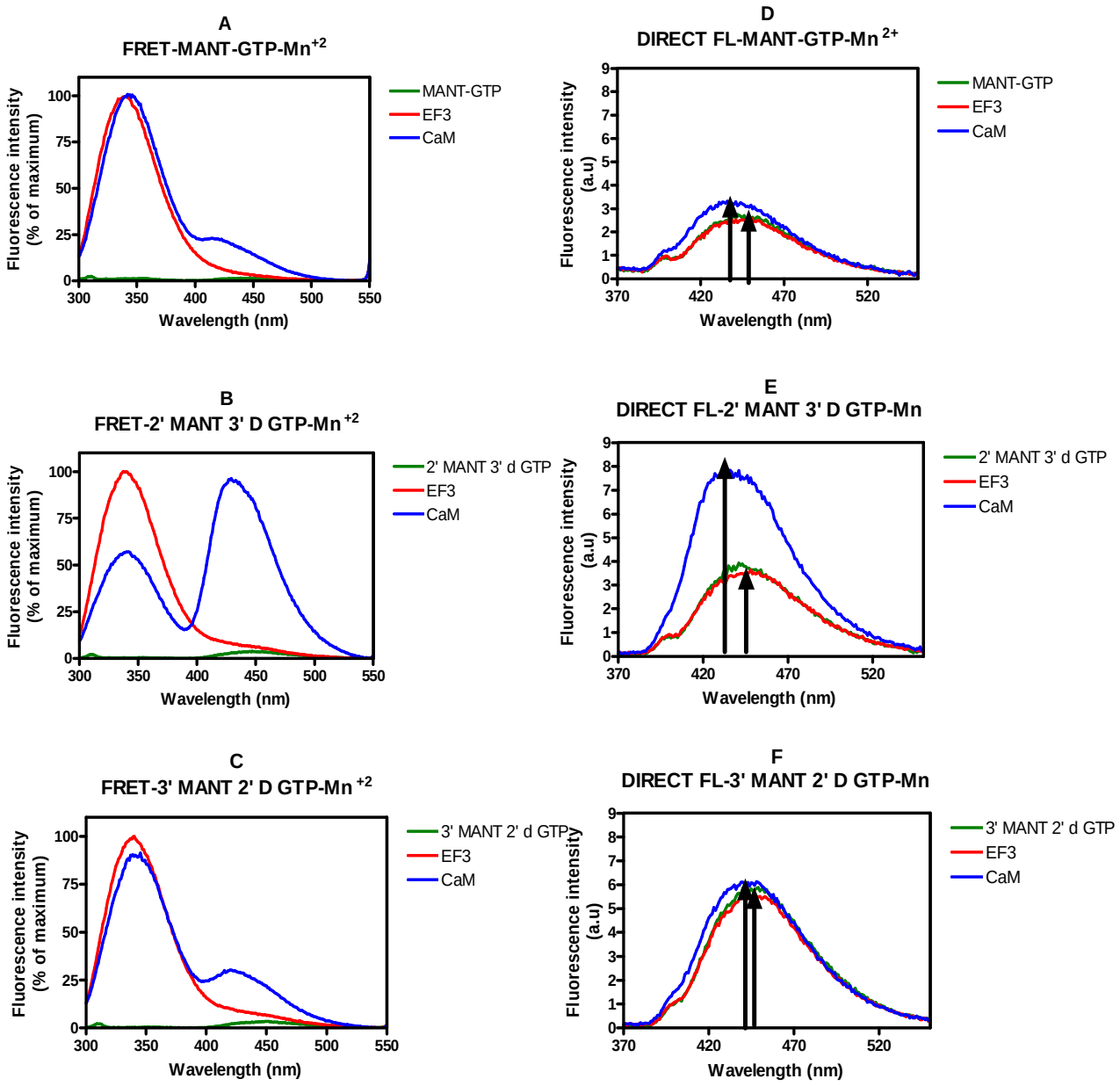
A
FRET-MANT-GTP-Mn+2
Fluorescence intensity (% of maximum)
Wavelength (nm)
MANT-GTP
EF3
CaM
D
DIRECT FL-MANT-GTP-Mn 2+
Fluorescence intensity (a.u)
Wavelength (nm)
MANT-GTP
EF3
CaM
B
FRET-2' MANT 3' D GTP-Mn +2
Fluorescence intensity (% of maximum)
Wavelength (nm)
2' MANT 3' d GTP
EF3
CaM
E
DIRECT FL-2' MANT 3' D GTP-Mn
Fluorescence intensity (a.u)
Wavelength (nm)
2' MANT 3' d GTP
EF3
CaM
C
FRET-3' MANT 2' D GTP-Mn +2
Fluorescence intensity (% of maximum)
Wavelength (nm)
3' MANT 2' d GTP
EF3
CaM
F
DIRECT FL-3' MANT 2' D GTP-Mn
Fluorescence intensity (a.u)
Wavelength (nm)
3' MANT 2' d GTP
EF3
CaM

- ***Enzyme saturation experiments and determination of K_d values***

Enzyme saturation experiments were carried out to determine the apparent K_d values of the MANT-nucleotides for EF3 in the presence of Mn^{2+}. K_d values help understand the binding affinity of the ligand to the receptor and therefore FRET saturation experiments were carried out. The excitation wavelength of 280 nm was used to measure intrinsic protein fluorescence and 350 nm for MANT-nucleotide fluorescence. EF3 and CaM were added to the cuvette first and the emission spectra were recorded at 280 nm and 350 nm. Increasing concentrations of MANT-nucleotide were then added to observe increases in fluorescence until saturation was reached (Figure 4-5 A). Fluorescence spectra of increasing MANT-nucleotide concentrations were also recorded in the absence of EF3/CaM at 280 nm (Figure 4-5 B). These values were later subtracted from the FRET signals in the presence of EF3/CaM. After correction for the inner filter effect, saturation curves were generated for the specific MANT-nucleotide (Figure 4-6) and the apparent K_d values were calculated (Table 4-2). Slight inconsistencies between the K_d values and the K_i values obtained in AC assays were observed. The K_i and K_d values especially in the case of MANT-GTP isomers were more consistent compared to the other MANT-nucleotides studied. These slight differences in K_i and K_d values can be attributed to experimental conditions such as salt concentration, pH and temperature. Most importantly, since MANT-nucleotides are extremely sensitive probes, the relative orientation and the

local environment of the nucleotide plays a very important role in any changes observed in fluorescence. Another important difference between Kd and Ki values is also the fact that the EF concentrations in AC assays and FRET assays were largely different. Higher EF concentrations were used in FRET assays. When the affinity of the ligand for EF is high, the higher protein concentrations largely underestimate the affinity of the ligand for EF. Nonetheless, the order of affinity of the MANT-nucleotides studied matched well with the K_i values obtained in AC assays. 3' MANT-2'd-ATP showed the lowest K_d value (K_d = 0.065 μM) compared to other MANT-nucleotides indicating higher affinity for EF3/CaM. MANT-GTP showed the lowest affinity for EF3/CaM and the K_d value (K_d = 0.79 μM) was slightly lower compared to the K_i value obtained in AC assays (K_d = 1.08 μM).

Collectively, the results of the fluorescence and enzymatic studies indicate that the 2' and 3' isomers of MANT-ATP and MANT-GTP have different fluorescence and inhibitory properties for EF3. The MANT-group positioning and the base are extremely critical for binding and inhibition of EF3 catalytic activity. Furthermore, similar to mACs and CyaA, the catalytic core of EF3 in the presence of CaM is spacious enough to accommodate various MANT-nucleotides with differences in the MANT-group positioning and the nucleobase (Mou et al., 2006; Gottle et al., 2007). Knowledge of the inhibitory properties of the different MANT-nucleotide analogs should facilitate rational design of potent EF3 inhibitors.

Figure 4-5 EF3 saturation experiments using FRET measurements probed by 2' MANT-3'd-ATP in the presence of Mn^{2+}

EF saturation experiments were carried out as explained in section 4.3.2 in the presence of Mn^{2+} with sequential addition of buffer, 300 nM EF3, 300 nM CaM and increasing concentrations of MANT-nucleotides ranging from 165 nM to 1.3 μM (A). Steady-state emission spectra were recorded with λ_{ex} = 280 nm (λ_{em} = 300 – 500 nm) for FRET saturation measurements. Experiments were also carried out in the absence of EF3/CaM (B). Graphs were generated using Prism 4.0 software. Fluorescence intensity in A is shown as percentage of the maximal emission spectra obtained for the respective experiment. Fluorescence intensity in B is shown as percentage of the emission maximum obtained in A for comparison. Data shown here are representative experiments with 2' MANT-3'd-ATP. Similar results were obtained for all the MANT-nucleotides studied in 2-3 independent experiments.

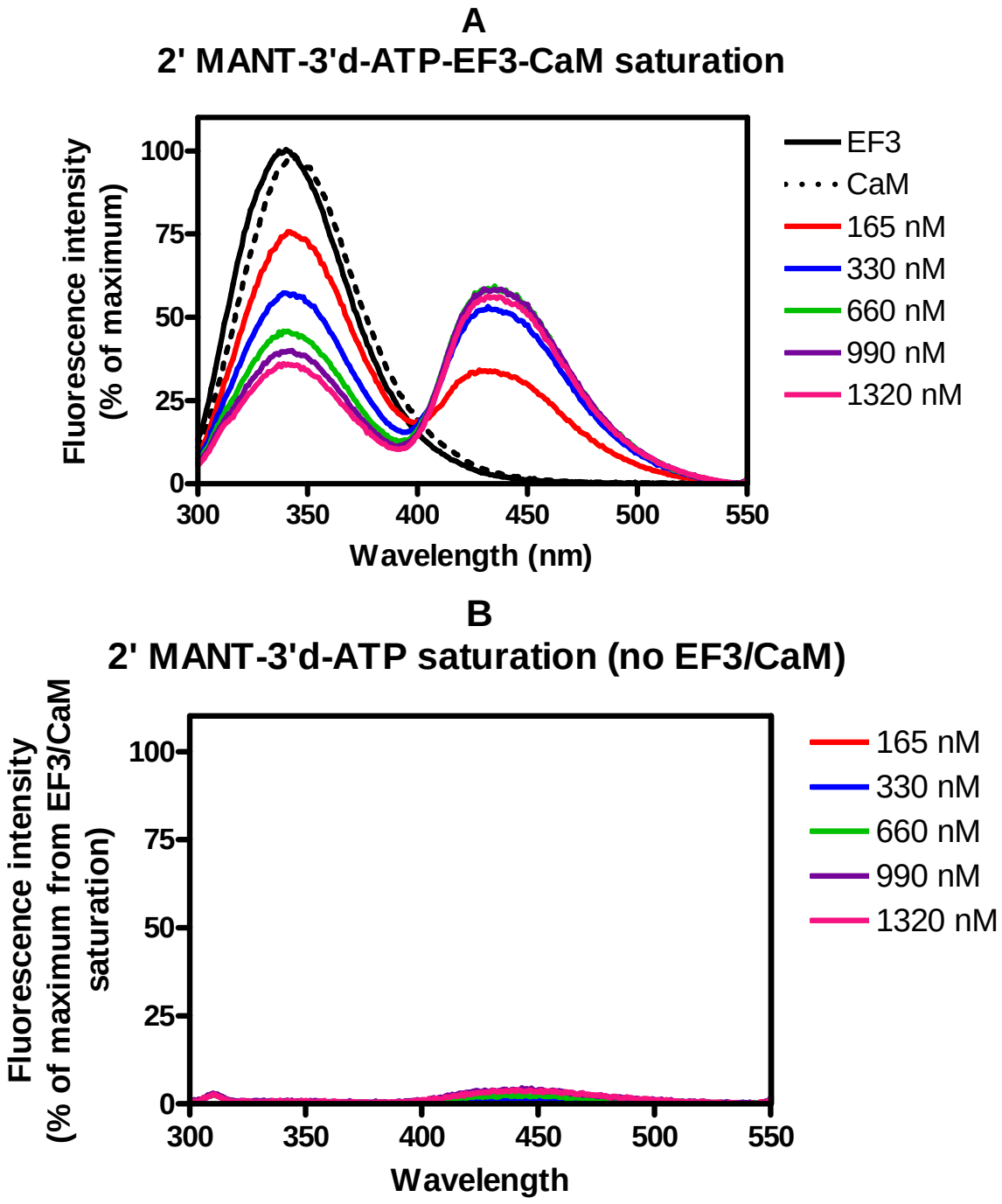
A
2' MANT-3'd-ATP-EF3-CaM saturation
Fluorescence intensity
(% of maximum)
100
75
50
25
0
300
350
400
450
500
550
Wavelength (nm)
EF3
CaM
165 nM
330 nM
660 nM
990 nM
1320 nM
B
2' MANT-3'd-ATP saturation (no EF3/CaM)
Fluorescence intensity
(% of maximum from EF3/CaM
saturation)
100
75
50
25
0
300
350
400
450
500
550
Wavelength
165 nM
330 nM
660 nM
990 nM
1320 nM

Figure 4-6 Nucleotide saturation curve for EF3 in the presence of Mn^{2+}

EF saturation experiments were carried out as explained in section 4.3.2 in the presence of Mn^{2+} with sequential addition of buffer, 300 nM EF3, 300 nM CaM and increasing concentrations of MANT-nucleotides ranging from 165 nM to 1.3 μM. MANT-nucleotide fluorescence was first corrected for the inner filter effect by recording the absorbance spectra of the respective MANT-nucleotide at the highest concentration in the presence of EF3 and CaM. The absorption wavelength was then subtracted depending on the concentrations of the MANT-nucleotides used in the saturation experiments. Additionally values from experiments conducted in the absence of Ef3/CaM (Figure 4-4 B) were subtracted from values obtained in Figure 4-4 A. Saturation curves were obtained by non-linear regression analysis using Prism 4.0 software. Fcorr is the fluorescence intensity in arbitrary units (a.u) after correction for the inner filter effect. Data shown are for a representative experiment with 2' MANT-3'd-ATP. Similar results were obtained for all the MANT-nucleotides studied in 2-3 independent experiments.

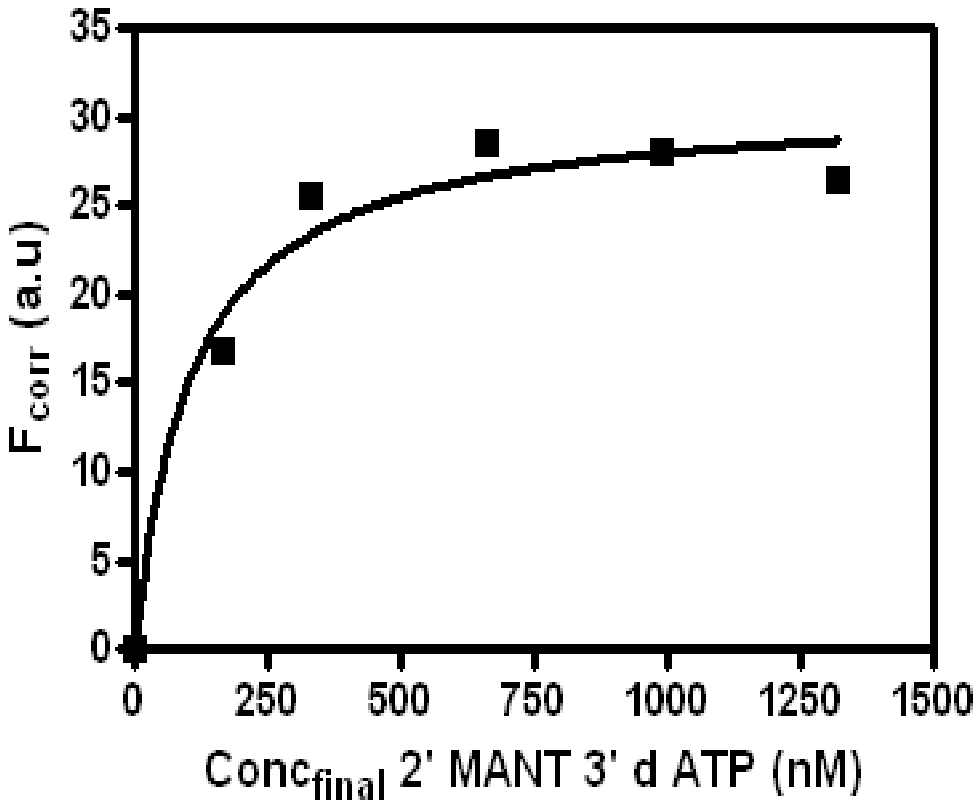
35
30
25
20
15
10
5
0
F_{corr} (a.u)
0
250
500
750
1000
1250
1500
$Conc_{final}$ 2' MANT 3' d ATP (nM)

Table 4-2 Comparison of K_d values in fluorescence assays and K_i values in AC assays for MANT-nucleotides

Shown here is a comparison of K_d values and K_i values obtained in AC assays. K_d values of MANT-nucleotides for EF3 were determined as explained in section 4.3.2. Experiments were carried out in the presence of Mn^{2+} with sequential addition of buffer, 300 nM EF3, 300 nM CaM and increasing concentrations of MANT-nucleotides ranging from 165 nM to 1.3 μM. MANT-nucleotide fluorescence was first corrected for the inner filter effect and values from experiments conducted in the absence of Ef3/CaM (Figure 4-4 B) were subtracted from values obtained in Figure 4-4 A. K_d values were determined by non-linear regression analysis using Prism 4.0 software. K_i values were calculated in AC assays as described in section 4.3.2. K_d and K_i values are expressed in μM. Similar results were obtained for all the MANT-nucleotides studied in 2-3 independent experiments.

		K_i Values (μM)	K_d values (μM)
MANT-ATP		0.36 ± 0.18	0.19 ± 0.2
2' MANT 3' d ATP		0.04 ± 0.002	0.1 ± 0.03
3' MANT 2' d ATP		0.011 ± 0.002	0.065 ± 0.005
MANT-GTP		1.08 ± 0.4	0.7 ± 0.3
2' MANT 3' d GTP		0.05 ± 0.01	0.06 ± 0.02
3' MANT 2' d GTP		0.36 ± 0.1	0.37 ± 0.2

-***Fluorescence analysis of the nucleotide-binding site of EF3 by competition with 2'5'dd 3'-ATP***

To confirm the presence of a single nucleotide-binding site in EF3, experiments were carried out with 2'5'-dd-3'-ATP to observe the displacement of MANT-nucleotide from the catalytic site of EF3. The non-fluorescent ATP analog, 2'5'-dd-3'-ATP, is a potent inhibitor of mACs (Desaubry et al., 1996) and displaces MANT- and TNP-nucleotides from the catalytic site of C1/C2 (Gille et al., 2004; Chapter 2 data). Fluorescence experiments were carried out in the dual-kinetic mode to observe the rate of change in EF3 (λ = 280 – 450 nm, Figure 4-6, red trace) and MANT-nucleotide fluorescence respectively (λ = 350-450 nm, Figure 4-6, blue trace). 2'5'dd-3'-ATP displaced 2' MANT-3'd-ATP almost completely from the catalytic site of EF3 in a concentration-dependent manner. This clearly indicates that the catalytic site of EF3 possesses a single nucleotide-binding site and MANT-nucleotides bind reversibly to the catalytic site of EF3. Steady-state emission spectra were also recorded at 280 nm for changes in intrinsic EF3 fluorescence and at 350 nm for MANT-nucleotide fluorescence. In FRET measurements, 10 μM concentration of 2'5'-dd-3'-ATP caused a decrease in intrinsic EF3 fluorescence as well as a decrease in FRET from EF3 to the MANT-group in the presence of CaM (Figure 4-7 A, black trace). A decrease in FRET is reflective of longer distances between MANT-group and the tryptophan and tyrosine residues in EF3. In direct fluorescence measurements, a decrease in

MANT-fluorescence due to addition of 2’5’-dd-3’-ATP (Figure 4-7 B, black trace) indicates that the MANT-group is in a more polar environment and, therefore, displaced competitively by the non-fluorescent nucleotide from the catalytic pocket of EF3. Overall, it is clear that MANT-nucleotide binds to the same site as substrate ATP and competitively inhibits EF3.

.

Figure 4-7 Kinetic analysis of the displacement of bound 2' MANT-3'd-ATP from the catalytic site of EF3 by 2'5'-dd-3'-ATP

Fluorescence experiments were conducted as described in section 4.3.2. Kinetics of 2' MANT-3'd-ATP displacement by 2'5' dd 3' ATP from the EF3 catalytic site were carried out in dual-kinetic mode to observe the rate of change in EF3 (λ = 280 – 450 nm, red trace) and MANT-nucleotide fluorescence (λ = 350 – 450 nm, blue trace). Cuvettes contained 300 nM each of EF3, CaM and MANT-nucleotide in the presence of buffer containing10 mM $MnCl_2$. Increasing concentrations of 2'5'- dd -3'-ATP varying from 1 μM to 10 μM were added until saturation was achieved. In the graph, fluorescence intensity in arbitrary units is measured as a function of time in minutes. Fluorescence recordings were analyzed using the spectrum package of the Cary Eclipse software. Similar results were obtained from 3 – 4 independent experiments conducted for all the MANT-nucleotides studied in this chapter.

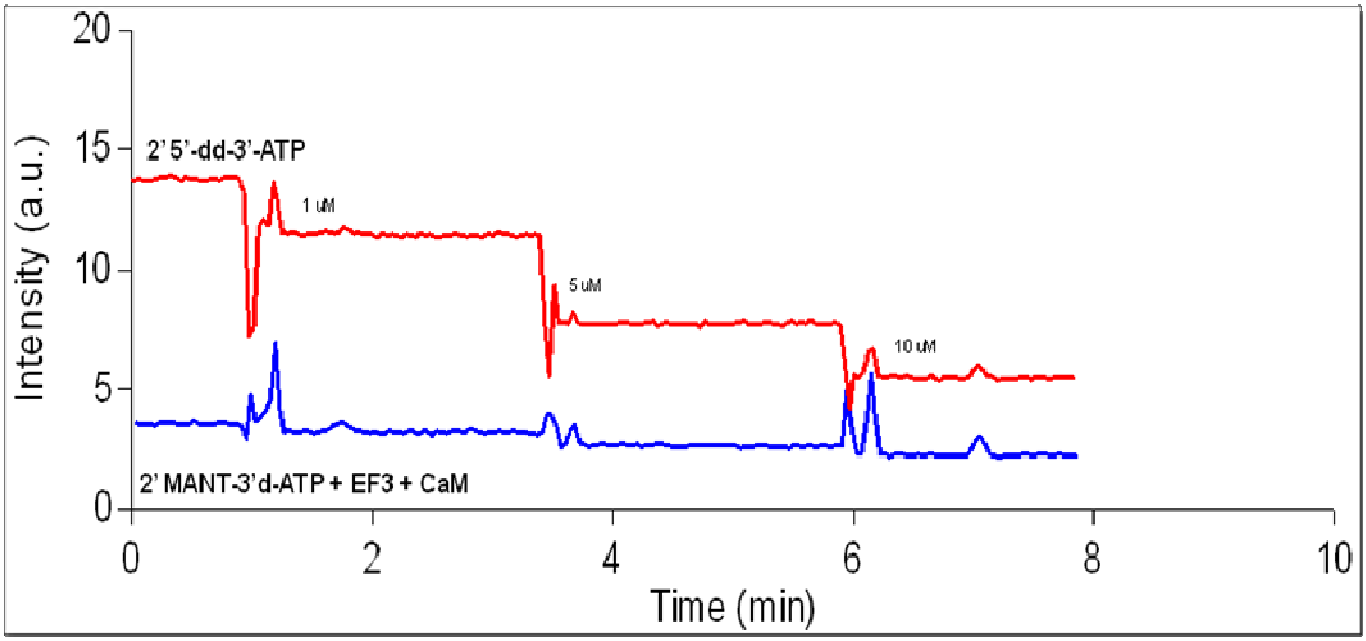
20
15
10
5
0
Intensity (a.u.)
2' 5'-dd-3'-ATP
1 uM
5 uM
10 uM
2' MANT-3'd-ATP + EF3 + CaM
0
2
4
6
8
10
Time (min)

Figure 4-8 FRET and direct fluorescence measurements of the displacement of 2' MANT-3'd-ATP from EF3 catalytic site by 2'5'-dd-3'-ATP

FRET and direct fluorescence experiments were carried out as described in section 4.3.2. Steady-state emission spectra were recorded with λ_{ex} = 280 nm (λ_{em} = 300 – 500 nm) for intrinsic EF3 fluorescence (Figure A) and λ_{ex} = 350 nm (λ_{em} = 370 – 500 nm) for MANT-nucleotide fluorescence (Figure B). Experiments were carried out with sequential addition of reaction mixtures containing 100 mM KCl, 10 mM $MnCl_2$ and 25 mM HEPES/NaOH, pH 7.4, 300 nM 2' MANT-3'd-ATP (green trace), 300 nM EF3 (red trace) and 300 nM CaM (blue trace), followed by addition of 10 μM 2'5'-dd-3'-ATP (black trace). The final assay volume was 150 μl. Graphs were generated using Prism 4.0 software. Baseline fluorescence (buffer alone) was subtracted from the spectra. Fluorescence intensity in A and B are shown as percentage of the maximal emission obtained for the respective experiment. Data shown here are conducted with 2' MANT-3'd-ATP and similar results were obtained from experiments with all the MANT-nucleotides studied in this chapter.

A

FRET measurements - Inhibition by 2'5'-dd-3'-ATP

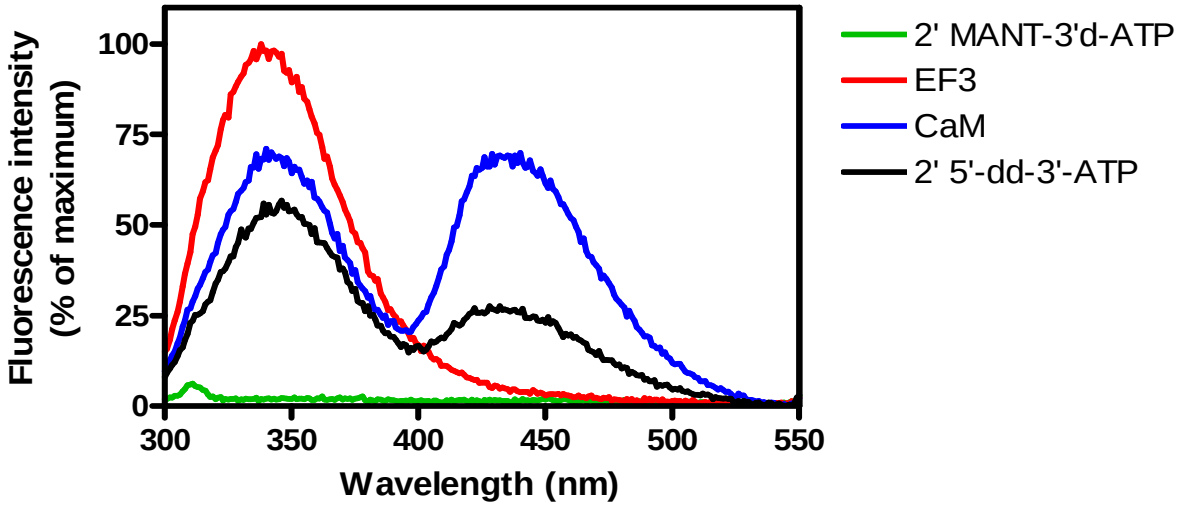

B

Direct fluorescence - Inhibition by 2'5'-dd-3'-ATP

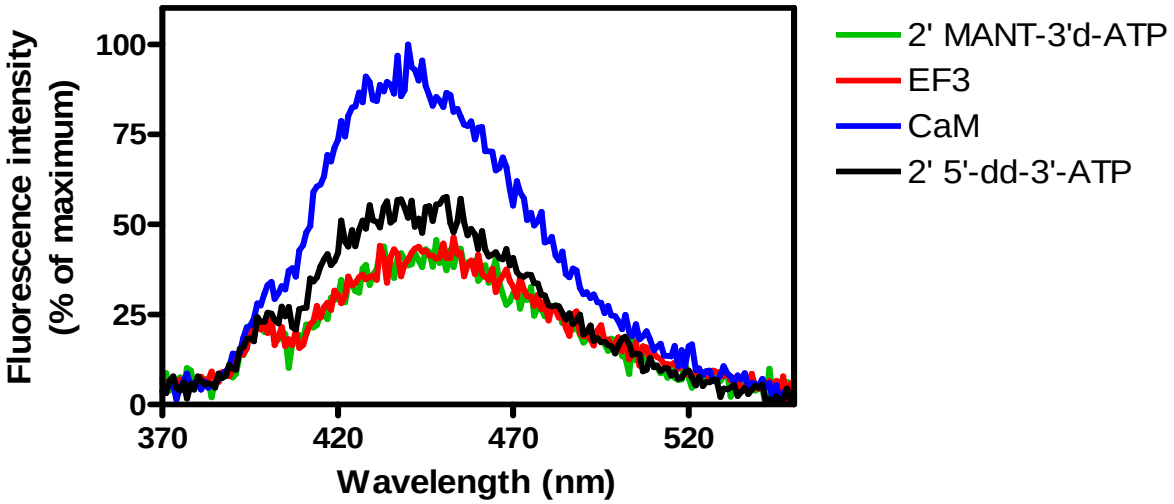

4.4.3 Molecular modeling studies of MANT-nucleotide binding to EF3-CaM

Enzymatic studies have shown that MANT-ATP and its 2’ and 3’ isomers are more potent at inhibiting EF3 than MANT-GTP and its analogs. Furthermore, 3’ MANT-2’d-ATP was 3-fold more potent than 2’ MANT-3’d-ATP. In sharp contrast, 2’ MANT-2’d-GTP was at least 7-fold more potent than 3’ MANT-2’d-GTP. In fluorescence assays with EF3 and CaM, the 2’ isomers of MANT-ATP and MANT-GTP were more favorable for FRET and for showing the increase in direct fluorescence of the MANT-group compared to other MANT-nucleotides studied in this chapter. So far, several crystal structures of EF-CaM with fluorescent and non-fluorescent nucleotides have been solved, however, crystallographic studies of EF3-CaM in complex with MANT-nucleotides has not. Due to differences observed in enzymatic and fluorescence studies and a lack of crystal structure of EF3-CaM in complex with MANT-nucleotide, molecular modeling studies were carried out to predict the specific interaction of MANT-nucleotides with the amino acid residues in EF3.

Molecular docking studies carried out in collaboration with Dr.G.H.Lushington (University of Kansas) predict that MANT-nucleotides are stabilized in the catalytic pocket of EF3 by Van der Waals and electrostatic interactions with several residues in EF3. The NHCH3-group of MANT-ATP

interacts with F586, Q588 and N583 of EF3 (Figure 4-8). Amino acid residues T548 and T579 further enhance this interaction by stabilizing the base of the nucleotide. More specifically, the anthraniloyl ring of the MANT-group is aligned parallel to F586 and is stabilized by π–stacking interactions with F586 in the catalytic site of EF3. Furthermore, the distances between the MANT-group and the tryptophan residues W357, W552, W608 and W645 in EF3 are predicted to be 16 Å, 22 Å, 14 Å and 17 Å respectively. This proximity between the tryptophan residues (donor) and the MANT-group (acceptor) explains the occurrence of significant FRET in our fluorescence experiments (Lakowicz, 1999).

The triphosphate chains of the MANT-nucleotides are stabilized by their interaction with residues R329, K346, K353, S354 and K372 of EF3 (Figure 4-10). The γ-phosphate and the oxygen of the β-phosphate interact with R329, K353 and K372. The β-phosphate and the α,β-bridging oxygen are stabilized by interactions with S354 and K346. The β, γ-bridging oxygen is predicted to form hydrogen bonds with K353. As expected in the crystal structure of EF3, the metal atoms are coordinated by H577, a pair of conserved aspartate residues D491 and D493 and the non-bridging oxygens of the phosphate chain.

Molecular docking studies predicted differential binding of the MANT-ATP and MANT-GTP isomers in the active site of EF3. Residues T548 and T579

may interact with the adenine base. This may explain why MANT-ATP analogs are more potent than MANT-GTP analogs. Also, in the case of MANT-ATP analogs, the 3' MANT isomer is more aligned to form π-stacking interactions with F586 explaining its greater affinity for EF3 (Figure 4-8). However, the orientation of the MANT-group of 3' MANT-2'd-GTP placed it further away from F586 than its 2' isomer (Figure 4-9). This is also consistent with our experimental data that indicated that the 2' MANT isomer of MANT-GTP is more potent in AC assays and is more favorable for FRET and direct fluorescence effects. This is especially surprising because in ACs, a preference for the 3'-conformation of MANT-ATP and MANT-GTP was observed (Gille et al., 2004; Mou et al., 2005). Therefore, a preference for the 2'-conformation of MANT-GTP has been demonstrated for the first time. Since, molecular modeling studies only predict the interaction of the MANT-nucleotides with the catalytic site of EF3, future crystallographic studies of EF3-CaM in complex with the isomers of MANT-ATP and MANT-GTP will be required to explain the exact differences in their binding and affinities for EF3.

Figure 4-9 Predicted differential interaction of MANT-ATP isomers with amino acid residues in the catalytic site of EF3

A superimposition of 2' and 3' isomers of MANT-ATP in the space filling model of EF3 is shown. Only important residues are shown in the model and the colors on the surface of EF3 are depicted as follows: Hydrophobic surfaces = yellow, acidic surfaces = red, basic regions = blue, neutral/polar = white. Ligands are depicted in stick form and are represented in the following colors: C = gray, H = light blue, N = dark blue, O = red, P = orange.

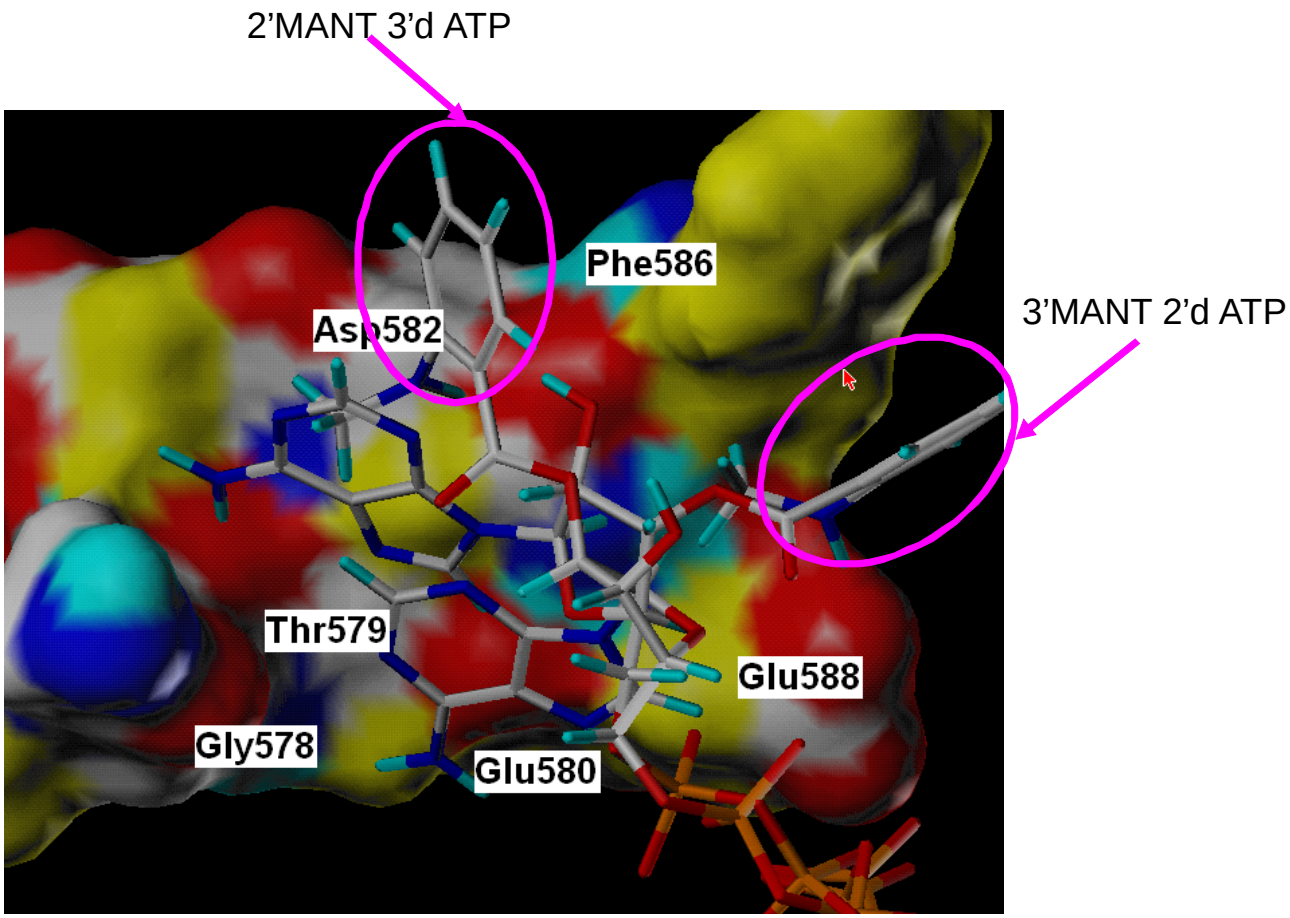

Figure 4-10 Comparison of the predicted interaction of 2' and 3' isomers of MANT-GTP with amino acid residues in the catalytic site of EF3

A plot of predicted 2' MANT-3'd-GTP (stick with purple C-atoms) and 3'MANT-2'd-GTP (stick with green C-atoms) binding conformers within the EF3 receptor is shown. Sterically important residues are indicated. Gold-lined Connolly surfaces represent favorable Van der Waals interactions of residues with ligands and blue-lined surfaces depict unfavorable interactions. Except for carbon atoms, all the other atoms are depicted as follows: H = cyan, N = blue, O = red, P = orange. The MANT-group of 2' MANT-3'd-GTP faces towards F586 whereas in the case of 3' MANT-2'd-GTP, the MANT-group faces towards G352.

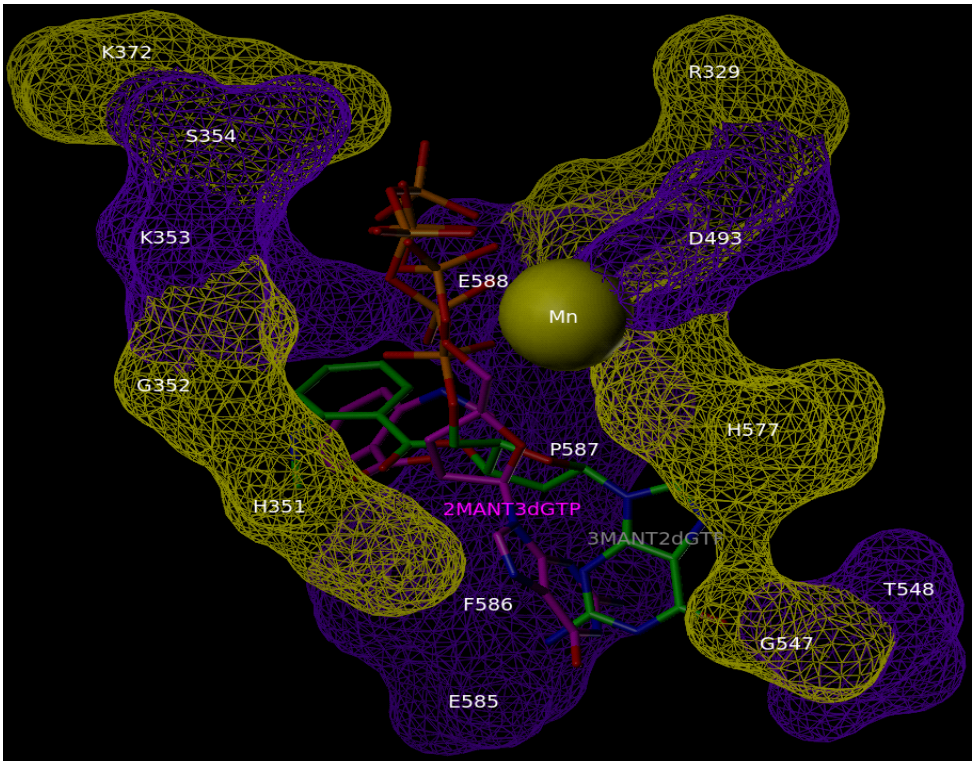

Figure 4-11 Predicted interaction of the triphosphate chain of MANT-nucleotides with the amino acid residues in the catalytic site of EF3

A superimposition of the triphosphate chain of MANT-nucleotides in the space filling model of EF3 is shown. Only important residues are shown in the model and the colors on the surface of EF3 are depicted as follows: Hydrophobic surfaces = yellow, acidic surfaces = red, basic regions = blue, neutral/polar = white. Ligands are depicted in stick form and are represented in the following colors: C = gray, H = light blue, N = dark blue, O = red, P = orange.

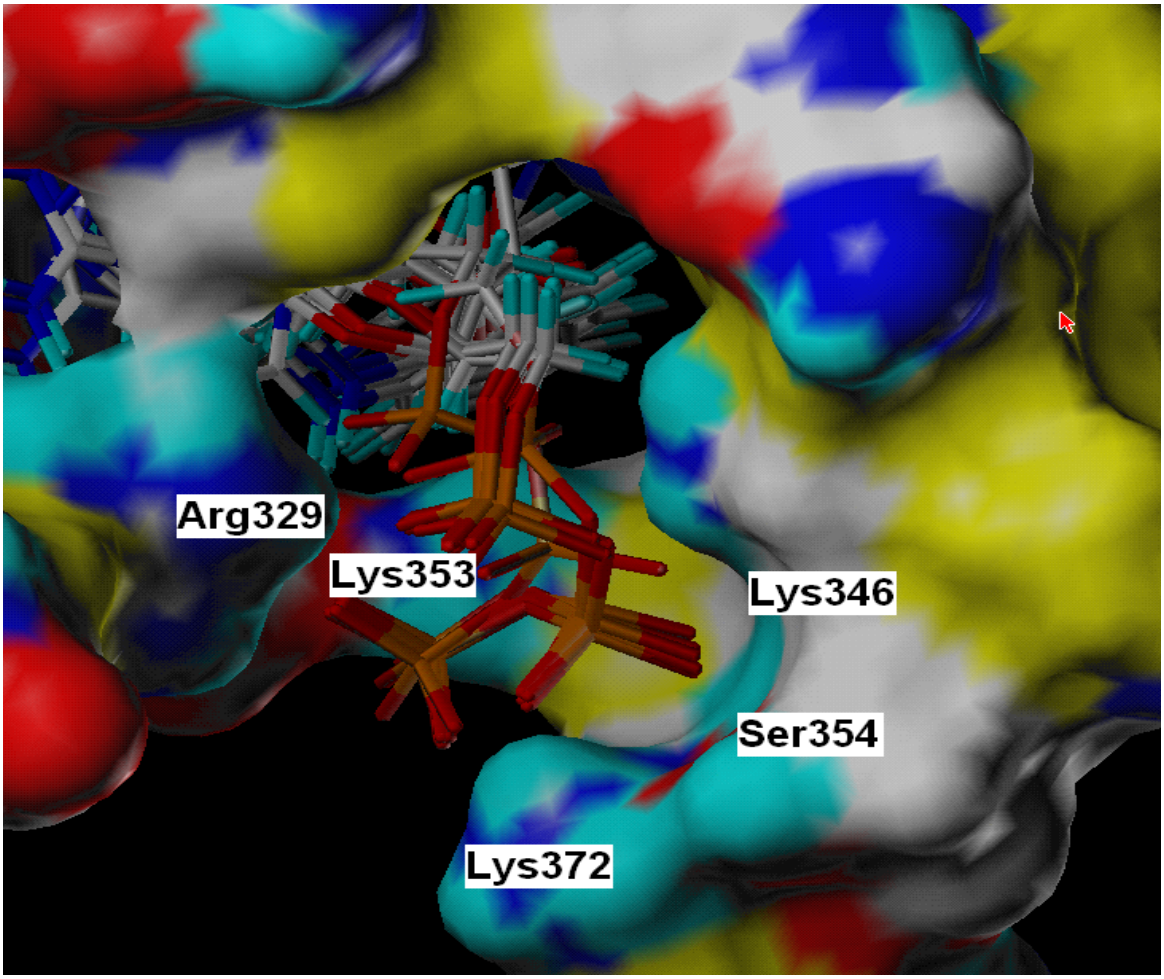

4.4.4 Characterization of the EF-CaM interaction probed by MANT-nucleotides

Binding of CaM to EF is the first step in the toxic mechanism of EF. As mentioned in the introduction section of chapter 1, EF consists of three domains CA, CB and a helical domain connected to CA by a linker region. CA and CB domains form the catalytic core of EF. CaM binding to EF causes the helical, linker and CA domain to completely wrap around the CaM. In addition to these domains, switch sgments A, B and C of EF also undergo conformational changes due to CaM binding (Drum et al., 2002). Residues corresponding to switches A and C are most important for interaction with EF. The switch B region of EF consists of residues important for catalysis and makes extensive contacts with switch C. Several hydrophobic and hydrophilic contacts stabilize the interaction between EF and CaM. Extensive binding surface area between EF and CaM is observed in the crystal structure of the EF-CaM complex. The CA domain of EF binds to helices IV, V and VI of CaM. The helical domain of EF and residues corresponding to switch C interact with and stabilize the N-terminal domain of CaM. The K525 residue in EF was identified as a “hotspot” for binding to CaM and forms a salt bridge with E114 of CaM. D647of EF can also form a salt bridge with R90 of CaM. Therefore it was proposed that CaM first binds with residues from switch A followed by interaction with residues from switch C. Switch B is disordered in the structure of EF alone. However in the structure of the EF-CaM complex, switch B is

ordered indicating that CaM-binding to switch C induces the ordering of switch B (Drum et al., 2002).

Furthermore, it has been observed that EF binds to the N-terminus of CaM in a closed and Ca^{2+} independent manner, whereas binding of EF to the C-terminus of CaM is Ca^{2+} dependent. EF interacts weakly with a closed N-CaM in a Ca^{2+} independent manner to initiate a tighter interaction with an open and Ca^{2+} loaded C-CaM (Shen et al., 2002; Shen et al., 2005).

In addition to identifying inhibitors for EF AC activity, it is also important to identify inhibitors that block the binding of CaM to EF. It is difficult to inhibit CaM, since CaM is a ubiquitous protein that can bind to several effector proteins and plays an important role in signal transduction. Therefore, it is important to identify regions in EF that specifically bind to CaM. This study is aimed at understanding EF-CaM binding to help identify inhibitors that exclusively block this interaction.

- Inhibition of EF3-CaM interaction with Calmidazolium chloride (Cz.Cl) probed by 2' MANT-3'd-ATP

Calmidazolium chloride (Cz.Cl) is a classic inhibitor of CaM (IC50 = 10 nM) and can, therefore, inhibit CaM-activated enzymes. Cz.Cl binds specifically to CaM and is therefore not expected to compete with the MANT-nucleotide for the nucleotide-binding site of EF3. Binding of Cz.Cl to CaM and its indirect impact on the EF-CaM interaction was probed by 2' MANT-3'd-ATP using

fluorescence spectroscopy. Fluorescence experiments were carried out in both steady-state and kinetic modes to observe changes in EF3 and MANT-nucleotide fluorescence due to binding of Cz.Cl. In kinetic mode, with a sequential addition of Cz.Cl ranging from 1 nM to 300 nM, a gradual decrease in EF3 fluorescence was observed in the presence of CaM (Figure 4-11, red trace). However, with the addition of Cz.Cl, there was no change in MANT-nucleotide fluorescence in the presence of CaM (Figure 4-11, blue trace). In steady-state fluorescence experiments, at an excitation wavelength of 280 nm, with the addition of Cz.Cl to EF3/CaM and MANT-nucleotide, a decrease in EF3 fluorescence and a shift to longer wavelength at around 355 nm was observed (Figure 4-12 A, black trace). Shifts to longer wavelengths indicate the presence of tryptophan residues of EF3 in a more polar environment. Additionally, a decrease in FRET at around 440 nm was observed. This indicates that Cz.Cl binds and inhibits CaM that can in turn bring about conformational changes in EF3 causing a change in the local environment of the tryptophan residues in EF3. Furthermore, this change in the local environment of tryptophan residues also causes a decrease in FRET to MANT-nucleotide possibly due to an increased distance between them.

At an excitation wavelength of 350 nm, in the presence of EF3/MANT-nucleotide, as expected, an increase in fluorescence was observed with the addition of CaM (Figure 4-12 B, blue trace). This is due to CaM-induced conformational changes in EF3 so that MANT-nucleotide can bind to a

hydrophobic site in EF3. Therefore with the addition of Cz.Cl, a decrease in MANT-nucleotide fluorescence can be expected because Cz.Cl inhibits CaM. However, it was surprising to observe that even in the presence of Cz.Cl, there was no change in MANT-nucleotide fluorescence (Figure 4-12 B, black trace). MANT- nucleotide was bound to a hydrophobic pocket in EF3 even after inhibition of CaM. Based on our experiments, two possibilities cannot be ruled out. One, CaM is not completely inhibited by calmidazollium and therefore can still bind to and induce conformational changes in EF3. Two, though it is too early to suggest that EF3 may possess an exposed/accessible nucleotide binding pocket that can accommodate a nucleotide in the absence of CaM, it is possible that MANT-nucleotide can bind to EF3 in a CaM-independent manner. It is also possible that nucleotide binding to EF in the absence of CaM is an intermediate or transition state between EF alone and EF-CaM-nucleotide complex. Future biochemical, enzymatic, crystallographic and biophysical studies will be required to understand if substrate or substrate analogs could bind to EF3 in the absence of CaM.

Figure 4-12 Kinetic analysis of the inhibition of EF3-CaM binding with calmidazolium chloride probed by 2' MANT-3'd-ATP

Fluorescence experiments were conducted as described in section 4.3.2. Kinetics of inhibition of EF3-CaM binding by calmidazolium chloride was carried out in dual-kinetic mode to observe the rate of change in EF3 (λ = 280 – 450 nm, red trace) and MANT-nucleotide fluorescence (λ = 350 – 450 nm, blue trace). Cuvettes contained 300 nM each of EF3, CaM and MANT-nucleotide in the presence of buffer containing10 mM $MnCl_2$. Increasing concentrations of calmidazolium chloride varying from 1 nM to 300 nM were added. In the graph, fluorescence intensity in arbitrary units is measured as a function of time in minutes. Fluorescence recordings were analyzed using the spectrum package of the Cary Eclipse software. Similar results were obtained from 2 – 3 independent experiments conducted with 2' MANT-3'd-ATP as probe.

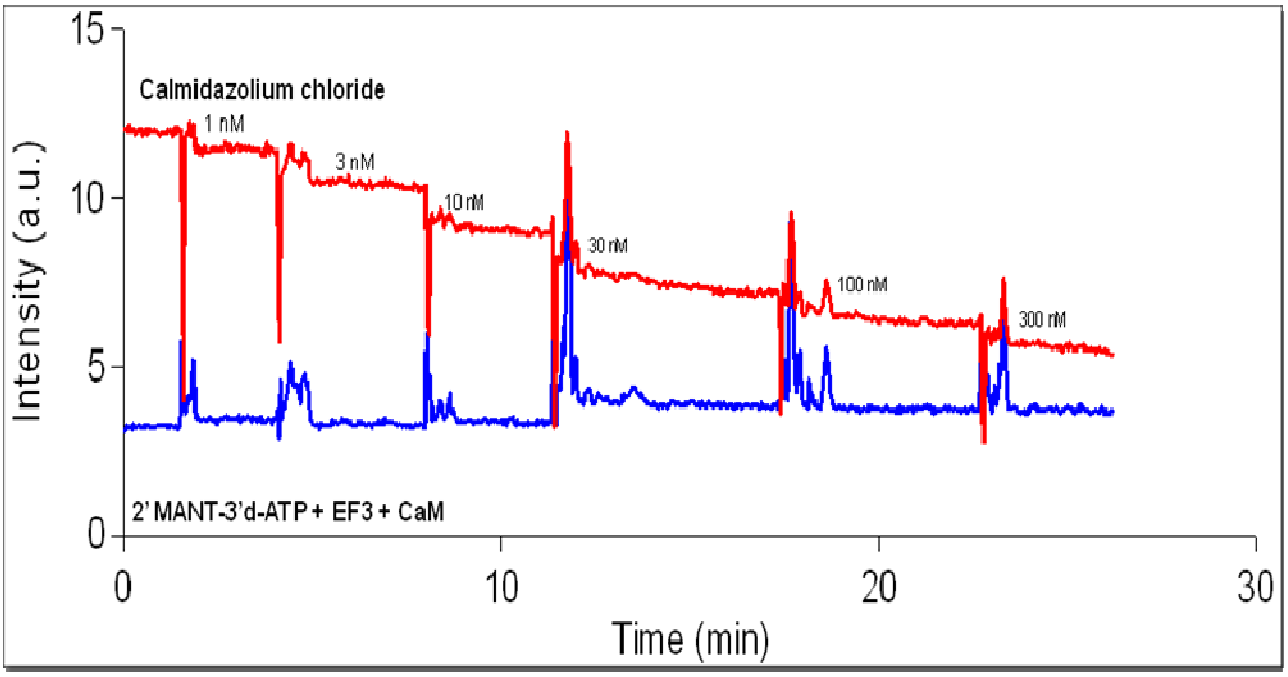
Calmidazolium chloride
1 nM
3 nM
10 nM
30 nM
100 nM
300 nM
2' MANT-3'd-ATP + EF3 + CaM
Intensity (a.u.)
Time (min)
0
5
10
15
0
10
20
30

Figure 4-13 FRET and direct fluorescence experiments examining the effect of calmidazolium chloride on EF3-CaM binding probed by 2' MANT-3'd-ATP

FRET and direct fluorescence experiments were carried out as described in section 4.3.2. Steady-state emission spectra were recorded with λ_{ex} = 280 nm (λ_{em} = 300 – 500 nm) for intrinsic EF3 fluorescence (Figure A) and λ_{ex} = 350 nm (λ_{em} = 370 – 500 nm) for MANT-nucleotide fluorescence (Figure B). Experiments were carried out with sequential addition of reaction mixtures containing 100 mM KCl, 10 mM $MnCl_2$ and 25 mM HEPES/NaOH, pH 7.4, 300 nM 2' MANT-3'd-ATP (green trace), 300 nM EF3 (red trace) and 300 nM CaM (blue trace) followed by addition of 300 nM calmidazolium chloride (black trace). The final assay volume was 150 μl. Graphs were generated using Prism 4.0 software. Baseline fluorescence (buffer alone) was subtracted from all spectra. Fluorescence intensity in A and B are shown as percentage of the maximal emission data obtained for the respective experiment. Data shown here are representative of 2 – 3 independent experiments conducted with 2' MANT-3'd-ATP.

A

FRET measurements - Effect of Calmidazolium Chloride

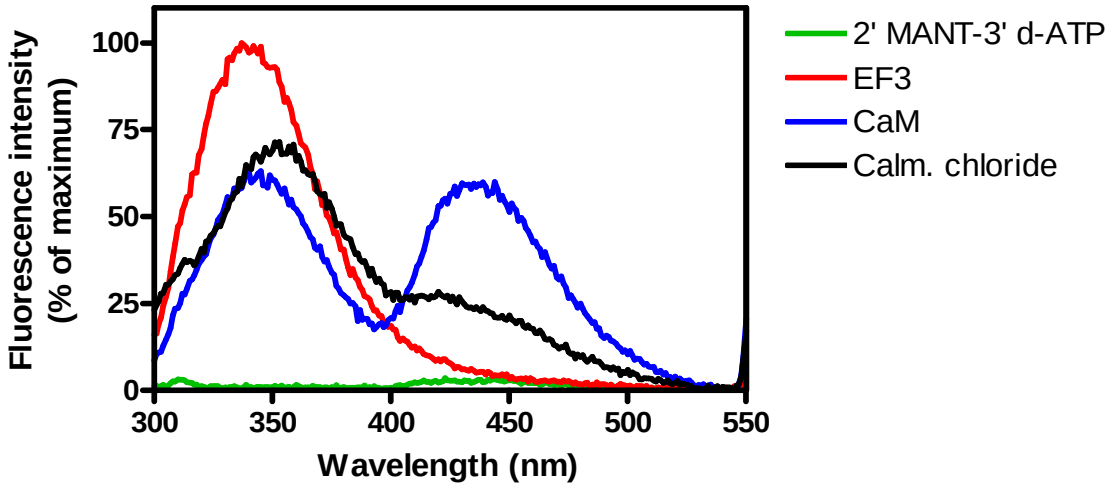

B

Direct fluorescence - Effect of Calmidazolium chloride

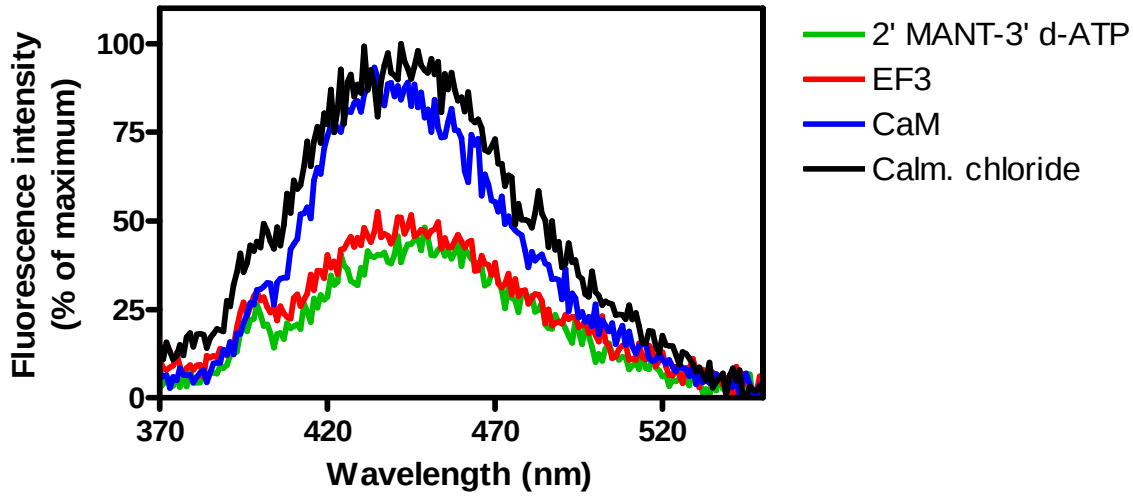

-***Calcium dependent/independent interaction of CaM with EF3 probed by 2' MANT-3'd-ATP***

A high binding affinity of EF and CaM (K_d = 20 nM) is dependent on calcium (Shen et al., 2002 and 2005; Ulmer et al., 2003). CaM possesses four calcium binding sites (2 each in N and C-terminal domain) and exists in three calcium loading states namely apo-CaM (no Ca^{2+} bound), 2 Ca^{2+} state (2 Ca^{2+} ions bound to C-CaM and N-CaM in apo state) and a 4 Ca^{2+} state (both N and C-CaM bound to calcium). EF binds to CaM in a 2 Ca^{2+} loaded state with N-CaM in apo state and C-CaM bound to calcium ions. Experiments with CaM mutants suggest that mutations in calcium binding sites 1 and 2 did not have an effect on EF-CaM activation. Mutations in calcium binding sites 3 and 4, especially 4 had a significant effect on EF-CaM activation (Shen et al., 2002). This clearly indicated that EF can bind to N-CaM irrespective of its calcium loaded state but EF binding to C-CaM is strongly dependent on calcium.

A combination of enzymatic, spectroscopic and NMR studies have demonstrated that EF activation by CaM requires a physiological calcium concentration of about 1 μM. In fluorescence experiments probed by 2'd-3' ANT-ATP, up to 2 μM Ca^{2+} was required for EF-CaM activation. Higher calcium concentrations inhibit EF activity by competing with Mg^{2+} ion for the metal-ion binding site (Shen et al., 2002).

The current study is aimed at understanding the importance of calcium ions in the EF-CaM interaction probed by 2' MANT-3'd-ATP. Fluorescence experiments at excitation of 280 nm (Figure 4-13 A, B and C) and 350 nm (Figure 4-13 D, E and F) were carried out in three different conditions namely 1, in the presence of 100 μM Ca^{2+} (Figure 4-13 A and D). 2, in the presence of 100 μM EGTA (to bind to any free Calcium ions) (Figure 4-13 B and E). 3, in the absence of both EGTA and calcium (Figure 4-13 C and F). EGTA is a calcium chelator and can effectively bind to free calcium if present in the experiment. Calcium or EGTA were added to the HEPES buffer to observe their effect on intrinsic EF3 or MANT-nucleotide fluorescence. Under all three conditions studied, no change in intrinsic EF3 fluorescence, FRET or direct MANT-nucleotide fluorescence was observed. This indicates that irrespective of the presence of calcium, MANT-nucleotide can bind to a hydrophobic site formed by CaM-bound EF3. Our results are surprising in view of the fact that CaM-dependent activation and catalysis of EF3 is dependent on optimal calcium concentrations. In EF AC inhibition studies, the affinity of MANT-nucleotides depended on optimal free calcium concentrations. However, in fluorescence assays, no difference in MANT-nucleotide binding to EF3-CaM was observed in the presence or absence of calcium.

In experiments carried out with N-CaM and C-CaM separately, it was observed that N-CaM but not C-CaM partially activated EF (Shen et al., 2002). Based on the observations that EF locks N-CaM in a calcium-

independent manner, we predict that in experiments with 2' MANT-3'd-ATP, the fluorescence changes in nucleotide binding to EF3 is almost entirely due to EF3 binding to N-CaM in a calcium independent manner.

Previous observations suggest that the helical domain and switch C of EF bind to N-CaM which later triggers a tighter interaction of other regions of EF with C-CaM (Drum et al., 2002; Shen et al., 2002). From molecular modeling and fluorescence studies, we predicted that the stabilization of the MANT-group is due to π-stacking interactions with F586. It is also known that switch C makes large contacts with switch B and F586 is a residue in switch B. Therefore, we predict that binding and activation of EF3-CaM probed by 2'MANT-3'd-ATP is a multi-step process as follows.

1. The helical domain and switch C region of EF3 make initial contacts with N-CaM (calcium-independent)

2. Switch C binding to N-CaM causes the ordering of switch B in EF3 which can now accommodate and stabilize the MANT-nucleotide in a hydrophobic pocket by π-stacking interactions with F586

1. N-CaM binding to EF3 triggers a stronger interaction with C-CaM in a calcium dependent manner to fully activate EF3.

It is also clear that binding of CaM and activation of EF are two independent events where amino acid residues in EF3 responsible for binding

are completely different from the ones needed for nucleotide-binding and catalysis. Site-directed mutagenesis experiments with CaM, crystallographic studies of EF3-CaM in complex with 2' MANT-3'd-ATP and molecular modeling approaches will be needed to completely understand the role of calcium in binding and activation of EF3-CaM.

Figure 4-14 Calcium-dependent/independent-binding of CaM to EF3 probed by 2'MANT-3'd-ATP

FRET and direct fluorescence experiments were carried out as described in section 4.3.2 in three different conditions namely 1, in the presence of 100 μM Ca^{2+} (Figure A and D). 2, in the presence of 100 μM EGTA (Figure B and E). 3, in the absence of both EGTA and calcium (Figure C and F). Steady-state emission spectra were recorded with λ_{ex} = 280 nm (λ_{em} = 300 – 500 nm) for intrinsic EF3 fluorescence (Figure A, B and C) and λ_{ex} = 350 nm (λ_{em} = 370 – 500 nm) for MANT-nucleotide fluorescence (Figure D, E and F). Experiments were carried out with sequential addition of reaction mixtures containing 100 mM KCl, 10 mM $MnCl_2$ and 25 mM HEPES/NaOH, pH 7.4, with calcium or EGTA followed by addition of 300 nM 2' MANT-3'd-ATP (green trace), 300 nM EF3 (red trace) and 300 nM CaM (blue trace). The final assay volume was 150 μl. Graphs were generated using Prism 4.0 software. Baseline fluorescence (buffer alone) was subtracted from all spectra. Fluorescence intensities in A, B and C are shown as percentage of the maximal emission data obtained for the respective experiment. Fluorescence intensity in D, E and F are shown in arbitrary units (a.u). Data shown here are representative of 2 – 3 independent experiments conducted with 2' MANT-3'd-ATP.

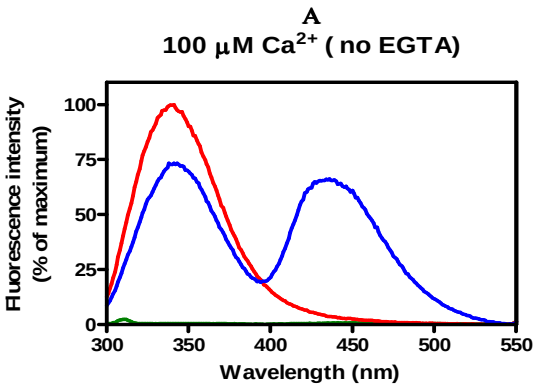
A
100 µM Ca2+ (no EGTA)
Fluorescence intensity (% of maximum)
Wavelength (nm)

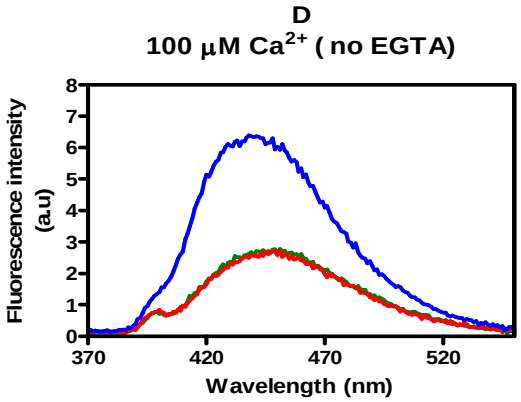
D
100 µM Ca2+ (no EGTA)
Fluorescence intensity (a.u)
Wavelength (nm)

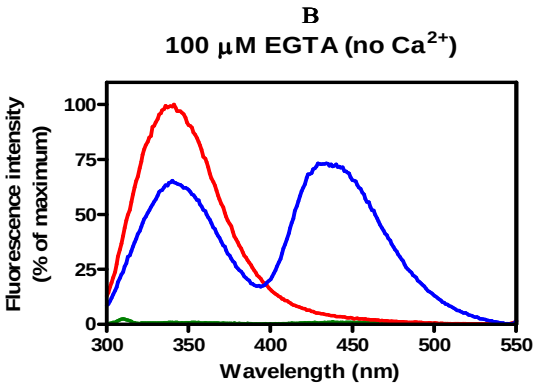
B
100 µM EGTA (no Ca2+)
Fluorescence intensity (% of maximum)
Wavelength (nm)

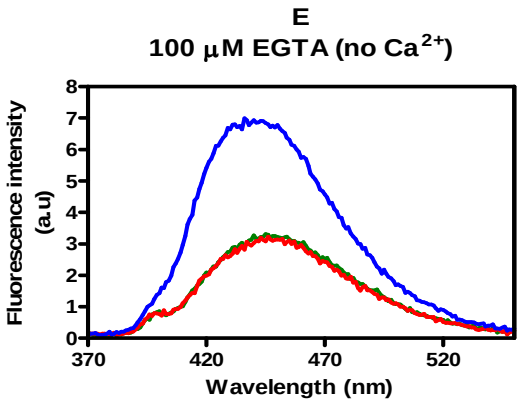
E
100 µM EGTA (no Ca2+)
Fluorescence intensity (a.u)
Wavelength (nm)

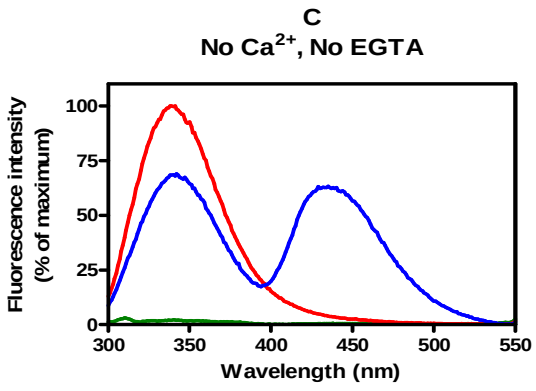
C
No Ca2+, No EGTA
Fluorescence intensity (% of maximum)
Wavelength (nm)

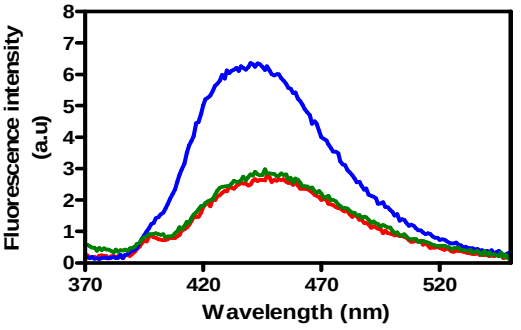
F
No Ca2+, No EGTA
Fluorescence intensity (a.u)
Wavelength (nm)

Figure 4-15 Schematic representation of the proposed mechanism of EF-CaM binding and activation

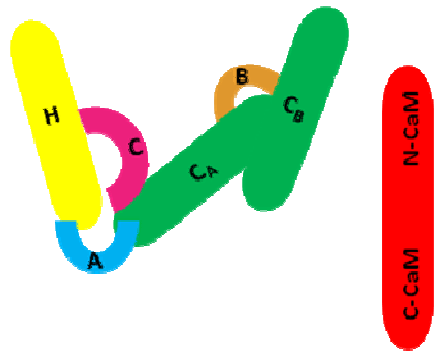

Shown here is EF alone with different domains depicted as yellow = H, helical domain; green = C_A-C_B catalytic domain; blue, pink and orange = A, B and C switch regions that undergo major conformational changes due to CaM-binding. CaM (red) with N and C-terminus shown.

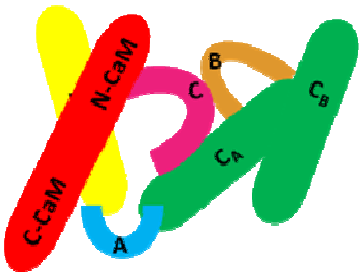

EF-CaM interaction is initiated by binding of N-CaM to helical domain and switch C region in a calcium-independent manner. Switch C interacts with and stabilizes switch B due to CaM-binding.

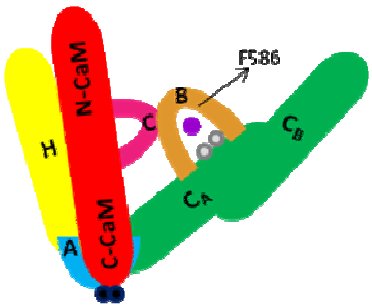

Switch B consists of residues for nucleotide binding. Due to N-CaM-binding, nucleotide (purple sphere) stabilizes itself in the catalytic core by π-stacking interactions with F586. C-CaM binding to EF occurs in calcium-dependent manner (Ca^{2+} ions – black spheres) triggering activation and catalysis of EF. Metal ions depicted as grey spheres.

- ***Modulation of EF-CaM interaction by oxidation of CaM***

Reactive oxygen species oxidize specifically the cysteine and methionine residues in proteins (Levine et al., 1999). CaM consists of nine methionine residues and these residues are particularly sensitive to ROS-induced oxidation (Yin et al., 2000). CaM (O) (oxidized CaM) cannot efficiently bind to and activate its effector proteins such as Ca^{2+}-ATPase in the plasma membrane. Specifically, oxidation of M144 and M145 in CaM abolishes the CaM-dependent activation of Ca^{2+}-ATPase (Bartlett et al., 2003). It has also been observed in nitric oxide synthases that CaM (O) has a decreased affinity for the enzyme (Montgomery et al., 2003). CaM (O) is also unable to activate CaM kinase II and prevents autophosphorylation (Robison et al., 2007). Clearly, the reduced state of methionine residues is crucial for interaction of CaM with its effector proteins. Fluorescence and circular dichroism (CD) studies have shown that the central helix in CaM loses its stabilizing interactions due to oxidation (Gao et al., 1998). Furthermore, compared to C-CaM, increased local structural changes were observed in N-CaM due to oxidation of methionine residues.

CyaA, the AC toxin from *Bordetella pertussis* specifically targets neutrophils and macrophages by binding to CD11b/CD18 integrin during infection (Guermonprez et al., 2001). Neutrophil activation results in ROS production that can in turn oxidize a number of proteins including CaM.

Therefore it was important to determine whether oxidized CaM could bind to and activate CyaA. Activation of CyaA was completely abolished by CaM oxidation (Wolff et al., 1980). CyaA was activated by partially oxidized CaM indicating an important role for the toxin in exerting its pathophysiological effects even in the presence of CaM (O). Methionines 109, 124 and 145 were identified as important residues for binding and activation of CyaA enzymatic activity (Vougier et al., 2004).

EF and LF together inhibit NADPH oxidase activity that generates ROS to cause bacterial killing (Crawford et al., 2006). However, it is not known if stimulation of NADPH oxidase activity can cause oxidation of CaM and, therefore, result in inactivation of EF. The goal of this study is to understand the importance of methionine residues in EF-CaM binding and if they play an important role in CaM oxidation in the EF toxic mechanism.

In this study, a qualitative analysis of the binding of CaM (O) to EF3 probed by MANT-nucleotides was carried out by fluorescence spectroscopy. CaM was oxidized as explained in Vougier et al., (2004) and in section 4.3.2. CaM without oxidation CaM(N), was used as control in all the experiments to compare the effects with CaM (O). In steady-state fluorescence experiments at an excitation wavelength of 280 nm, CaM (N) was added to EF3/MANT-nucleotide (Figure 4-14 and 4-15 A and C). As expected, FRET occurred from the tryptophan and tyrosine residues to the MANT-group. In experiments with

CaM(O), in the presence of EF3/MANT-nucleotide, the intensity of FRET reduced several-fold (Figure 4-14 and 4-15 B and D). To monitor changes in MANT-nucleotide fluorescence, CaM (N) was added to EF3/MANT-nucleotide and excited at 350 nm (Figure 4-14 and 4-15 E and G). A several-fold increase in fluorescence was observed. With the addition of CaM (O) (Figure 4-14 and 4-15 F and H), the intensity of MANT-nucleotide fluorescence was reduced compared to CaM (N).

In both FRET and direct MANT-nucleotide fluorescence measurements, with the addition of CaM (O), a decrease in fluorescence intensity compared to CaM (N) indicates that CaM (O) does not bind to EF3 efficiently. Additionally, we observed that a decrease in fluorescence intensity with CaM(O) varied for each nucleotide studied. A 63% and a 42% decrease in the intensity of FRET and direct fluorescence respectively was observed with CaM (O) in the presence of 2' MANT-3'd-ATP (Figure 4-15, B and F). Irrespective of the nucleotide studied, an overall decrease in fluorescence intensity indicates that CaM (O) cannot bind properly to EF3 as compared to CaM (N).

Fluorescence experiments were carried out in the kinetic mode to monitor the rate of binding of CaM (N) and CaM (O) to EF3 (Figure 4-16). Irrespective of the MANT-nucleotide studied, binding of CaM (N) to EF3 showed a higher association rate constant (1.6 min-1 ± 0.2) compared to binding of CaM (O) to

EF3 (0.69 min-1 ± 0.4). This indicates that CaM (N) associates faster with EF3 compared to CaM (O). Furthermore, the t1/2 values obtained from the results are also reflective of the rate of binding of CaM to EF3. The half life in this case indicates the time taken for half of CaM to bind to EF3. Half life obtained for CaM (N) and CaM (O) are 0.4 min ± 0.1 and 0.9 min ± 0.2 respectively. This shows that CaM (O) binds at least 50% slower than CaM (N) to EF3/MANT-nucleotide.

Collectively, a qualitative and a quantitative difference in the binding of CaM (N) and CaM (O) to EF3 was observed. It is clear that CaM (O) shows inefficient binding to EF3 and therefore, it can be suggested that methionine residues in CaM play an important role in the EF3-CaM interaction. However, it remains to be seen if CaM (O) can affect the catalytic activity of EF3. It is also not known if the oxidation of CaM can be reduced by the endogenous methionine sulfoxide reductases (Msr). Future experiments in this area of research must include identifying the specific methionine residues responsible for the EF3-CaM interaction. In addition to design of inhibitors for EF catalytic activity, a clearer understanding of the mechanism EF3-CaM binding will aid in the developments of inhibitors to specifically block this protein-protein interaction.

Figure 4-16 FRET and direct fluorescence measurements of CaM (N) and CaM (O) binding to EF3 probed by MANT-ATP and MANT-GTP

CaM oxidation and fluorescence experiments were carried out as described in section 4.3.2. Steady-state emission spectra were recorded with λ_{ex} = 280 nm (λ_{em} = 300 – 500 nm) for intrinsic EF3 fluorescence (Figure A, B, C and D) and λ_{ex} = 350 nm (λ_{em} = 370 – 500 nm) for MANT-nucleotide fluorescence (Figure E, F, G and H). Figures A, B, E and F correspond to MANT-ATP and Figures C, D, G and H correspond to MANT-GTP. Experiments were carried out with sequential addition of reaction mixtures containing 100 mM KCl, 10 mM $MnCl_2$ and 25 mM HEPES/NaOH, pH 7.4 followed by addition of 300 nM MANT-nucleotide (green trace), 300 nM EF3 (red trace) and 300 nM CaM (N) or 300 nM CaM (O) (blue trace). The final assay volume was 150 μl. Graphs were generated using Prism 4.0 software. Baseline fluorescence (buffer alone) was subtracted from all spectra. Fluorescence intensities in A, B, C and D are shown as percentage of the maximal emission data obtained for the respective experiment. Fluorescence intensity in E, F, G and H are shown in arbitrary units (a.u). Data shown here are representative of 2 – 3 independent experiments for each MANT-nucleotide studied.

A
FRET-MANT-ATP-CaM (N)

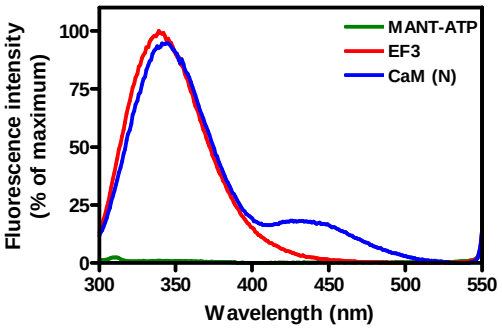

E
DIRECT FL-MANT-ATP- CaM (N)

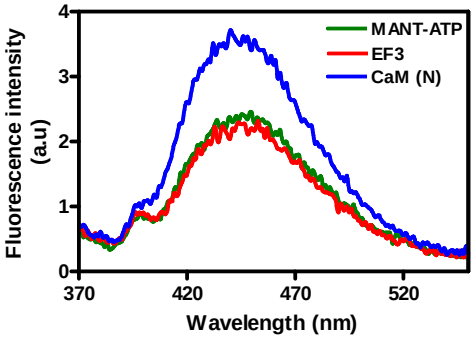

B
FRET-MANT-ATP-CaM (O)

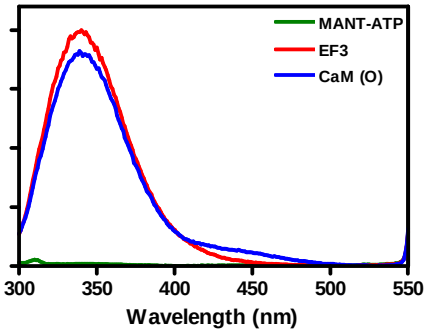

F
DIRECT FL-MANT-ATP-CaM(O)

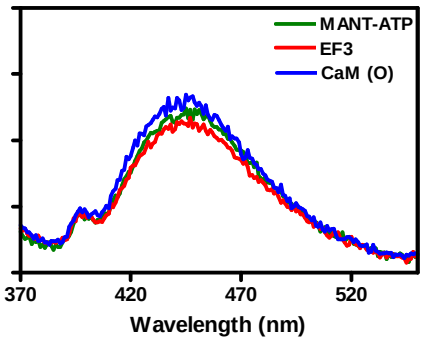

C
FRET-MANT-GTP-CaM (N)

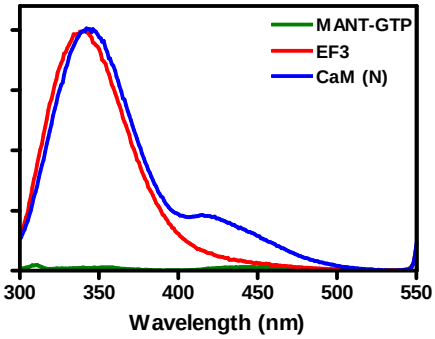

G
DIRECT FL-MANT-GTP-CaM (N)

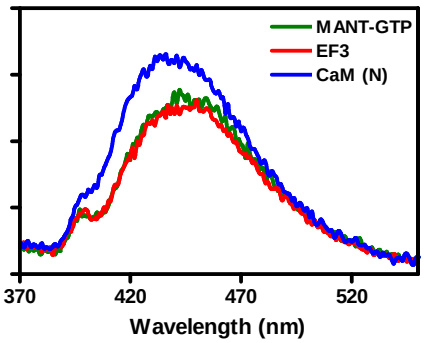

D
FRET-MANT-GTP-CaM (O)

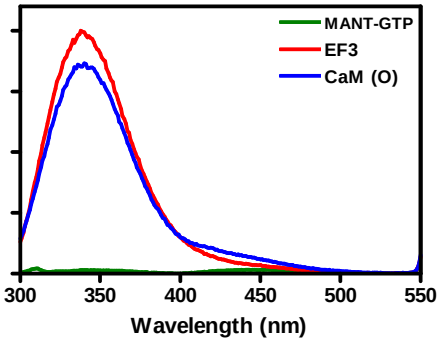

H
DIRECT FL-MANT-GTP-CaM(O)

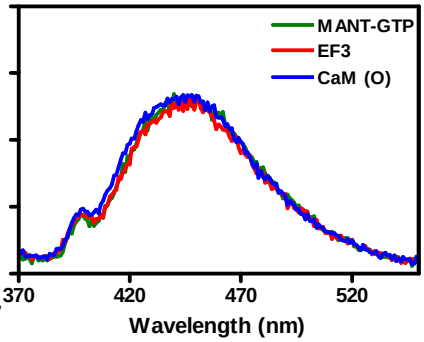

Figure 4-17 FRET and direct fluorescence measurements of CaM (N) and CaM (O) binding to EF3 probed by 2'MANT-3'd-ATP and 3'MANT-2'd-ATP

CaM oxidation and fluorescence experiments were carried out as described in section 4.3.2. Steady-state emission spectra were recorded with λ_{ex} = 280 nm (λ_{em} = 300 – 500 nm) for intrinsic EF3 fluorescence (Figure A, B, C and D) and λ_{ex} = 350 nm (λ_{em} = 370 – 500 nm) for MANT-nucleotide fluorescence (Figure E, F, G and H). Figures A, B, E and F correspond to 2' MANT-3'd-ATP and Figures C, D, G and H correspond to 3' MANT-2'd-ATP. Experiments were carried out with sequential addition of reaction mixtures containing 100 mM KCl, 10 mM $MnCl_2$ and 25 mM HEPES/NaOH, pH 7.4 followed by addition of 300 nM MANT-nucleotide (green trace), 300 nM EF3 (red trace) and 300 nM CaM (N) or 300 nM CaM (O) (blue trace). The final assay volume was 150 μl. Graphs were generated using Prism 4.0 software. Baseline fluorescence (buffer alone) was subtracted from all spectra. Fluorescence intensities in A, B, C and D are shown as percentage of the maximal emission data obtained for the respective experiment. Fluorescence intensities in E, F, G and H are shown in arbitrary units (a.u). Data shown are representative of 2 – 3 independent experiments for each MANT-nucleotide studied.

A
FRET-2' MANT 3' D ATP-CaM(N)

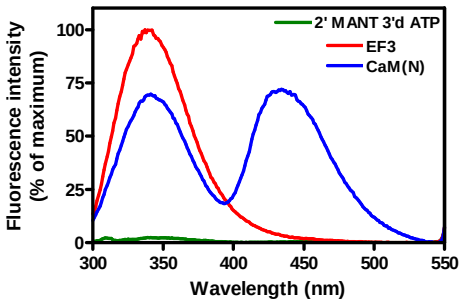

B
FRET-2' MANT 3' D ATP-CaM(O)

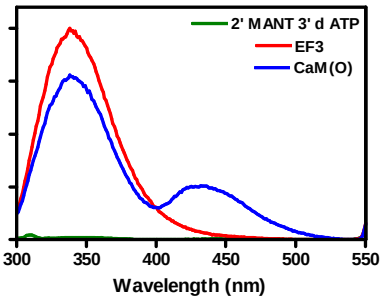

C
FRET-3' MANT 2' D ATP-CaM(N)

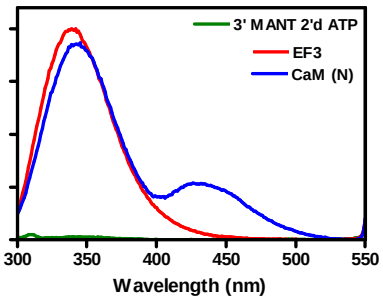

D
FRET-3' MANT 2' D ATP-CaM(O)

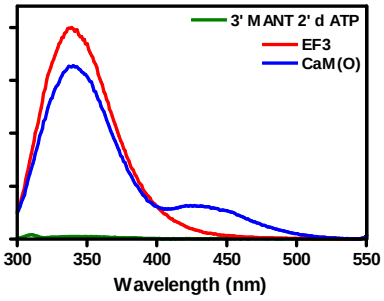

E
DIRECT FL-2' MANT 3' D ATP
CaM(N)

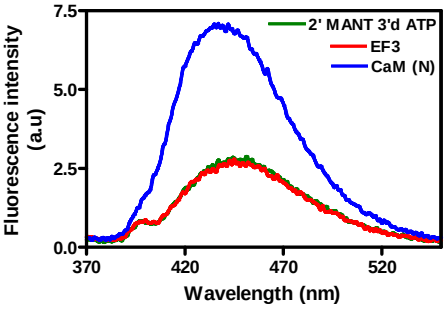

F
DIRECT FL-2' MANT 3' D ATP
CaM(O)

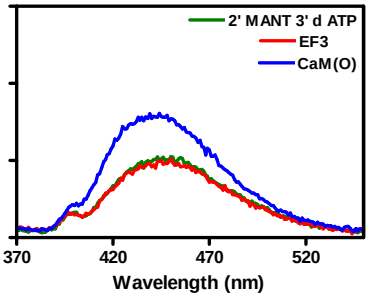

G
DIRECT FL-3' MANT 2' D ATP
CaM(N)

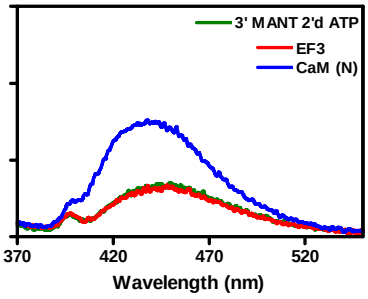

H
DIRECT FL-3' MANT 2' D ATP
CaM(O)

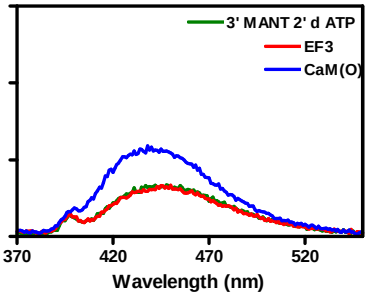

Figure 4-18 Kinetic analysis of the rate of binding of CaM (N) and CaM (O) to EF3

Fluorescence experiments were carried out in the kinetic mode as described in section 4.3.2 to determine the rate of binding of CaM (N) and CaM (O) to EF3. Experiments were carried out with sequential addition of reaction mixtures containing 100 mM KCl, 10 mM $MnCl_2$ and 25 mM HEPES/NaOH, pH 7.4 followed by addition of 300 nM MANT-nucleotide, 300 nM EF3 and 300 nM CaM (N) or 300 nM CaM (O). Experiments were carried out in kinetic mode with wavelength ranging from 280-450 nm. Kinetics of CaM (N) and CaM (O) binding to EF3 were analyzed by the one-phase exponential association equation in Graphpad prism 4.0 software. Baseline fluorescence (buffer + nucleotide + EF3) and initial time before the addition of CaM was subtracted from the graph plotted between fluorescence intensity (a.u) and time (min). Independent experiments with CaM (N) and CaM (O) are plotted in the same graph for comparison. K is the association rate constant expressed in min^{-1} and half life expressed in min is the time required for CaM to bind 50% of the available EF3 molecules. Data shown here are representative of 2 independent experiments for MANT-ATP. Similar results were obtained for all the MANT-nucleotides studied.

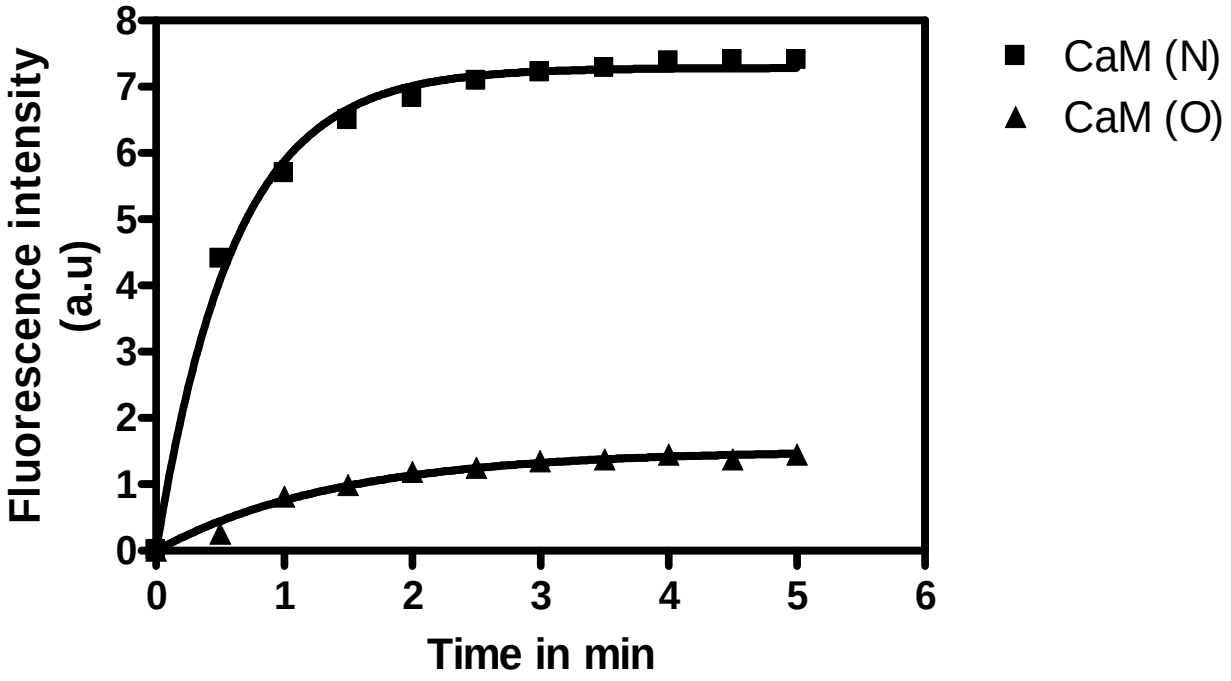

	CaM (N)	CaM (O)
K	1.644	0.6978
HalfLife	0.4217	0.9933

4.5 Conclusions

In conclusion, the 2' and 3' isomers of MANT-ATP and MANT-GTP respectively are useful probes in studying EF-CaM interaction and EF catalytic activity. MANT-GTP analogs have not been studied yet in other AC systems but clearly, enzymatic studies show that MANT-ATP analogs are the most potent inhibitors for EF compared to CyaA, C1/C2 and mAC isoforms (Gille et al., 2004; Gottle et al., 2007).

Though 2' isomers of MANT-ATP and MANT-GTP are more favorable for FRET and direct fluorescence studies, 3' MANT-2'd-ATP is the most potent inhibitor of EF reported so far (K_i = 11 nM). Our molecular modeling studies predict that the 3' MANT-substituent of ATP is better aligned to form π-stacking interactions with F586 and thereby stabilizes itself in the catalytic site of EF3. However, the 2' MANT-substituent of GTP was more potent than its corresponding 3' MANT-substituent as an inhibitor in enzymatic studies. Molecular modeling studies also predict that the MANT-group of 2'MANT-3'd-GTP is oriented towards F586 resulting in more stabilizing interactions with EF. Our studies clearly show that the MANT-group positioning is critical for binding and inhibition of EF3.

Enzymatic, fluorescence and molecular modeling approaches have shown that, though there are slight differences in the binding of the 2' and 3' isomers of MANT-ATP and MANT-GTP, the catalytic site of EF is spacious enough to

accommodate bulky purine nucleotides with modified ribose substituents. Crystallographic studies of the EF-CaM in complex with MANT-ATP and MANT-GTP analogs will help understand the differential binding of these nucleotides. Similar to the tripartite pharmacophore model for mACs (Mou et al., 2006), generation of a pharmacophore model for EF based on the crystal structures of EF-CaM in complex with various nucleotides will help in the design of potent EF inhibitors.

We observed that binding of CaM to EF is Ca^{2+}independent while activation of EF catalytic activity was dependent on calcium. Therefore, a multi-step hypothesis was proposed stating that binding and activation of EF by interaction with CaM are two independent steps involving two different sets of amino acid residues in EF. Future studies, more specifically, experiments with CaM mutants with mutations at the calcium binding sites, will be required to test our hypothesis.

Methionine residues play an important role in recognition and binding of CaM to EF3. Oxidation of methionine residues in CaM resulted in inefficient and a slower binding of CaM to EF3. Based on the important role of methionine residues in EF-CaM interaction, three questions arise. 1. What are the specific methionine residues involved in the EF-CaM interaction? CaM consists of nine methionine residues with five residues in N-CaM and 4 residues in C-CaM (pdb structure 2F3Z, 1J7O, 1J7P, Fallon et al., 2005;

Chou et al., 2001). In the case of CyaA, it was observed that methionine residues at 109, 124, 144 and 145 in C-CaM are important for interaction with CyaA AC (Vougier et al., 2004). Site-directed mutagenesis and Mass-spectroscopic experiments will be required to identify the specific methionine residues involved in EF-CaM interaction. 2. Does CaM (O) alter the catalytic activity of EF? Though it is clear that CaM (O) shows a reduced binding affinity for EF, it is not known if CaM (O) can modulate EF AC activity. It has been observed that CyaA AC activity can be completely abolished by CaM (O) though CyaA can be resistant to partial oxidation of CaM (Wolff et al., 1980; Vougier et al., 2004). This also indicated that even in the presence of CaM (O), CyaA toxin can exert its pathophysiological effect. Enzymatic studies of EF with CaM (O) will be required to observe the effect of CaM oxidation on EF AC activity. In addition, it will also be important to observe the reversal of CaM oxidation by the endogenous methionine sulfoxide reductase enzymes.

Collectively, these properties should help gain insights into EF-CaM interaction to aid in the design of specific EF-CaM inhibitors.

4.6 References

Babu YS, Sack JS, Greenhough TJ, Bugg CE, Means AR and Cook WJ (1985) Three-dimensional structure of calmodulin. *Nature* **315**(6014):37-40.

Bartlett RK, Bieber Urbauer RJ, Anbanandam A, Smallwood HS, Urbauer JL and Squier TC (2003) Oxidation of Met144 and Met145 in calmodulin blocks calmodulin dependent activation of the plasma membrane Ca-ATPase. *Biochemistry* **42**(11):3231-3238.

Bauer CB, Kuhlman PA, Bagshaw CR and Rayment I (1997) X-ray crystal structure and solution fluorescence characterization of Mg.2'(3')-*O*-(N-methylanthraniloyl) nucleotides bound to the *Dictyostelium discoideum* myosin motor domain. *J Mol Biol* **274**(3):394-407.

Bhatnagar R and Batra S (2001) Anthrax toxin. *Crit Rev Microbiol* **27**(3):167-200.

Boyd AP, Ross PJ, Conroy H, Mahon N, Lavelle EC and Mills KH (2005) *Bordetella pertussis* adenylate cyclase toxin modulates innate and adaptive immune responses: distinct roles for acylation and enzymatic activity in immunomodulation and cell death. *J Immunol* **175**(2):730-738.

Brandwein HJ, Lewicki JA, Waldman SA and Murad F (1982) Effect of GTP analogues on purified soluble guanylate cyclase. *J Biol Chem* **257**(3):1309-1311.

Carbonetti NH, Artamonova GV, Andreasen C and Bushar N (2005) Pertussis toxin and adenylate cyclase toxin provide a one-two punch for establishment of *Bordetella pertussis* infection of the respiratory tract. *Infect Immun* **73**(5):2698-2703.

Chen D, Misra M, Sower L, Peterson JW, Kellogg GE and Schein CH (2008) Novel inhibitors of anthrax edema factor. *Bioorg Med Chem* **16**(15):7225-7233.

Chou JJ, Li S, Klee CB and Bax A (2001) Solution structure of $Ca(^{2+})$-calmodulin reveals flexible hand-like properties of its domains. *Nat Struct Biol* **8**(11):990-997.

Confer DL and Eaton JW (1982) Phagocyte impotence caused by an invasive bacterial adenylate cyclase. *Science, NY* **217**(4563):948-950.

Crawford MA, Aylott CV, Bourdeau RW and Bokoch GM (2006) *Bacillus anthracis* toxins inhibit human neutrophil NADPH oxidase activity. *J Immunol* **176**(12):7557-7565.

Deisseroth K, Heist EK and Tsien RW (1998) Translocation of calmodulin to the nucleus supports CREB phosphorylation in hippocampal neurons. *Nature*

392(6672):198-202.

Desaubry L, Shoshani I and Johnson RA (1996) 2',5'-Dideoxyadenosine 3'-polyphosphates are potent inhibitors of adenylyl cyclases. *J Biol Chem* **271**(5):2380-2382.

Dixon TC, Meselson M, Guillemin J and Hanna PC (1999) Anthrax. Anthrax. *N Engl J Med* **341**(11):815-826.

Drum CL, Yan SZ, Bard J, Shen YQ, Lu D, Soelaiman S, Grabarek Z, Bohm A and Tang WJ (2002) Structural basis for the activation of anthrax adenylyl cyclase exotoxin by calmodulin. *Nature* **415**(6870):396-402.

Drum CL, Yan SZ, Sarac R, Mabuchi Y, Beckingham K, Bohm A, Grabarek Z and Tang WJ (2000) An extended conformation of calmodulin induces interactions between the structural domains of adenylyl cyclase from *Bacillus anthracis* to promote catalysis. *J Biol Chem* **275**(46):36334-36340.

Fallon JL, Halling DB, Hamilton SL and Quiocho FA (2005) Structure of calmodulin bound to the hydrophobic IQ domain of the cardiac Ca(v)1.2 calcium channel. *Structure* **13**(12):1881-1886.

Firoved AM, Moayeri M, Wiggins JF, Shen Y, Tang WJ and Leppla SH (2007) Anthrax edema toxin sensitizes DBA/2J mice to lethal toxin. *Infect Immun* **75**(5):2120-2125.

Gallay J, Vincent M, Li de la Sierra IM, Munier-Lehmann H, Renouard M, Sakamoto H, Barzu O and Gilles AM (2004) Insight into the activation mechanism of *Bordetella pertussis* adenylate cyclase by calmodulin using fluorescence spectroscopy. *Eur J Biochem / FEBS* **271**(4):821-833.

Gao J, Yin DH, Yao Y, Sun H, Qin Z, Schoneich C, Williams TD and Squier TC (1998) Loss of conformational stability in calmodulin upon methionine oxidation. *Biophys J* **74**(3):1115-1134.

Gille A, Lushington GH, Mou TC, Doughty MB, Johnson RA and Seifert R (2004) Differential inhibition of adenylyl cyclase isoforms and soluble guanylyl cyclase by purine and pyrimidine nucleotides. *J Biol Chem* **279**(19):19955-19969.

Gille A and Seifert R (2003) 2'(3')-*O*-(N-methylanthraniloyl)-substituted GTP analogs: a novel class of potent competitive adenylyl cyclase inhibitors. *J Biol Chem* **278**(15):12672-12679.

Gottle M, Dove S, Steindel P, Shen Y, Tang WJ, Geduhn J, Konig B and Seifert R (2007) Molecular analysis of the interaction of *Bordetella pertussis* adenylyl cyclase with fluorescent nucleotides. *Mol Pharmacol* **72**(3):526-535.

Guermonprez P, Khelef N, Blouin E, Rieu P, Ricciardi-Castagnoli P, Guiso N, Ladant D and Leclerc C (2001) The adenylate cyclase toxin of Bordetella pertussis binds to target cells via the α(M)β(2) integrin (CD11b/CD18). *J Exp Med* **193**(9):1035-1044.

Hazlett TL, Moore KJ, Lowe PN, Jameson DM and Eccleston JF (1993) Solution dynamics of p21ras proteins bound with fluorescent nucleotides: a time-resolved fluorescence study. *Biochemistry* **32**(49):13575-13583.
Hewlett EL, Gordon VM, McCaffery JD, Sutherland WM and Gray MC (1989) Adenylate cyclase toxin from *Bordetella pertussis*. Identification and purification of the holotoxin molecule. *J Biol Chem* **264**(32):19379-19384.

Hiratsuka T (1983) Acrylamide fluorescence quenching studies on the actin-induced change in protein dynamics in the subfragment-1/subfragment-2 link region of cardiac myosin. *J Biochem* **93**(3):875-882.

Ikura M (1996) Calcium binding and conformational response in EF-hand proteins. *Trends Biochem Sci* **21**(1):14-17.

Jameson DM and Eccleston JF (1997) Fluorescent nucleotide analogs: synthesis and applications. *Methods Enzymol* **278**:363-390.

Johnson RA and Shoshani I (1990) Inhibition of *Bordetella pertussis* and *Bacillus anthracis* adenylyl cyclases by polyadenylate and "P"-site agonists. *J Biol Chem* **265**(31):19035-19039.

Kammer GM (1988) The adenylate cyclase-cAMP-protein kinase A pathway and regulation of the immune response. *Immunol Today* **9**(7-8):222-229.

Kyriakis JM and Avruch J (2001) Mammalian mitogen-activated protein kinase signal transduction pathways activated by stress and inflammation. *Physiol Rev* **81**(2):807-869.

Ladant D and Ullmann A (1999) *Bordatella pertussis* adenylate cyclase: a toxin with multiple talents. *Trends Microbiol* **7**(4):172-176.

Lee YS, Bergson P, He WS, Mrksich M and Tang WJ (2004) Discovery of a small molecule that inhibits the interaction of anthrax edema factor with its cellular activator, calmodulin. *Chem Biol* **11**(8):1139-1146.

Leppla SH (1982) Anthrax toxin edema factor: a bacterial adenylate cyclase that increases cyclic AMP concentrations of eukaryotic cells. *Proc Natl Acad Sci U S A* **79**(10):3162-3166.

Levine RL, Berlett BS, Moskovitz J, Mosoni L and Stadtman ER (1999) Methionine residues may protect proteins from critical oxidative damage. *Mech Ageing Dev* **107**(3):323-332.

Mock M and Ullmann A (1993) Calmodulin-activated bacterial adenylate cyclases as virulence factors. *Trends Microbiol* **1**(5):187-192.

Montgomery HJ, Bartlett R, Perdicakis B, Jervis E, Squier TC and Guillemette JG (2003) Activation of constitutive nitric oxide synthases by oxidized calmodulin mutants. *Biochemistry* **42**(25):7759-7768.
Mou TC, Gille A, Fancy DA, Seifert R and Sprang SR (2005) Structural basis for the inhibition of mammalian membrane adenylyl cyclase by 2 '(3')-*O*-(N-Methylanthraniloyl)-guanosine 5 '-triphosphate. *J Biol Chem* **280**(8):7253-7261.

Mou TC, Gille A, Suryanarayana S, Richter M, Seifert R and Sprang SR (2006) Broad specificity of mammalian adenylyl cyclase for interaction with 2',3'-substituted purine- and pyrimidine nucleotide inhibitors. *Mol Pharmacol* **70**(3):878-886.

Nelson MR and Chazin WJ (1998) An interaction-based analysis of calcium-induced conformational changes in Ca^{2+} sensor proteins. *Protein Sci* **7**(2):270-282.

Ortiz AR, Pisabarro MT, Gago F and Wade RC (1995) Prediction of drug binding affinities by comparative binding energy analysis. *J Med Chem* **38**(14):2681-2691.

Pini A, Runci Y, Falciani C, Lelli B, Brunetti J, Pileri S, Fabbrini M, Lozzi L, Ricci C, Bernini A, Tonello F, Dal Molin F, Neri P, Niccolai N and Bracci L (2006) Stable peptide inhibitors prevent binding of lethal and oedema factors to protective antigen and neutralize anthrax toxin *in vivo*. *Biochem J* **395**(1):157-163.

Rarey M, Kramer B, Lengauer T and Klebe G (1996) A fast flexible docking method using an incremental construction algorithm. *J Mol Biol* **261**(3):470-489.

Robison AJ, Winder DG, Colbran RJ and Bartlett RK (2007) Oxidation of calmodulin alters activation and regulation of CaMKII. *Biochem Biophys Res*

Commun **356**(1):97-101.

Sarfati RS, Kansal VK, Munier H, Glaser P, Gilles AM, Labruyere E, Mock M, Danchin A and Barzu O (1990) Binding of 3'-anthraniloyl-2'-deoxy-ATP to calmodulin-activated adenylate cyclase from *Bordetella pertussis* and *Bacillus anthracis*. *J Biol Chem* **265**(31):18902-18906.

Shen Y, Guo Q, Zhukovskaya NL, Drum CL, Bohm A and Tang WJ (2004) Structure of anthrax edema factor-calmodulin-adenosine 5'-(α,β-methylene)-triphosphate complex reveals an alternative mode of ATP binding to the catalytic site. *Biochem Biophys Res Commun* **317**(2):309-314.

Shen Y, Lee YS, Soelaiman S, Bergson P, Lu D, Chen A, Beckingham K, Grabarek Z, Mrksich M and Tang WJ (2002) Physiological calcium concentrations regulate calmodulin binding and catalysis of adenylyl cyclase exotoxins. *Embo J* **21**(24):6721-6732.

Shen Y, Zhukovskaya NL, Guo Q, Florian J and Tang WJ (2005) Calcium-independent calmodulin binding and two-metal-ion catalytic mechanism of anthrax edema factor. *Embo J* **24**(5):929-941.

Shen Y, Zhukovskaya NL, Zimmer MI, Soelaiman S, Bergson P, Wang CR, Gibbs CS and Tang WJ (2004) Selective inhibition of anthrax edema factor by adefovir, a drug for chronic hepatitis B virus infection. *Proc Natl Acad Sci U S A* **101**(9):3242-3247.

Shoshani I, Laux WH, Perigaud C, Gosselin G and Johnson RA (1999) Inhibition of adenylyl cyclase by acyclic nucleoside phosphonate antiviral agents. *J Biol Chem* **274**(49):34742-34744.

Soelaiman S, Wei BQ, Bergson P, Lee YS, Shen Y, Mrksich M, Shoichet BK and Tang WJ (2003) Structure-based inhibitor discovery against adenylyl cyclase toxins from pathogenic bacteria that cause anthrax and whooping cough. *J Biol Chem* **278**(28):25990-25997.

Tesmer JJ, Dessauer CW, Sunahara RK, Murray LD, Johnson RA, Gilman AG and Sprang SR (2000) Molecular basis for P-site inhibition of adenylyl cyclase. *Biochemistry* **39**(47):14464-14471.

Ulmer TS, Soelaiman S, Li S, Klee CB, Tang WJ and Bax A (2003) Calcium dependence of the interaction between calmodulin and anthrax edema factor. *J Biol Chem* **278**(31):29261-29266.

Vougier S, Mary J, Dautin N, Vinh J, Friguet B and Ladant D (2004) Essential

role of methionine residues in calmodulin binding to *Bordetella pertussis* adenylate cyclase, as probed by selective oxidation and repair by the peptide methionine sulfoxide reductases. *J Biol Chem* **279**(29):30210-30218.

Wolff J, Cook GH, Goldhammer AR and Berkowitz SA (1980) Calmodulin activates prokaryotic adenylate cyclase. *Proc Natl Acad Sci U S A* **77**(7):3841-3844.

Yin D, Kuczera K and Squier TC (2000) The sensitivity of carboxyl-terminal methionines in calmodulin isoforms to oxidation by H_2O_2 modulates the ability to activate the plasma membrane Ca-ATPase. *Chem Res Toxicol* **13**(2):103-110.

Zhang M, Tanaka T and Ikura M (1995) Calcium-induced conformational transition revealed by the solution structure of apo calmodulin. *Nat Struct Biol* **2**(9):758-767.

Chapter 5: Future directions

5.1 Understanding AC regulation and inhibition

5.1.1 Structural basis for the interaction of the TNP-nucleotides with C1/C2 and holo-AC isoforms

The work presented in chapter 2 clearly indicates that there are subtle differences in the interaction of TNP-GTP and TNP-ATP with C1/C2. Since the crystal structure of C1/C2-$G_s\alpha$-FS in complex with TNP-ATP is already available (Mou et al., 2006), crystallographic studies of C1/C2 in complex with TNP-GTP should be carried out to compare and explain the differences in the interaction of these nucleotides with C1/C2.

Compared to other proteins studied with TNP-nucleotides as probes, TNP-nucleotides have the highest affinity for mACs (Hiratsuka, 1982; Broglie and Takahashi, 1983; Thomas et al., 1991). TNP-nucleotides are known to bind to a number of nucleotide-binding proteins so it is challenging to establish their usefulness as specific inhibitors for ACs (Liu and Sharom, 1997; Stewart et al., 1998; Hiratsuka, 2003) Among the ACs, we have seen that TNP-nucleotides are more potent at inhibiting mACs compared to bacterial AC toxins such as EF and CyaA (data not shown). From the crystal structure of C1/C2-$G_s\alpha$-FS in complex with TNP-ATP (Mou et al., 2006), it is clear that

introduction of the bulky, aromatic TNP group at the 2' and the 3' position of the ribose moiety of ATP can give rise to a new class of inhibitors for mACs. Additionally, we have also observed that TNP-UTP and TNP-CTP are highly potent at inhibiting both C1/C2 (K_i = 92 nM and 310 nM respectively) and mAC isoforms indicating that a smaller base may also help in higher potency at AC inhibition. Since the TNP-pyrimidine nucleotides have not yet been reported to bind to, and inhibit other proteins, they can serve as starting points for development of potent inhibitors for mACs.

There are nine different AC isoforms with differential localization, regulation and interaction with different proteins (Sunahara et al., 1996; Hanoune and Defer, 2001). Therefore, it has been extremely difficult to identify potent isoform-specific activators and inhibitors of mACs. While studying the inhibitory effects of TNP-nucleotides on holo-AC isoforms, specifically AC1, AC2 and AC5, TNP-nucleotides inhibited the holo-ACs in an isoform-selective manner. TNP-ATP was the most potent inhibitor of the AC5 isoform reported so far (K_i = 4 nM). Furthermore, in our fluorescence assays, we have observed that all the TNP-nucleotides can be utilized as probes to study conformational changes in C1/C2.

We have also observed that TNP-NDPs can serve as substrates for selective kinases (Chapter 2). Therefore TNP-NDPs could serve as models for developing pro-drugs at inhibiting ACs, where they can be converted into

their active-NTP form in the presence of the specific phosphorylating systems.

All our studies have been carried out with C1 (from AC5) and C2 (from AC2) as models for mAC regulation and catalysis (Gille et al., 2004; Mou et al., 2005 and 2006). However, it will be important to carry out enzymatic, fluorimetric, molecular modeling and crystallographic studies of C1 and C2 from the same isoforms with TNP-nucleotides. This approach will also help understand the isoform-selective inhibition of mACS by TNP-nucleotides.

Collectively, based on the AC-isoform-selective inhibitory properties of TNP-nucleotides and their binding to C1/C2 monitored by fluorescence spectroscopy, sensitive fluorescence-based assays can be developed to identify potent isoform-specific AC inhibitors. Additionally, development of cell-based assays will be required for the identification of cell-permeable AC inhibitors.

5.1.2 Analysis of the mechanism of homodimerization of C1 and C2 subunits of mAC and a potential physiological role of AC dimerization in cAMP signaling

In addition to forming multimeric complexes with GPCRS and G-proteins, ACs are also known to dimerize *via* their transmembrane domains (Neer et

al., 1984; Yeager et al., 1985; Smigel, 1986; Gu et al., 2001 and 2002; Cooper and Crossthwaithe, 2006). In chapter 3, we have observed that the individual subunits of mACs, C1 possess very low catalytic activity and C2 exhibits almost no catalytic activity. We have observed that C1 and C2 subunits can form homodimers. Although, it is proposed that the dimer is the minimum functional unit of mACs, it is also important to understand if the C1 and C2 subunits can form only homodimers or higher-order oligomers. It was proposed that ACs dimerize in a head-to-tail fashion, thereby bringing the two C1 and the two C2 subunits from different ACs molecules together (Gu et al., 2001 and 2002; Cooper and Crossthwaithe, 2006). Future studies should focus on analyzing the properties of C1 and C2 homodimers from various AC isoforms. It would also be interesting to see if C1 and C2 subunits from two different AC isoforms can homodimerize. More specifically, FRET and BRET studies in live cells should be carried out to examine the possibility of homodimerization. Chimeric ACs should also be constructed, for example, C1 from ACX and C1 from ACY, to analyze the homodimerization.

Although ACs can dimerize, a physiological role of AC dimerization in the production of cAMP is not yet known. Studies should focus on understanding the consequences of C1 and C2 homodimerization. It is possible that C1 and C2 homodimers serve as a checkpoint to control excess cAMP production. Therefore, further insights into the physiological significance of C1 and C2

homodimerization will greatly impact the development of activators and inhibitors of dimerized ACs.

5.2 Molecular analysis of EF catalytic activity and its interaction with other proteins.

5.2.1 Understanding the mechanism of the interaction of EF with other proteins

EF and LF bind to PA and PA mediates entry of EF and LF into the cytosol ((Mock and Fouet, 2001; Mourez et al., 2002). Recent studies suggest that LF can bind to both monomeric and heptameric forms of PA (Lacy et al., 2005; Chvyrkova et al., 2007). An EF binding site has been mapped on PA (Lacy et al., 2002 and 2005) and though evidence suggests that the PA-binding domain of EF is not required for the potency of EF inside cells, it would be of considerable interest to inhibit EF alternatively by blocking its interaction with PA to prevent its entry into cells. Future studies should specifically focus on blocking this important interaction between EF and PA since this is the first step for the entry of EF into cells.

After PA-mediated entry of EF into the cytosol, CaM binds to, and activates EF (Leppla, 1982). We have proposed that CaM initially binds to EF in a calcium-independent manner followed by activation of EF catalytic activity

dependent on calcium ions. Furthermore, we have observed that methionine residues in CaM play an important role in EF-CaM binding. CaM is a ubiquitous protein that can bind to several effector proteins. Therefore, it would be worth studying the exact mechanism of the EF-CaM interaction to aid in the development of inhibitors that specifically block the binding of CaM to EF.

5.2.2 Structural basis for the interaction of MANT-nucleotides with EF and rational design of potent EF inhibitors

Our enzymatic, fluorescence and molecular modeling studies have shown that the 2' and 3' isomers of MANT-ATP and MANT-GTP interact differently with the catalytic site of EF3. Very recently, using a site-directed mutagenesis approach, we have identified important amino acid residues crucial for binding and stabilization of MANT-ATP to the EF3 catalytic site (Taha et al., 2008). Therefore, future studies should focus on solving the crystal structure of EF3-CaM in complex with the defined isomers of MANT-nucleotides to understand the structural basis for differential inhibition of EF3 by MANT-nucleotides. Very similar to mACs, it will be important to develop a pharmacophore model of EF3 for differential interaction of MANT-nucleotide inhibitors for rationale design of potent EF3 inhibitors.

Our fluorescence assays are extremely sensitive in identifying differences in the binding of different MANT-nucleotides to EF3. We have observed that

the 2’ isomers of MANT-ATP and MANT-GTP are more favorable for FRET and direct fluorescence studies. Therefore, based on our experiments, robust and non-radiometric fluorescence-based HTS assays can be developed for identification of potent EF inhibitors.

An important challenge in the development of potent EF inhibitors is the specificity of inhibitors for EF alone and not mACs. Though, EF and mACs are structurally different and are activated by different mediators, they both catalyze the conversion of ATP to cAMP using a two-metal ion catalytic mechanism and have a few common residues responsible for ATP-binding and catalysis (Tesmer et al., 1997 and 1999; Drum et al., 2002; Shen et al., 2005). Therefore, it is critical to develop potent inhibitors that specifically bind to EF and not to mACs.

References

Broglie KE and Takahashi M (1983) Fluorescence studies of threonine-promoted conformational transitions in aspartokinase I using the substrate analogue 2'(3')-*O*-(2,4,6-trinitrophenyl)adenosine 5'-triphosphate. *J Biol Chem* **258**(21):12940-12946.

Chvyrkova I, Zhang XC and Terzyan S (2007) Lethal factor of anthrax toxin binds monomeric form of protective antigen. *Biochem Biophys Res Commun* **360**(3):690-695.

Cooper DM and Crossthwaite AJ (2006) Higher-order organization and regulation of adenylyl cyclases. *Trends Pharmacol Sci* **27**(8):426-431.

Drum CL, Yan SZ, Bard J, Shen YQ, Lu D, Soelaiman S, Grabarek Z, Bohm A and Tang WJ (2002) Structural basis for the activation of anthrax adenylyl cyclase exotoxin by calmodulin. *Nature* **415**(6870):396-402.

Gille A, Lushington GH, Mou TC, Doughty MB, Johnson RA and Seifert R (2004) Differential inhibition of adenylyl cyclase isoforms and soluble guanylyl cyclase by purine and pyrimidine nucleotides. *J Biol Chem* **279**(19):19955-19969.

Gu C, Cali JJ and Cooper DM (2002) Dimerization of mammalian adenylate cyclases. *Eur J Biochem / FEBS* **269**(2):413-421.

Gu C, Sorkin A and Cooper DM (2001) Persistent interactions between the two transmembrane clusters dictate the targeting and functional assembly of adenylyl cyclase. *Curr Biol* **11**(3):185-190.

Hanoune J and Defer N (2001) Regulation and role of adenylyl cyclase isoforms. *Annu Rev Pharmacol Toxicol* **41**:145-174.

Hiratsuka T (1982) Biological activities and spectroscopic properties of chromophoric and fluorescent analogs of adenine nucleoside and nucleotides, 2',3'-*O*-(2,4,6-trinitrocyclohexadienylidene) adenosine derivatives. *Biochim Biophys Acta* **719**(3):509-517.

Hiratsuka T (2003) Fluorescent and colored trinitrophenylated analogs of ATP and GTP. *Eur J Biochem / FEBS* **270**(17):3479-3485.

Lacy DB, Lin HC, Melnyk RA, Schueler-Furman O, Reither L, Cunningham K, Baker D and Collier RJ (2005) A model of anthrax toxin lethal factor bound to protective antigen. *Proc Natl Acad Sci U S A* **102**(45):16409-16414.

Lacy DB, Mourez M, Fouassier A and Collier RJ (2002) Mapping the anthrax protective antigen binding site on the lethal and edema factors. *J Biol Chem* **277**(4):3006-3010.

Leppla SH (1982) Anthrax toxin edema factor: a bacterial adenylate cyclase that increases cyclic AMP concentrations of eukaryotic cells. *Proc Natl Acad Sci USA* **79**(10):3162-3166.

Liu R and Sharom FJ (1997) Fluorescence studies on the nucleotide binding domains of the P-glycoprotein multidrug transporter. *Biochemistry* **36**(10):2836-2843.

Mock M and Fouet A (2001) Anthrax. *Annu Rev Microbiol* **55**:647-671.

Mou TC, Gille A, Fancy DA, Seifert R and Sprang SR (2005) Structural basis for the inhibition of mammalian membrane adenylyl cyclase by 2 '(3')-*O*-(N-Methylanthraniloyl)-guanosine 5 '-triphosphate. *J Biol Chem* **280**(8):7253-

7261.

Mou TC, Gille A, Suryanarayana S, Richter M, Seifert R and Sprang SR (2006) Broad specificity of mammalian adenylyl cyclase for interaction with 2',3'-substituted purine- and pyrimidine nucleotide inhibitors. *Mol Pharmacol* **70**(3):878-886.

Mourez M, Lacy DB, Cunningham K, Legmann R, Sellman BR, Mogridge J and Collier RJ (2002) 2001: a year of major advances in anthrax toxin research. *Trends Microbiol* **10**(6):287-293.

Neer EJ, Lok JM and Wolf LG (1984) Purification and properties of the inhibitory guanine nucleotide regulatory unit of brain adenylate cyclase. *J Biol Chem* **259**(22):14222-14229.

Shen Y, Zhukovskaya NL, Guo Q, Florian J and Tang WJ (2005) Calcium-independent calmodulin binding and two-metal-ion catalytic mechanism of anthrax edema factor. *Embo J* **24**(5):929-941.

Smigel MD (1986) Purification of the catalyst of adenylate cyclase. *J Biol Chem* **261**(4):1976-1982.

Stewart RC, VanBruggen R, Ellefson DD and Wolfe AJ (1998) TNP-ATP and TNP-ADP as probes of the nucleotide binding site of CheA, the histidine protein kinase in the chemotaxis signal transduction pathway of Escherichia coli. *Biochemistry* **37**(35):12269-12279.

Sunahara RK, Dessauer CW and Gilman AG (1996) Complexity and diversity of mammalian adenylyl cyclases. *Annu Rev Pharmacol Toxicol* **36**:461-480.

Taha HM, Schmidt J, Gottle M, Suryanarayana S, Shen Y, Tang WJ, Gille A, Geduhn J, Konig B, Dove S and Seifert R (2008) Molecular Analysis of the Interaction of Anthrax Adenylyl Cyclase Toxin, Edema Factor, with 2'(3')-O-(N-(methyl)anthraniloyl)-Substituted Purine and Pyrimidine Nucleotides. *Mol Pharmacol*.

Thomas PJ, Shenbagamurthi P, Ysern X and Pedersen PL (1991) Cystic fibrosis transmembrane conductance regulator: nucleotide binding to a synthetic peptide. *Science, NY* **251**(4993):555-557.